The Chemistry of Tris(phosphino)borate Manganese and Iron Platforms

Thesis by

Connie Chih Lu

In partial fulfillment of the requirements for the degree of Doctor of Philosophy

California Institute of Technology

Pasadena, California

2006

(Defended May 26, 2006)

Acknowledgments

One of the pleasures of finishing this document is the opportunity to thank the many people who have helped me through these past years. My advisor, Jonas Peters, is an inspiration. Jonas is a great model of someone who truly loves what he does. His tenacity and passion for science are traits that I encounter nearly every time I speak with him. My committee members, John Bercaw, Brian Stoltz, and Bill Goddard, were helpful in preparing me for this final hurdle. I would like to thank John for his many words of wisdom packed into short amounts of time, especially during my prop exam.

The Peters group has been a second family and a good source of support and entertainment. My colleagues from the start are an unforgetful bunch of characters. My first boxmate, Chris Thomas, welcomed me to the lab and taught me to be a meticulous and skeptical scientist. Ted Betley and Steve Brown were the strongmen of the group, and they pulled their weight to keep the lab shipshape for everyone. I recall fondly working with Dave Jenkins on many problem sets. Seth Harkins had many pearls of wisdom, though unfortunately, I won't be able to repeat them here. Chris(tine) Thomas has also been a supportive labmate, and it has been an inspiration to see her succeed.

Many talented post-docs have trekked through the lab. I would like to thank Cora MacBeth foremost because she single-handedly had the strongest influence on me during my time at Caltech. She taught me nearly half of the physical methods I use today. Her generosity and her good deeds place her in a realm above most of us. Mark Mehn has been my trustworthy scientific critic these past few years. Bruce MacKay, Xile Hu, Arjun Mendiratta, Eric Rivard, and Philip Collier have generously provided feedback on proposals/papers at different stages of my grad studies. I would be remiss not to thank

Parisa Mehrkhodavandi and Paula Diaconescu for acting as my mentors since my undergrad days.

I've also had the pleasure of working with Erin Daida, Claire Jacobs, Baixin Qian, and Megumi Abe. Also, there is the new Peters avant-garde to recognize. Matt Whited and Neal Mankad are leaders who are bringing the lab and its science to the next stage. I am grateful to Caroline Saouma for maintaining the glove-box and editing my drafts. Alex Miller has been patient and helpful with my computer problems. I wish Valerie Scott, Jill Dempsey, and the rest of the Peters crew successes and happiness in the upcoming years. I would also like to thank Kathleen Hand for her kind friendship throughout the years.

The mechanism of doing research would not have been possible without the efforts of many staff personnel. Larry Henling has spent much of his time teaching and re-teaching crystal structure refinement. I would also like to thank Mike Day, Mona Shahgholi, Angelo di Bilio, Dr. Robert Lee, Scott Ross, and Dan Nieman for technical assistance. I thank Dian Buchness, Pat Anderson, Shirley Feng, and Tess Legaspi for making paperwork and scheduling meetings as painless as possible. Bill Gunderson and Professor Mike Hendrich provided the Mössbauer data. Todd Younkin and Andy Waltman helped set up my earliest polymerization experiments.

Finally, I would like to give thanks to my friends for all the great memories I can take with me, and my family for their encouragement and support. Special thanks are in order for Carole and Atti, who gave me extra servings of food, love, and happiness.

Abstract

The coordination chemistry of monovalent and divalent manganese complexes supported by the anionic tris(phosphino)borate ligand, [PhBP$^{i\mathrm{Pr}}_3$] (where [PhBP$^{i\mathrm{Pr}}_3$] = [PhB($CH_2P^iPr_2$)$_3$]$^-$), is presented. The halide complexes, [PhBP$^{i\mathrm{Pr}}_3$]MnCl and [PhBP$^{i\mathrm{Pr}}_3$]MnI, have been characterized by X-ray diffraction, SQUID magnetometry, and EPR spectroscopy. The halide [PhBP$^{i\mathrm{Pr}}_3$]MnI serves as a precursor to a series of manganese azide, alkyl, and amide species: [PhBP$^{i\mathrm{Pr}}_3$]Mn(N_3), [PhBP$^{i\mathrm{Pr}}_3$]Mn(CH_2Ph), [PhBP$^{i\mathrm{Pr}}_3$]Mn(Me), [PhBP$^{i\mathrm{Pr}}_3$]Mn(NH(2,6-^{i}Pr$_2$Ph)), [PhBP$^{i\mathrm{Pr}}_3$]Mn(dbabh), and [PhBP$^{i\mathrm{Pr}}_3$]Mn(1-Ph(isoindolate)). Collectively, they represent an uncommon structural motif of low-coordinate polyphosphine-supported manganese species. Two monovalent manganese species have also been prepared. These include the Tl-Mn adduct, [PhBP$^{i\mathrm{Pr}}_3$]Tl-$MnBr(CO)_4$, and the octahedral complex [PhBP$^{i\mathrm{Pr}}_3$]Mn(CN^tBu)$_3$. Some of our initial synthetic efforts to generate [PhBP$^{i\mathrm{Pr}}_3$]Mn≡N_x species are briefly described, as are theoretical DFT studies that probe the electronic viability of these types of multiply bonded target structures.

Two new tris(phosphino)borate ligands, [PhB(CH_2P(*m*-terphenyl)$_2$)$_3$]$^-$ ([PhBP$^{\mathrm{ter}}_3$]) and [PhB($CH_2P(CH_2Cy)_2$)$_3$]$^-$ ([PhBP$^{CH_2Cy}_3$]), are introduced that feature terphenyl and methylcyclohexyl groups on the phosphine arms, respectively. The iron chlorides, [PhBP$^{\mathrm{ter}}_3$]FeCl and [PhBP$^{CH_2Cy}_3$]FeCl, have been characterized by crystallography and cyclic voltammetry. The Fe(II)/Fe(I) potential of [PhBP$^{CH_2Cy}_3$]FeCl at -1.94 V is ~100 mV more anodic relative to the potential of [PhBP$^{i\mathrm{Pr}}_3$]FeCl. A similar shift is observed for [PhBP$^{\mathrm{ter}}_3$]FeCl relative to [$PhBP_3$]FeCl. The preparation of iron nitrides has been probed with the nitride transfer reagent, Li(dbabh) (where dbabh = 2,3:5,6-dibenzo-7-

azabicyclo[2.2.1]hepta-2,5-diene). Whereas [PhBP$^{ter}_3$]FeCl and Li(dbabh) gave an ill-defined mixture, [PhBP$^{CH_2Cy}_3$]FeCl and Li(dbabh) produced the terminal nitride, [PhBP$^{CH_2Cy}_3$]Fe(N), cleanly at -50 ºC. The ^{15}N NMR spectrum of the labeled species, [PhBP$^{CH_2Cy}_3$]Fe(^{15}N), contains a peak at 929 ppm, consistent with a terminal nitride functionality. Mössbauer spectroscopy of the nitride shows a low isomer shift value of -0.34(1) mm/s, which is consistent with high valent iron, and an exceptionally large quadrupole splitting of 6.01(1) mm/s.

The sodium amalgam reduction of [PhBP$^{CH_2Cy}_3$]FeCl gives a masked iron(I) species that is highly reactive. Combustion analysis of this species is consistent with "[PhBP$^{CH_2Cy}_3$]Fe." Other physical methods including VT NMR, EPR, and IR spectroscopies suggest the presence of a paramagnetic S = ½ species in equilibrium with a diamagnetic species. The paramagnetic component is postulated to be an Fe(III) hydride, wherein a ligand C-H bond has been cyclometalated at the metal center. The reactivity of "[PhBP$^{CH_2Cy}_3$]Fe" is consistent with iron(I). For example, its reaction with PMe_3 and 1-adamantylazide affords the phosphine adduct, [PhBP$^{CH_2Cy}_3$]Fe(PMe_3), and the iron imide, [PhBP$^{CH_2Cy}_3$]Fe(NAd), respectively. Interestingly, "[PhBP$^{CH_2Cy}_3$]Fe" undergoes redox reactions with benzene to give initially a benzene adduct, {[PhBP$^{CH_2Cy}_3$]Fe}$_2$(μ-η^3:η^3-C_6H_6), which decomposes to {[PhBP$^{CH_2Cy}_3$]Fe}$_2$(μ-η^5:η^5-6,6'-bicyclohexadienyl) via radical C-C bond coupling. Finally, "[PhBP$^{CH_2Cy}_3$]Fe" readily reduces CO_2 at rt to give as the major product {[PhBP$^{CH_2Cy}_3$]Fe}$_2$(μ-CO)(μ-O), wherein a C=O bond has been cleaved. The minor product has not been definitively established, but one possibility is the oxalate-bridged dimer {[PhBP$^{CH_2Cy}_3$]Fe}$_2$(μ-η^2:η^2-O_2CCO_2) that results from reductive coupling of two CO_2 molecules.

Table of Contents

List of Figures

List of Tables

List of Abbreviations and Nomenclature

$[BP_3]$	general tris(phosphino)borate ligand
$[PhBP_3]$	$[PhB(CH_2PPh_2)_3]^-$
$[PhBP^{CH_2Cy}{}_3]$	$[PhB(CH_2P(CH_2Cy)_2)_3]^-$
$[PhBP^{iPr}{}_3]$	$[PhB(CH_2P^iPr_2)_3]^-$
$[PhBP^{ter}{}_3]$	$[PhB(CH_2P(m\text{-terphenyl})_2)_3]^-$
$[PhBP^{tBu}{}_2(pz)]$	$[PhB(CH_2P^tBu_2)_2(pyrazolyl)]^-$
$[Ph_2BP_2]$	$[Ph_2B(CH_2PPh_2)_2]^-$
(Ph_2SiP_2)	$Ph_2Si(CH_2PPh_2)_2$
$[PhTp^{tBu}]$	phenyl tris(3-*tert*-butylpyrazolyl)borate
$\{^1H\}$	hydrogen-1 decoupled
°	degrees, a measure of angle
°C	degrees Celsius
^1H	hydrogen-1
^{11}B	boron-11
^{15}N	nitrogen-15
^{19}F	fluorine-19
^{31}P	phosphorus-31
Å	Angstrom, 10^{-10} m
A_x	EPR coupling constant where X is the nucleus coupling to the unpaired electron
ACN	acetonitrile
Ad	1-adamantyl

Anal. Calcd.	elemental analysis calculated
atm	atmosphere
ave	average
B3LYP	Becke three-parameter function with Lee-Yang-Parr correlation
br	broad
^{n}Bu	n-butyl
^{s}Bu	*sec*-butyl
^{t}Bu	*tert*-butyl
C_3, C_s	Schoenflies symmetry designations
ca.	circa
CCD	charge-coupled device
CCDC	Cambridge Crystallographic Data Centre
cm	centimeter(s)
cm^{-1}	inverse centimeters or wavenumbers
cm^3	cubic centimeters
COD	1,5-cyclooctadiene
Cp	cyclopentadienyl
Cp^*	pentamethylcyclopentadienyl
Cy	cyclohexyl
d	doublet
d^n	d-electron count of n-electrons for a transition metal
dbabh	2,3:5,6-dibenzo-7-aza bicycle[2.2.1]hepta-2,5-diene
D_{calc}	calculated density

dd	doublet of doublets
deg	degrees
DFT	density functional theory
dippp	1,3-diisopropylphosphinopropane
dppp	1,3-diphenylphosphinopropane
dt	doublet of triplets
E	an atom or functional group forming a metal-ligand multiple bond
E/D	rhombicity of a metal center
EPR	electron paramagnetic resonance
equiv	equivalents
ESI/MS	electrospray ionization mass spectrometry
Et_2O	diethylether
EtOH	ethanol
eV	electron volt
EXAFS	extended X-ray absorption fine structure
F_c	calculated structure factor
Fc/Fc^+	ferrocene/ferrocenium
F_o	observed structure factor
fw	formula weight
g	gram(s)
g	g-factor
G	Gauss
GC/MS	gas chromatography mass spectrometry

GHz	gigahertz
GPC	gel permeation chromatography
h	hour(s)
H	applied magnetic field
H_m	meta-H
H_o	ortho-H
HOMO	highest occupied molecular orbital
H_p	para-H
Hz	hertz
I	intensity
I_n	nuclear spin of atom n
IR	infrared
$^nJ_{A\text{-}B}$	coupling constant between nuclei A and B over n bonds (NMR)
k	rate constant
K	degrees in Kelvin
kcal	kilocalories
K_{eq}	equilibrium constant
kHz	kilohertz
k_{obs}	observed rate constant
L	dative ligand for a transition metal
LACVP	Los Alamos core valence potential
LN_2	liquid nitrogen
LUMO	lowest unoccupied molecular orbital

m	multiplet
M	concentration in molarity
M	general transition metal
m-	meta position of an aryl ring
Me	methyl
mg	milligram(s)
MHz	megahertz, 10^6 Hertz
min	minute(s)
mL	milliliter(s)
mm	millimeter
mmol	millimole(s)
MO	molecular orbital
mol	mole(s)
m_s	intrinsic spin quantum number
ms	millisecond(s)
MS	mass spectrometry
mT	millitesla(s)
mV	millivolt(s)
mW	milliwatt(s)
NIR	near-infrared
nm	nanometer(s)
NMR	nuclear magnetic resonance
N_x	general nitrogen-bound ligand

OTf	$-OSO_2CF_3$
p-	*para* position of an aryl ring
P_{ax}	axial phosphorous
Ph	phenyl
pin	pinacol
ppm	parts per million
psi	pound-force per square inch
q	quartet
R	general alkyl or aryl substituents
R_1	R-factor (XRD)
rt	room temperature
s	second(s)
s	singlet
S	spin
SCF	self-consistent field
SD	standard deviation
SOMO	singly occupied molecular orbital
SQUID	superconducting quantum interference device
sqrt	square root
t	triplet
T	temperature
T_d	tetrahedral symmetry
THF	tetrahydrofuran

THF-d_8	tetrahydrofuran-d_8
tmeda	tetramethylethylenediamine
TMS	trimethylsilyl
tol	toluene
tolyl	$-C_6H_4CH_3$
TON	turnover number
Tp	general hydrotris(pyrazolyl)borate ligand
Tp^{Me2}	hydrotris(3,5-dimethylpyrazolyl)borate
triphos	$H_3CC(CH_2PPh_2)_3$
UV-vis	ultraviolet-visible
V	volume
VT NMR	variable temperature nuclear magnetic resonance
wR_2	weighted R-factor (XRD)
X	monoanionic atom or group, e.g., halide
XAS	X-ray absorption spectroscopy
XRD	X-ray diffraction
χ	magnetic susceptibility
χ_M	molar magnetic susceptibility
δ	chemical shift
δ	isomer shift
ΔE_Q	quadrupole splitting
ε	extinction coefficient in M^{-1} cm^{-1}
η^n	hapticity of order n

λ	wavelength
λ_{max}	wavelength of maximum absorption
μ	absorption coefficient (XRD)
μ-A	bridging atom
μ_B	Bohr magnetons
μ_{eff}	effective magnetic moment
µL	microliter(s)
µmol	micromole(s)
ν	frequency
ω	omega (XRD)
φ	phi (XRD)
π	bonding interaction that has a nodal plane including the internuclear axis
π^*	anti-bonding interaction with a node that is perpendicular to the internuclear axis
σ	bonding interaction that contains the internuclear axis with no nodes
σ^*	anti-bonding interaction with a node along the internuclear axis

Chapter 1: Introduction to Tripodal (Phosphino)borate Metal Platforms

1.1 Overview of (Phosphino)borate Ligands

The properties of a transition metal center are strongly influenced by the electronics and sterics of its ligand environment. Even subtle changes in the ligand architecture may induce novel reactivity at a metal site. One area of research in the Peters lab has been the study of the effect of adding an anionic borate to the backbone of polyphosphines.[1-7] These ligands become more electron-releasing due to the addition of the charge. This effect has been observed in several systems featuring mid-to-late transition metals and may manifest in quicker reactivity, higher catalytic activity, a change in the reaction mechanism, and/or a different product outcome.[8-13]

In particular, the tris(phosphino)borate ligands, [$PhBP_3$] and [$PhBP^{iPr}_3$], and the hybrid bis(phosphino)pyrazolyl borate ligands [$PhBP_2(pz)$] (shown in Figure 1.1) have highlighted fundamentally new aspects in the coordination chemistry of both cobalt and iron.[14-20] These ligands have stabilized the first examples of mononuclear terminal imides and nitrides (M≡N) of cobalt and iron.[16-19] The ligands are structurally similar to other tripodal ligands, including triphos, hydrotris(pyrazolyl)borates (Tp), tris(thioether)borates,[21-26] and the recent tris(carbenes)[27-31] and tris(carbene)borates.[32-34] They are also comparable by isolobal analogy to the well-known family of cyclopentadienyl ligands. Nonetheless, comparative studies have demonstrated that the [$PhBP_3$] ligand is significantly more electron-releasing than either Cp^* or Tp^{Me2}.[5] The strong-ligand-field attribute of [$PhBP_3$] may be further underscored by the fact that the only other four-coordinate cobalt imides, which feature $Tp^{Me,tBu}$ and the tris(carbene) as ligands, are less stable.[35, 36]

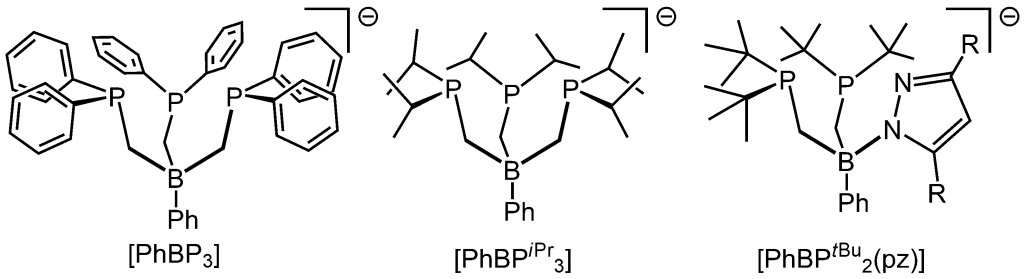

Figure 1.1. Tripodal (phosphino)borate ligands featuring various ligand arms.

1.2 Electronic Structure and Implications for M≡N$_x$ Species

An early demonstration that the tripodal (phosphino)borate ligands can reveal novel aspects in the metal's coordination chemistry was provided by the cobalt complex, [PhBP$_3$]CoI.[14] Its low-spin ground state is unprecedented for tetrahedral or distorted tetrahedral Co(II), which are exclusively high spin otherwise. The low-spin configuration is consistent with a two-over-three d-orbital splitting diagram, which would result if a high-lying orbital in the *t* set drops to low energy (Figure 1.2). The near 90° P-Co-P angles observed in [PhBP$_3$]CoI represent an axial distortion from T_d symmetry. One consequence of this distortion is that the d_{z2} orbital can be significantly stabilized to produce the two-over-three splitting diagram.

The two high-energy orbitals are symmetrically poised to form two equivalent π-bonds with a ligand in the apical site. These π-interactions do not change the two-over-three splitting diagram as these orbitals are already destabilized by σ* interactions with the phosphines. Indeed, the d^6 [BP$_3$]-supported cobalt imides are stable and exhibit singlet ground states.[18]

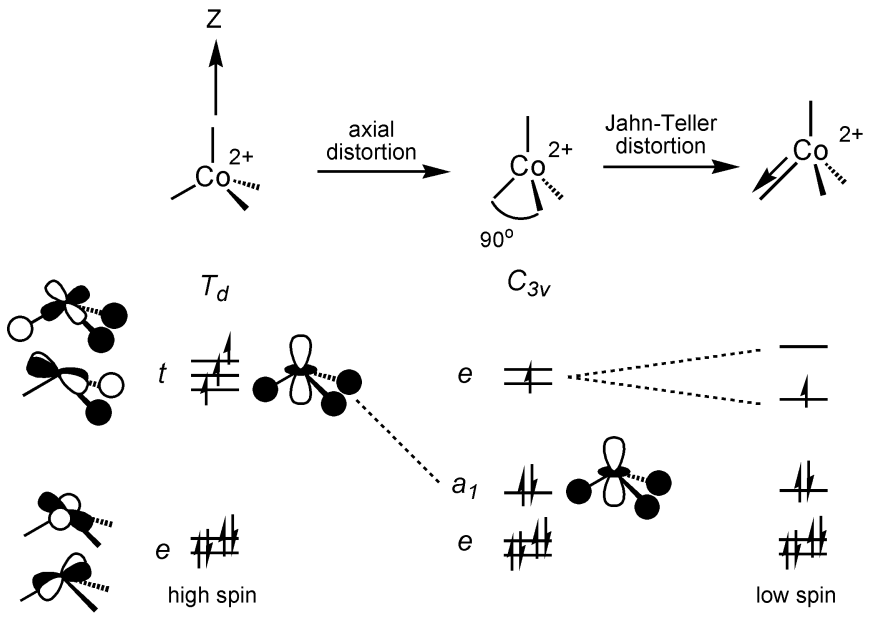

Figure 1.2. Comparison of d-orbital splitting diagrams for Co^{2+} in T_d, C_{3v} (with axial distortion), and C_s geometry.

The discovery of the first cobalt imide was inspiring because metal-ligand multiply bonded species are rare for the late transition metals, especially for the first-row metals. An inspection of the d-orbital splitting diagram led to speculations that the d^5 electronic configuration may be viable. The formal removal of an electron should not alter the M-N bond order if the three low-lying orbitals are truly non-bonding. Indeed, the d^6 Fe(II) and d^5 Fe(III) imides supported by [$PhBP_3$] have nearly identical Fe-N bond lengths in their solid-state structures (Figure 1.3).[17, 37] Also quite interesting is that the unprecedented Fe(IV) imides of the type [$PhBP_2$(pz)]Fe(NR)$^+$ exhibit an S = 3/2 ground state and show remarkably similar Fe-N bond distances.[19]

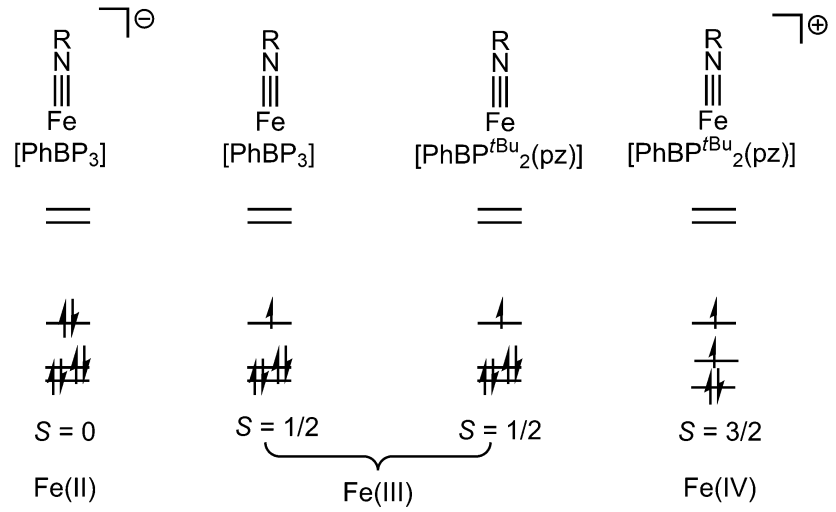

Figure 1.3. The electronic configurations for structurally related iron imides in three different oxidation states and spin states.

The stability of the various electronic configurations for the iron imides suggests that $M{\equiv}N_x$ species of other mid-to-late transition metals may be electronically accessible. One plausible target is the d^4 manganese imide $[BP_3]Mn(NR)$. This hypothetical species is isolobal to the Fe(IV) imides and is an unusual example of a low-valent manganese imide.

By switching to the $[PhBP^{iPr}_3]$ ligand, the novel Fe(IV) terminal nitride $[PhBP^{iPr}_3]Fe(N)$ was prepared.[16] This species is stable at 0 °C, but it thermally degrades via bimolecular coupling to the bridged-dinitrogen dimer, $\{[PhBP^{iPr}_3]Fe\}_2(\mu\text{-}N_2)$. The few examples of terminal iron nitrides are generated and characterized at very low temperatures (30 to 70 K),[38-42] so this species shows dramatically increased stability. Compared to the imides, the nitride has a different orbital splitting diagram in which the d_{z2} orbital is strongly destabilized by increased antibonding interactions with the nitride and phosphines. Because only two orbitals remain at low energy, the d^4 configuration of

this species is stable and consistent with its singlet nature. In analogy to the d^6 and d^5 iron imides, it is also worthwhile to consider the stability of a d^3 metal nitride such as the hypothetical manganese nitride, $[BP_3]Mn(N)$. General efforts to prepare manganese imides and nitrides are presented in Chapter 2. Also, efforts to prepare stable iron(IV) nitrides motivated the development of new $[BP_3]$ ligands. The ligand preparations and their ability to stabilize Fe(IV) nitrides are discussed in Chapter 3.

1.3 Redox Reactivity of the Iron Systems– Towards Activation of Small Molecules

Another facet of these ligands is that they support a wide range of metal oxidation states. In particular, the versatility of $[PhBP^{iPr}_3]Fe$ to accommodate multiple redox states is highlighted by the variety of nitrogen-containing ligands, ranging from the π-acidic N_2 to the π-basic imides and nitrides that are supported on this single platform.[15, 16] Collectively, these compounds, which are shown in Figure 1.4, may represent intermediates in the transformation of dinitrogen to ammonia at a single iron site in a Chatt-type cycle. Therefore, an understanding of their spectroscopy and reactivity patterns may elucidate structure-function relationships that are relevant to dinitrogen fixation. Indeed, some of the proposed steps in dinitrogen fixation have already been demonstrated using these complexes. For instance, the $Fe(N_2)$ adduct, $[[PhBP^{iPr}_3]Fe(N_2)]_2[Mg(THF)_4]$, reacts with 2 equivalents of MeOTs to yield 2 equivalents of the diazenido species, $[PhBP^{iPr}_3]Fe(N_2Me)$.[15]

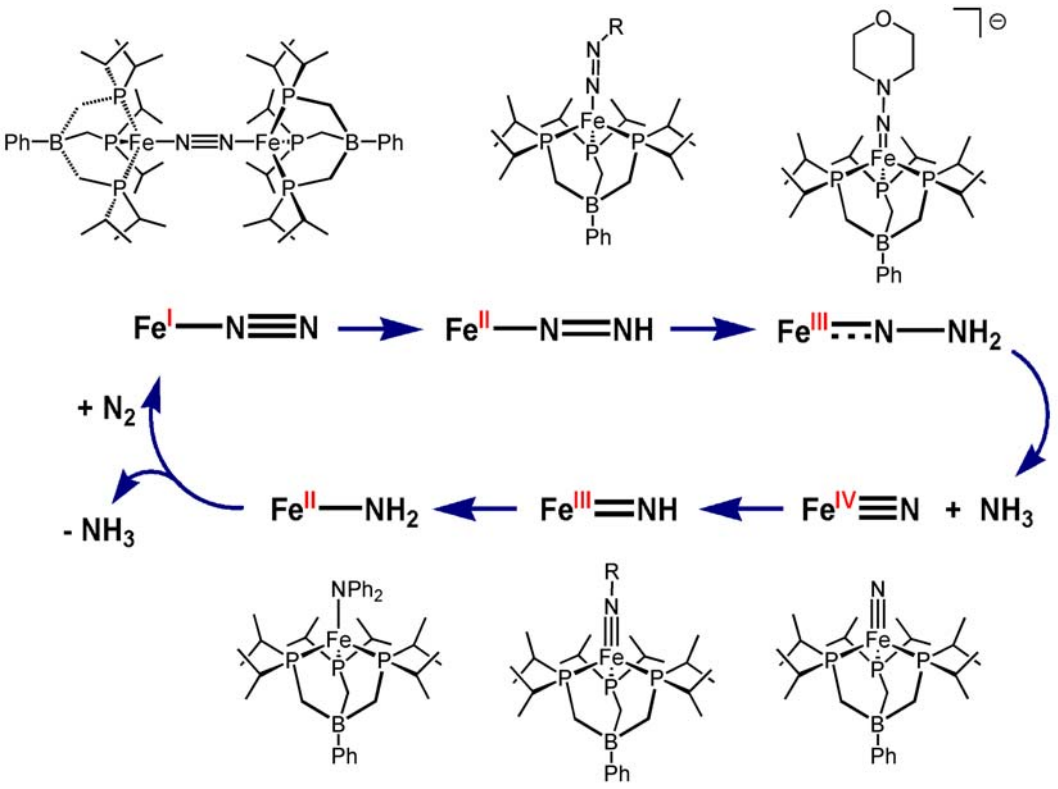

Figure 1.4. [PhBP$^{iPr}_3$]Fe complexes with a wide range of nitrogenous ligands are structurally similar to proposed intermediates in a Chatt-type cycle at a single iron site.

The conversion of dinitrogen to ammonia occurs naturally within nitrogenases and industrially in the Haber-Bosch process (Figure 1.5). Despite detailed structural knowledge of the FeMo cofactor in the MoFe-nitrogenases,[43-46] the site(s) of N_2 binding and reduction are not well understood.[47-49] Molybdenum and iron are both implicated as the active sites, though iron is the only transition metal common to all nitrogenases. Iron is also the preferred catalyst for the Haber-Bosch process. The chemical equation by which nitrogenases reduce N_2 to ammonia utilizes protons and electrons (Figure 1.5). The Haber-Bosch process, on the other hand, uses hydrogen at high pressures and

temperatures.[50,51] Both processes are challenging to study intimately, and thus, their mechanisms are virtually unknown.

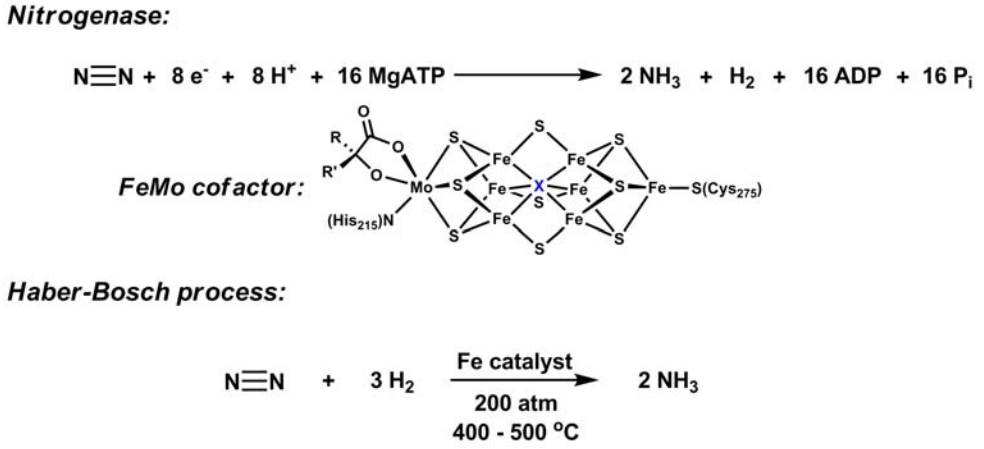

Figure 1.5. Nitrogenases and the Haber-Bosch process reduce dinitrogen to ammonia.

The recent discovery of well-defined $[BP_3]Fe{\equiv}N_x$ species provides a unique opportunity to study their plausible roles as intermediates in dinitrogen fixation. Interestingly, the $Fe{\equiv}N_x$ species show a propensity to undergo functionalization at the nitride and imide moiety, sometimes with full scission of the Fe-N linkage. For example, the nitride $[PhBP^{iPr}_3]Fe(N)$ liberates ammonia in moderate yield (~50%) upon exposure to protons and electrons.[16] Another interesting reaction is the hydrogenation of the bridged iron nitrides, $[\{[PhBP_3]Fe\}_2(\mu\text{-}N)]^n$ (where n = 0, -1), to give the bridged imides, $[\{[PhBP_3]Fe\}_2(\mu\text{-}NH)(\mu\text{-}H)]^n$.[52] Additionally, the hydrogenation of the iron imide $[PhBP_3]Fe(N(p\text{-tolyl}))$ gives initially the iron amide, which reacts further with hydrogen to liberate the amine and generate a solvent-trapped iron hydride.[53]

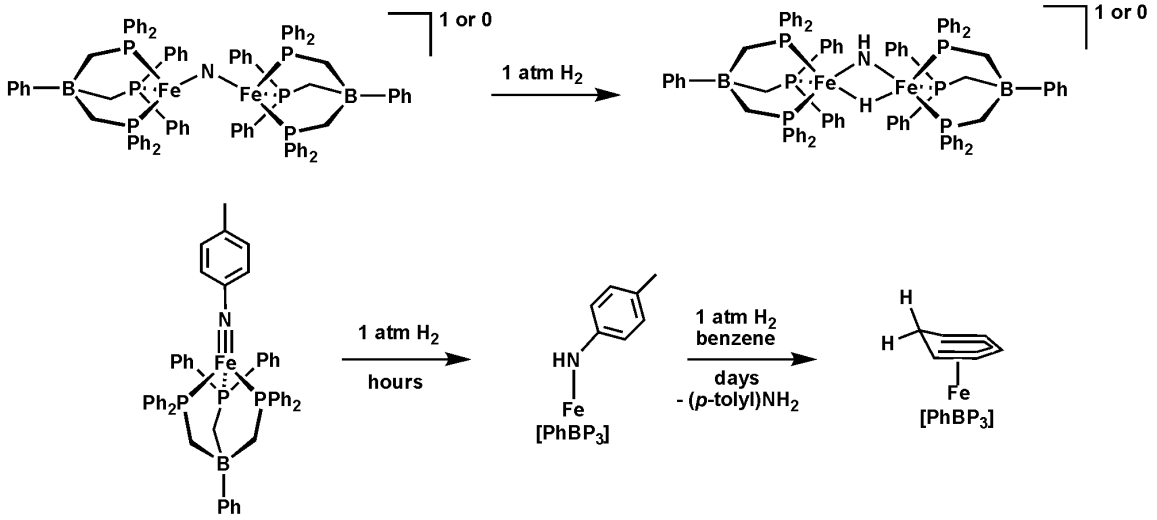

Figure 1.6. Examples of hydrogenations of Fe-N bonds that are relevant to N_2 reduction.

The above discussions showcase the rich redox chemistry of the $[BP_3]Fe$ platforms for the fixation of N_2. This redox versatility, however, may be generally exploited for the activation of other small molecules. For instance, the conversion of CO_2, an abundant pollutant, to a useful precursor for chemical synthesis or fuel production is highly desirable. The potential utility of the $[BP_3]Fe$ scaffolds for activating CO_2 and other small substrates is explored in Chapter 4.

1.4 Chapter Summaries

Chapter 2 presents aspects of the coordination chemistry of monovalent and divalent manganese complexes supported by $[PhBP^{iPr}_3]$. The halide complex $[PhBP^{iPr}_3]MnI$ serves as a useful precursor to a series of Mn azide, alkyl, and amide species. These pseduotetrahedral compounds represent an uncommon structural motif for low-coordinate, polyphosphine-supported Mn complexes. Two monovalent manganese

species have also been prepared. Initial synthetic efforts to generate $[PhBP^{iPr}_3]Mn{\equiv}N_x$ species are briefly described, as are theoretical DFT studies that probe the electronic viability of these types of multiply bonded target structures.

Chapter 3 introduces two new tris(phosphino)borate ligands, $[PhB(CH_2P(m\text{-terphenyl})_2)_3]^-$ and $[PhB(CH_2P(CH_2Cy)_2)_3]^-$, which feature terphenyl and methylcyclohexyl groups on the phosphine arms, respectively. The ligand syntheses and their iron metallation are described. Notably, a terminal iron nitride supported by the methylcyclohexyl ligand can be prepared and characterized, albeit only at temperatures below -50 °C. One interesting feature of this nitride is an unusually large quadrupole splitting observed by Mössbauer spectroscopy.

Chapter 4 describes the reduction of $[PhBP^{CH2Cy}_3]FeCl$ to give a masked iron(I) species. Though the exact nature of this compound remains unknown, it is highly reactive and reductively activates a host of small molecules. Of particular interest is the reductive cleavage of CO_2 to give the iron dimer, $\{[PhBP^{CH2Cy}_3]Fe\}_2(\mu\text{-CO})(\mu\text{-O})$, wherein a C=O bond has been cleaved by two electrons. Another possible functionalization of CO_2 is presented, where two CO_2 molecules are reductively coupled to generate an oxalate functionality.

References Cited

1. Betley, T. A.; Peters, J. C. *Inorg. Chem.* **2003**, *42*, 5074.

2. Shapiro, I. R.; Jenkins, D. M.; Thomas, J. C.; Day, M. W.; Peters, J. C. *Chem. Commun.* **2001**, 2152.

3. Thomas, C. M.; Peters, J. C. *Inorg. Chem.* **2004**, *43*, 8.

4. Thomas, J. C.; Peters, J. C. *Inorg. Chem.* **2003**, *42*, 5055.

5. Feldman, J. D.; Peters, J. C.; Tilley, T. D. *Organometallics* **2002**, *21*, 4050.

6. Barney, A. A.; Heyduk, A. F.; Nocera, D. G. *Chem. Commun.* **1999**, 2379.

7. Thomas, J. C.; Peters, J. C. *Inorg. Synth.* **2004**, *34*, 8.

8. Lu, C. C.; Peters, J. C. *J. Am. Chem. Soc.* **2004**, *126*, 15818.

9. Thomas, J. C.; Peters, J. C. *J. Am. Chem. Soc.* **2003**, *125*, 8870.

10. Betley, T. A.; Peters, J. C. *Angew. Chem. Int. Ed.* **2003**, *42*, 2385.

11. Lu, C. C.; Peters, J. C. *J. Am. Chem. Soc.* **2002**, *124*, 5272.

12. Thomas, J. C.; Peters, J. C. *J. Am. Chem. Soc.* **2001**, *123*, 5100.

13. Daida, E. J.; Peters, J. C. *Inorg. Chem.* **2004**, *43*, 7474.

14. Jenkins, D. M.; Di Bilio, A. J.; Allen, M. J.; Betley, T. A.; Peters, J. C. *J. Am. Chem. Soc.* **2002**, *124*, 15336.

15. Betley, T. A.; Peters, J. C. *J. Am. Chem. Soc.* **2003**, *125*, 10782.

16. Betley, T. A.; Peters, J. C. *J. Am. Chem. Soc.* **2004**, *126*, 6252.

17. Brown, S. D.; Betley, T. A.; Peters, J. C. *J. Am. Chem. Soc.* **2003**, *125*, 322.

18. Jenkins, D. M.; Betley, T. A.; Peters, J. C. *J. Am. Chem. Soc.* **2002**, *124*, 11238.

19. Thomas, C. M.; Mankad, N. P.; Peters, J. C. *J. Am. Chem. Soc.* **2006**, *128*, 4956.

20. Thomas, C. M.; Peters, J. C. *Angew. Chem. Int. Ed.* **2006**, *45*, 776.

21. Fujita, K.; Rheingold, A. L.; Riordan, C. G. *Dalton Trans.* **2003**, 2004.

22. Schebler, P. J.; Mandimutsira, B. S.; Riordan, C. G.; Liable-Sands, L. M.; Incarvito, C. D.; Rheingold, A. L. *J. Am. Chem. Soc.* **2001**, *123*, 331.

23. Ohrenberg, C.; Riordan, C. G.; Liable-Sands, L.; Rheingold, A. L. *Coord. Chem. Rev.* **1998**, *174*, 301.

24. Schebler, P. J.; Riordan, C. G.; Guzei, I. A.; Rheingold, A. L. *Inorg. Chem.* **1998**, *37*, 4754.

25. Ge, P. H.; Riordan, C. G.; Yap, G. P. A.; Rheingold, A. L. *Inorg. Chem.* **1996**, *35*, 5408.

26. Ohrenberg, C.; Ge, P. H.; Schebler, P.; Riordan, C. G.; Yap, G. P. A.; Rheingold, A. L. *Inorg. Chem.* **1996**, *35*, 749.

27. Hu, X.; Castro-Rodriguez, I.; Meyer, K. *Organometallics* **2003**, *22*, 3016.

28. Hu, X.; Meyer, K. *J. Organomet. Chem.* **2005**, *690*, 5474.

29. Hu, X. L.; Castro-Rodriguez, I.; Meyer, K. *Chem. Commun.* **2004**, 2164.

30. Hu, X. L.; Castro-Rodriguez, I.; Olsen, K.; Meyer, K. *Organometallics* **2004**, *23*, 755.

31. Hu, X. L.; Castro-Rodriguez, I.; Meyer, K. *J. Am. Chem. Soc.* **2003**, *125*, 12237.

32. Nieto, I.; Cervantes-Lee, F.; Smith, J. M. *Chem. Commun.* **2005**, 3811.

33. Fränkell, R.; Birg, C.; Kernbach, U.; Habereder, T.; Noth, H.; Fehlhammer, W. P. *Angew. Chem. Int. Ed.* **2001**, *40*, 1907.

34. Kernbach, U.; Ramm, M.; Luger, P.; Fehlhammer, W. P. *Angew. Chem., Int. Ed. Eng.* **1996**, *35*, 310.

35. Shay, D. T.; Yap, G. P. A.; Zakharov, L. N.; Rheingold, A. L.; Theopold, K. H. *Angew. Chem. Int. Ed.* **2005**, *44*, 1508.

36. Hu, X.; Meyer, K. *J. Am. Chem. Soc.* **2004**, *126*, 16322.

37. Brown, S. D.; Peters, J. C. *J. Am. Chem. Soc.* **2005**, *127*, 1913.

38. Aliaga-Alcalde, M.; George, S. D.; Mienert, B.; Bill, E.; Wieghardt, K.; Neese, F. *Angew. Chem. Int. Ed.* **2005**, *44*, 2908.

39. Grapperhaus, C. A.; Mienert, B.; Bill, E.; Weyhermüller, T.; Wieghardt, K. *Inorg. Chem.* **2000**, *39*, 5306.

40. Meyer, K.; Bill, E.; Mienert, B.; Weyhermüller, T.; Wieghardt, K. *J. Am. Chem. Soc.* **1999**, *121*, 4859.

41. Wagner, W. D.; Nakamoto, K. *J. Am. Chem. Soc.* **1989**, *111*, 1590.

42. Wagner, W. D.; Nakamoto, K. *J. Am. Chem. Soc.* **1988**, *110*, 4044.

43. Einsle, O.; Tezcan, F. A.; Andrade, S. L. A.; Schmid, B.; Yoshida, M.; Howard, J. B.; Rees, D. C. *Science* **2002**, *297*, 1696.

44. Howard, J. B.; Rees, D. C. *Chem. Rev.* **1996**, *96*, 2965.

45. Kim, J. S.; Rees, D. C. *Nature* **1992**, *360*, 553.

46. Kim, J. S.; Rees, D. C. *Science* **1992**, *257*, 1677.

47. Rees, D. C.; Howard, J. B. *Curr. Opin. Chem. Biol.* **2000**, *4*, 559.

48. Burgess, B. K.; Lowe, D. J. *Chem. Rev.* **1996**, *96*, 2983.

49. MacKay, B. A.; Fryzuk, M. D. *Chem. Rev.* **2004**, *104*, 385.

50. Ertl, G. *Chem. Rec.* **2001**, *1*, 33.

51. Ertl, G., *Catalytic Ammonia Synthesis: Fundamentals and Practice*. Plenum Press: New York, 1991; p 109.

52. Brown, S. D.; Mehn, M. P.; Peters, J. C. *J. Am. Chem. Soc.* **2005**, *127*, 13146.

53. Brown, S. D.; Peters, J. C. *J. Am. Chem. Soc.* **2004**, *126*, 4538.

Chapter 2: Pseudotetrahedral Manganese Complexes Supported by the Anionic Tris(phosphino)borate Ligand [PhBP^{i}Pr$_3$]

2.1 Introduction

Transition metal complexes containing metal-ligand multiple bonds figure prominently in coordination chemistry, especially in atom- and group-transfer processes.[1, 2] Metal species of the types $L_nM{=}E$ and $L_nM{\equiv}E$, where E = O, NR, CR_2, can act as intermediates in numerous catalytic reactions including epoxidation,[3-6] aziridination,[7-10] cyclopropanation,[11-13] olefin metathesis,[14-17] and C-H bond insertion.[10, 18] Besides having broad synthetic utility, metal-to-ligand multiply bonded species also serve as biomimetic models of active sites in metalloenzymes.[19-22] Until a few years ago, examples of stable complexes featuring metal-to-ligand multiple bonds were rare for the later metals,[23-25] especially for those in the first row.[26] While the paucity of these compounds was typically attributed to an inherent incompatibility of high d-electron counts with multiply bonded π-donor substituents, low-coordinate geometries have provided one strategic path to circumvent this limitation. The recent rise in literature reports of well-defined $L_nM{=}E$ and $L_nM{\equiv}E$ systems for the metals M = Fe,[27-33] Co,[34-38] Ni,[39-43] and Cu[44, 45] strongly attests to the viability of these types of species for the first-row, mid-to-late metals.

Manganese compounds featuring multiply bonded terminal functionalities such as nitrides and imides are far more abundant than their later first-row counterparts.[46] For example, Mn(V) nitrides are well known to be stabilized by various ligand auxiliaries, including porphyrins,[47-51] macrocyclic amines,[52, 53] cyanides,[54] and Schiff bases.[55-58] In contrast, Mn(VI) and Mn(VII) nitrides are rare. Wieghardt and coworkers prepared two examples of Mn(VI) nitrides *in situ*, but neither compound has been fully characterized.[52, 54] Hursthouse and coworkers isolated the sole example of a Mn(VII) nitride,

$[Mn(N)(NtBu)_3]^{2-}$, which is supported by imido ligands.[59] Other relevant manganese imides from the Hursthouse group include species of the type $Mn^{VII}(N^tBu)_3X$, as well as the homoleptic compound $[Mn^{VI}(N^tBu)_4]^{2-}$.[60-62] Terminal Mn(V) imides are also stabilized by corroles, as recently reported by Abu-Omar and coworkers.[63-65] Finally, elegant work from Groves and Carreira strongly implicates Mn(V) acylimides (generated *in situ* from the nitrides) as effective group-transfer catalysts to olefin and enol ether substrates.[47, 55, 66]

We have been investigating the tris(phosphino)borate (generally denoted as $[BP_3]$) and hybrid bis(phosphino)pyrazolylborate ($[PhBP_2(pz)]$) ligands as scaffolds for M≡E linkages. Thus far, these ligands have stabilized Co(III)[36] and Fe(II/III) imides, [27, 29] as well as distinctive examples of Fe(IV) imides and nitrides.[28, 67] Motivated by these results, we wish to extend this chemistry to other mid-to-late first-row metals such as Ni[68] and Mn. In particular, we are interested in whether $[BP_3]Mn{\equiv}N_x$ species (d^3 and d^4) are electronically accessible and in defining synthetic methods for their generation. In pursuit of this task, we began to study aspects of the fundamental coordination chemistry of previously unexplored $[BP_3]$Mn-systems. In this chapter, the synthesis and characterization of a family of mono- and divalent manganese compounds supported by the $[PhBP^{iPr}_3]$ ligand (where $[PhBP^{iPr}_3] = [PhB(CH_2P^iPr_2)_3]^-$) are reported. Complementary theoretical studies are described for hypothetical imide $[PhBP^{iPr}_3]Mn(N^tBu)$ and nitride $[PhBP^{iPr}_3]Mn(N)$ systems. These species appear to be plausible target structures based upon electronic considerations. While studies towards well-defined $[BP_3]Mn{\equiv}N_x$ systems are ongoing, the four-coordinate $[PhBP^{iPr}_3]$Mn(II)

species that are described here represent structurally unusual examples of low-coordinate manganese complexes supported by polyphosphine ligands.

2.2 Results and Discussion

2.2.1 Synthesis and Characterization of [PhBP$^{iPr}_3$]Mn(II) Halides

The Mn(II) halides [PhBP$^{iPr}_3$]MnCl (**2.1**) and [PhBP$^{iPr}_3$]MnI (**2.2**) were readily prepared by mixing the thallium reagent [PhBP$^{iPr}_3$]Tl with MnX_2 (where X = Cl or I) (Equation 2.1).[69] This methodology has been used previously to prepare related compounds of divalent Fe, Ru, Co, and Ni.[68, 70, 71] The halides **2.1** and **2.2** are colorless in solution and can be crystallized from benzene/petroleum ether. Compound **2.1** provided light pink blocks in low yield (33%), while **2.2** was obtained as colorless blocks in moderate yield (62%). Because of its higher crystalline yield, compound **2.2** was used as the preferred starting material throughout the research described herein.

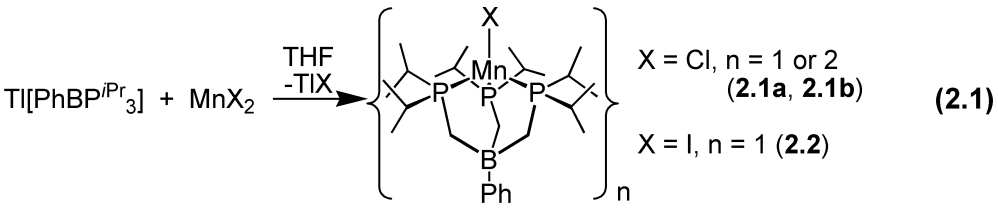

(2.1)

The halides **2.1** and **2.2** were characterized by various techniques including X-ray crystallography, SQUID magnetometry, and EPR spectroscopy. The solid-state structures of **2.1** and **2.2** are shown in Figures 2.1 and 2.2. The chloride complex **1** crystallizes as a mixture of its monomer (**2.1a**) and its dimer {[PhBP$^{iPr}_3$]Mn(μ-Cl)}$_2$ (**2.1b**), whereas the iodide complex **2.2** crystallizes exclusively as a monomer. A similar monomer-dimer equilibrium was observed for [PhBP$_3$]CoX systems in solution (where X = Cl or Br).[71] Solid-state structures of monomeric **2.1a** and **2.2** are pseudotetrahedral with approximate

three-fold symmetry about the axis containing B, Mn, and X (I-Mn-B = 176.6°, Cl-Mn-B = 175.5°). The Mn-P bond distances are nearly equal, as well as the P-Mn-P bond angles. For example, monomer **2.1a** has Mn-P distances of 2.53 Å and P-Mn-P angles that are near 90º (90.6 to 92.6°). Likewise, compound **2.2** exhibits a narrow spread in its Mn-P bond distances (2.524 to 2.538 Å) and P-Mn-P angles (90.7 to 91.4°). The Mn-P bond distances are not unusual for high-spin Mn(II),[72] but are significantly longer than those of tris(phosphino)borate complexes of later first-row transition metal ions. The series of structurally characterized chloride complexes, $[PhBP^{iPr}_3]MCl$ for M = Mn, Fe, Co, and Ni, shows decreasing M-P bond distances, which reflect both their decreasing ionic radii across the series as well as their total spin *S*.

The dimer $\{[PhBP^{iPr}_3]Mn(\mu\text{-}Cl)\}_2$ (**2.1b**) crystallizes in the triclinic crystal system $P\bar{1}$ and features a Mn_2Cl_2 core that contains an inversion center. The chloride and one P^iPr_2 unit are disordered, but both can be independently refined in two positions of nearly equal populations. The solid-state structure of one conformer is shown in Figure 2.2 (top). A simplified structure containing all of the disordered atoms in the core is shown below it. In the dimer, the Mn center is five-coordinate and roughly square pyramidal. Two phosphorus atoms and two chlorides comprise the base, with an axial phosphine at the apex of the pyramid. The Mn-P bond distances in the dimer are even more elongated relative to the monomer **2.1a** (Mn-P = 2.613, 2.616, and 2.552 Å). One of these bonds (Mn-P3) is slightly shorter than the other two and corresponds to the $Mn\text{-}P_{ax}$ bond. The Mn-Cl bonds in the dimer are also significantly longer (2.463 and 2.533 Å) compared to the monomer (2.269 Å).

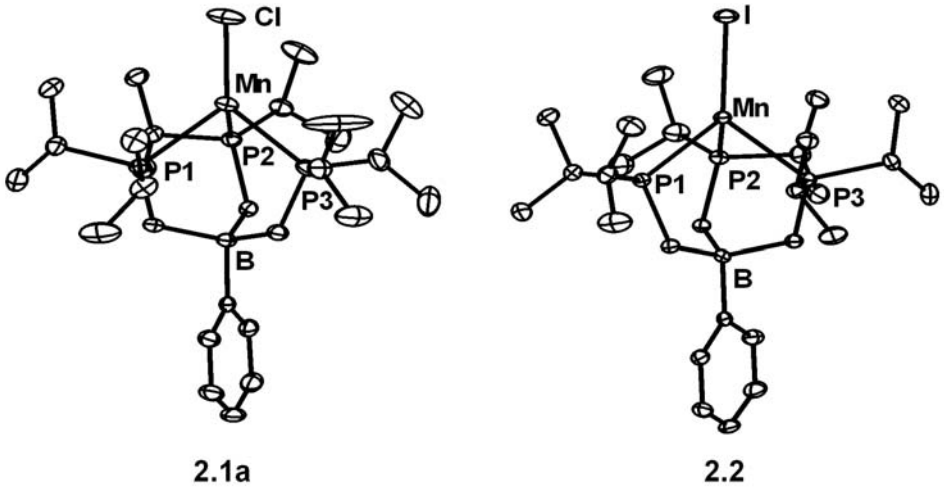

2.1a 2.2

Figure 2.1. 50% thermal ellipsoid representations of [PhBP$^{i\text{Pr}}_3$]MnCl (**2.1a**) and [PhBP$^{i\text{Pr}}_3$]MnI (**2.2**). Hydrogen atoms and solvent molecules have been omitted for clarity. Selected bond distances (Å) and angles (deg.) for **2.1a**: Mn–Cl 2.2687(7), Mn–P1 2.5300(6), Cl–Mn–P1 125.38(2), Mn–P2 2.5298(6), Mn–P3 2.5289(6), Cl–Mn–P2 120.22(2), Cl–Mn–P3 126.14(2), P1–Mn–P2 90.55(2), P2–Mn–P3 92.64(2), P1–Mn–P3 92.22(2). For **2.2**: Mn–I 2.6394(4), Mn–P1 2.5351(7), Mn–P2 2.5238(7), Mn–P3 2.5379(6), P1–Mn–I 127.19(2), P2–Mn–I 122.27(2), P3–Mn–I 124.09(2), P1–Mn–P2 91.39(2), P2–Mn–P3 90.68(2), P1–Mn–P3 90.95(2).

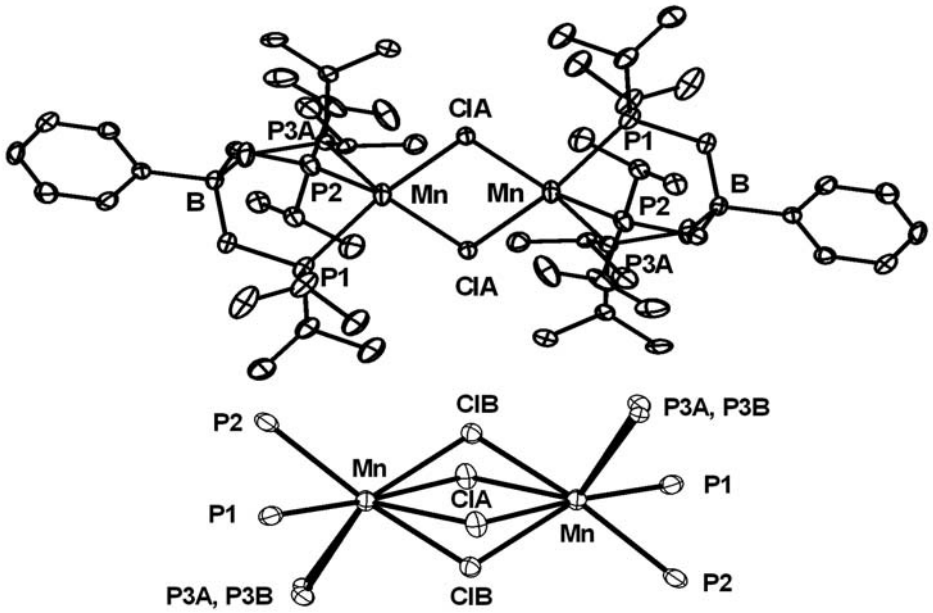

Figure 2.2. 50% thermal ellipsoid representations of $\{[PhBP^{iPr}_3]Mn(\mu\text{-}Cl)\}_2$ (**2.1b**) (top). Hydrogen atoms have been omitted for clarity. Selected bond distances (Å) and angles (deg.) for **2.1b**: Mn–ClA 2.4625(9), Mn–ClA 2.5327(9), Mn–ClB 2.4630(9), Mn–ClB 2.525(1), Mn–P1 2.6162(7), Mn–P2 2.6132(7), Mn–P3A 2.552(4), Mn–P3B 2.580(4), P1–Mn–P2 86.38(2), P3A–Mn–P1 87.13(7), P3B–Mn–P1 94.03(7), P3A–Mn–P2 92.55(8), P3B–Mn–P2 86.26(7). View of the core of **2.1b** showing both positions of the disordered chloride and P3 atom (bottom). The angle between the $Mn_2(ClA)_2$ and $Mn_2(ClB)_2$ planes is 41 degrees.

Magnetic susceptibility (SQUID) data were obtained on polycrystalline samples of **2.1** and **2.2**. The μ_{eff} versus T plots are nearly identical and show very little temperature dependence (Figure 2.3A). From 60 to 300 K, the μ_{eff} values average 5.94 μ_B for **1** (calculated as a monomer) and 5.97 μ_B for **2.2**. The μ_{eff} value for **2.1** is identical to its solution magnetic moment of 5.9(1) in benzene, where we presume the monomeric form is favored over the dimer form (Evans method, 3 runs).[73, 74] These values are consistent with five unpaired electrons per Mn, verifying the high-spin configuration of these [PhBP$^{i\text{Pr}}_3$]MnX species. The proximity of μ_{eff} to the spin-only value (5.92 μ_B) further suggests that the ground states of **2.1** and **2.2** are orbitally nondegenerate as expected for a ground-state electronic configuration where all the d-orbitals are singly populated (^{6}S). The $\chi_M T$ versus T plots for **2.1** and **2.2** are also similar, but distinct at very low temperatures. From 4 to 75 K, $\chi_M T$ dips slightly for **2.2**, perhaps due to intermolecular paramagnetic quenching (Figure 2.3B). The $\chi_M T$ versus T plot for **2.1**, however, shows a gradual increase in $\chi_M T$ in the same temperature range. The small rise in $\chi_M T$ from 4.43 to 4.71 cm^3 K/mol might be indicative of weak ferromagnetic coupling. Similarly weak coupling has been observed in another Mn(μ-Cl) dimer and might thus arise from the presence of the dimer **2.1b**.[75]

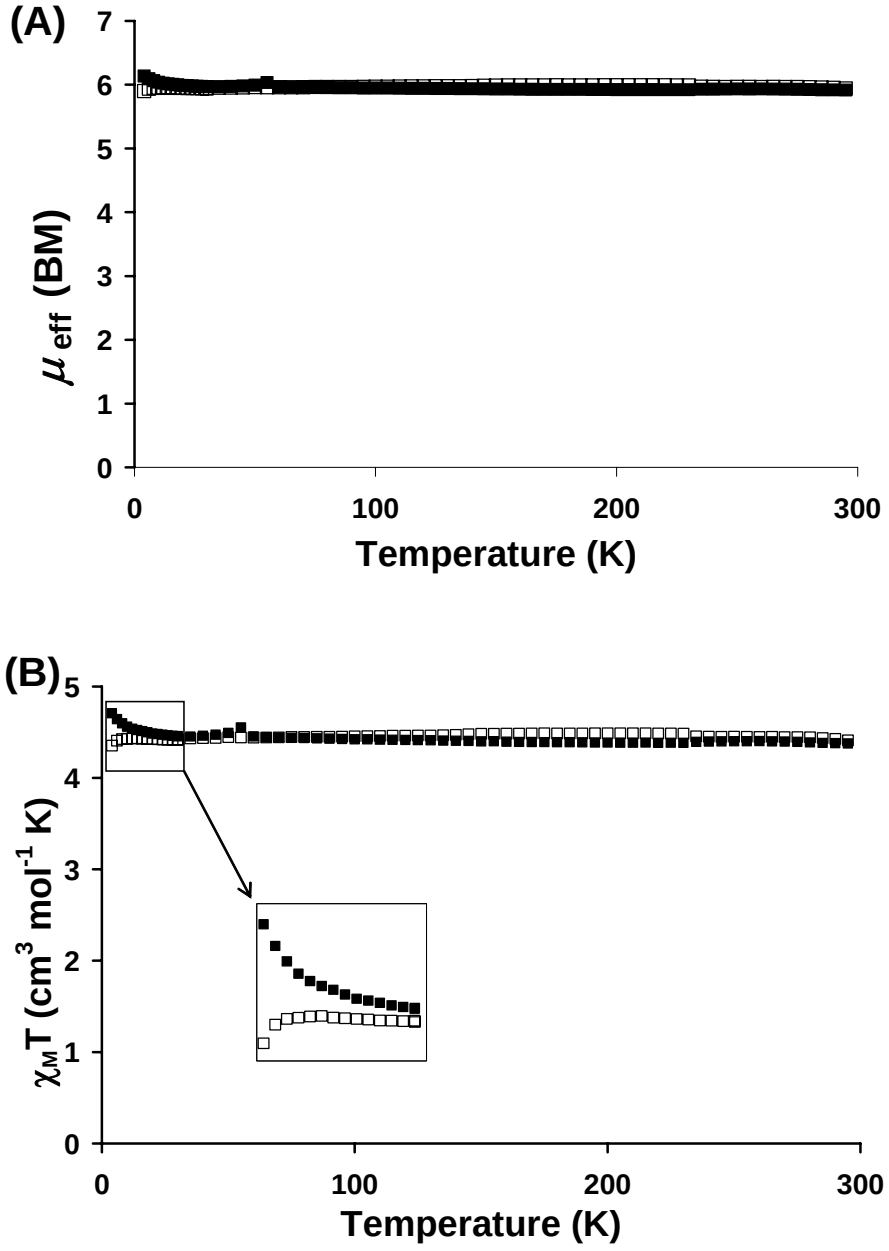

Figure 2.3. (A) SQUID plots of μ_{eff} (μ_B) versus T and (B) $\chi_M T$ (cm^3K/mol) versus T for [PhBP$^{i\text{Pr}}_3$]MnCl, **2.1**, (■), and [PhBP$^{i\text{Pr}}_3$]MnI, **2.2**, (□). An expansion of the $\chi_M T$ versus T plot at low temperatures (4 to 30 K) is shown in the inset.

EPR spectra were also recorded on the halides in methyl-THF glass at 8 K. The iodide **2.2** has an axial spectrum with transitions at ~120 and 330 mT (Figure 2.4A). The observed g values, ~ 6 and 2, match the calculated transitions for the $m_s = \pm ½$ states of a $S = 5/2$ paramagnet with E/D ~ 0. Hyperfine structure due to the ^{55}Mn nucleus ($I = 5/2$) is evident in the $g = 2$ signal, which shows a six-line splitting with A ~ 63 G. The octahedral complexes $MnX_2(dmpe)_2$ (where X = Br, I) show nearly identical EPR signatures.[76] Unlike **2.2**, the chloride **2.1** has an EPR spectrum with numerous transitions occurring from 0 to 1000 mT (Figure 2.4B). The complicated spectrum is difficult to interpret and is tentatively attributed to a superposition of the monomer (~ 130 and 360 mT) and dimer forms of **2.1**. The dimer, an $S = 5$ paramagnet, could itself give rise to multiple transitions. For both **2.1** and **2.2**, hyperfine coupling to the ^{31}P nucleus ($I = ½$) is not observed, suggesting that the spin density is tightly localized on Mn and therefore indicative of attenuated covalent character at the Mn-P bond by comparison to other $[BP_3]$M paramagnets we have studied.[27, 71, 77]

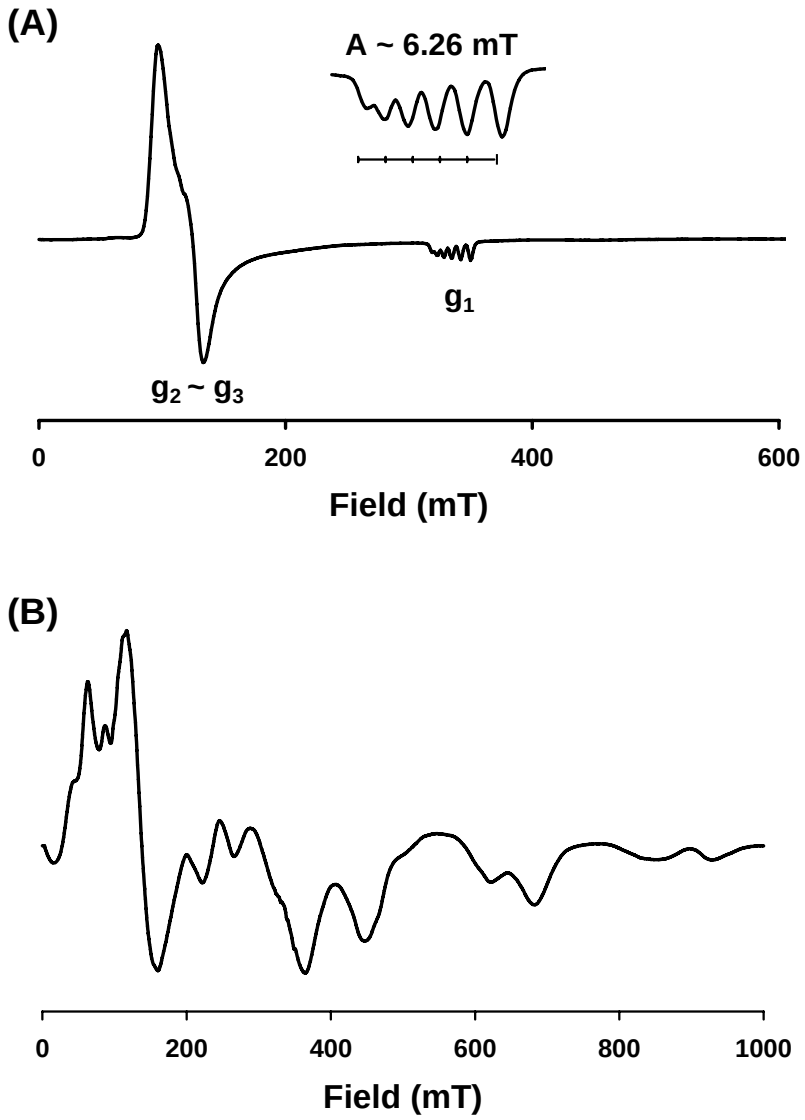

Figure 2.4. EPR spectra of glassy 2-(methyl)THF solutions of (A) [PhBP$^{i\mathrm{Pr}}_3$]MnI (**2.2**) and (B) [PhBP$^{i\mathrm{Pr}}_3$]MnCl (**2.1**) at 8 K. Instrumental parameters: ν = 9.38 GHz, modulation frequency = 100 kHz, modulation amplitude = 5 G, microwave power = 0.064 mW, conversion time = 81.9 ms, time constant = 20.5 ms, sweep time = 83.9 ms, 3 scans.

Compounds **2.1** and **2.2** were also studied by NMR spectroscopy and electrochemistry, but these data proved relatively uninformative. The ^{1}H NMR spectra contained a few resolvable resonances, and those that could be resolved were unusually broad by comparison to related [PhBP$^{i\mathrm{Pr}}_3$]FeX and [PhBP$^{i\mathrm{Pr}}_3$]CoX systems. The cyclic voltammograms of **2.1** and **2.2** did not reveal any reversible features (0.35 M [^{n}Bu$_4$N][PF$_6$] in THF). The lack of any reversible redox couples also contrasts the analogous halide complexes of Fe, Co, and Ni, all of which exhibit at least pseudo-reversible M^{II}/M^{I} redox couples.

Surprisingly, a survey of the CCDC revealed only three structures of monomeric four-coordinate Mn halide complexes with one or two phosphine donor(s).[72, 78, 79] No such structures with three phosphine donors were found. Even monomeric five-coordinate polyphosphine-ligated Mn halides are few in number, with only three structurally characterized examples.[80-82] Low-coordinate Mn halides are also known for the related tridentate ligand tris(pyrazoyl)borate (Tp). A handful of monomeric four-coordinate manganese structures featuring these ligands have been reported.[83-87]

2.2.2 Synthesis and Characterization of [PhBP$^{i\mathrm{Pr}}_3$]Mn(II) Azide, Alkyls, and Amides

A series of divalent manganese complexes featuring other X-type ligands were readily prepared from the iodide **2.2** via metathesis (Equation 2.2). For example, addition of excess sodium azide to **2.2** produced off-white [PhBP$^{i\mathrm{Pr}}_3$]Mn(N$_3$) (**2.3**) in good yield (73%). Compound **2.3** features a terminal azide ligand with a characteristic ν(N$_3$) stretch at 2070 cm^{-1} (KBr, THF). Its solid-state structure is shown in Figure 2.5. Not surprisingly, the pseudohalide **2.3** exhibits a similar molecular geometry to the

monomeric halides **2.1** and **2.2**. In a CCDC search of all structurally characterized Mn complexes containing a terminal azide, the mean Mn-N_{azide} bond distance is 2.190 Å with a standard deviation of 0.096 Å. The Mn-N bond distance of 2.046(3) Å in **2.3** is therefore unusually short. Manganese complexes featuring similarly short Mn-N bond distances for terminal azides are typically in the oxidation state +3.[53, 88-91]

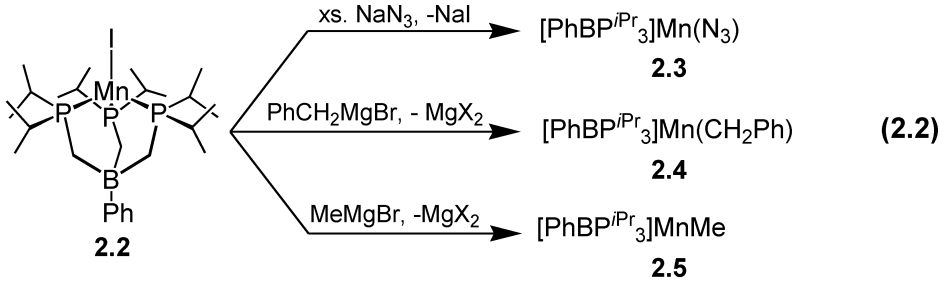

(2.2)

Manganese alkyl compounds were also readily prepared from the addition of the Gringards $PhCH_2MgBr$ and MeMgBr to **2.2** at -90° in THF. The bright yellow complex [$PhBP^{iPr}_3$]Mn(CH_2Ph) (**2.4**) and pale yellow complex [$PhBP^{iPr}_3$]Mn(Me) (**2.5**) are soluble in hydrocarbons and can be crystallized from cyclopentane at -30 °C. The benzyl complex **2.4** was characterized by X-ray diffraction, and its solid-state structure is shown in Figure 2.5. Related examples of low-coordinate monomeric organomanganese compounds are known and include trigonal (*β*-diketiminato)MnR and tetrahedral (P_2)MnR_2 species, where P_2 represents bidentate phosphine or two PR_3 ligands.[92-94] Despite the low valence electron count of these Mn systems, rather little has been reported concerning their reactivity patterns. One interesting exception concerns tetrahedral Mn(II) dialkyl compounds supported by diimine ligands that readily undergo alkyl migration to the diimine ligand at ambient temperatures.[95] We have found that the [$PhBP^{iPr}_3$]-supported manganese alkyls **2.4** and **2.5** are thermally stable up to 65 °C even

under an atmosphere of dihydrogen or CO. This sharply contrasts the related iron(II) alkyls [PhBP$^{i\mathrm{Pr}}_3$]Fe-R, which lose alkane upon exposure to H_2 and bind CO readily.[96]

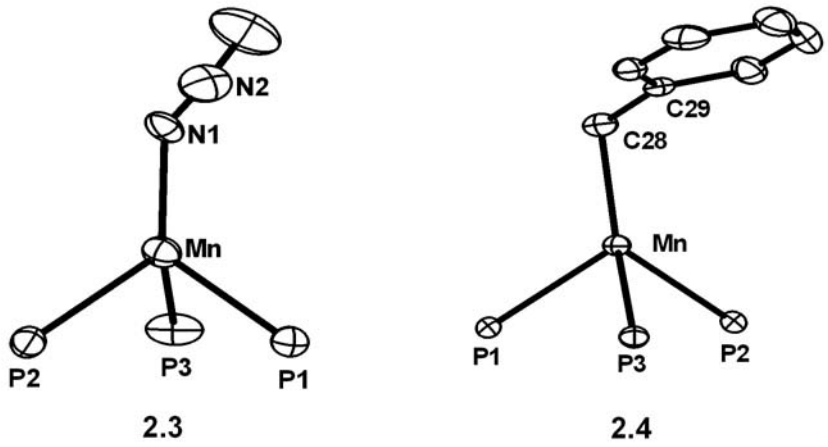

Figure 2.5. 50% thermal ellipsoid representations of [PhBP$^{i\mathrm{Pr}}_3$]Mn(N_3) (**2.3**) and [PhBP$^{i\mathrm{Pr}}_3$]Mn(CH_2Ph) (**2.4**). For clarity, hydrogen atoms have been omitted and only the phosphorous atoms of the ligand are shown. For **2.3**, only one of the two molecules in the asymmetric unit is shown. Selected bond distances (Å) and angles (deg.) for **2.3**: Mn–N1 2.046(3), Mn–P1 2.534(1), Mn–P2 2.522(1), Mn–P3 2.521(2), N1–N2 1.112(5), N2–N3 1.202(6), N2–N1–Mn 128.8(3), P1–Mn–P2 92.33(4), P2–Mn–P3 93.21(5), P1–Mn–P3 91.04(5), N1–Mn–P1 123.1(1), N1–Mn–P2 125.7(1), N1–Mn–P3 122.2(1). For **2.4**: Mn–C28 2.138(2), Mn–P1 2.5679(4), Mn–P2 2.5507(5), Mn–P3 2.5620(5), P1–Mn–P2 91.46(1), P2–Mn–P3 89.44(1), P1–Mn–P3 89.90(1), C28–Mn–P1 117.86(5), C28–Mn–P2 126.42(5), C28–Mn–P3 130.59(5), Mn–C28–C29 111.5(1).

Manganese amides were generated by the addition of lithium and potassium amides to **2.2** at -90° in THF. In the metathesis reactions with lithium amides, a common side-product was the free ligand [PhBP$^{i\mathrm{Pr}}_3$][Li], easily identified by ^{31}P NMR spectroscopy. Replacement of lithium by potassium minimizes the liberation of the [PhBP$^{i\mathrm{Pr}}_3$] anion. For example, 2,6-diispropylaniline can be deprotonated with KH and added to **2.2** to produce yellow [PhBP$^{i\mathrm{Pr}}_3$]Mn(NH(2,6-^{i}Pr$_2$Ph)) (**2.6**) in high yield (90%) (Equation 2.3).

$$\underset{\textbf{2.2}}{[\mathrm{PhBP}^{i\mathrm{Pr}}_3]\mathrm{MnI}} \xrightarrow[\text{THF, -90 °C}]{\mathrm{K(NH(2,6\text{-}}{}^{i}\mathrm{Pr}_2\mathrm{Ph))}} \underset{\textbf{2.6}}{[\mathrm{PhBP}^{i\mathrm{Pr}}_3]\mathrm{Mn(NH(2,6\text{-}}{}^{i}\mathrm{Pr}_2\mathrm{Ph))} \qquad \textbf{(2.3)}}$$

This strategy was also employed to install 2,3:5,6-dibenzo-7-azabicyclo[2.2.1]hepta-2,5-diene (Hdbabh) as the amide functionality. The lithium amide Li(dbabh) is a particularly interesting reagent to investigate because it has been successfully exploited as an N-atom transfer reagent to both Cr and Fe centers with concomitant loss of anthracene.[28, 97] Methathesis of **2.2** and Li(dbabh) resulted in a mixture of the amide compound [PhBP$^{i\mathrm{Pr}}_3$]Mn(dbabh) (**2.7**), the bridged amide complex {(Hdbabh)MnI(μ-*N*-dbabh)}$_2$, and the ligand [PhBP$^{i\mathrm{Pr}}_3$][Li] (Equation 2.4). Though the yield of the desired compound **2.7** was quite low, yellow crystals of **2.7** could be cleanly chosen from the colorless crystals of the byproducts. Attempts to improve the yield of **2.7** by using K(dbabh) were unsuccessful. Deprotonation of Hdbabh with KH or benzyl potassium afforded a bright yellow-green solution; upon addition of **2.2** at -90°C, the reaction solution turned orange. Red-orange crystals were grown from this solution that were clearly indicative of a species different from **2.7**. An X-ray diffraction study revealed the product to be a different Mn amide, [PhBP$^{i\mathrm{Pr}}_3$]Mn(1-Ph(isoindolate)) (**2.8**),

an isomer of **2.7** wherein one of the five-membered rings has opened by an overall C-C bond cleavage (Equation 2.4). This decomposition most likely occurs during the deprotonation stage of the reaction since the solution turns brilliant yellow-green upon addition of the potassium base, whereas solutions of Li(dbabh) are pale pink. Competitive deprotonation of the benzylic proton could possibly induce this C-C bond cleavage.

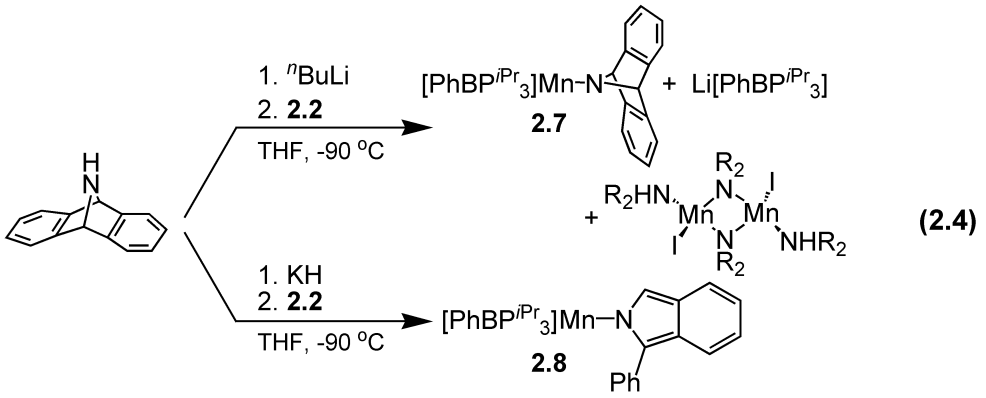

(2.4)

The solid-state structures of the Mn(II) amides **2.6**, **2.7**, and **2.8** are shown in Figure 2.6. Collectively, these amides are similar to the other pseudotetrahedral, high-spin [PhBP$^{iPr}_3$]Mn(II) species reported here in that they have typical Mn-P bond distances (ca. 2.55 Å) and P-Mn-P bond angles (ca. 90°). The apical N atom of **2.7** lies on the Mn-B axis, whereas compounds **2.6** and **2.8** exhibit a slightly canted N atom with N-Mn-B angles of 156° and 167°, respectively. The Mn-N bond distances follow the order: **2.7** (1.948(1) Å) < **2.6** (1.997(2) Å) < **2.8** (2.054(2) Å). This trend likely reflects the relative steric repulsion between the amide groups and the isopropyl groups of the [PhBP$^{iPr}_3$] ligand.

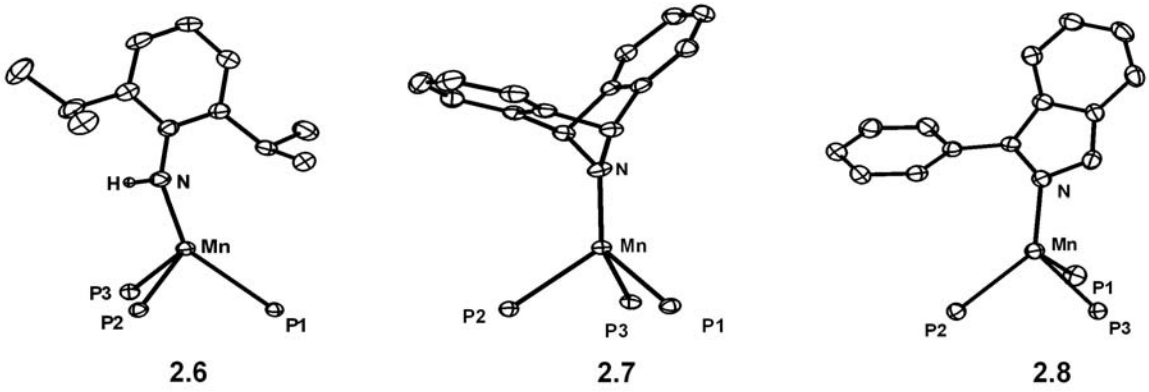

Figure 2.6. 50% thermal ellipsoid representations of [PhBP$^{i\mathrm{Pr}}_3$]Mn(NH(2,6-^{i}Pr$_2$Ph)) (**2.6**), [PhBP$^{i\mathrm{Pr}}_3$]Mn(dbabh) (**2.7**), and [PhBP$^{i\mathrm{Pr}}_3$]Mn(1-Ph(isoindolate)) (**2.8**). For clarity, hydrogen atoms (except N-*H*) have been omitted, and only the phosphorous atoms of the ligand are shown. Selected bond distances (Å) and angles (deg.) for **2.6**: Mn–N 1.997(2), Mn–P1 2.5877(6), Mn–P2 2.5813(6), Mn–P3 2.5637(6), P1–Mn–P2 87.96(2), P2–Mn–P3 89.95(2), P1–Mn–P3 93.11(2), N–Mn–P1 144.77(5), N–Mn–P2 105.73(5), N–Mn–P3 118.63(5). For **2.7**: Mn–N 1.948(1), Mn–P1 2.5357(5), Mn–P2 2.5473(5), Mn–P3 2.5503(5), P1–Mn–P2 90.46(2), P2–Mn–P3 89.51(2), P1–Mn–P3 90.71(2), N–Mn–P1 126.19(4), N–Mn–P2 126.13(4), N–Mn–P3 122.92(4). For **2.8**: Mn–N 2.054(2), Mn–P1 2.5308(7), Mn–P2 2.5550(7), Mn–P3 2.5718(6), P1–Mn–P2 95.13(2), P1–Mn–P3 89.54(2), P2–Mn–P3 90.09(2), N–Mn–P1 111.98(5), N–Mn–P2 136.31(5), N–Mn–P3 122.30(5).

The Mn(II) alkyls and amides were studied by cyclic voltammetry in THF with 0.35 M [^{n}Bu$_4$N][PF$_6$] as the supporting electrolyte and Ag/AgNO$_3$ as the reference electrode. Interestingly, amide **2.7** is distinct amongst this series of complexes in that it exhibits a reversible 1-electron redox couple centered at -0.26 V (vs. Fc/Fc$^+$, scan rate = 50 mV/s), indicative of a Mn^{II}/Mn^{III} redox event (Figure 2.7). The amides **2.6** and **2.8** exhibit irreversible oxidative events near this same potential.

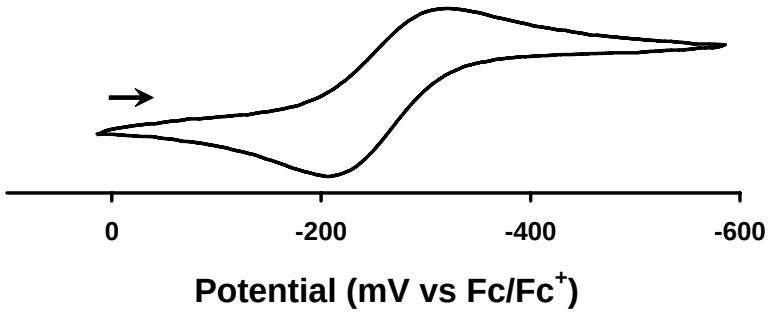

Figure 2.7. Cyclic voltammogram of [PhBP$^{iPr}_3$]Mn(dbabh) (**2.7**) recorded at a scan rate of 50 mV/s in THF with 0.35 M [^{n}Bu$_4$][PF$_6$] as the supporting electrolyte. Potentials are internally referenced to Fc/Fc$^+$.

2.2.3 Synthesis and Characterization of [PhBP$^{iPr}_3$]Mn(I) Compounds

Monovalent manganese compounds may prove to be valuable precursors to Mn≡NR multiply bonded species in future studies. Indeed, oxidative nitrene transfer to monovalent Fe and Co precursors has proven highly effective in the synthesis of related Fe≡NR, Co≡NR, and Co=NR species.[29, 34-36, 98, 99] While monovalent manganese complexes are numerous, they typically are octahedral 18-electron species stabilized by carbonyl ligands.[100-104] Low-coordinate and unsaturated Mn(I) compounds, on the other

hand, are uncommon. Notable examples of this latter class include a three-coordinate Mn(I) dimer supported by bulky β-diketiminate ligands and several five-coordinate Mn compounds of the type $(P\hat{}P)_2Mn(CO)^+$ (where P^P is a bidentate phosphine).[105-108]

To pursue a low-coordinate Mn(I) precursor, $[PhBP^{iPr}_3]Tl$ and $MnBr(CO)_5$ were heated in benzene at 50 °C for several hours. The resulting yellow solution contained some TlBr precipitate, but to our surprise, the major product was a Tl-Mn adduct, $[PhBP^{iPr}_3]Tl\text{-}MnBr(CO)_4$ (**2.9**), which was isolated in 39% crystalline yield. Compound **2.9** is diamagnetic and exhibits a doublet in the ^{31}P NMR spectrum (45.4 ppm, $J_{Tl\text{-}P}$ = 8060 Hz) that is shifted relative to $[PhBP^{iPr}_3]Tl$ (24.3 ppm, $J_{Tl\text{-}P}$ = 5913 Hz). The solid-state structure of **2.9** is shown in Figure 2.8.

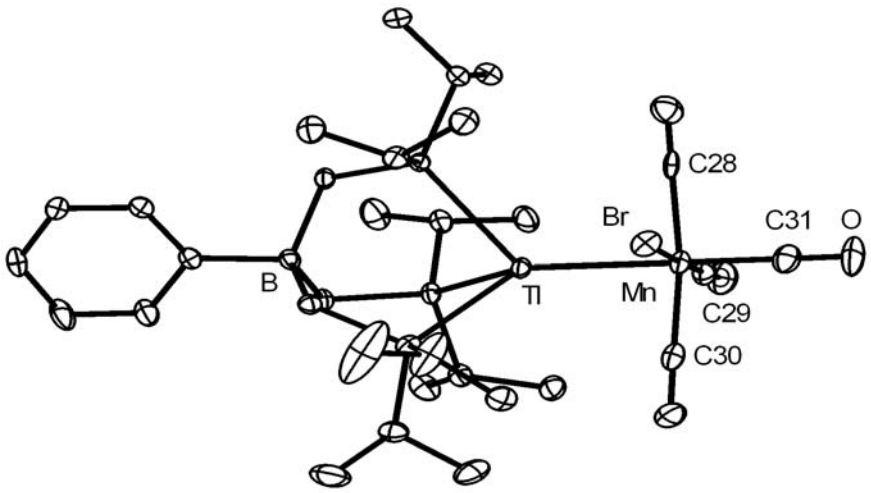

Figure 2.8. 50% thermal ellipsoid representation of $[PhBP^{iPr}_3]Tl–MnBr(CO)_4$ (**2.9**). For clarity, hydrogen atoms have been omitted. Selected bond distances (Å) and angles (deg.) for **2.9**: Mn–Tl 2.6437(4), Mn–C28 1.913(3), Mn–C29 1.799(3), Mn–C30 1.851(3), Mn–C31 1.823(3), Mn–Br 2.5299(4), C31–Mn–Tl 172.74(8), Br–Mn–Tl 86.11(1), C29–Mn–C28 92.6(1), C29–Mn–C30 91.1(1), C28–Mn–Br 85.39(7), C29–Mn–Br 177.98(8), C30–Mn–Br 90.94(8), C31–Mn–Br 86.73(8).

There are several crystal structures featuring a Tl-Mn bond, and the Tl-Mn bond of 2.6437(4) Å is similar to those reported previously.[109, 110]

Prolonged heating of a benzene solution of **2.9** resulted in its decomposition. By ^{31}P NMR spectroscopy, one major product forms upon thermolysis, characterized by a broad peak at ~50 ppm. An IR spectrum revealed two sharp stretches at 1999 and 1906 cm^{-1} (KBr/THF). We propose this species to be the monovalent tricarbonyl compound, $[PhBP^{iPr}_3]Mn(CO)_3$ (Equation 2.5). Indeed, the isoelectronic compound, $[PhBP^{iPr}_3]Mn(CN^tBu)_3$ (**2.10**), can be prepared by the reduction of $[PhBP^{iPr}_3]MnI$ with sodium napthalenide followed by addition of excess CN^tBu. Compound **2.10** is isolated in pure form but in low yield (22%) due in part to the competitive formation of $[PhBP^{iPr}_3]Na$.[111] Similarly, reduction of $[PhBP^{iPr}_3]MnI$ with sodium napthalenide under CO produces the presumed degradation product of **2.9**, $[PhBP^{iPr}_3]Mn(CO)_3$. Unfortunately, this species has not been isolated in pure form. The solid-state structure of **2.10** confirms its assignment as a monovalent Mn complex with three isocyanides (Figure 2.9). Relative to the high-spin Mn(II) species, the Mn-P bonds (2.36 to 2.38 Å) are more than 0.15 Å shorter. The P-Mn-P bond angles are also slightly contracted (86.5 to 89.2°). Compound **2.10** is also characterized by a reversible redox process at -0.66 V in its cyclic voltammogram, shown in Figure 2.10 (vs. Fc/Fc^+, scan rate = 100 mV/s).

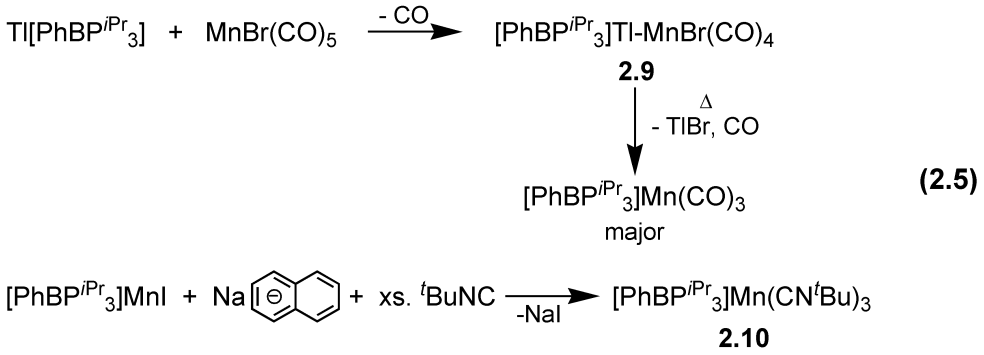

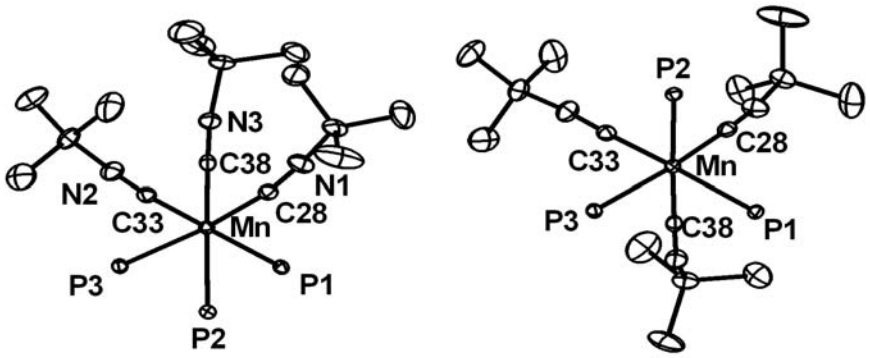

Figure 2.9. 50% thermal ellipsoid representation of [PhBP$^{i\mathrm{Pr}}_3$]Mn(CN^{t}Bu)$_3$ (**2.10**) viewing along (left) and down the Fe-B vector (right). For clarity, hydrogen atoms have been omitted, and only the phosphorous atoms of the ligand are shown. Selected bond distances (Å) and angles (deg.) for **2.10**: Mn–C28 1.870(1), Mn–C33 1.864(1), Mn–C38 1.835(1), N1–C28 1.176(2), N2–C33 1.176(2), N3–C38 1.185(2), Mn–P1 2.3597(4), Mn–P2 2.3831(4), Mn–P3 2.3655(3), P1–Mn–P2 88.59(1), P2–Mn–P3 86.49(1), P1–Mn–P3 89.17(1), C33–Mn–C28 83.75(5), C38–Mn–C28 85.26(5), C38–Mn–C33 89.12(5).

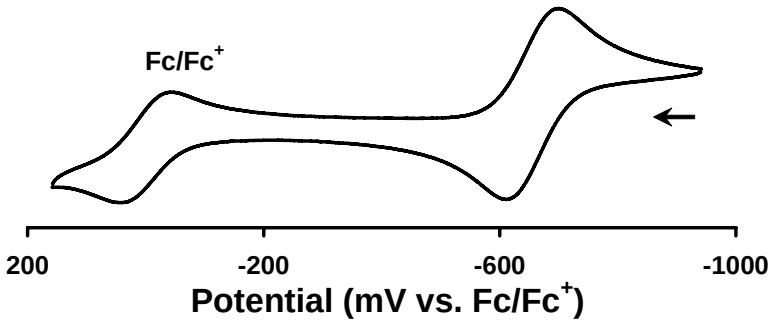

Figure 2.10. Cyclic voltammogram of [PhBP$^{i\mathrm{Pr}}_3$]Mn(CN^{t}Bu)$_3$ (**2.10**) recorded at a scan rate of 100 mV/s in THF with 0.35 M [^{n}Bu$_4$][PF$_6$] as the supporting electrolyte. Potentials are internally referenced to Fc/Fc$^+$.

2.2.4 DFT Models of Mn=N^{t}Bu and Mn≡N Species

DFT studies were undertaken to obtain some insight into the electronic viability of two species, [PhBP$^{i\mathrm{Pr}}_3$]Mn$^{\mathrm{III}}$≡N^{t}Bu and [PhBP$^{i\mathrm{Pr}}_3$]Mn$^{\mathrm{IV}}$≡N. We have previously used DFT methods to probe the electronic structures of [BP$_3$]M species with terminally bound N$_x$-functionalities that are strongly π-donating, for example [PhBP$_3$]Co$^{\mathrm{III}}$≡N(*p*-tolyl), [PhBP$_3$]Fe$^{\mathrm{III}}$≡N^{t}Bu, and [PhBP$^{i\mathrm{Pr}}_3$]Fe$^{\mathrm{IV}}$≡N.[29, 36, 28]

For the low-spin Fe and Co imides, a general d-orbital splitting diagram has been forwarded based upon these DFT studies. The d-orbitals, which transform as a_1 + 2 e under idealized three-fold symmetry, split into two high-lying and three lower-lying orbitals. The higher-energy e-set, which in simplest terms can be thought of as comprising d_{xz} and d_{yz}, is destabilized by σ^* and π^* interactions with the phosphines and imide functionality, respectively. The remaining orbitals, of predominant d_{z2} (a_1), and d_{xy} and $d_{x2\text{-}y2}$ (e) character, lie at lower energy and are predominantly non-bonding in nature.[27]

If we apply this qualitative d-orbital picture to the hypothetical d^4 imide, [PhBP$^{i\mathrm{Pr}}_3$]Mn≡N^{t}Bu, the two ground states, low-spin (S = 0) and intermediate-spin (S = 1), need to be considered. Recently, we have reported the characterization of an unusual Fe$^{\mathrm{IV}}$ imide that exhibits a triplet ground state.[67] Because this species is isoelectronic to the hypothetical Mn(III) imide under consideration here, we might expect the latter to be a triplet as well. To test this from a theoretical standpoint, the imide [PhBP$^{i\mathrm{Pr}}_3$]Mn≡N^{t}Bu was optimized as a singlet and a triplet using the Jaguar computational program (B3LYP/LACVP**). The input geometry was derived from the crystal structure coordinates of [PhBP$^{i\mathrm{Pr}}_3$]Fe(NAd), where the metal and N$_x$-functionality were changed to

Mn and N^{t}Bu, respectively. A geometry optimization was then performed using a spin-unrestricted calculation and conducted without any symmetry constraints.

The predicted structures for the singlet and triplet states of [PhBP$^{i\text{Pr}}_3$]Mn≡N^{t}Bu differ quite remarkably from one another (Figure 2.11). The optimized singlet structure has a bent Mn-N-C angle (145º) with expanded P-Mn-P angles (97-98º), whereas the optimized triplet structure features a linear Mn-N-C angle (179º) with characteristic P-Mn-P angles (90-92º). The triplet state exhibits what appears to be a more likely geometry, in accord with the fact that it is predicted by DFT to be more energetically stable by 0.74 eV than the singlet state.

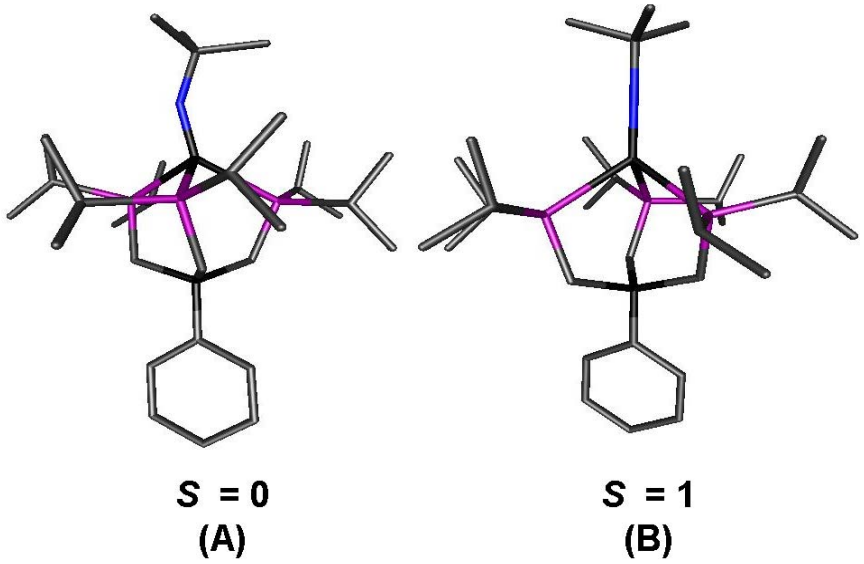

Figure 2.11. DFT-optimized structures (Jaguar 5.0, B3LYP/LACVP**) for (**A**) singlet [PhBP$^{i\text{Pr}}_3$]Mn(N^{t}Bu) and (**B**) triplet [PhBP$^{i\text{Pr}}_3$]Mn(N^{t}Bu). Selected bond distances (Å) and angles (deg.) for (**A**): Mn–N 1.63; Mn–P 2.28, 2.36, 2.36; Mn–N–C 144.8; P–Mn–P 96.8, 97.2, 97.7; N–Mn–P 104.7, 126.2, 127.2. For (**B**): Mn–N 1.66; Mn–P 2.40, 2.44, 2.45; Mn–N–C 179.2; P–Mn–P 89.5, 89.8, 91.5; N–Mn–P 121.9, 126.2, 127.0.

Based on DFT studies, the known nitride $[PhBP^{iPr}_3]Fe^{IV}{\equiv}N$ has a splitting diagram that differs from the structurally analogous imides in that the a_1 orbital of dz^2 parentage is more appreciably destabilized by sigma antibonding interactions with the nitride functionality and the phosphine donors.[28] This situation leaves only two orbitals at very low energy, giving rise to the singlet ground state of $[PhBP^{iPr}_3]Fe^{IV}{\equiv}N$. Based on this splitting scheme, the hypothetical Mn nitride $[PhBP^{iPr}_3]Mn{\equiv}N$ might be expected to populate a doublet ground state. To ascertain whether this would be the case, the Mn nitride $[PhBP^{iPr}_3]Mn(N)$ was modeled as both an S = 1/2 and S = 3/2 system. In the optimized quartet structure, the nitride atom is severely tilted off the Mn-B axis by 30° (Figure 2.12) in what appears to be an unfavorable geometry. The P-Mn-P bond angles (90 to 91°) and Mn-P bond distances (2.48 to 2.60 Å) are, however, typical of the pseudotetrahedral $[PhBP^{iPr}_3]Mn(II)$ complexes described here. The Mn-N bond length of 1.62 Å seems excessively long for known Mn≡N species, which typically have Mn-N bond lengths in the range of 1.50 to 1.55 Å. These distortions in the optimized quartet structure presumably arise from population of the antibonding d_{z2} orbital.

Relative to the quartet state, the doublet state is energetically preferred by 0.41 eV and exhibits what appears to be a more reasonable geometry (Figure 2.12). The nitride atom is canted off the Mn-B axis by only 9° and binds tightly to Mn with a Mn-N bond length of 1.50 Å. The P-Mn-P bond angles are slightly expanded (95 to 97º), approaching a more tetrahedral geometry. Similar parameters were found in the DFT optimized structure of $[PhBP^{iPr}_3]Fe^{IV}{\equiv}N$, which features expanded P-Fe-P bond angles (99 to 101º) and an Fe-N bond length of 1.49 Å. It is the combination of these two structural

parameters that renders the a_1 (d_{z^2}) orbital more antibonding for the metal nitrides than in the case of the related metal imides.

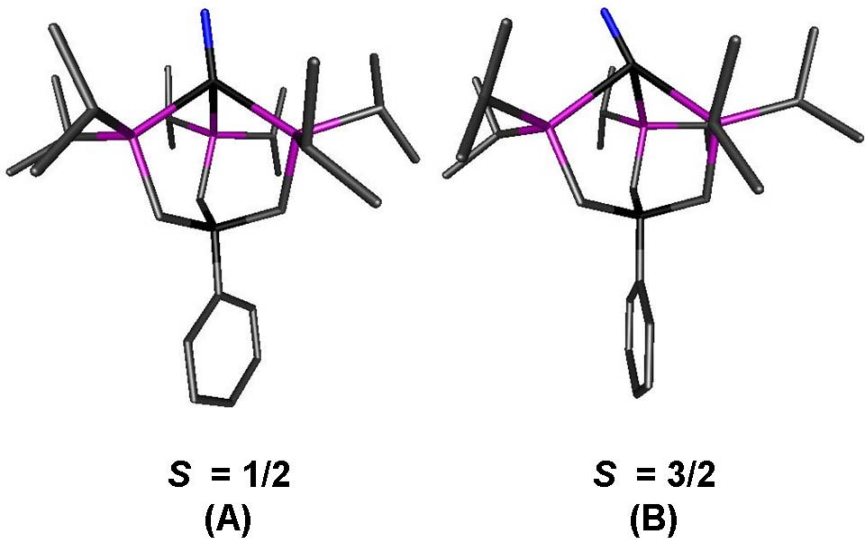

Figure 2.12. DFT-optimized structures (Jaguar 5.0, B3LYP/LACVP**) for (**A**) doublet [PhBP$^{i\text{Pr}}_3$]Mn(N) and (**B**) quartet [PhBP$^{i\text{Pr}}_3$]Mn(N). Selected bond distances (Å) and angles (deg.) for (**A**): Mn–N 1.50; Mn–P 2.35, 2.41, 2.45; N–Mn–P 112.1, 122.3, 127.5; P–Mn–P 94.8, 95.6, 97.2. For (**B**): Mn–N 1.62; Mn–P 2.48, 2.49, 2.60; N–Mn–P 103.9, 109.3, 155.3; P–Mn–P 89.9, 90.5, 91.2.

2.3 Concluding Remarks

With this report, we have extended our study of the coordination chemistry of first-row mid-to-late transistion metals supported by electron-releasing [BP_3] ligands. As with Fe, Co, and Ni, the [PhBP$^{i\text{Pr}}_3$] scaffold readily supports divalent Mn complexes in a pseudotetrahedral geometry. The preparative significance of the systems described herein is best underscored by noting how uncommon low-coordinate manganese complexes

supported by polyphosphines are. The high donor strength and anionic charge of the [PhBP$^{i\mathrm{Pr}}_3$] ligand may be advantageous over polyphosphine ligands in general by helping to attenuate problematic phosphine dissociation. These two ligand properties are not always sufficient, however, as evident from the observed propensity to substitute manganese by an alkali metal cation or by thallium in the [PhBP$^{i\mathrm{Pr}}_3$] binding pocket under certain metathetical exchange reactions. Fortunately, the halide [PhBP$^{i\mathrm{Pr}}_3$]MnI does serve as a sufficiently useful reagent for most metathetical reactions, allowing the preparation of [PhBP$^{i\mathrm{Pr}}_3$]Mn(II) azide, alkyl, and amide species.

DFT calculations of the hypothetical Mn(III) imide [PhBP$^{i\mathrm{Pr}}_3$]Mn(N^{t}Bu) and nitride [PhBP$^{i\mathrm{Pr}}_3$]Mn(N) structures suggest that their preferred ground states will be triplet and doublet, respectively. While the preparation of Mn≡N$_x$ species of these types has, at this stage, only been cursorily canvassed it is worth noting a few experimental observations. For instance, we have explored whether the monovalent complex **10** might undergo facile oxidative group transfer in the presence of organic aryl and alkylazides. We have also canvassed conditions that might have effected the oxidative deprotonation of the anilide species **2.6**.[42] Finally, attempts to generate a Mn(IV) nitride species, including thermolysis and photolysis of the amide complex [PhBP$^{i\mathrm{Pr}}_3$]Mn(dbabh) **2.7**, as well as photolysis of the Mn azide **2.3**, have been explored. As yet, none of these straightforward approaches have provided a tractable Mn≡N$_x$ species. Therefore, while the preparation of well-defined low-valent Mn complexes with multiply bonded linkages remains a challenge, it is one that should be surmountable. Our hope is that manganese imides and nitrides of these types will benefit from synthetic access to unsaturated Mn(I) precursors, such as a four-coordinate [PhBP$^{i\mathrm{Pr}}_3$]Mn-PR$_3$ species. Oxidative nitrene or

nitride group transfer might then prove synthetically more fruitful. Efforts along these lines are part of ongoing studies.

2.4 Experimental Section

2.4.1 General Considerations

All manipulations were carried out using standard Schlenk or glovebox techniques under a dinitrogen atmosphere. Unless otherwise noted, solvents were deoxygenated and dried by thorough sparging with N_2 gas followed by passage through an activated alumina column. Nonhalogenated solvents were tested with a standard purple solution of benzophenone ketyl in THF to confirm effective oxygen and moisture removal. Deuterated solvents were purchased from Cambridge Isotopes Laboratories, Inc. and were degassed and stored over activated 3-Å molecular sieves prior to use. Elemental analyses were performed by Desert Analytics, Tucson, AZ. Varian 300 MHz spectrometers were used to record the ^{1}H NMR and ^{31}P NMR spectra at ambient temperature. ^{1}H chemical shifts were referenced to residual solvent, while ^{31}P NMR chemical shifts were referenced to 85% H_3PO_4 at δ 0 ppm. IR measurements were obtained with a KBr solution cell using a Bio-Rad Excalibur FTS 3000 spectrometer controlled by Bio-Rad Merlin Software (v. 2.97) set at 4 cm^{-1} resolution.

2.4.2 Magnetic Measurements

Magnetic measurements were recorded using a Quantum Designs SQUID magnetometer running Magnetic Property Measurement System Rev. 2 software. Data were recorded at 5000 G. The sample was suspended in the magnetometer in a plastic straw sealed under nitrogen with Lilly No. 4 gel caps. Loaded samples were centered

within the magnetometer using the DC centering scan at 35 K and 5000 G. Data were acquired at 4 to 30 K (one data point every 2 K) and 30 to 300 K (one data point every 5 K). The magnetic susceptibility was adjusted for diamagnetic contributions using the constitutive corrections of Pascal's constants. The molar magnetic susceptibility (χ_m) was calculated by converting the calculated magnetic susceptibility (χ) obtained from the magnetometer to a molar susceptibility (using the multiplication factor {(molecular weight)/[(sample weight)(field strength)]}). Effective magnetic moments were calculated using the following equation:

$$\mu_{eff} = (7.997\chi_m T)^{1/2}$$

2.4.3 EPR Measurements

X-band EPR spectra were obtained on a Bruker EMX spectrometer (controlled by Bruker Win EPR Software v. 3.0) equipped with a rectangular cavity working in the TE_{102} mode. Variable temperature measurements were conducted with an Oxford continuous-flow helium cryostat (temperature range 3.6 to 300 K). Accurate frequency values were provided by a frequency counter built into the microwave bridge. Solution spectra were acquired in 2-(methyl)THF. Sample preparation was performed under a dinitrogen atmosphere in an EPR tube equipped with a ground glass joint.

2.4.4 Electrochemical Measurements

Electrochemical measurements were recorded in a glovebox under a dinitrogen atmosphere using a BAS CV 100W (Bioanalytical Systems Inc., West Lafayette, IN). A glassy carbon working electrode, a platinum wire auxiliary electrode, and an $Ag/AgNO_3$ non-aqueous reference electrode were used in the electrochemical studies.

2.4.5 DFT Calculations

All calculations were performed using the Jaguar 5.0 program package (Jaguar 5.0, Schrodinger, LLC, Portland, OR, 2002). The calculation employed the hybrid DFT functional B3LYP and the basis set LACVP**. Input coordinates for the geometry optimizations were derived from the solid-state structure of [PhBP$^{i\text{Pr}}_3$]Fe≡NAd, where Fe was replaced by Mn.[98] For the Mn imide, the adamantyl group was truncated to a *tert*-butyl group; and for the nitride, the adamantyl group was removed completely. Spin states and molecular charges were imposed as described in the text. The calculations were spin unrestricted, and no symmetry constraints were used. The default values for geometry and SCF iteraction cutoffs were used, and all structures converged under these criteria.

2.4.6 Starting Materials and Reagents

The compounds [PhBP$^{i\text{Pr}}_3$]Tl,[70] benzyl potassium,[112] and Li(dbabh)[97] were prepared according to literature procedures. The reagents 2,6-diisopropyl aniline and ^{t}BuNC were dried over sieves prior to use. Sodium azide was *carefully* dried by heating at 50 °C under vacuum for two days. (CAUTION: Azides are potentially explosive and should generally be stored away from heat and ignition sources.) Potassium hydride was crushed into a fine powder, washed liberally with petroleum ether, and stored at -30 °C. All other reagents were purchased from commercial vendors and used without further purification.

2.4.7 Synthesis of Compounds

Synthesis of [PhBP$^{i\text{Pr}}_3$]MnCl, 2.1: A THF solution (18 mL) of [PhBP$^{i\text{Pr}}_3$]Tl (250.0 mg, 36.46 mmol) was added dropwise to a stirring suspension of $MnCl_2$ (46.3 mg,

36.36 mmol). The reaction mixture was stirred for 24 h and filtered through a Celite pad. The colorless solution was concentrated under reduced pressure to dryness to yield an off-white solid. After washing the solid liberally with petroleum ether, the product was extracted into benzene. Vapor diffusion of petroleum ether into the benzene solution resulted in pale-pink blocks (80 mg, 33% yield). ^{1}H NMR (C_6D_6, 300 MHz) δ ~20 (v. br), 10.3 (br), 8.1 (br). Anal. Calcd. for $C_{27}H_{53}BClMnP_3$: C 56.71; H 9.34; N 0. Found: C 56.43; H 9.44; N 0.19.

Synthesis of [PhBP$^{i\mathrm{Pr}}_3$]MnI, 2.2: A THF solution (20 mL) of [PhBP$^{i\mathrm{Pr}}_3$]Tl (284.7 mg, 41.52 mmol) was added dropwise to a stirring suspension of MnI_2 (129.5 mg, 41.52 mmol). The reaction mixture was stirred for 12 h and filtered through a Celite pad. The colorless solution was concentrated under reduced pressure to dryness to yield an off-white solid. After washing the solid liberally with petroleum ether, the product was extracted into hot benzene. Vapor diffusion of petroleum ether into the benzene solution resulted in colorless crystals (172 mg, 62% yield). ^{1}H-NMR (C_6D_6, 300 MHz) δ 21 (v. br), 8.8 (br), 6.6 (br). Anal. Calcd. for $C_{27}H_{53}BIMnP_3$: C 48.89; H 8.05; N 0. Found: C 49.12; H 7.54; N < 0.05.

Synthesis of [PhBP$^{i\mathrm{Pr}}_3$]Mn(N$_3$), 2.3: A THF solution (15 mL) of [PhBP$^{i\mathrm{Pr}}_3$]MnI (406.0 mg, 0.612 mmol) was added to a suspension of NaN_3 (203.0 mg, 3.06 mmol). The reaction mixture was stirred for 12 h and filtered through a Celite pad. The cream-colored filtrate was concentrated under reduced pressure to dryness and extracted with benzene (258 mg, 73% yield). Single crystals suitable for X-ray diffraction were grown from vapor diffusion of petroleum ether into the benzene solution. ^{1}H NMR (C_6D_6, 300 MHz)

δ 11 (v. br), 8.3 (br). Anal. Calcd. for $C_{27}H_{53}BMnN_3P_3$: C 56.07; H 9.24; N 7.26. Found: C 55.67; H 8.85; N 7.34.

Synthesis of [PhBP$^{iPr}_3$]Mn(CH$_2$Ph), 2.4: An Et_2O solution of benzylmagnesium bromide (107 μL, 1.41 M) was added dropwise to a THF solution of [PhBP$^{iPr}_3$]MnI (100.0 mg, 0.151 mmol) chilled to -90 °C. The solution was allowed to warm slowly to rt. The yellow solution was filtered through a Celite pad, concentrated under reduced pressure to dryness, and extracted with petroleum ether (83.4 mg, 88 % yield). Yellow block crystals suitable for X-ray diffraction were grown from cyclopentane at -30 °C. ^{1}H-NMR (C_6D_6, 300 MHz) δ 16 (v. br), 10.3 (br), 8.3 (br). Anal. Calcd. for $C_{34}H_{60}BMnP_3$: C 65.08; H 9.64; N 0. Found: C 64.98; H 9.32; N <0.05.

Synthesis of [PhBP$^{iPr}_3$]Mn(Me), 2.5: An Et_2O solution of methylmagnesium bromide (53.5 μL, 2.82 M) was added dropwise to a THF solution of [PhBP$^{iPr}_3$]MnI (100.0 mg, 0.151 mmol) chilled to -90 °C. The solution was allowed to warm slowly to rt. The pale-yellow solution was filtered through a Celite pad, concentrated under reduced pressure to dryness, and extracted with petroleum ether (74.1 mg, 89% crude yield). Crystals were grown from cyclopentane at -30 °C (42.3 mg, 51% yield). ^{1}H NMR (C_6D_6, 300 MHz) δ ~ 17 (v. br), 10.1 (br), 8.3 (br). Anal. Calcd. for $C_{28}H_{56}BMnP_3$: C 60.99; H 10.24; N 0. Found: C 60.85; H 9.94; N < 0.05.

Synthesis of [PhBP$^{iPr}_3$]Mn(NH(2,6-^{i}Pr$_2$Ph)), 2.6: A THF solution (8 mL) of 2,6-diisopropylaniline (25.1 mg, 0.142 mmol) was added dropwise to a suspension of KH (5.7 mg, 0.142 mmol) chilled to -90 °C. The solution was allowed to warm slowly to rt. After stirring for 12 h, the solution was rechilled to -90 °C and a THF solution (8 mL) of [PhBP$^{iPr}_3$]MnI (93.9 mg, 0.142 mmol) was added dropwise. After slowly warming to rt,

the bright-yellow reaction was concentrated under reduced pressure to dryness. The product was extracted with petroleum ether, filtered through a Celite pad to remove salts, and concentrated under reduced pressure to afford yellow solids (90.9 mg, 90% yield). Single crystals suitable for X-ray diffraction were grown from TMS_2O/petroleum ether at -30 °C. ^{1}H NMR (C_6D_6, 300 MHz) δ 16.3 (v. br), 10.7 (br), 8.1 (br). Anal. Calcd. for $C_{39}H_{71}BMnNP_3$: C 65.73; H 10.04; N 1.97. Found: C 65.81; H 9.71; N 1.88.

Synthesis of [PhBP$^{iPr}_3$]Mn(dbabh), 2.7: A THF solution (5 mL) of [PhBP$^{iPr}_3$]MnI (142.2 mg, 0.214 mmol) was added dropwise to a Et_2O suspension (10 mL) of Li(dbabh) (42.7 mg, 0.214 mmol) chilled to -90 °C. The solution was allowed to warm slowly to rt. The yellow solution was filtered through a Celite pad, concentrated under reduced pressure to dryness, and extracted with hot Et_2O. Cooling the ether solution to -30 °C afforded yellow blocks (49.7 mg, 32% yield). ^{1}H NMR (C_6D_6, 300 MHz) δ 21 (v. br), 10.3 (br), 8.1 (br). Anal. Calcd. for $C_{41}H_{63}BMnNP_3$: C 67.59; H 8.72; N 1.92. Found: C 66.28; H 8.40; N 1.77.

Synthesis of [PhBP$^{iPr}_3$]Mn(1-Ph(isoindolate)), 2.8: A THF solution (10 mL) of benzyl potassium (40.0 mg, 0.307 mmol) was added to a solution of Hdbabh (59.4 mg, 0.307 mmol) chilled to -90 °C. The solution was allowed to warm slowly to rt. After stirring for 24 h, the solution was rechilled to -90 °C and a THF solution (10 mL) of [PhBP$^{iPr}_3$]MnI (203.9 mg, 0.307 mmol) was added dropwise. After slowly warming to rt, the orange solution was filtered through a Celite pad, concentrated under reduced pressure to dryness, washed with petroleum ether, and extracted with hot Et_2O. Cooling the ether solution to -30 °C afforded red-orange crystals (71.8 mg, 35% yield). ^{1}H NMR

(C_6D_6, 300 MHz) δ 11 (v. br), 8.2 (br). Anal. Calcd. for $C_{41}H_{63}BMnNP_3$: C 67.59; H 8.72; N 1.92. Found: C 66.34; H 9.83; N 1.82.

Synthesis of [PhBP$^{iPr}_3$]Tl-MnBr(CO)$_4$, 2.9: [PhBP$^{iPr}_3$]Tl (150.0 mg, 0.219 mmol) and $MnBr(CO)_5$ (73.6 mg, 0.262 mmol) were mixed together in 10 mL of benzene. The reaction mixture was heated at 50 °C for 7 h. After cooling, the solution was concentrated under reduced pressure to dryness, extracted with benzene, filtered through a glass wool pipette, and concentrated to dryness. The yellow solids were washed liberally with petroleum ether and extracted with benzene. Vapor diffusion of petroleum ether into the solution afforded yellow-orange crystals (79.2 mg, 39% yield). ^{1}H NMR (C_6D_6, 300 MHz) δ 7.76 (d, J = 6.9 Hz, 2H, H$_o$ of Ph), 7.53 (t, J = 6.9 Hz, 2H, H$_m$ of Ph), 7.30 (t, J = 6.9 Hz, 1H, H$_p$ of Ph), 2.00 (m, 6H, CH_2P), 1.26 (m, 6H, C*H*MeMe′), 1.09 (d, J = 6.9 Hz, 18H, CH*Me*Me′), 1.01 (d, J = 6.9 Hz, 18H, CHMe*Me*′). ^{31}P NMR (C_6D_6, 121 MHz) δ 45.4 ppm (d, $J_{Tl\text{-}P}$ = 8060 Hz). Anal. Calcd. for $C_{31}H_{53}BBrMnO_4P_3Tl$: C 39.92; H 5.73; N 0. Found: C 40.35; H 5.83; N 0.06.

Synthesis of [PhBP$^{iPr}_3$]Mn(CN^{t}Bu)$_3$, 2.10: A THF solution (5 mL) of sodium naphthalenide (0.237 mmol, prepared by stirring excess Na and stoichiometric naphthalene in THF for 2 h and filtering prior to use) was added to a stirring solution of [PhBP$^{iPr}_3$]MnI (150.0 mg, 0.226 mmol). ^{t}Butylisocyanide (43.7 μL, 0.724 mmol) was then quickly added to the mixture. After 11 h, the reaction mixture was concentrated under reduced pressure to dryness, extracted with Et_2O, and filtered through a glass wool pipette. The solution was again concentrated under reduced pressure to dryness, extracted with petroleum ether, and filtered through a glass wool pipette. Cooling of the solution to -30 °C afforded pale-yellow crystals (39.4 mg, 22% yield). ^{1}H NMR (C_6D_6, 500 MHz)

δ 8.15 (br, 2H), 7.63 (br, 2H), 7.34 (br, 1H), 2.19 (br, 6H), 1.54 (br, 18H), 1.39 (br, 18H), 1.27 (s, 27H), 0.94 (br, 6H). ^{31}P NMR (C_6D_6, 121 MHz) δ 55.6 ppm (br). Anal. Calcd. for $C_{42}H_{80}BMnN_3P_3$: C 64.20; H 10.26; N 5.35. Found: C 63.84; H 10.10; N 5.22. IR (KBr/THF): ν(cm^{-1}) 2048 (br).

2.4.8 X-ray Experimental Data

X-ray diffraction studies were carried out in the Beckman Institute Crystallographic Facility on a Bruker Smart 1000 CCD diffractometer under a stream of dinitrogen. Data were collected using the Bruker SMART program, collecting ω scans at 5 ϕ settings. Data reduction was performed using Bruker SAINT v6.2. Structure solution and structure refinement were performed using SHELXS-97 (Sheldrick, 1990) and SHELXL-97 (Sheldrick, 1997). All structural representations were produced using the Diamond software program. Crystallographic data are summarized in Table 2.1-2.4.

Table 2.1. Crystallographic data for [PhBP$^{i\mathrm{Pr}}_3$]MnCl, **2.1a**; {[PhBP$^{i\mathrm{Pr}}_3$]Mn(μ-Cl)}$_2$, **2.1b**; and [PhBP$^{i\mathrm{Pr}}_3$]MnI, **2.2**.

	2.1a	**2.1b**	**2.2**·C_6H_6
chemical formula	$0.98C_{27}H_{53}BP_3MnCl$ ·0.02 $Tl\,C_{27}H_{53}BP_3$	$C_{54}H_{106}B_2Cl_2Mn_2P_6$	$C_{27}H_{53}BP_3MnI\cdot C_6H_6$
fw	573.66	1143.61	741.36
T (K)	100	100	100
λ (Å)	0.71073	0.71073	0.71073
a (Å)	14.493(2)	10.950(2)	9.5424(8)
b (Å)	12.928(2)	11.718(2)	9.9006(8)
c (Å)	34.850(5)	13.432(3)	19.668(2)
α (°)	90	68.000(3)	89.780(1)
β (°)	100.344(3)	76.424(4)	89.920(1)
γ (°)	90	78.528(3)	82.662(1)
V (Å^3)	6424(2)	1541.5(5)	1842.9(3)
space group	*C2/c* (# 15)	*P-1* (# 2)	*P-1* (# 2)
Z	8	1	2
D_{calc} (g/cm^3)	1.186	1.232	1.336
μ (cm^{-1})	7.3	6.9	13.5
R1, wR2[a] ($I > 2\sigma(I)$)	0.0422, 0.0720	0.0356, 0.0674	0.0305, 0.0586

[a] $R1 = \Sigma||F_o| - |F_c||/\Sigma|F_o|$, $wR2 = \{\Sigma[w(F_o^2 - F_c^2)^2]/\Sigma[w(F_o^2)^2]\}^{1/2}$

Table 2.2. Crystallographic data for [PhBP$^{i\mathrm{Pr}}_3$]Mn(N_3), **2.3**; [PhBP$^{i\mathrm{Pr}}_3$]Mn(CH_2Ph), **2.4**; and [PhBP$^{i\mathrm{Pr}}_3$]Mn(NH(2,6-$^{i}Pr_2Ph$)), **2.6**.

	2.3	**2.4**	**2.6**
chemical formula	$0.77C_{27}H_{53}BP_3MnN_3$ $\cdot 0.05TlC_{27}H_{53}BP_3$ $\cdot 0.18C_{27}H_{53}BP_3MnCl$	$C_{34}H_{60}BMnP_3$	$C_{39}H_{71}BMnNP_3$
fw	1165.21	627.48	712.63
T (K)	100	100	100
λ (Å)	0.71073	0.71073	0.71073
a (Å)	11.946(2)	9.4120(6)	10.690(1)
b (Å)	34.586(7)	11.8746(8)	11.249(1)
c (Å)	15.423(3)	16.736(1)	18.718(2)
α (°)	90	90	98.393(2)
β (°)	90	105.605(1)	101.614(2)
γ (°)	90	90	107.482(2)
V (Å^3)	6372(2)	1801.6(2)	2050.8(4)
space group	*Pnc2* (# 30)	*P2$_1$* (# 4)	*P-1* (# 2)
Z	4	2	2
D_{calc} (g/cm^3)	1.215	1.157	1.154
μ (cm^{-1})	8.3	5.2	4.7
R1, wR2[a] ($I > 2\sigma(I)$)	0.0938, 0.0783	0.0328, 0.0570	0.0419, 0.0694

[a] $R1 = \Sigma||F_o| - |F_c||/\Sigma|F_o|$, $wR2 = \{\Sigma[w(F_o^2 - F_c^2)^2]/\Sigma[w(F_o^2)^2]\}^{1/2}$

Table 2.3. Crystallographic data for [PhBP$^{i\mathrm{Pr}}_3$]Mn(dbabh), **2.7**; [PhBP$^{i\mathrm{Pr}}_3$]Mn(1-Ph(isoindolate)), **2.8**; and [PhBP$^{i\mathrm{Pr}}_3$]Tl-MnBr(CO)$_4$, **2.9**.

	2.7	**2.8**·0.5$C_4H_{10}O$	**2.9**
chemical formula	$C_{41}H_{63}BMnNP_3$	$C_{41}H_{63}BMnNP_3$ ·0.5$C_4H_{10}O$	$C_{31}H_{53}BBrMnO_4P_3Tl$
fw	728.58	765.64	932.67
T (K)	100	98	100
λ (Å)	0.71073	0.71073	0.71073
a (Å)	10.4294(9)	19.6218(9)	10.2574(5)
b (Å)	16.812(1)	77.737(4)	18.6613(8)
c (Å)	23.393(2)	11.2629(6)	19.9243(9)
α (°)	90	90	90
β (°)	97.476(1)	90	100.590(1)
γ (°)	90	90	90
V (Å^3)	4066.7(6)	17180(2)	3748.9(3)
space group	$P2_1/c$ (# 14)	$Fdd2$ (# 43)	$P2_1/n$ (# 14)
Z	4	16	4
D_{calc} (g/cm^3)	1.190	1.184	1.652
μ (cm^{-1})	4.7	4.5	58.6
R1, wR2[a] ($I > 2\sigma(I)$)	0.0409, 0.0724	0.0514, 0.0731	0.0355, 0.0532

[a] $R1 = \Sigma||F_o| - |F_c||/\Sigma|F_o|$, $wR2 = \{\Sigma[w(F_o^2 - F_c^2)^2]/\Sigma[w(F_o^2)^2]\}^{1/2}$

Table 2.4. Crystallographic data for $[PhBP^{iPr}_3]Mn(CN^tBu)_3$, **2.10**.

	2.10
chemical formula	$C_{42}H_{80}BMnN_3P_3$
fw	785.75
T (K)	100
λ (Å)	0.71073
a (Å)	11.2996(7)
b (Å)	17.578(1)
c (Å)	23.108(1)
α (°)	90
β (°)	93.660(2)
γ (°)	90
V (Å^3)	4580.4(5)
space group	$P2_1/n$ (# 14)
Z	4
D_{calc} (g/cm^3)	1.139
μ (cm^{-1})	4.2
R1, wR2[a] ($I > 2\sigma(I)$)	0.0437, 0.0707

[a] $R1 = \Sigma||F_o| - |F_c||/\Sigma|F_o|$, $wR2 = \{\Sigma[w(F_o^2 - F_c^2)^2]/\Sigma[w(F_o^2)^2]\}^{1/2}$

References Cited

1. Nugent, W. A.; Mayer, J. M., *Metal-Ligand Multiple Bonds*. Wiley: New York, 1988.
2. Holm, R. H. *Chem. Rev.* **1987**, *87*, 1401.
3. Jorgensen, K. A. *Chem. Rev.* **1989**, *89*, 431.
4. Gao, Y.; Hanson, R. M.; Klunder, J. M.; Ko, S. Y.; Masamune, H.; Sharpless, K. B. *J. Am. Chem. Soc.* **1987**, *109*, 5765.
5. Collman, J. P.; Zhang, X. M.; Lee, V. J.; Uffelman, E. S.; Brauman, J. I. *Science* **1993**, *261*, 1404.
6. Collman, J. P.; Brauman, J. I.; Meunier, B.; Raybuck, S. A.; Kodadek, T. *Proc. Natl. Acad. Sci. U. S. A.* **1984**, *81*, 3245.
7. Li, Z.; Quan, R. W.; Jacobsen, E. N. *J. Am. Chem. Soc.* **1995**, *117*, 5889.
8. Evans, D. A.; Woerpel, K. A.; Hinman, M. M.; Faul, M. M. *J. Am. Chem. Soc.* **1991**, *113*, 726.
9. Jacobsen, E. N., *Comprehensive Asymmetric Catalysis*. Springer: Hamburg, 1999.
10. Müller, P.; Fruit, C. *Chem. Rev.* **2003**, *103*, 2905.
11. Brookhart, M.; Studabaker, W. B. *Chem. Rev.* **1987**, *87*, 411.
12. Doyle, M. P. *Chem. Rev.* **1986**, *86*, 919.
13. Doyle, M. P.; McKervey, M. A.; Ye, T., *Modern Catalytic Methods for Organic Synthesis with Diazo Compounds*. Wiley: New York, 1997.
15. Grubbs, R. H.; Chang, S. *Tetrahedron* **1998**, *54*, 4413.
16. Hoveyda, A. H.; Schrock, R. R. *Chem. Eur. J.* **2001**, *7*, 945.
17. Feldman, J.; Schrock, R. R. *Prog. Inorg. Chem.* **1991**, *39*, 1.

18. Davies, H. M. L.; Hansen, T.; Churchill, M. R. *J. Am. Chem. Soc.* **2000**, *122*, 3063.

19. Groves, J. T.; Han, Y.-Z., *Cytochrome P450: Structure, Mechanism, and Biochemistry*. Plenum Press: New York, 1995; p 3.

20. Abu-Omar, M. M.; Loaiza, A.; Hontzeas, N. *Chem. Rev.* **2005**, *105*, 2227.

21. Nakamoto, K. *Coord. Chem. Rev.* **2002**, *226*, 153.

22. Costas, M.; Mehn, M. P.; Jensen, M. P.; Que, L. *Chem. Rev.* **2004**, *104*, 939.

23. Glueck, D. S.; Wu, J. X.; Hollander, F. J.; Bergman, R. G. *J. Am. Chem. Soc.* **1991**, *113*, 2041.

24. Glueck, D. S.; Hollander, F. J.; Bergman, R. G. *J. Am. Chem. Soc.* **1989**, *111*, 2719.

25. Hay-Motherwell, R. S.; Wilkinson, G.; Hussain-Bates, B.; Hursthouse, M. B. *Polyhedron* **1993**, *12*, 2009.

26. Verma, A. K.; Nazif, T. N.; Achim, C.; Lee, S. C. *J. Am. Chem. Soc.* **2000**, *122*, 11013.

27. Brown, S. D.; Peters, J. C. *J. Am. Chem. Soc.* **2005**, *127*, 1913.

28. Betley, T. A.; Peters, J. C. *J. Am. Chem. Soc.* **2004**, *126*, 6252.

29. Brown, S. D.; Betley, T. A.; Peters, J. C. *J. Am. Chem. Soc.* **2003**, *125*, 322.

30. Klinker, E. J.; Kaizer, J.; Brennessel, W. W.; Woodrum, N. L.; Cramer, C. J.; Que, L. *Angew. Chem. Int. Ed.* **2005**, *44*, 3690.

31. Rohde, J. U.; In, J. H.; Lim, M. H.; Brennessel, W. W.; Bukowski, M. R.; Stubna, A.; Münck, E.; Nam, W.; Que, L. *Science* **2003**, *299*, 1037.

32. Kaizer, J.; Klinker, E. J.; Oh, N. Y.; Rohde, J. U.; Song, W. J.; Stubna, A.; Kim, J.; Münck, E.; Nam, W.; Que, L. *J. Am. Chem. Soc.* **2004**, *126*, 472.

33. Bart, S. C.; Lobkovsky, E.; Bill, E.; Chirik, P. J. *J. Am. Chem. Soc.* **2006**, *128*, 5302.

34. Shay, D. T.; Yap, G. P. A.; Zakharov, L. N.; Rheingold, A. L.; Theopold, K. H. *Angew. Chem. Int. Ed.* **2005**, *44*, 1508.

35. Dai, X. L.; Kapoor, P.; Warren, T. H. *J. Am. Chem. Soc.* **2004**, *126*, 4798.

36. Jenkins, D. M.; Betley, T. A.; Peters, J. C. *J. Am. Chem. Soc.* **2002**, *124*, 11238.

37. Termaten, A. T.; Aktas, H.; Schakel, M.; Ehlers, A. W.; Lutz, M.; Spek, A. L.; Lammertsma, K. *Organometallics* **2003**, *22*, 1827.

38. Sanchez-Nieves, J.; Sterenberg, B. T.; Udachin, K. A.; Carty, A. J. *J. Am. Chem. Soc.* **2003**, *125*, 2404.

39. Mindiola, D. J.; Hillhouse, G. L. *Chem. Commun.* **2002**, 1840.

40. Mindiola, D. J.; Hillhouse, G. L. *J. Am. Chem. Soc.* **2002**, *124*, 9976.

41. Melenkivitz, R.; Mindiola, D. J.; Hillhouse, G. L. *J. Am. Chem. Soc.* **2002**, *124*, 3846.

42. Mindiola, D. J.; Hillhouse, G. L. *J. Am. Chem. Soc.* **2001**, *123*, 4623.

43. Kogut, E.; Wiencko, H. L.; Zhang, L. B.; Cordeau, D. E.; Warren, T. H. *J. Am. Chem. Soc.* **2005**, *127*, 11248.

44. Dai, X. L.; Warren, T. H. *J. Am. Chem. Soc.* **2004**, *126*, 10085.

45. Straub, B. F.; Hofmann, P. *Angew. Chem. Int. Ed.* **2001**, *40*, 1288.

46. Eikey, R. A.; Abu-Omar, M. M. *Coord. Chem. Rev.* **2003**, *243*, 83.

47. Groves, J. T.; Takahashi, T. *J. Am. Chem. Soc.* **1983**, *105*, 2073.

48. Buchler, J. W.; Dreher, C.; Lay, K. L.; Lee, Y. J. A.; Scheidt, W. R. *Inorg. Chem.* **1983**, *22*, 888.

49. Hill, C. L.; Hollander, F. J. *J. Am. Chem. Soc.* **1982**, *104*, 7318.

50. Buchler, J. W.; Dreher, C.; Lay, K. L. *Z. Naturforsch., B: Chem. Sci.* **1982**, *37*, 1155.

51. Dehnicke, K.; Strahle, J. *Angew. Chem., Int. Ed. Eng.* **1981**, *20*, 413.

52. Meyer, K.; Bendix, J.; Metzler-Nolte, N.; Weyhermüller, T.; Wieghardt, K. *J. Am. Chem. Soc.* **1998**, *120*, 7260.

53. Niemann, A.; Bossek, U.; Haselhorst, G.; Wieghardt, K.; Nuber, B. *Inorg. Chem.* **1996**, *35*, 906.

54. Bendix, J.; Meyer, K.; Weyhermüller, T.; Bill, E.; Metzler-Nolte, N.; Wieghardt, K. *Inorg. Chem.* **1998**, *37*, 1767.

55. Du Bois, J.; Tomooka, C. S.; Hong, J.; Carreira, E. M. *Acc. Chem. Res* **1997**, *30*, 364.

56. Du Bois, J.; Tomooka, C. S.; Hong, J.; Carreira, E. M.; Day, M. W. *Angew. Chem., Int. Ed. Eng.* **1997**, *36*, 1645.

57. Chang, C. J.; Connick, W. B.; Low, D. W.; Day, M. W.; Gray, H. B. *Inorg. Chem.* **1998**, *37*, 3107.

58. Chang, C. J.; Low, D. W.; Gray, H. B. *Inorg. Chem.* **1997**, *36*, 270.

59. Danopoulos, A. A.; Wilkinson, G.; Sweet, T. K. N.; Hursthouse, M. B. *J. Chem. Soc., Dalton Trans.* **1995**, 205.

60. Danopoulos, A. A.; Green, J. C.; Hursthouse, M. B. *J. Organomet. Chem.* **1999**, *591*, 36.

61. Danopoulos, A. A.; Wilkinson, G.; Sweet, T. K. N.; Hursthouse, M. B. *J. Chem. Soc., Dalton Trans.* **1995**, 937.

62. Danopoulos, A. A.; Wilkinson, G.; Sweet, T. K. N.; Hursthouse, M. B. *J. Chem. Soc., Dalton Trans.* **1994**, 1037.

63. Abu-Omar, M. M.; Shields, C. E.; Edwards, N. Y.; Eikey, R. A. *Angew. Chem. Int. Ed.* **2005**, *44*, 6203.

64. Edwards, N. Y.; Eikey, R. A.; Loring, M. I.; Abu-Omar, M. M. *Inorg. Chem.* **2005**, *44*, 3700.

65. Eikey, R. A.; Khan, S. I.; Abu-Omar, M. M. *Angew. Chem. Int. Ed.* **2002**, *41*, 3592.

66. Du Bois, J.; Hong, J.; Carreira, E. M.; Day, M. W. *J. Am. Chem. Soc.* **1996**, *118*, 915.

67. Thomas, C. M.; Mankad, N. P.; Peters, J. C. *J. Am. Chem. Soc.* **2006**, *128*, 4956.

68. MacBeth, C. E.; Thomas, J. C.; Betley, T. A.; Peters, J. C. *Inorg. Chem.* **2004**, *43*, 4645.

69. Shapiro, I. R.; Jenkins, D. M.; Thomas, J. C.; Day, M. W.; Peters, J. C. *Chem. Commun.* **2001**, 2152.

70. Betley, T. A.; Peters, J. C. *Inorg. Chem.* **2003**, *42*, 5074.

71. Jenkins, D. M.; Di Bilio, A. J.; Allen, M. J.; Betley, T. A.; Peters, J. C. *J. Am. Chem. Soc.* **2002**, *124*, 15336.

72. Hebendanz, N.; Köhler, F. H.; Müller, G. *Inorg. Chem.* **1984**, *23*, 3043.

73. Sur, S. K. *J. Magn. Reson.* **1989**, *82*, 169.

74. Evans, D. F. *J. Chem. Soc.* **1959**, 2003.

75. Armentano, D.; de Munno, G.; Guerra, F.; Faus, J.; Lloret, F.; Julve, M. *Dalton Trans.* **2003**, 4626.

76. Girolami, G. S.; Wilkinson, G.; Galas, A. M. R.; Thornton-Pett, M.; Hursthouse, M. B. *J. Chem. Soc., Dalton Trans.* **1985**, 1339.

77. Brown, S. D.; Mehn, M. P.; Peters, J. C. *J. Am. Chem. Soc.* **2005**, *127*, 13146.

78. Godfrey, S. M.; McAuliffe, C. A.; Ndifon, P. T.; Pritchard, R. G. *J. Chem. Soc., Dalton Trans.* **1993**, 3373.

79. Godfrey, S. M.; McAuliffe, C. A.; Pritchard, R. G. *J. Chem. Soc., Dalton Trans.* **1993**, 371.

80. Cecconi, F.; Ghilardi, C. A.; Midollini, S.; Orlandini, A. *J. Chem. Soc., Dalton Trans.* **1992**, 33.

81. Beagley, B.; McAuliffe, C. A.; Minten, K.; Pritchard, R. G. *J. Chem. Soc., Dalton Trans.* **1987**, 1999.

82. Beagley, B.; McAuliffe, C. A.; Minten, K.; Pritchard, R. G. *J. Chem. Soc., Chem. Commun.* **1984**, 658.

83. Komatsuzaki, H.; Sakamoto, N.; Satoh, M.; Hikichi, S.; Akita, M.; Moro-oka, Y. *J. Am. Chem. Soc.* **1998**, *37*, 6554.

84. Matsunaga, Y.; Fujisawa, K.; Ibi, N.; Miyashita, Y.; Okamoto, K. *Inorg. Chem.* **2005**, *44*, 325.

85. Nabika, M.; Seki, Y.; Miyatake, T.; Ishikawa, Y.; Okamoto, K.; Fujisawa, K. *Organometallics* **2004**, *23*, 4335.

86. Brunker, T. J.; Hascall, T.; Cowley, A. R.; Rees, L. H.; O'Hare, D. *Inorg. Chem.* **2001**, *40*, 3170.

87. Komatsuzaki, H.; Nagasu, Y.; Suzuki, K.; Shibasaki, T.; Satoh, M.; Ebina, F.; Hikichi, S.; Akita, M.; Moro-oka, Y. *J. Chem. Soc., Dalton Trans.* **1998**, 511.

88. Wieghardt, K.; Bossek, U.; Nuber, B.; Weiss, J. *Inorg. Chim. Acta* **1987**, *126*, 39.

89. Hubin, T. J.; McCormick, J. M.; Alcock, N. W.; Busch, D. H. *Inorg. Chem.* **2001**, *40*, 435.

90. Mantel, C.; Hassan, A. K.; Pecaut, J.; Deronzier, A.; Collomb, M. N.; Duboc-Toia, C. *J. Am. Chem. Soc.* **2003**, *125*, 12337.

91. Saha, S.; Mal, D.; Koner, S.; Bhattacherjee, A.; Gutlich, P.; Mondal, S.; Mukherjee, M.; Okamoto, K. I. *Polyhedron* **2004**, *23*, 1811.

92. Chai, J. F.; Zhu, H. P.; Fan, H. J.; Roesky, H. W.; Magull, J. *Organometallics* **2004**, *23*, 1177.

93. Howard, C. G.; Girolami, G. S.; Wilkinson, G.; Thornton-Pett, M.; Hursthouse, M. B. *J. Chem. Soc., Dalton Trans.* **1983**, 2631.

94. Chai, J. F.; Zhu, H. P.; Roesky, H. W.; He, C.; Schmidt, H. G.; Noltemeyer, M. *Organometallics* **2004**, *23*, 3284.

95. Riollet, V.; Copéret, C.; Basset, J. M.; Rousset, L.; Bouchu, D.; Grosvalet, L.; Perrin, M. *Angew. Chem. Int. Ed.* **2002**, *41*, 3025.

96. Daida, E. J.; Peters, J. C. *Inorg. Chem.* **2004**, *43*, 7474.

97. Mindiola, D. J.; Cummins, C. C. *Angew. Chem. Int. Ed.* **1998**, *37*, 945.

98. Betley, T. A.; Peters, J. C. *J. Am. Chem. Soc.* **2003**, *125*, 10782.

99. Hu, X.; Meyer, K. *J. Am. Chem. Soc.* **2004**, *126*, 16322.

100. Baker, R. J.; Edwards, P. G.; Gracia-Mora, J.; Ingold, F.; Malik, K. M. A. *J. Chem. Soc., Dalton Trans.* **2002**, 3985.

101. Bond, A. M.; Colton, R.; van den Bergen, A.; Walter, J. N. *Inorg. Chem.* **2000**, *39*, 4696.

102. Connolly, J.; Genge, A. R. J.; Levason, W.; Orchard, S. D.; Pope, S. J. A.; Reid, G. *J. Chem. Soc., Dalton Trans.* **1999**, 2343.

103. Connor, J. A.; Hudson, G. A. *J. Organomet. Chem.* **1974**, *73*, 351.

104. Reimann, R. H.; Singleton, E. *J. Chem. Soc., Dalton Trans.* **1973**, 841.

105. Sorace, L.; Golze, C.; Gatteschi, D.; Bencini, A.; Roesky, H. W.; Chai, J.; Stückl, A. C. *Inorg. Chem.* **2006**, *45*, 395.

106. Chai, J. F.; Zhu, H. P.; Stückl, A. C.; Roesky, H. W.; Magull, J.; Bencini, A.; Caneschi, A.; Gatteschi, D. *J. Am. Chem. Soc.* **2005**, *127*, 9201.

107. King, W. A.; Scott, B. L.; Eckert, J.; Kubas, G. J. *Inorg. Chem.* **1999**, *38*, 1069.

108. King, W. A.; Luo, X. L.; Scott, B. L.; Kubas, G. J.; Zilm, K. W. *J. Am. Chem. Soc.* **1996**, *118*, 6782.

109. Schollenberger, M.; Nuber, B.; Ziegler, M. L.; Hey-Hawkins, E. *J. Organomet. Chem.* **1993**, *460*, 55.

110. Guilard, R.; Zrineh, A.; Ferhat, M.; Tabard, A.; Mitaine, P.; Swistak, C.; Richard, P.; Lecomte, C.; Kadish, K. M. *Inorg. Chem.* **1988**, *27*, 697.

111. Attempts to minimize formation of [PhBP$^{i\mathrm{Pr}}_3$]Na by adding CN^{t}Bu to **2.2** prior to the addition of sodium napthalenide or by adding sodium napthalenide to **2.2** at low temperatures lead to less clean reactions.

112. Bailey, P. L.; Coxall, R. A.; Dick, C. M.; Fabre, S.; Henderson, L. C.; Herber, C.; Liddle, S. T.; Lorono-Gonzalez, D.; Parkin, A.; Parsons, S. *Chem. Eur. J.* **2003**, *9*, 4820.

Chapter 3: Targeting Terminal Iron Nitrides Using the Bulky Tripodal Phosphine Ligands [PhBP$^{ter}_3$] and [PhBP$^{CH_2Cy}_3$]

3.1 Introduction

Iron complexes featuring a terminal nitride functionality are extremely rare.[1] The first examples of terminal iron nitrides were generated at very low temperatures and based on *in situ* spectroscopic evidence (Figure 3.1). When Nakamoto and coworkers irradiated thin films of [(porphyrin)]Fe(N_3) species at 30 K, they detected a transient species, which they assigned as an iron(V) nitride. Consistent with this assignment, these species exhibited resonance Raman signatures near 870 cm^{-1} that shift in isotopic studies in accord with an Fe=N stretching vibration.[2] Upon warming, these species degrade to the μ-N iron dimer. Wieghardt and coworkers have also observed an intermediate species during the photolysis of frozen solutions of *trans*-[(cyclam)Fe(N_3)$_2$] and [(cyclam-acetato)Fe(N_3)] at 77 K. Based on Mössbauer spectroscopy, these species were proposed to be iron(V) nitrides.[3] Recent XAS data have corroborated this assignment by revealing a short Fe-N bond length of 1.61 Å.[4]

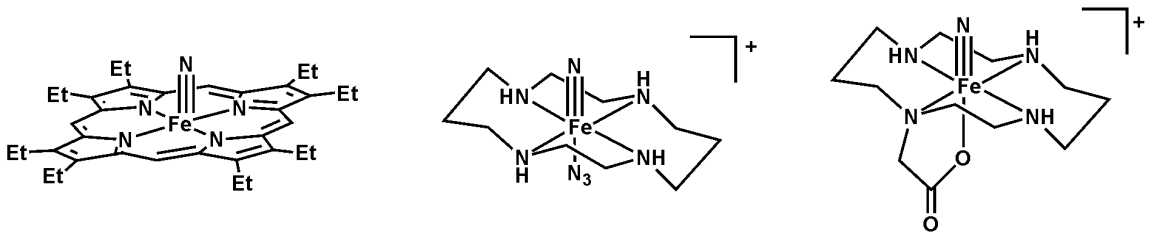

Figure 3.1. Examples of iron(V) nitrides stabilized by porphyrin and cyclam ligands.

Thus far, the most stable terminal iron nitride was reported by Betley and Peters. The proposed species, [PhBP$^{i\mathrm{Pr}}_3$]Fe^{IV}(N), is generated *in situ* by the thermal degradation of [PhBP$^{i\mathrm{Pr}}_3$]Fe(dbabh), where dbabh is 2,3:5,6-dibenzo-7-azabicyclo[2.2.1]hepta-2,5-diene,[5] a known N-atom transfer reagent that can expel anthracene (Equation 3.1).[6]

Evidence for a terminal nitride includes a ^{15}N NMR resonance at 952 ppm, an IR stretch at 1034 cm^{-1} that is sensitive to ^{15}N-substitution, and EXAFS data that reveal an Fe-N bond length of 1.54 Å.[7] The nitride species is stable at 0 °C under dilute conditions, but eventually degrades via bimolecular coupling to the dinitrogen-bridged dimer, $\{[PhBP^{iPr}_3]Fe\}_2(\mu\text{-}N_2)$.[8]

Scheme 3.1

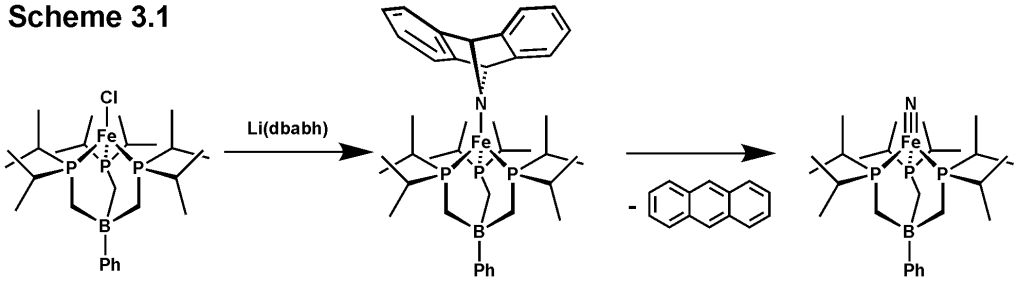

The preparation of stable iron terminal nitrides remains a challenge. One strategy is to hinder the bimolecular decomposition pathways by incorporating sterically encumbering groups into the ligand scaffolds. The $[PhBP^{iPr}_3]$ system is particularly amenable to this approach due to the synthetic modularity of the $[BP_3]$ ligands. In this chapter, we introduce two new ligands, $[PhB(CH_2P(m\text{-terphenyl})_2)_3]^-$ ($[PhBP^{ter}_3]$) and $[PhB(CH_2P(CH_2Cy)_2)_3]^-$ ($[PhBP^{CH_2Cy}_3]$), which feature terphenyl and methylcyclohexyl groups on the phosphine arms, respectively. Their synthesis and iron metalation are described, as well as some initial attempts to generate terminal iron nitrides.

3.2 Results and Discussion

3.2.1 Preparation and Characterization of $[PhBP^R_3]Tl$ Species

The synthesis of the Tl-ligand adduct, $[PhBP^{ter}_3]Tl$, which is adapted from the protocol used for $[PhBP_3]Tl$,[9] consists of three steps starting from *m*-terphenyl bromide

(Scheme 3.2). Lithium-halogen exchange of *m*-terphenyl bromide with ^{n}BuLi occurs at -78 ºC.[10] Subsequent quenching with $MePCl_2$ generates the phosphine, MeP(*m*-terphenyl)$_2$ (**3.1**), which is obtained in good yield (84%). Next, the deprotonation of **3.1** is effected by the combination of ^{s}BuLi and tmeda to give (*m*-terphenyl)$_2$PCH$_2$Li(tmeda) (**3.2**). Finally, addition of **3.2** to $PhBCl_2$ followed by *in situ* transmetalation with $TlPF_6$ leads directly to [PhBP$^{ter}_3$]Tl (**3.3**). The ^{31}P NMR spectrum of **3.3** contains a wide doublet with a splitting that is diagnostic of thallium-phosphorus coupling (J = 4870 Hz).

Scheme 3.2

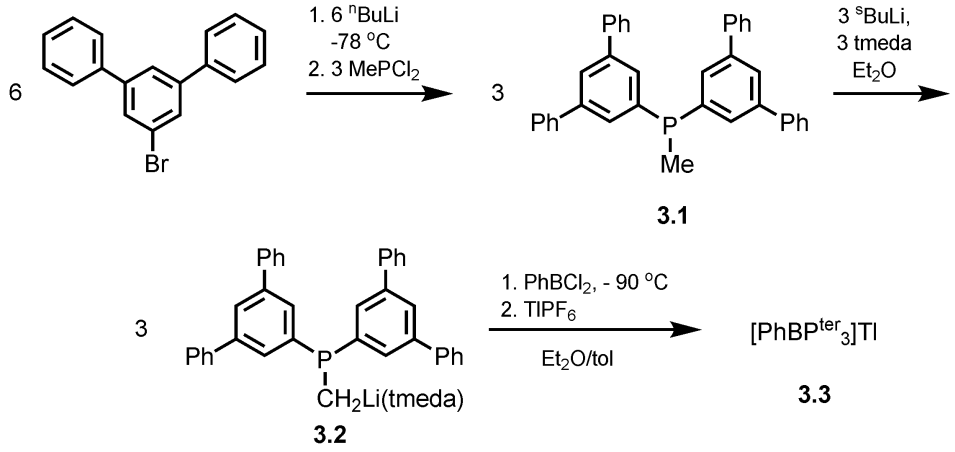

The synthesis of the methylcyclohexyl derivative [PhBP$^{CH_2Cy}_3$]Tl is derived from the protocol developed for [PhBP$^{iPr}_3$]Tl (Scheme 3.3).[11] The phosphine MeP(CH$_2$Cy)$_2$ (**3.4**) is generated from the Gringard CyCH$_2$MgBr and $MePCl_2$ in high yield (98%). Deprotonation of **3.4** is achieved by heating the neat phosphine with solid ^{t}BuLi at 90 °C for 4 h.[12] The lithio species, LiCH$_2$P(CH$_2$Cy)$_2$ (**3.5**), is thus obtained in 94% yield. The delivery of **3.5** to $PhBCl_2$ followed by addition of $TlPF_6$ provides the ligand, [PhBP$^{CH_2Cy}_3$]Tl (**3.6**).

Scheme 3.3

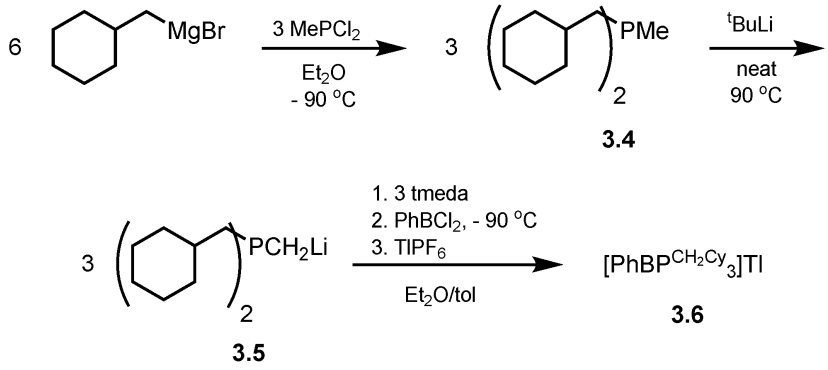

3.2.2 Preparation and Characterization of [PhBP$^{R}_{3}$]Fe Complexes

Thallium complexes of poly(phosphino)borates have proven to be synthetically useful for delivering these ligands onto various transition metals.[9,11,13] Both [PhBP$^{ter}_{3}$]Tl (**3.3**) and [PhBP$^{CH_2Cy}_{3}$]Tl (**3.6**) react cleanly with $FeCl_2$ to generate the complexes, [PhBP$^{ter}_{3}$]FeCl (**3.7**) and [PhBP$^{CH_2Cy}_{3}$]FeCl (**3.8**), respectively, in good yields (Equation 3.1).

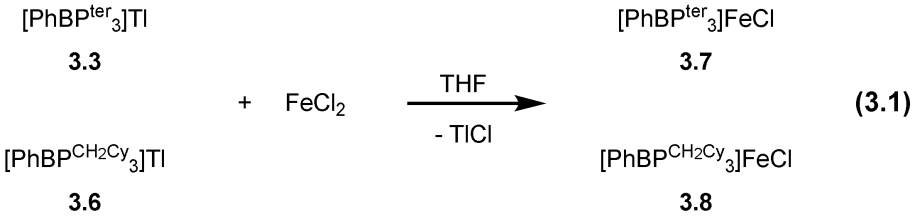

X-ray analysis revealed that complexes **3.7** and **3.8** are monomeric and pseudotetrahedral species in the solid state (Figure 3.2). For both **3.7** and **3.8**, the phosphine substituents extend well above the chloride atom and, thus, may obstruct any dimerization processes in the coordination chemistry of their respective [PhBP$^{R}_{3}$]Fe systems. The bond distances and angles for **3.7** and **3.8** as well for their parent congeners, [PhBP$_3$]FeCl and [PhBP$^{iPr}_{3}$]FeCl are presented together in Table 3.1.

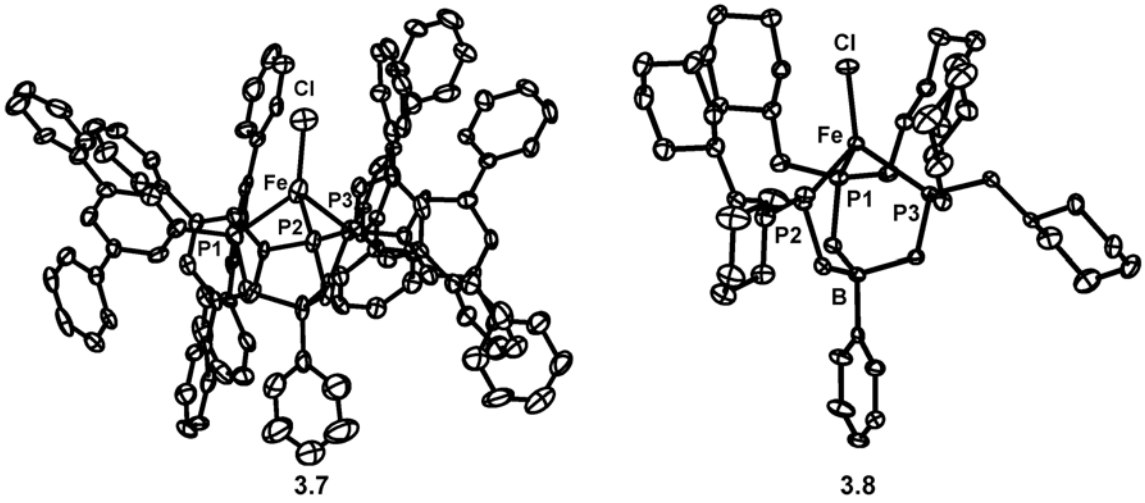

Figure 3.2. 50% thermal ellipsoid representations of [PhBP$^{ter}_3$]FeCl (**3.7**) and [PhBP$^{CH_2Cy}_3$]FeCl (**3.8**). Hydrogen atoms have been omitted for clarity.

Table 3.1. Selected bond distances (Å) and angles (deg.) for [PhBP$^{ter}_3$]FeCl (**3.7**), [PhBP$_3$]FeCl, [PhBP$^{CH_2Cy}_3$]FeCl (**3.8**), and [PhBP$^{iPr}_3$]FeCl.

	3.7	[PhBP$_3$]FeCl	**3.8**	[PhBP$^{iPr}_3$]FeCl
Fe-Cl	2.191(2)	2.205(1)	2.2173(6)	2.2204(9)
Fe-P	2.410(2)	2.417(1)	2.4146(8)	2.4146(9)
	2.432(2)	2.427(1)	2.4227(8)	2.4281(9)
	2.467(2)	2.432(1)	2.4254(7)	2.431(1)
P-Fe-P	91.01(7)	89.76(3)	92.55(2)	93.24(3)
	91.63(8)	93.19(4)	93.55(3)	94.10(3)
	92.98(8)	94.29(4)	94.07(2)	94.49(3)
P-Fe-Cl	115.74(9)	110.57(4)	111.96(3)	122.12(4)
	127.43(9)	129.63(4)	124.53(3)	122.52(4)
	128.0(1)	129.60(4)	131.04(3)	122.62(4)
Cl-Fe-B	171.08(9)	166.56(4)	167.43(3)	179.79(4)

The iron chlorides show little variation in their bonding parameters, and they all exhibit approximate C_3 symmetry. However, the range of Cl-Fe-P angles in [PhBP$^{i\mathrm{Pr}}_3$]FeCl is notably tighter than in the other complexes, and the Cl-Fe-B angle deviates the least from linearity. The higher C_3 symmetry exhibited by [PhBP$^{i\mathrm{Pr}}_3$]FeCl is attributed to the ligand's rigidity, which is partly enforced by the tight packing of the isopropyl groups. In comparison, the methylcyclohexyl derivative **3.8** exhibits a wider range of Cl-Fe-P angles and a significantly bent Cl-Fe-B angle (167.43(3)°). The substitution of isopropyl with methylcyclohexyl groups may unfortunately *decrease* the overall bulk in the immediate coordination sphere around the metal center. In other words, the methylcyclohexyl groups impart additional flexibility to the metal pocket wherein the chloride atom resides. The bonding parameters for **3.7** and [PhBP$_3$]FeCl do not show significant differences.

Besides sterics, the electron-releasing character of the [PhBP$^{\mathrm{ter}}_3$] and [PhBP$^{\mathrm{CH_2Cy}}_3$] ligands was assessed by studying the cyclic voltammetry of their respective iron chlorides. [PhBP$^{\mathrm{ter}}_3$]FeCl **3.7** exhibits a fully reversible Fe(II)/Fe(I) couple at -1.52 V, while [PhBP$^{\mathrm{CH_2Cy}}_3$] exhibits a quasi-reversible Fe(II)/Fe(I) couple at -1.94 V (Figure 3.3). These potentials are similar, though slightly anodic relative to those for the parent species, [PhBP$_3$]FeCl (-1.61 V) and [PhBP$^{i\mathrm{Pr}}_3$]FeCl (-2.03 V).

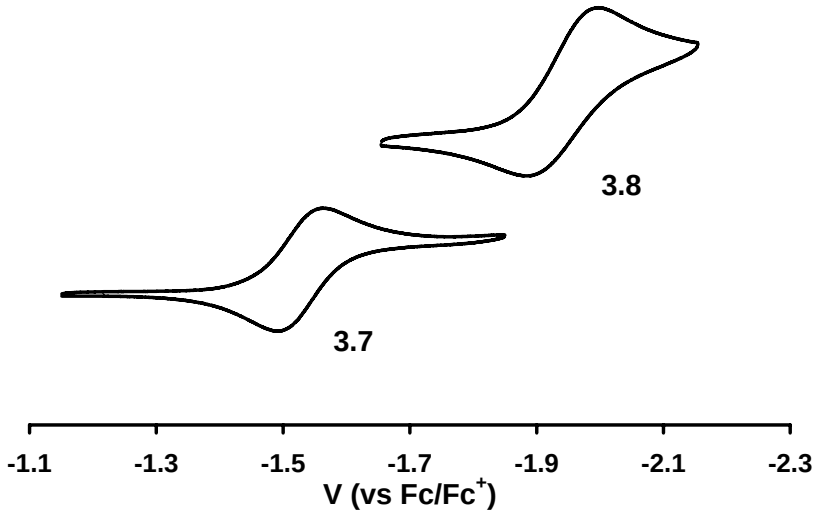

Figure 3.3. Cyclic voltammograms of [PhBP$^{ter}_3$]FeCl (**3.7**) and [PhBP$^{CH_2Cy}_3$]FeCl (**3.8**) recorded at scan rates of 10 and 50 mV/s, respectively, in THF with 0.35 M [^{n}NBu$_4$][PF$_6$] as the supporting electrolyte. Potentials are internally referenced to Fc/Fc$^+$.

3.2.3 Targeting [PhBP$^R_3$]Fe(N) Complexes

The installation of a terminal nitride functionality onto the new [PhBP$^R_3$]Fe scaffolds was investigated. As mentioned previously, the thermal degradation of [PhBP$^{iPr}_3$]Fe(dbabh), which results from the reaction of [PhBP$^{iPr}_3$]FeCl and Li(dbabh), leads to the clean production of [PhBP$^{iPr}_3$]Fe(N) and one equivalent of anthracene. In contrast, [PhBP$_3$]FeCl does not react cleanly with Li(dbabh) and gives an ill-defined mixture.[14] Not surprisingly then, the reaction of compound **3.7** and Li(dbabh) resulted in a mixture of several species even at -50 ºC based on NMR spectroscopy.

Similar to the [PhBP$^{i\mathrm{Pr}}_3$]Fe system, [PhBP$^{\mathrm{CH_2Cy}}_3$]FeCl reacts with Li(dbabh) to give cleanly the iron(IV) nitride, [PhBP$^{\mathrm{CH_2Cy}}_3$]Fe(N) (**3.9**), and one equivalent of anthracene (^{1}H and ^{31}P NMR, Scheme 3.4). However, [PhBP$^{\mathrm{CH_2Cy}}_3$]FeCl converts directly to the nitride **3.9** at -50 °C without the observation of the intermediate iron amide, "[PhBP$^{\mathrm{CH_2Cy}}_3$]Fe(dbabh)." Steric repulsion between the bulkier [PhBP$^{\mathrm{CH_2Cy}}_3$] ligand and dbabh may accelerate the rate of anthracene expulsion.

Scheme 3.4

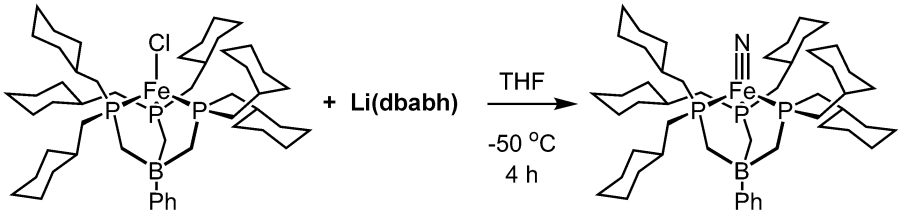

The formulation of **3.9** as a terminal nitride was confirmed by a peak at 929 ppm in the ^{15}N NMR spectrum of ^{15}N-**3.9**. The Mössbauer spectrum of **3.9** contains two doublets (Figure 3.4), revealing a mixture of **3.9** (~75%) and an unknown diamagnetic impurity (~25%).[15] The larger doublet for **3.9** has an isomer shift (δ) of -0.34(1) mm/s and a quadrupole splitting (ΔE_Q) of 6.01(1) mm/s. The low isomer shift corroborates the assignment of a high valent iron center, while the quadrupole splitting indicates a non-spherical distribution of nuclear electron density. These values are identical to those observed for [PhBP$^{i\mathrm{Pr}}_3$]Fe(N), although the spectrum only contained 35% of the desired species and was complicated by the presence of [PhBP$^{i\mathrm{Pr}}_3$]FeCl, [PhBP$^{i\mathrm{Pr}}_3$]Fe(dbabh), and {[PhBP$^{i\mathrm{Pr}}_3$]Fe}$_2$(μ-N$_2$) (Figure 3.4).

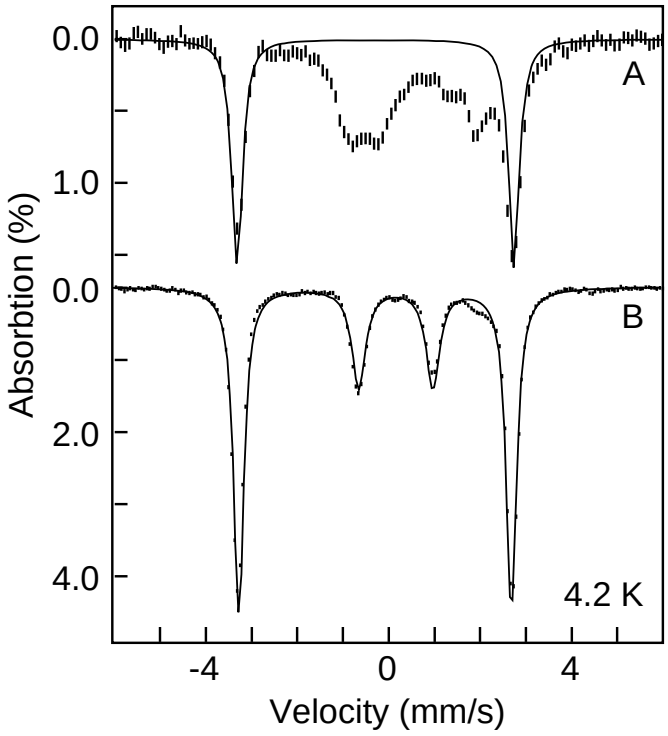

Figure 3.4. Mössbauer spectra of 40 mM (A) [PhBP$^{i\mathrm{Pr}}_3$]Fe≡N in THF and (B) 35 mM [PhBP$^{\mathrm{CH_2Cy}}_3$]Fe≡N (**3.9**) in THF recorded at 4.2 K with an applied field of 45 mT. The vertical lines are the experimental data and the solid lines are fits using the following parameters: (A) δ = -0.34 mm/s, ΔE_Q = 6.0 mm/s (35%); and (B) δ = -0.34(1) mm/s, ΔE_Q = 6.01(1) mm/s (75%). The other species in (B) has the following values: δ = 0.15 mm/s, ΔE_Q =1.61 mm/s (25%).

The Mössbauer parameters for several iron(IV) complexes are presented in Table 3.2 for comparison. Iron(IV), though uncommon, is an important oxidation state because it is believed to function in metalloenzymes.[16] Many well-defined iron(IV) compounds feature a bridging or terminal oxo ligand, although there are several exceptions including (cyclam-acetato)Fe(N_3),[17] [NEt_4][(L_4)FeCl][18] (where L_4 is a tetraanionic macrocyclic ligand), (L_4)Fe(CN^tBu)$_2$,[19] Fe(1-norbornyl)$_4$,[20] (triamido(amine))Fe(CN),[21] [$PhBP^{iPr}_3$]Fe(H)$_3$(PMe_3),[22] and the nitride compounds described here. The δ values for the majority of these iron(IV) species are near zero. The δ values of -0.34 mm/s for the iron nitrides is slightly different, but they are consistent with high valent iron and similar to (triamido(amine))Fe(CN). Unlike the isomer shift, no consistent trend is observable for the quadrupole splitting, which ranges from 0.6 to 6 mm/s. Notably, the ΔE_Q values for the iron nitrides are by far the largest.

Table 3.2. Mössbauer parameters for various iron(IV) species.

Iron(IV) Species [a]	S	δ (mm/s)	ΔE_Q (mm/s)
[(tris(2-pyridylmethyl)amine)Fe=O]$^{2+}$ [23]	2	0.01(2)	0.92(2)
[(L_4)FeCl]$^-$	2	-0.04(2)	0.89(2)
[(Me_4-cyclam)Fe=O(CH_3CN)]$^{2+}$ [24]	1	0.17(1)	1.24(1)
[(cyclam-acetato)Fe=O]$^+$ [3b]	1	0.01	1.39
(L_4)Fe(CN^tBu)$_2$	1	-0.04	3.38
[(cyclam-acetato)Fe(N_3)]$^{2+}$	1	0.11	1.92
(triamido(amine))Fe(CN)	1	-0.22	3.28
[$PhBP^{iPr}_3$]Fe(H)$_3$(PMe_3)	0	0.01(2)	0.58(2)
[$PhBP^{iPr}_3$]Fe≡N	0	-0.34(1)	6.01(1)
[$PhBP^{MeCy}_3$]Fe≡N (**3.9**)	0	-0.34(1)	6.01(1)

[a] References are provided in the main text if not given here.

There are only a handful of iron complexes with uncharacteristically large quadrupole splittings, but even so, their values are on the order of 4 mm/s.[25] Most of these examples are of the type [(porphyrin)FeX]$^-$ (where X = halide, OR, OCOR) that feature a five-coordinate iron(II) center (Figure 3.5).[25a-e] One exception is an iron(II) complex of a macrocyclic tetrathioether ligand reported by Silver and coworkers.[25f] Although two iodides are located in the axial positions above and below the square plane of the ligand, the Fe-I bond distances are extremely long at 2.8896(2) Å. Moreover, the complex shows no proclivity to bind CH_3CN. Based on these observations, Silver and coworkers report this species as an unusual example of square-planar iron(II).

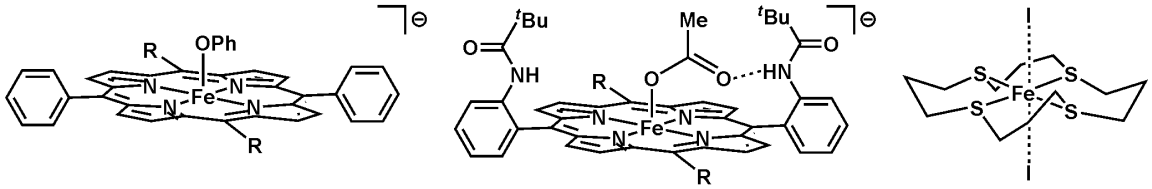

Figure 3.5. Representative examples of iron complexes with unusually large quadrupole splittings.

Comparing the quadrupole splittings featured in Figure 3.5, the ΔE_Q value of 6.0 mm/s observed for the iron(IV) nitrides is the largest quadrupole splitting reported for any iron complex. One explanation for the exceptionally large quadrupole splitting is due to a very aspherical nuclear electron density. The disposition of the trianionic nitride and the monoanionic borate moiety on the pseudo three-fold axis creates a highly anisotropic

field gradient. The charges strongly interact with the iron nucleus and thus are responsible for the large asymmetry.

Compound **3.9** is stable at -50 ºC for at least 8 h. However, it is thermally unstable and begins to decompose at -40 ºC. The decomposition of **3.9** was monitored by NMR spectroscopy at -40 ºC. After 10 h, an ill-defined mixture of several species was observed. The decreased thermal stability of **3.9** relative to [PhBP$^{i\mathrm{Pr}}_3$]Fe(N) was surprising, as the bulkier ligand was expected to hinder dimerization. However, subsequent coordination chemistry of [PhBP$^{\mathrm{CH2Cy}}_3$]Fe reveals that the methylcyclohexyl groups impart more flexibility than the isopropyl groups, and hence, may allow dimerization processes to occur more readily (*vide infra*). Moreover, other decomposition pathyways may also be operative and need to be considered.

3.3 Conclusions

The family of [BP$_3$] ligands has been expanded with these recent additions of the [PhBP$^{\mathrm{ter}}_3$] and [PhBP$^{\mathrm{CH2Cy}}_3$] ligands. The electron-releasing character of these ligands is similar to the known [PhBP$_3$] and [PhBP$^{i\mathrm{Pr}}_3$] ligands, respectively. However, the steric properties of the ligands have been dramatically altered. For example, the formation of [PhBP$^{\mathrm{CH2Cy}}_3$]Fe(N) occurs readily at significantly lower temperatures relative to [PhBP$^{i\mathrm{Pr}}_3$]Fe(N) (-50 vs. 0 ºC) . The Mössbauer spectrum for this species exhibits a low isomer shift value, which is consistent with a high valent iron center and reveals a distinctively large quadrupole splitting, due to the asymmetry of the electric field. The influence of sterics on the coordination chemistry of iron will continue to be investigated for both these ligands.

3.4 Experimental Section

3.4.1 General Considerations

General considerations are outlined in Section 2.4.1. ^{15}N NMR data were collected on an Inova 500 MHz spectrometer, and chemical shifts were referenced to neat CH_3NO_2 at δ 380.23. Solution magnetic moments were measured using the Evans method.[26]

3.4.2 Electrochemical Measurements

Electrochemical data was acquired as described in Section 2.4.4.

3.4.3 Mössbauer Measurements

Mössbauer samples were loaded under nitrogen into Delrin Mössbauer cups or quartz tubes and shipped in a liquid nitrogen chilled transport dewar to Carnegie Mellon for analysis. Mössbauer spectra were recorded on a constant acceleration instrument with an available temperature range of 1.5 to 200 K. An applied magnetic field of 45 mT was applied to the samples. Isomer shifts are reported relative to Fe metal at 298 K. Least-square fitting of quadrupole doublet is performed with the WMOSS software package (WEB Research, Edina, MN).

3.4.4 Starting Materials and Reagents

All reagents were purchased from commercial vendors and used without further purification unless otherwise noted. $TlPF_6$ and $FeCl_2$ were dried *in vacuo* for 12 to 24 h to remove moisture. Tmeda and $CyCH_2Br$ were degassed and stored over 3 Å sieves. Terphenyl bromide was prepared according to literature protocol.[27]

3.4.5 Synthesis of Compounds

Synthesis of MeP(*m*-terphenyl)$_2$, 3.1: Terphenyl bromide (8.909 g, 28.81 mmol) was dissolved in 75 mL THF and chilled at -78 °C. ^{n}BuLi (1.6 M in hexanes, 28.8 mmol) was added dropwise over 15 min, and the reaction was stirred cold for 1 h. In the meantime, $MePCl_2$ (1.736 g, 14.4 mmol) was diluted in 15 mL toluene and chilled at -78 °C. After the 1 h, the phosphine was added dropwise over 10 min to the reaction, which was then stirred for 15 h, slowly warming to rt. The reaction solution was concentrated *in vacuo*. The resulting residue was washed profusely with petroleum ether, giving cream-colored solids (5.765 g, 84% yield). ^{1}H NMR (C_6D_6, 300 MHz) δ 7.92 (d, J = 6.9 Hz, 4H), 7.73 (s, 2H), 7.46 (d, J = 6.9 Hz, 8H), 7.18 – 7.11 (m, 12H), 1.56 (d, $^2J_{H\text{-}P}$ = 3.6 Hz, 3H, CH_3P). ^{31}P NMR (C_6D_6, 121 MHz) δ -24.2 ppm.

Synthesis of (*m*-terphenyl)$_2$PCH$_2$Li(tmeda), 3.2: In a 125 mL Erlenmeyer flask with a stir bar, MeP(*m*-terphenyl)$_2$ (2.986 g, 6.25 mmol**)** was dissolved in Et_2O and chilled to 0 °C. ^{s}BuLi (1.4 M in cyclohexane, 7.50 mmol) was mixed with tmeda (0.800 g, 6.88 mmol) and chilled to 0 °C. The mixture ^{s}BuLi/tmeda was added to the phosphine, and the reaction was slowly warmed to rt. The next day, brown-yellow solids had precipitated. They were collected on a frit and washed profusely with 5:1 petroleum ether/Et_2O and then with minimal Et_2O to obtain yellow solids (1.227 g, 33% yield). ^{1}H NMR (THF-d_8, 300 MHz) δ 7.92 (d, J = 6.9 Hz, 4H), 7.63 (d, J = 6.9 Hz, 8H), 7.50 (s, 2H), 7.35 (t, J = 6.9 Hz, 8H), 7.23 (t, J = 6.9 Hz, 4H), 2.30 (4H), 2.15 (12H), -0.14 (d, $^2J_{H\text{-}P}$ = 3.3 Hz, 2H). ^{31}P NMR (THF, 121 MHz) δ -4.08 ppm.

Synthesis of [PhBP$^{ter}_3$]Tl, 3.3: In a vial, (*m*-terphenyl)$_2$PCH$_2$Li(tmeda) (365.0 mg, 608.6 μmol) was dissolved in 10 mL Et_2O and then chilled to -90 °C**.** $PhBCl_2$ (33.2 mg, 202.8 μmol) was diluted in 3 mL toluene and added dropwise to the solution. The

reaction was stirred for 18 h, slowly warming to rt to give [$PhBP^{ter}_3$]Li(tmeda) (^{31}P NMR: -10.4 ppm). The reaction was concentrated under reduced pressure to dryness and then suspended in 10 mL EtOH. $TlPF_6$ (61.1 mg, 202.8 mmol) was added, and the reaction was stirred for 12 h. The white solids in the reaction were collected on a frit and washed with EtOH and petroleum ether (237.1 mg, 62% yield). ^{1}H NMR (C_6D_6, 500 MHz) δ 8.65 (br d, J = 6.0 Hz, 2H), 7.88 – 7.85 (m, 13H), 7.68 (t, J = 6.0 Hz, 2H), 7.16 – 7.13 (overlaps with solvent peak, ~18H), 7.00 – 6.99 (overlapping s, 48H), 2.77 (br, 6H). ^{31}P NMR (C_6D_6, 121 MHz) δ 21.7 ppm (d, $J_{Tl\text{-}P}$ = 4870 Hz).

Synthesis of $MeP(CH_2Cy)_2$, 3.4: Magnesium coils (6.15 g, 0.253 mol) were placed inside a 250 mL Erlenmeyer flask with a long stir bar. THF (25 mL) and a crystal of I_2 were added, and the mixture was stirred until the yellow iodine color had faded. More THF (75 mL) was then added. $CyCH_2Br$ (19.67 g, 0.111 mol) in 25 mL THF was added slowly dropwise over 30 min. The reaction was then heated gently at 50 °C for 5 h. After cooling, the Gringard solution was filtered through a frit lined with Celite and titrated (86.6 mmol, 78% yield). $MePCl_2$ (5.04 g, 42.2 mmol) was diluted in 50 mL Et_2O in a 500 mL Erlenmeyer flask at -90 ºC. $CyCH_2MgBr$ solution in THF was added dropwise, and the reaction was stirred for 14 h, slowly warming to rt. The reaction was then filtered through a frit lined with Celite, quenched with 2 mL MeOH, and concentrated under reduced pressure. Upon precipitation of more salts, the filtrate was again filtered through a frit lined with Celite and concentrated under reduced pressure to a thick oil. The oil was flashed through a 2″-silica plug to obtain a pale-yellow oil (9.94 g, 98% yield). ^{1}H NMR (C_6D_6, 300 MHz) δ 1.87 (br dd, J = 27.6 & 11.7 Hz, 4H), 1.69 – 1.58 (m, 6H), 1.43 – 1.09 (m, 12H), 1.04 – 0.93 (m, 4H), 0.88 (d, $^2J_{H\text{-}P}$ = 2.1 Hz, 3H,

C*H*$_3$P). ^{13}C NMR ($CDCl_3$, 75 MHz) δ 41.0 (d, *J* = 13.4 Hz), 36.5 (d, *J* = 12.5 Hz), 36.0 (d, *J* = 8.8 Hz), 35.6 (d, *J* = 9.7 Hz), 27.2, 14.2 (d, *J* = 16.8 Hz). ^{31}P NMR (C_6D_6, 121 MHz) δ -53.5 ppm.

Synthesis of $LiCH_2P(CH_2Cy)_2$, 3.5: To a 250 mL schlenk RB flask, ^{t}BuLi (1.7 M, 86.7 mmol) was added and concentrated under reduced pressure to dryness. $MeP(CH_2Cy)_2$ (17.48 g, 72.7 mmol) was added to the flask. The reaction was heated under sparging N_2 at 90 °C for 4 h or until the reaction had completely solidified. The cream-colored solids were collected on a frit, mashed into a fine powder, and washed profusely with petroleum ether. (16.79 g, 94% yield). ^{31}P NMR (THF, 121 MHz) δ -28.5 ppm.

Synthesis of $[PhBP^{CH_2Cy}_3]Tl$, 3.6: $LiCH_2P(CH_2Cy)_2$ (5.0690 g, 20.58 mmol) and tmeda (2.3916 g, 20.58 mmol) were stirred together in 100 mL Et_2O and then chilled to -90 °C. $PhBCl_2$ (1.1232 g, 6.86 mmol) was diluted in 10 mL toluene and added dropwise to the solution. The reaction was stirred for 12 h, slowly warming to rt. The reaction was then filtered through a glass frit with Celite, and $TlPF_6$ (2.4706 g, 6.86 mmol) was added to the filtrate. The reaction was stirred for 12 h or until $[PhBP^{CH_2Cy}_3]Li(tmeda)$ was consumed (^{31}P NMR: -37.6 ppm). The reaction was again filtered through a Celite-lined glass frit and and concentrated under reduced pressure to a goo. The goo was then taken up in minimal petroleum ether (~ 15 mL) to precipitate solids. The solids were collected on a frit, washed sparingly with petroleum ether, and washed profusely with CH_3CN. The petroleum ether filtrate can be stored at -30 °C to obtain a second crop of white solids that are similarly washed. (1.748 g, 25% yield). ^{1}H NMR (C_6D_6, 500 MHz) δ 7.92 (br d, *J* = 6.0 Hz, 2H, H$_o$ of Ph), 7.54 (t, *J* = 7.0 Hz, 2H, H$_m$ of Ph), 7.28 (t, *J* = 7.0 Hz, 1H, H$_p$ of

Ph), 2.00 – 1.91 (m, 18 H), 1.75 – 1.58 (m, 30H), 1.31 – 1.23 (m, 18H), 1.18 – 1.02 (m, 18H). ^{13}C NMR (C_6D_6, 500 MHz) δ 168.1 (br m, C_{ipso} of BPh), 132.2, 127.8, 124.0, 39.5 (br), 36.7 (br), 36.0, 27.1, 27.0, 22.1 (m, *C*H_2PPh_2). ^{31}P NMR (C_6D_6, 121 MHz) δ 9.8 ppm (d, $J_{Tl\text{-}P}$ = 5570 Hz). Anal. Calcd. for $C_{51}H_{89}BP_3Tl$: C 60.63; H 8.88; N 0. Found: C 60.38; H 8.59; N <0.05.

Synthesis of [PhBP$^{ter}_3$]FeCl, 3.7: [PhBP$^{ter}_3$]Tl (0.473 g, 0.262 mmol) and $FeCl_2$ (0.034 g, 0.262 mmol) were stirred in 8 mL THF for 12 h. The reaction was filtered through Celite and concentrated under reduced pressure to dryness. The yellow residue was mashed to a fine powder and washed with petroleum ether and Et_2O (0.369 g, 83%). Single crystals suitable for X-ray diffraction can be grown from vapor diffusion of petroleum ether into a benzene solution. ^{1}H NMR (C_6D_6, 300 MHz) δ 206.09, 40.86, 19.79, 18.35, 7.09, 6.94, 3.62, -14.32, -37.29**.** Evans Method (C_6D_6): 5.32 B.M. Anal. Calcd. for $C_{117}H_{89}BClFeP_3$: C 83.15; H 5.31; N 0. Found: C 80.64; H 5.39; N <0.05.

Synthesis of [PhBP$^{CH_2Cy}_3$]FeCl, 3.8: [PhBP$^{CH_2Cy}_3$]Tl (3.2328, 3.20 mmol) and $FeCl_2$ (0.4138 g, 3.20 mmol) were stirred in 25 mL THF for 12 h. The reaction was filtered through Celite and concentrated under reduced pressure to dryness. The residue is then extracted with 1:1 THF/petroleum ether, filtered through glass wool, and concentrated to dryness. The yellow solids are washed profusely with petroleum ether (2.4509 g, 85%). Single crystals suitable for X-ray diffraction can be grown from an Et_2O solution at -25 °C. ^{1}H NMR (C_6D_6, 300 MHz) δ 186.64, 40.16, 19.63, 18.05, 2.24, 1.22, 0.24, -0.39, -5.01, -5.62, -13.24, -16.37, -28.80, -39.98**.** Evans method (C_6D_6): 5.39 B.M. Anal. Calcd. for $C_{51}H_{89}BClFeP_3$: C 68.27; H 10.00; N 0. Found: C 67.89; H 9.77; N <0.05.

Synthesis of [PhBP$^{CH_2Cy}_3$]Fe(N), 3.9: [PhBP$^{CH_2Cy}_3$]FeCl (47.1 mg, 52.5 μmol) was dissolved in 0.5 mL THF and chilled at -90 ºC. Li(dbabh) (13.4 mg, 67.3 μmol) was dissolved in 0.5 mL THF and chilled with a stir bar at -90 ºC. The frozen solution of [PhBP$^{CH_2Cy}_3$]FeCl was thawed, immediately added to Li(dbabh) at -90 ºC, and rinsed with 0.5 mL of chilled THF. The reaction mixture was then warmed to -50 ºC (octane/dry ice bath) and stirred at this temperature for 4 to 5 h. The solution of [PhBP$^{CH_2Cy}_3$]Fe(N) is stable at -50 ºC for 8 h, but begins to decompose at -40 ºC within 2 h. Besides anthracene, trace solvents, and residual Li(dbabh), [PhBP$^{CH_2Cy}_3$]Fe(N) was observed cleanly by ^{1}H NMR spectroscopy in THF-d_8. ^{1}H NMR (THF-d_8, 202 MHz, -50 ºC) δ 6.94 (br, 2H), 6.88 (t, J = 6.5 Hz, 2H), 6.74 (t, J = 6.5 Hz, 1H), 2.14 – 1.67 (m, 42H), 1.40 – 1.12 (m, 30H), 0.92 – 0.78 (m, 12H). ^{31}P NMR (THF, 202 MHz, -50 ºC) δ 52.29. ^{15}N NMR (THF, 51 MHz, -50 ºC) δ 929.4.

3.4.6 X-ray Experimental Data

Crystallographic procedures are outlined in Section 2.4.8. Crystallographic data are summarized in Table 3.3.

Table 3.3. Crystallographic data for [PhBP$^{ter}_3$]FeCl, **3.7**; [PhBP$^{CH_2Cy}_3$]FeCl, **3.8**.

	3.7	**3.8**
Chemical formula	$C_{117}H_{89}BClFeP_3$	$C_{51}H_{87}BClFeP_3$
Fw	1689.90	895.23
T (K)	100	100
λ (Å)	0.71073	0.71073
a (Å)	13.578(1)	11.2119(4)
b (Å)	15.882(1)	37.519(1)
c (Å)	22.286(2)	13.2026(5)
α (°)	75.466(2)	90
β (°)	80.341(2)	112.318(1)
γ (°)	77.215(2)	90
V (Å^3)	4504.5(6)	5137.7(3)
space group	*P-1*	*P2$_1$/c*
Z	2	4
D_{calc} (g/cm^3)	1.246	1.157
μ (cm^{-1})	3.0	4.71
R1, wR2[a] ($I > 2\sigma(I)$)	0.0862, 0.1962	0.0694, 0.1094

[a] $R1 = \Sigma||F_o| - |F_c||/\Sigma|F_o|$, $wR2 = \{\Sigma[w(F_o^2 - F_c^2)^2]/\Sigma[w(F_o^2)^2]\}^{1/2}$

References Cited

[1] Mehn, M. P.; Peters, J. C. *J. Inorg. Biochem.* **2006**, *100*, 634.

2 (a) Wagner, W.-D.; Nakamoto, K. *J. Am. Chem. Soc.* **1989**, *111*, 1590. (b) Wagner, W.-D.; Nakamoto, K. *J. Am. Chem. Soc.* **1988**, *110*, 4044.

3 (a) Meyer, K.; Bill, E.; Mienert, T.; Weyhermüller, K.; Wieghardt, K. *J. Am. Chem. Soc.* **1999**, *121*, 4859. (b) Grapperhaus, C. A.; Meinert, B.; Bill, E.; Weyhermüller, K.; Wieghardt, K. *Inorg. Chem.* **2000**, *39*, 5306.

4 Aliaga-Alcalde, N.; George, S. D.-B.; Meinert, B.; Bill, E.; Weyhermüller, K.; Wieghardt, K.; Neese, F. *Angew. Chem. Int. Ed.* **2005**, *44*, 2908.

5 Mindiola, D. J.; Cummins, C. C. *Angew. Chem. Int. Ed.* **1998**, *37*, 945.

6 Betley, T. A.; Peters, J. C. *J. Am. Chem. Soc.* **2004**, *126*, 6252.

7 Betley, T. A. **2005** (Ph.D. Thesis), California Institute of Technology.

8 Betley, T. A.; Peters, J. C. *J. Am. Chem. Soc.* **2003**, *125*, 10782.

9 Shapiro, I. R.; Jenkins, D. M.; Thomas, J. C.; Day, M. W.; Peters, J. C. *Chem. Commun.* **2001**, 2152.

10 Niyomura, O.; Tokunaga, M.; Obora, Y.; Iwasawa, T.; Tsuji, Y. *Angew. Chem. Int. Ed.* **2003**, *42*, 1287.

11 Betley, T. A.; Peters, J. C. *Inorg. Chem.* **2003**, *42*, 5074.

12 Karsch, H. H.; Schmidbaur, H. *Z. Naturforsch.* **1977**, *32b*, 762.

13 (a) MacBeth, C. E.; Thomas, J. C.; Betley, T. A. *Inorg. Chem.* **2004**, *43*, 4645. (b) Brown, S. D.; Peters, J. C. *J. Am. Chem. Soc.* **2003**, *125*, 332.

14 Brown, S. D.; Peters, J. C. *J. Am. Chem. Soc.* **2005**, *127*, 1913.

15 The 25% impurity may have formed during the shipping of the sample. NMR analysis of the sample batch prior to shipping showed clean formation of nitride. EPR and magnetic analysis of the nitride sample (**3.9**) showed insignificant amounts of paramagnetic species.

16 (a) Meunier, B. *Chem. Rev.* **1992**, *92*, 1411. (b) Costas, M.; Mehn, M. P.; Jensen, M. P.; Que Jr., L. *Chem. Rev.* **2004**, *104*, 939.

17 Berry, J. F.; Bill, E.; Bothe, E.; Weyhermüller, T.; Wieghardt, K. *J. Am. Chem. Soc.* **2005**, *127*, 11550.

18 Collins, T. J.; Fox, B. G.; Hu, Z. G.; Kostka, K. L.; Münck, E.; Rickard, C. E. F.; Wright, L. J. *J. Am. Chem. Soc.* **1992**, *114*, 8724.

19 Kostka, K. L.; Fox, B. G.; Hendrich, M. P.; Collins, T. J.; Rickard, C. E. F.; Wright, L. J.; Münck, E. *J. Am. Chem. Soc.* **1993**, *115*, 6746.

20 Bower, B. K.; Tennet, H. G. *J. Am. Chem. Soc.* **1972**, *94*, 2512.

21 Cummins, C. C.; Schrock, R. R. *Inorg. Chem.* **1994**, *33*, 395.

22 Daida, E. J.; Peters, J. C. *Inorg. Chem.* **2004**, *43*, 7474.

23 Lim, M. H.; Rohde, J.-U.; Stubna, A.; Bukowski, M. R.; Costas, M.; Ho, R. Y. N.; Münck, E.; Nam, W.; Que, Jr., L. *PNAS* **2003**, *100*, 3665.

24 Rohde, J.-U.; In, J.-H.; Lim, M. H.; Brennessel, W. W.; Bukowski, M. R.; Stubna, A.; Münck, E.; Nam, W.; Que, Jr., L. *Science* **2003**, *299*, 1037.

25 (a) Shaevitz, B. A.; Lang, G.; Reed, C. A. *Inorg. Chem.* **1988**, *27*, 4607. (b) Silver, J.; Lukas, B. *Inorg. Chim. Acta* **1983**, *80*, 107. (c) Shappacher, M.; Richard, L.; Weiss, R.; Montiel-Toya, R.; Gouser, U. *Inorg. Chim. Acta* **1983**, *78*, L9. (d) Silver, J.; Lukas, B.; Al-Jaff, G. *Inorg. Chim. Acta* **1984**, *91*, 125. (e)

Narsi, H.; Fischer, J.; Weiss, R.; Bill, E.; Trautwein, A. *J. Am. Chem. Soc.* **1987**, *109*, 2549. (f) Hughes, D. L.; Jimenez-Tenorio, M.; Leigh, G. J.; Houlton, A.; Silver, J. *J. Chem. Soc., Dalton Trans.* **1992**, 2033.

26 (a) Sur, S. K. *J. Magn. Reson.* **1989**, *82,* 169. (b) Evans, D. F. *J. Chem. Soc.* **1959**, 2003.

27 Du, C.-J. F.; Hart, H.; Ng, K.-K. D. *J. Org. Chem.* **1986**, *51*, 3162.

Chapter 4: Reduction of Carbon Dioxide and Organic Molecules by a Masked Iron(I) Species

4.1 Introduction

Metalloenzymes use iron to mediate the reduction of protons, dioxygen, and perhaps even dinitrogen.[1] Thus, the preparation and study of iron complexes for effecting small molecule activation is important.[2] Additionally, the discovery of iron-based catalysts for functionalizing small molecules would be useful to the chemical industry since iron is an abundant metal. Low-coordinate iron complexes that feature a reduced metal center are particularly interesting because they are very reactive. For example, such species have been shown to bind and activate dinitrogen.[3] In this report, we present a masked iron(I) species, which readily binds and reduces small substrates by one or two electron(s) per metal. The iron chemistry reported here features the tris(phosphino)borate ligand, $[PhB(CH_2P(CH_2Cy)_2)_3]^-$ ($[PhBP^{CH_2Cy}_3]$), where the phosphine substituents are methylcyclohexyl groups. This masked iron(I) species exhibits unusual redox chemistry with substrates such as benzene, azobenzene, and CO_2.

4.2 Results and Discussion

4.2.1 Synthesis and Characterization of the Iron(I) Species, $[PhBP^{CH_2Cy}_3]Fe$

Previously, low-coordinate iron(I) complexes have been stabilized with capping π-acceptors such as CO, N_2, or phosphines.[3,4] For example, $[PhBP^{iPr}_3]FeCl$ undergoes reduction with Na/Hg under a dinitrogen atmosphere to yield the red-brown dinitrogen-bridged dimer $\{[PhBP^{iPr}_3]Fe\}_2(\mu\text{-}N_2)$.[3a] As noted previously, the cyclic voltammogram of $[PhBP^{CH_2Cy}_3]FeCl$ (**3.8**) contains a reversible Fe(II)/Fe(I) potential (-1.94 V) that is similar to that observed for $[PhBP^{iPr}_3]FeCl$ (-2.03 V, THF/[TBA][PF_6], vs. Fc/Fc^+).[5] However, when **3.8** is reduced with Na/Hg in THF, an intense lime-green solution results.

This dramatic difference in color suggests a different reaction outcome with Na/Hg for [PhBP$^{CH_2Cy}{}_3$]FeCl (**3.8**) versus [PhBP$^{iPr}{}_3$]FeCl.

To date, we have not been able to obtain suitable crystals of this product for an X-ray diffraction study. However, combustion analysis of the isolated product is consistent with "[PhBP$^{CH_2Cy}{}_3$]Fe" (**4.1**, Equation 4.1). Complex **4.1** exhibits complicated NMR solution spectra in THF-d_8. For example, the ^{31}P NMR spectrum features a single broad peak at -25 ppm, which is sensitive to temperature (Figure 4.1). This peak shifts from -29 ppm to 4 ppm when the temperature is varied from 60 to -60 °C, respectively. The ^{1}H NMR spectrum contains broad peaks ranging from -7 to 72 ppm, which also shift with changes in temperature. Collectively, the NMR spectroscopic data suggest that both a diamagnetic and a paramagnetic species are present in solution and are rapidly exchanging on the NMR timescale.

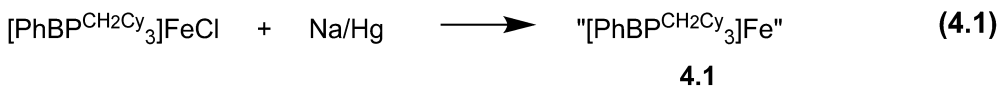

(4.1)

The paramagnetic component of **4.1** was studied by EPR spectroscopy. In THF glass at 4K, compound **4.1** exhibits an axial EPR signal that is consistent with a low-spin S = ½ ground state (Figure 4.2). Hyperfine structure due to the ^{31}P nucleus (I = 1/2) is evident in the g = 2 signal, which shows coupling to the three phosphorus atoms of the ligand with A ~ 37 G.

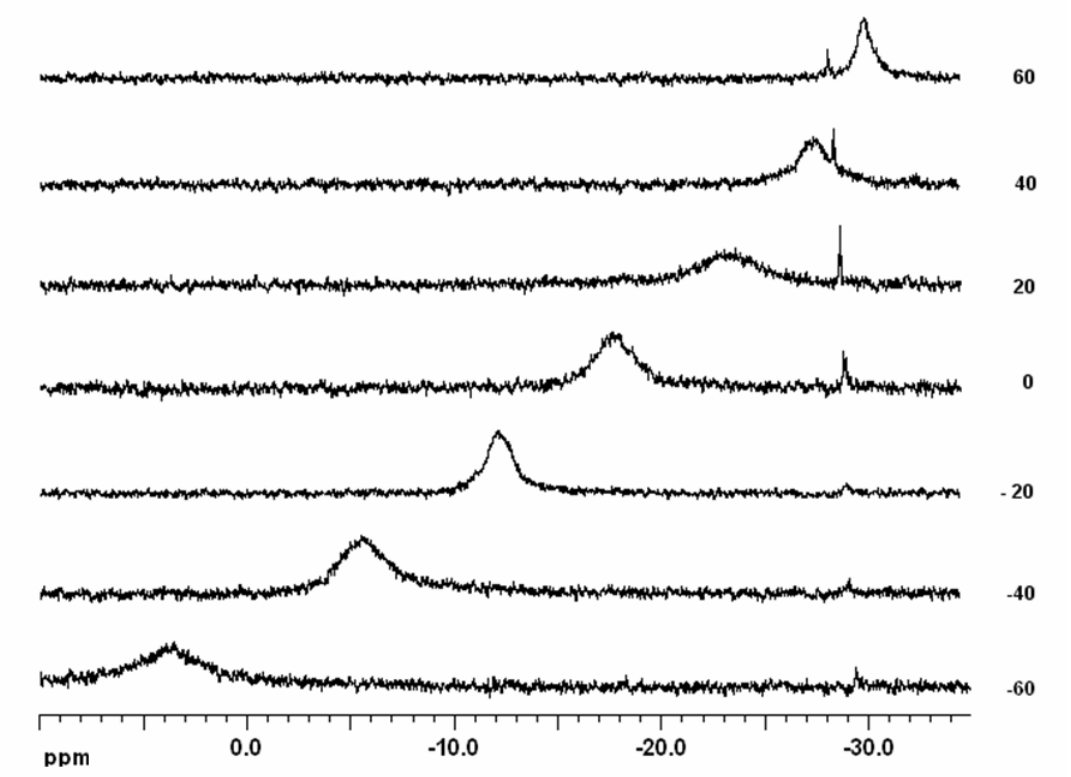

Figure 4.1. ^{31}P VT NMR spectra of "[PhBP$^{CH_2Cy}{}_3$]Fe" (**4.1**) in d_8-THF from -60 to 60 ºC. A small peak attributed to an unknown impurity is visible at -29 ppm and does not shift with temperature. Temperatures are indicated on the right in ºC.

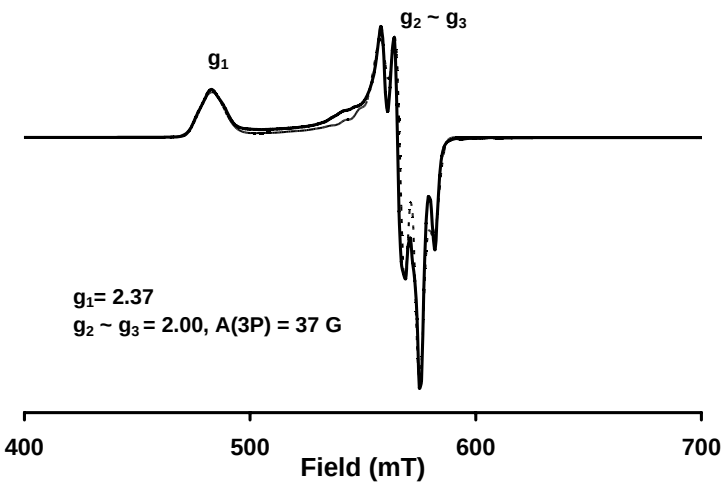

Figure 4.2. EPR spectrum of "[PhBP$^{CH_2Cy}{}_3$]Fe" (**4.1**) (THF glass at 4K, 9.37 GHz, X-band). Values for *g* and *A* were estimated by simulating the EPR spectrum (shown in dashed lines).

Possible identities for the paramagnetic and diamagnetic components of **4.1** are presented in Figure 4.3. The paramagnetic species is proposed to be either (**A**) an iron(I) complex with two THF ligands, or (**B**) an iron(III) hydride, wherein one of the cyclohexyl C-H bonds of the ligand has been cyclometalated by the iron center. Both species could give rise to the observed $S = ½$ signal in the EPR spectrum. The diamagnetic component of **4.1**, which gives rise to the single peak in the ^{31}P NMR spectrum, is proposed to be (**C**) an iron(I) dimer with a Fe-Fe bond or (**D**) an iron(III) bridging-hydride dimer. The dimers **C** and **D** can interconvert with species **A** and **B**, respectively. Moreover, **B** can also equillibrate with **C** by reversible cyclometalation and subsequent dimerization. Thus far, circumstantial evidence favors the assignment of the paramagnetic component as the cyclometalated Fe(III) species **B**. The data that implicate a metal hydride consist of an IR stretch at 2058 cm^{-1} (KBr pellet)[6] and the formation of

$CHCl_3$ (~ 40%, detected by ^1H and ^{13}C NMR) upon reaction of **4.1** with one equivalent of CCl_4 in d_8-THF.[7]

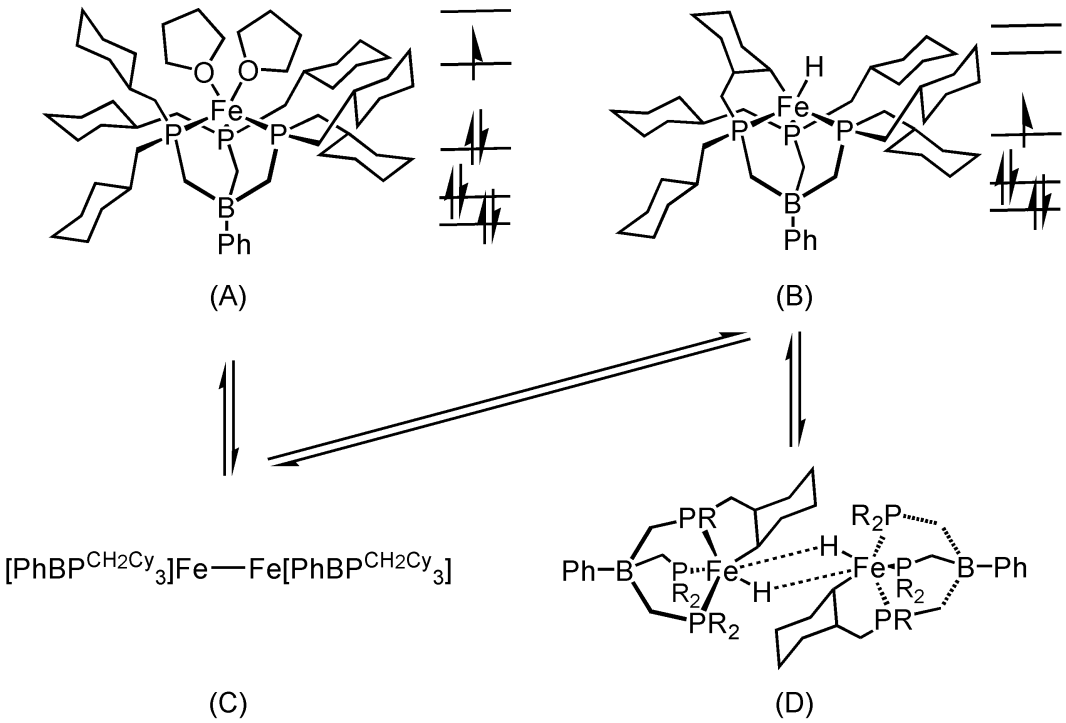

Figure 4.3. Possible structures and their interconversions for the components of "[PhBP^{CH_2Cy_3}]Fe" (**4.1**) in THF solution.

4.2.2 General Reactivity Studies

To gain further insight into the nature of **4.1**, we turned to studying its reactivity. Addition of PMe_3 to a THF solution of **4.1** cleanly generates the phosphine-capped iron(I) complex, [PhBP^{CH_2Cy_3}]Fe(PMe_3) (**4.2**, Equation 4.2).[4a-c] The solid-state structure of this compound is shown in Figure 4.4. Compound **4.1** reacts with one equivalent of 1-adamantyl azide to give the iron(III) imide, [PhBP^{CH_2Cy_3}]Fe≡NAd (**4.3**), quantitatively based on the ^1H NMR spectrum of the crude reaction (Equation 4.3).[8] This latter reaction

presumably occurs by oxidative nitrene transfer coupled to an Fe(I)/Fe(III) redox event.[3a, 4a-b] These two reactions strongly suggest that **4.1** is either a *bona fide* iron(I) species or an effective iron(I) precursor.

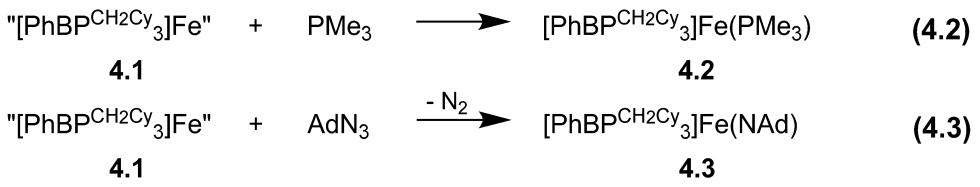

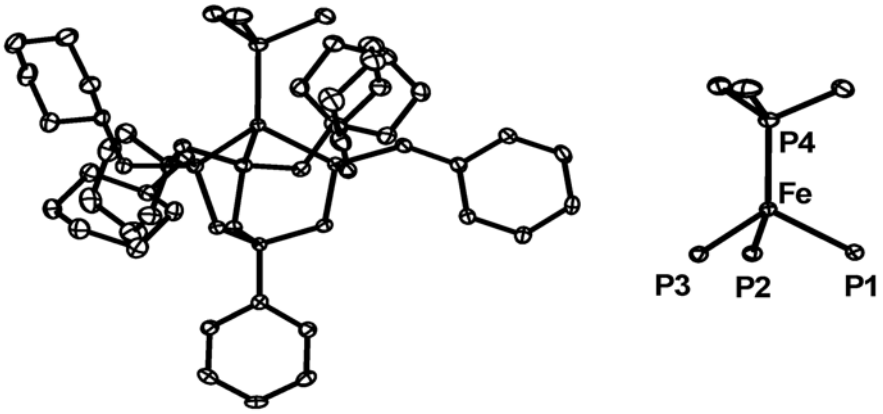

Figure 4.4. 50% thermal ellipsoid representation of [PhBP$^{CH_2Cy}_3$]Fe(PMe$_3$) (**4.2**). Hydrogen atoms have been omitted for clarity. To the right, only core atoms are shown. Selected bond distances (Å) and angles (deg.): Fe–P1 2.2876(6), Fe–P2 2.2999(5), Fe–P3 2.3058(5), Fe–P4 2.2871(6), P1–Fe–P2 97.71(2), P2–Fe–P3 97.33(2), P1–Fe–P3 97.21(2), P4–Fe–P1 119.10(2), P4–Fe–P2 119.23(2), P4–Fe–P3 121.13(2).

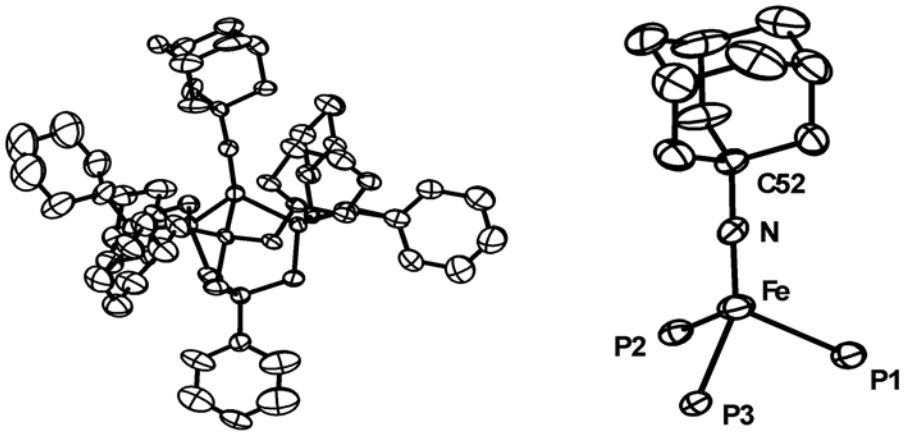

Figure 4.5. 50% thermal ellipsoid representation of [PhBP$^{CH_2Cy}{}_3$]Fe(NAd) (**4.3**) showing only the more populated position of the disordered [PhBP$^{CH_2Cy}{}_3$] ligand. Hydrogen atoms have been omitted for clarity. To the right, only the core atoms are shown. Selected bond distances (Å) and angles (deg.): Fe–P1 2.252(2), Fe–P2 2.151(2), Fe–P3 2.264(2), Fe–N 1.622(4), P1–Fe–P2 92.90(8), P2–Fe–P3 91.27(7), P1–Fe–P3 91.80(7), C52–N–Fe 176.3(4).

Compound **4.1** is extremely reactive and rapidly binds benzene even in trace amounts. Addition of benzene to **4.1** cleanly produces the dimer {[PhBP$^{CH_2Cy}{}_3$]Fe}$_2$(μ-η^3:η^3-C_6H_6) (**4.4**, Equation 4.4). The solid-state structure of **4.4**, which is shown in Figure 4.6, is a rare example of the *anti*-η^3(1,2,3):η^3(4,5,6) coordination mode for bridged arenes.[9,10] The C-C bond distances of the bound benzene are on average 1.396(5) Å. The other three examples of this bonding motif have average C-C bond distances of 1.41(2), 1.429(2), and 1.445(1) Å. The ^{1}H NMR spectrum of **4.4** contains a single broad peak at 4.91 ppm for the six equivalent protons of the bound benzene. One resonance structure for **4.4** localizes the electrons on the bridged benzene, which is formally

reduced by two electrons. This results in two allyl subunits that are each coordinated to an oxidized iron(II) center.

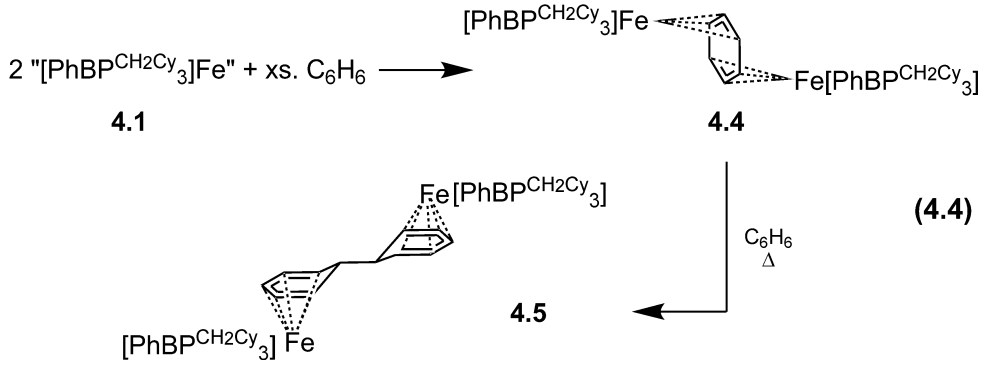

Compound **4.4** is thermally unstable and decomposes slowly at 25 °C to give the 18-electron species, {[PhBP^{CH_2Cy_3}]Fe}$_2$(μ-η^5:η^5-6,6'-bicyclohexadienyl) (**4.5**, Equation 4.4). The formation of **4.5** presumably results from the dimerization of an intermediate species, "[PhBP^{CH_2Cy_3}]Fe(C_6H_6)," which can undergo radical C-C bond coupling between the two benzene ligands. Similar reductive coupling of arenes has been previously observed in the related CpFe(η^6-arene) systems.[11]

The lability of the bound benzene in **4.4** was probed by heating a C_6D_6 solution of **4.4** to 50 ºC. By ^{31}P NMR spectroscopy, full conversion to compound **4.5** was observed after 8 h. By ^{1}H NMR spectroscopy, the proton signals for the bound bicyclohexadienyl group were completely absent, indicating that benzene exchange had occurred. As a control, a C_6D_6 solution of **4.5** was heated at 100 ºC for 72 h. The proton signals for the bicyclohexadienyl group are retained, confirming that benzene exchange occurs in **4.4** and that the newly formed C-C bond in **4.5** is not reversibly cleaved.

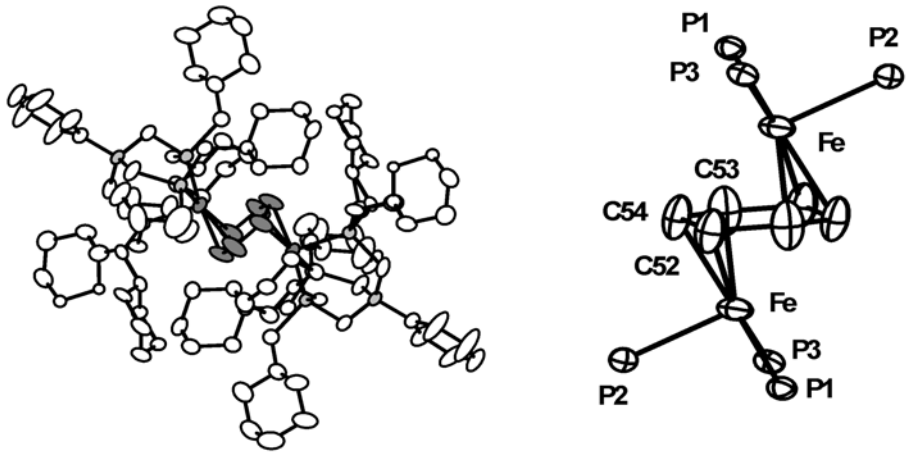

Figure 4.6. 50% thermal ellipsoid representation of $\{[PhBP^{CH_2Cy}{}_3]Fe\}_2(\mu\text{-}\eta^3\text{:}\eta^3\text{-}C_6H_6)$ (**4.4**) showing only the more populated position of the disordered $[PhBP^{CH_2Cy}{}_3]$ ligand. Hydrogen atoms have been omitted for clarity. To the right, only the core atoms are shown. Selected bond distances (Å) and angles (deg.): Fe–P1 2.234(2), Fe–P2 2.231(2), Fe–P3 2.268(2), Fe–C52 2.219(5), Fe–C54 2.169(5), Fe–C53 2.234(5), C54–C52 1.420(5), C53–C54 1.385(5), C52–C53′ 1.384(5), P1–Fe–P2 90.48(6), P2–Fe–P3 88.10(6), P1–Fe–P3 91.38(6).

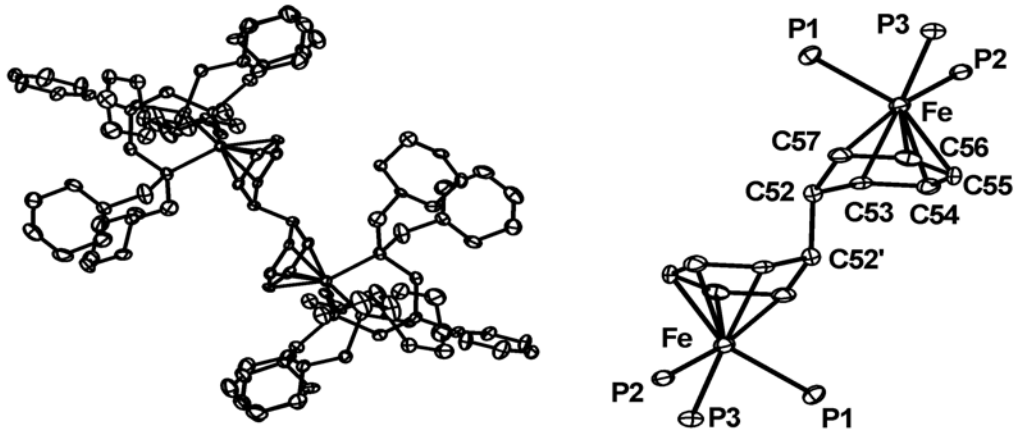

Figure 4.7. 50% thermal ellipsoid representation of {[PhBP$^{CH_2Cy}{}_3$]Fe}$_2$(μ-η^5:η^5-6,6'-bicyclohexadienyl) (**4.5**) showing only the more populated position of the disordered [PhBP$^{CH_2Cy}{}_3$] ligand. Hydrogen atoms have been omitted for clarity. To the right, only the core atoms are shown. Selected bond distances (Å) and angles (deg.): Fe–P1 2.262(2), Fe–P2 2.235(2), Fe–P3 2.250(2), Fe–C53 2.174(5), Fe–C54 2.100(5), Fe–C55 2.112(5), Fe–C56 2.103(5), Fe–C57 2.188(5), C52–C52′ 1.56(1), P1–Fe–P2 91.31(6), P2–Fe–P3 88.70(6), P1–Fe–P3 89.74(6).

We were interested in investigating the effectiveness of **4.1** to reductively cleave bonds in organic substrates such as diazenes. When azobenzene was added to the iron(I) species, the reaction turned dark red within minutes. The product was isolated and identified as the dimer $\{[PhBP^{CH_2Cy_3}]Fe\}_2(\mu\text{-}\eta^5\text{:}\eta^5\text{-azobenzene})$ (**4.6**), whose solid-state structure features an unprecedented binding mode for diazenes (Equation 4.5, Figure 4.8). Instead of coordinating to the nitrogen atom(s), the iron(II) centers coordinate the aryl rings in η^5-fashion as seen in compound **4.5**. Interestingly, the N-N bond distance is 1.340(9) Å, which is significantly reduced compared to free azobenzene, wherein the N=N bond distance is 1.23 Å.[12] The selectivity exhibited by **4.1** to coordinate the aryl ring rather than the nitrogen atom(s) likely derives from the stability of the 18-electron metal center with an η^5-capping ligand.[13]

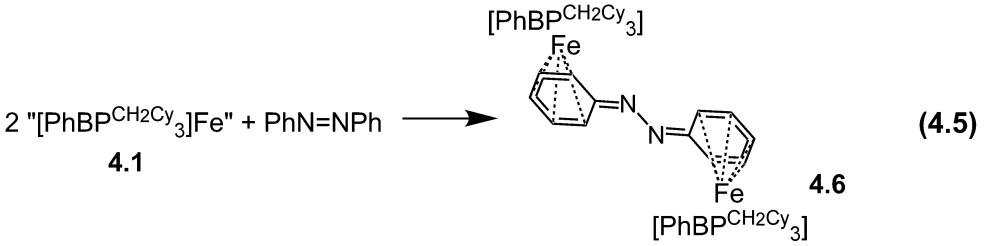

(4.5)

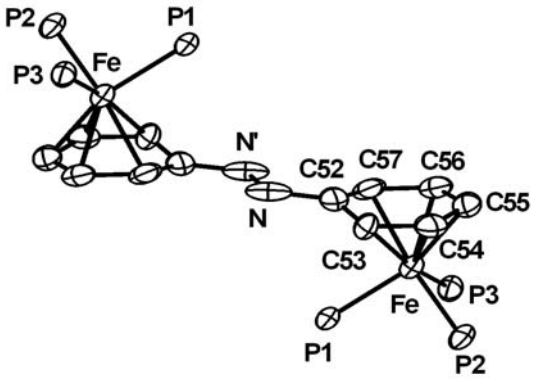

Figure 4.8. 50% thermal ellipsoid representation of $\{[PhBP^{CH_2Cy}{}_3]Fe\}_2(\mu\text{-}\eta^5\text{:}\eta^5\text{-}$azobenzene) (**4.6**) showing only the core atoms. Hydrogen atoms have been omitted for clarity. Selected bond distances (Å) and angles (deg.): Fe–P1 2.250(2), Fe–P2 2.230(2), Fe–P3 2.246(2), Fe–C53 2.238(6), Fe–C54 2.094(6), Fe–C55 2.089(6), Fe–C56 2.110(6), Fe–C57 2.212(6), N–C52 1.429(8), N–N′ 1.340(9), P1–Fe–P2 89.83(7), P2–Fe–P3 88.54(7), P1–Fe–P3 89.39(7).

4.2.3 Reduction of CO_2

Carbon dioxide is a pollutant and the single largest contributor to global warming. However, the abundance of CO_2 also makes it an ideal feedstock for chemical and fuel production. Utilization of CO_2 is thus highly desirable with the additional benefit of mitigating the greenhouse effect.

The activation of CO_2 is not trivial due to the molecule's thermodynamic and kinetic stability.[14] One paradigm of CO_2 activation mimics the action of the enzyme acetyl-CoA synthase/CO dehydrogenase, which reduces CO_2 to CO and water.[15] The formation of CO necessitates the splitting of a C=O bond, and such bond cleavage has been effected by several metal complexes.[16] On the other hand, the coupling of two CO_2 molecules is an intriguing case of CO_2 fixation. Though the coupling reaction occurs

readily via electrochemical reduction, examples of well-defined metal complexes that mediate the reductive coupling of CO_2 are rare.[17] This is somewhat surprising given the numerous examples of metal oxalato species.

Complex **4.1** reacts rapidly with one atmosphere of CO_2 as indicated by an immediate though subtle color change from lime-green to pine-green. Inspection of the reaction *in situ* by ^{1}H NMR spectroscopy reveals a clean mixture of two products, a diamagnetic and a paramagnetic species. The major product (75%, 5 equiv. CO_2, 3 runs) is diamagnetic with a single peak in the ^{31}P NMR spectrum at 51.9 ppm and an IR stretch at 1644 cm^{-1} (KBr, THF). X-ray diffraction studies of dark blue-green plates grown from benzene/petroleum ether revealed this product to be $\{[PhBP^{CH_2Cy}{}_3]Fe\}_2(\mu\text{-CO})(\mu\text{-O})$ (**4.7**, Equation 4.6). The solid-state structure for **4.7** is shown in Figure 4.9. Overall, two iron(I) centers effect the 2-electron reductive cleavage of CO_2. Though several metal complexes reductively cleave CO_2, the $\{L_nM\}_2(\mu\text{-O}{:}\mu\text{-CO})$ structure is unique.[18] The Fe-Fe bond distance is quite short at 2.39(4) Å, suggesting a direct metal-metal interaction. However, natural bond order analysis of a similar compound (*vide infra*) did not reveal any metal-metal bond. The iron centers can be assigned as low-spin iron(II), which is consistent with the diamagnetism of **4.7** and the lack of low-energy d-d transitions. The NIR spectrum for **4.7** looks remarkably similar to that for $[PhBP^{CH_2Cy}{}_3]Fe(NAd)$ (**4.3**) except that it is red-shifted (Figure 4.10).[19]

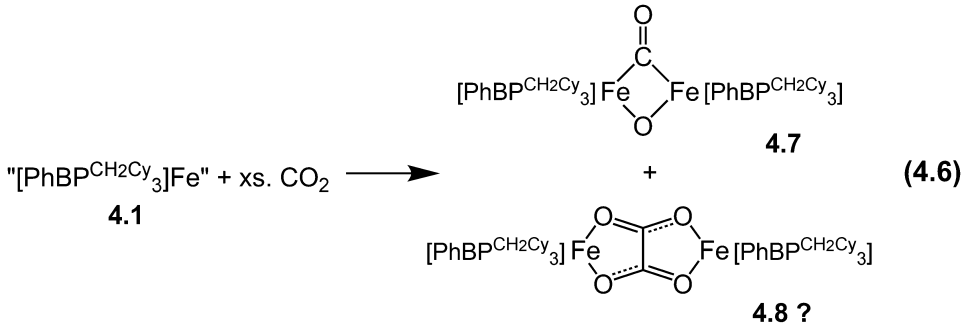

(4.6)

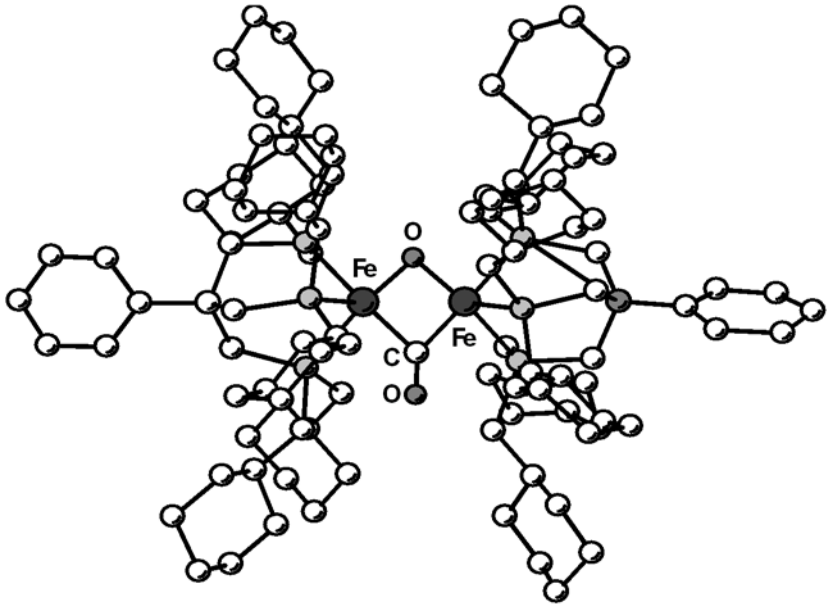

Figure 4.9. Ball and stick representation of $\{[PhBP^{CH_2Cy_3}]Fe\}_2(\mu\text{-CO})(\mu\text{-O})$ (**4.7**). Hydrogen atoms have been omitted for clarity. The quality of the X-ray data is insufficient for a detailed discussion of the bond distances and angles.

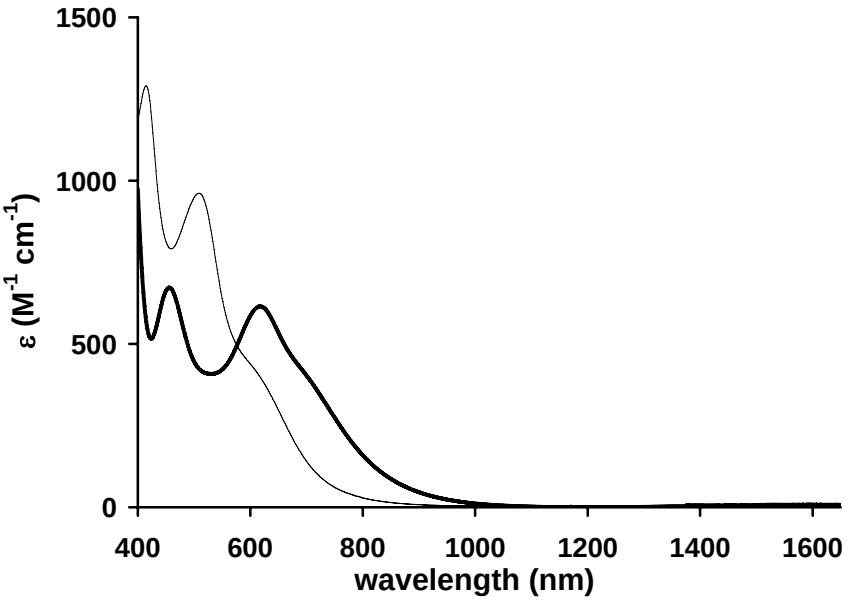

Figure 4.10. NIR data for {[PhBP$^{CH2Cy}_3$]Fe}$_2$(μ-CO)(μ-O) (**4.7**), shown in bold. For comparison, the NIR data for [PhBP$^{CH2Cy}_3$]Fe(NAd) (**4.3**) is also shown (in trace).

In an attempt to generate water via reduction of CO_2, compound **4.7** was reacted with various H sources. However, compound **4.7** showed essentially no reactivity with 1 equiv. of [H(Et_2O)][B(3,5-(CF_3)$_2$(C_6H_3))$_4$], K($HBEt_3$), or $HSnBu_3$ at rt in THF. Though the lack of reactivity was disappointing, it is consistent with the DFT study of an analogous compound, wherein the methylcyclohexyl groups have been simplified to methyls. The bridged CO and the bridged oxide ligands do not participate in either the HOMO or the LUMO. The HOMO is localized mainly on one borate phenyl ring whereas the LUMO involves Fe-P σ^* interactions (Figure 4.11). Compound **4.7** also did not react with $Me_3SiSiMe_3$ or pinBBpin up to 45 °C in benzene.

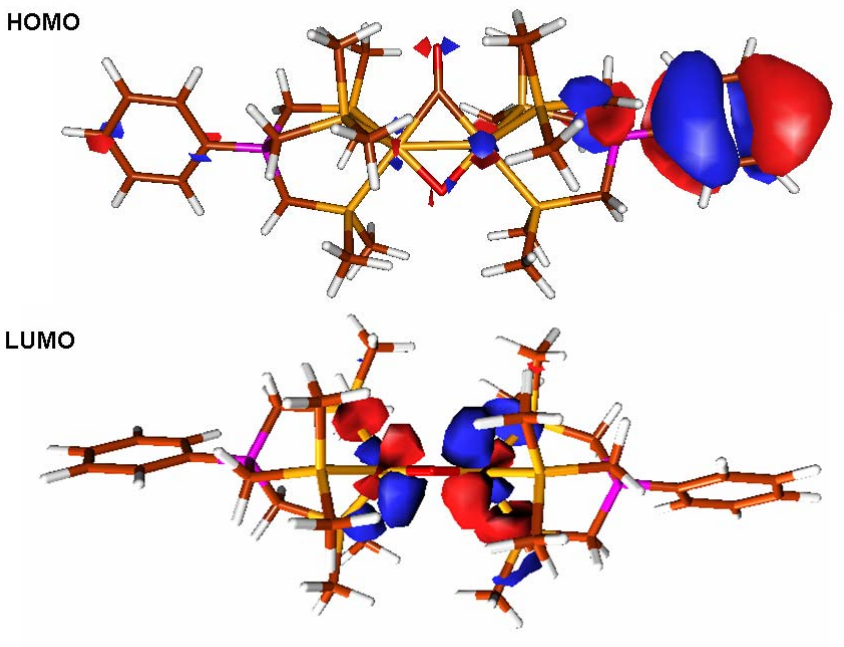

Figure 4.11. HOMO and LUMO diagrams for the hypothetical $\{[PhBP^{Me}_3]Fe\}_2(\mu\text{-}CO)(\mu\text{-}O)$, an analogue of **4.7**.

In addition to **4.7**, a minor product is consistently observed, irrespective of the reaction conditions. Varying the stoichiometry of CO_2 from 0.5 to 20 equivalents or the temperature from -78 to 25 °C did not significantly affect the yield of the minor species (~20 to 30% crude yield). Notably, the minor component does not appear to convert to **4.7** (and *vice versa*) upon heating, under excess CO_2, or with the addition of **4.1**.[20] Due to the low yields of this minor component, we have not been able to establish its identity unequivocally. However, ^{1}H NMR and IR spectra of the clean mixture indicate that the minor component is paramagnetic and is characterized by a stretch at 1730 cm^{-1}, respectively. Dichroic blue-green/yellow crystals were grown from THF/petroleum ether at -30 ºC that reveal a bridging-oxalato iron dimer, $\{[PhBP^{CH_2Cy}_3]Fe\}_2(\mu\text{-}\eta^2\text{:}\eta^2\text{-}O_2CCO_2)$

(**4.8**, Equation 4.6). Presumably, **4.8** arises from the bimolecular coupling of the radical species, "[PhBP$^{CH_2Cy}{}_3$]Fe$(CO_2)^{\bullet -}$" (Figure 4.12). Efforts are currently underway to prepare **4.8** by a different route and in sufficient quantity for complete characterization. Thus far, there are five reports of metal complexes mediating the reductive coupling of CO_2 to oxalate. However, most of these examples require several additives. The only example of a well-defined metal precursor is the samarium complex, $(C_5Me_5)_2Sm(THF)_2$, which reacts cleanly with CO_2 at rt to generate the bridging-oxalato species, $\{(C_5Me_5)_2Sm\}_2(\mu\text{-}\eta^2\text{:}\eta^2\text{-}O_2CCO_2)$, in >90% yield.[17a]

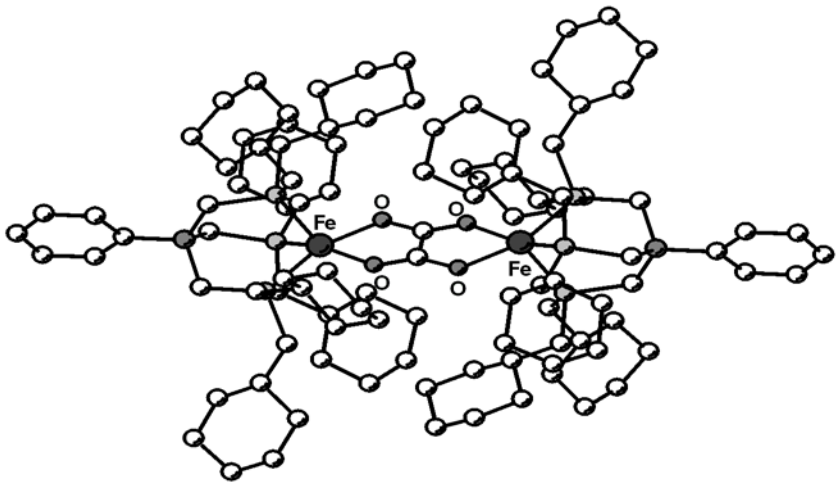

Figure 4.12. Ball and stick representation of $\{$[PhBP$^{CH_2Cy}{}_3$]Fe$\}_2(\mu\text{-}\eta^2\text{:}\eta^2\text{-}O_2CCO_2)$ (**4.8**). Hydrogen atoms have been omitted for clarity. The quality of the X-ray data is insufficient for a detailed discussion of the bond distances and angles.

4.3 Conclusions

In summary, compound **4.1** provides an interesting entry into the reduction chemistry of small organic molecules. Notably, **4.1** does not require a capping π-acceptor for stabilization. However, it may otherwise be stabilized as a masked iron(I) species. One plausible scenario is that **4.1** is an iron(III) species that results from cyclometalation of a ligand C-H bond. Reversible C-H bond elimination would unmask a naked iron(I) species that is highly reactive. The interesting redox chemistry exhibited by **4.1** includes bimolecular coupling of benzene and perhaps CO_2, as well as activating the N=N bond in azobenzene and the C=O bond in CO_2. Ongoing studies will focus on elucidating the exact nature of compound **4.1** and extending its redox chemistry to other small molecules.

4.4 Experimental Section

4.4.1 General Considerations

General considerations are outlined in Section 2.4.1. UV/vis/NIR measurements were taken in THF on a Cary 500 UV/vis/NIR spectrophotometer using a 0.1 cm quartz cell with a Teflon stopper, and the data for **4.1**, **4.2**, and **4.4** are shown below.

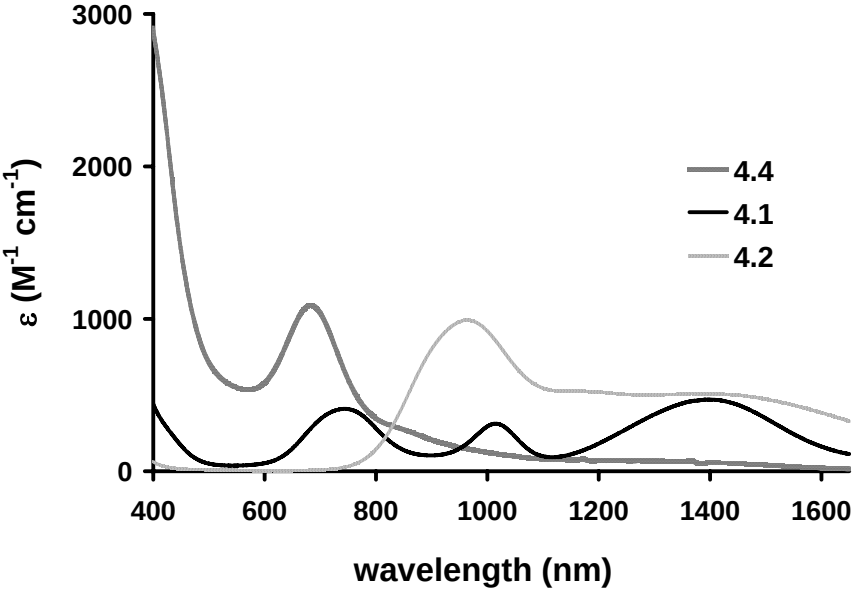

Figure 4.13. NIR data for "[PhBP$^{CH_2Cy}{}_3$]Fe" (**4.1**), [PhBP$^{CH_2Cy}{}_3$]Fe(PMe$_3$) (**4.2**), and {[PhBP$^{CH_2Cy}{}_3$]Fe}$_2$(μ-η^3:η^3-C$_6$H$_6$) (**4.4**) in THF.

4.4.2 EPR Measurements

EPR data was acquired as outlined in Section 2.4.3. Solution spectra were acquired in tetrahydrofuran. EPR simulations were performed with the program WINEPR *SimFonia* (Version 1.25, Bruker Analytische Messtechnik GmbH).

4.4.3 DFT Calculations

All calculations were performed using the Jaguar 5.0 program package (Jaguar 5.0, Schrodinger, LLC, Portland, OR, 2002). The calculation employed the hybrid DFT functional B3LYP[21] and the basis set LACVP**. Input coordinates for the geometry optimization were derived from the solid-state structure of {[PhBP$^{CH_2Cy}{}_3$]Fe}$_2$(μ-CO)(μ-O) (**4.7**). The ligand [PhBP$^{CH_2Cy}{}_3$] was simplified by replacing the methylcyclohexyl groups with methyl groups. Spin states and molecular charges were imposed. The

calculations were spin unrestricted, and no symmetry constraints were used. The default values for geometry and SCF iteration cutoffs were used, and the structure converged under these criteria. MO pictures were generated using Molden.

4.4.4 Starting Materials and Reagents

The reagents, azobenzene and 1-adamantyl azide, were dried *in vacuo* at rt under high vacuum for 24 h. The reagent PMe_3 was dried by storing over 3Å sieves. Sodium amalgam was used immediately after preparation or stored at -30 °C and used within a few days. All other reagents were purchased from commercial vendors and used without further purification unless otherwise stated.

4.4.5 Synthesis of Compounds

Synthesis of "[PhBP$^{CH_2Cy}{}_3$]Fe," 4.1: A 10 mL THF solution of [PhBP$^{CH_2Cy}{}_3$]FeCl (0.1119 g, 0.125 mmol) was stirred over sodium amalgam (0.4911 wt %, 0.131 mmol) with a glass stir bar for 2 to 3 h. The intense lime-green solution was then filtered through a Celite plug followed by a glass wool pipette. The solution can be used for reactions without further purification. Vapor diffusion of petroleum ether into the THF solution gave dark-green solids that tested analytically pure by combustion analysis. The ^{1}H NMR spectrum (THF-d_8) contains broad peaks ranging from -7 to 72 ppm. The peaks do not sharpen fully upon warming to 60 ºC (Figure 4.14). ^{31}P NMR (121 MHz, THF-d_8): δ -25.4 (br) ppm. UV-vis (THF) λ_{max}, nm (ε, M^{-1} cm^{-1}): 1395 (470), 1016 (310), 743 (410). Anal. Calcd. for $C_{51}H_{89}BFeP_3$: C 71.08; H 10.41; N 0. Found: C 71.09; H 10.25; N 0.06.

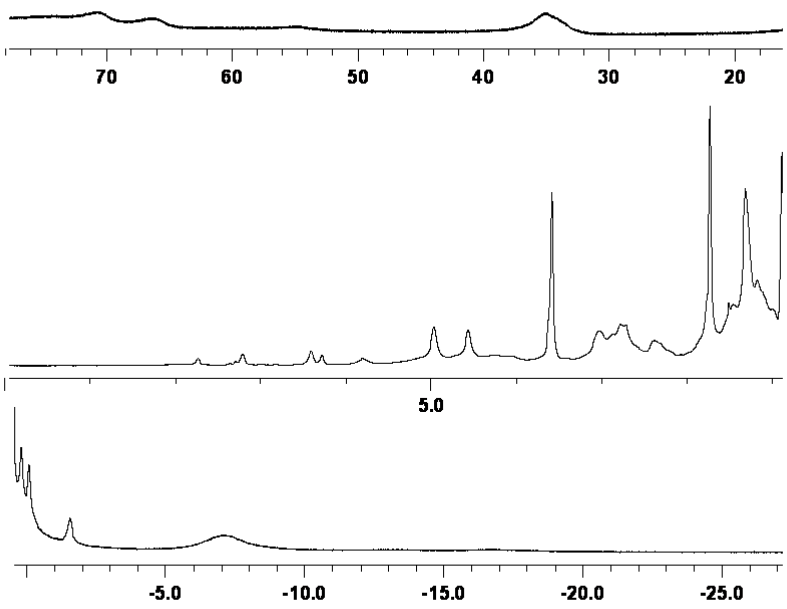

Figure 4.14. ^{1}H NMR spectrum for "[PhBP$^{CH2Cy}{}_3$]Fe" (**4.1**) in THF-d_8 at 60 °C.

Synthesis of [PhBP$^{CH_2Cy}{}_3$]Fe(PMe$_3$), 4.2: To an 8 mL THF solution of **4.1** (0.1114 mmol), PMe_3 (17.6 mL, 0.1649 mmol) was added via microsyringe, and within a few min, the solution changed from an intense lime-green to a pale-brown color. After stirring for 6 h, the solution was concentrated under reduced pressure to dryness. The residue was extracted with petroleum ether to give a pale-yellow-green solution, which formed pale-green crystals when stored at -30 °C (0.763 g, 72% yield). ^{1}H NMR (C_6D_6, 300 MHz) δ 87.74, 65.16, 11.56, 8.80, 8.72, 7.78, 4.97, 3.64, 3.14, 2.50, 1.20, 0.88, -11.59. UV-vis (C_6H_6) λ_{max}, nm (ε, M^{-1} cm^{-1}): 963 (990). Anal. Calcd. for $C_{51}H_{89}BFeP_4$: C 69.15; H 10.53; N 0. Found: C 69.65; H 10.68; N 0.14.

Synthesis of [PhBP$^{CH_2Cy}{}_3$]Fe(NAd), 4.3: To a 15 mL THF solution of **4.1** (0.2092 mmol), 1-adamantyl azide (35.6 mg, 0.2090 mmol) was added. Gradually, the

reaction mixture turned from intense lime-green to burgundy. After 8 h, the solution was concentrated under reduced pressure to dryness, washed with petroleum ether (4 x 2 mL), and extracted with benzene. Vapor diffusion of petroleum ether into the benzene solution afforded dark-maroon crystals. (192.0 mg, 91% yield) ^{1}H NMR (C_6D_6, 300 MHz) δ 24.38, 17.80, 12.98, 9.59, 8.99, 6.32, 5.00, 3.99, 1.59, 1.29, 0.89, 0.63, -0.06, -0.23, -0.55, -0.91, -1.18, -8.58, -12.25. UV-vis (C_6H_6) λ_{max}, nm (ε, M^{-1} cm^{-1}): 509 (960), 415 (1290). Anal. Calcd. for $C_{61}H_{104}BFeNP_3$: C 72.46; H 10.37; N 1.39. Found: C 72.23; H 10.09; N 1.52.

Synthesis of {[PhBP$^{CH_2Cy}{}_3$]Fe}$_2$(μ-η^3:η^3-C$_6$H$_6$), 4.4: A 10 mL THF solution of **4.1** (0.1847 mmol) was concentrated under reduced pressure to dryness. The green residue was washed liberally with petroleum ether, extracted with benzene, filtered through a glass wool pipette, and concentrated under reduced pressure to a dark-green powder (0.155 g, 93% yield). Single crystals suitable for X-ray diffraction can be grown from toluene/petroleum ether at -30 °C. ^{1}H NMR (C_6D_6, 300 MHz) δ 8.05 (d, *J* = 6.9 Hz, 4H), 7.55 (t, *J* = 6.9 Hz, 4H), 7.27 (t, *J* = 6.9 Hz, 2H), 4.91 (br s, 6H, C_6H_6), 2.27 (br d, *J* = 10.2 Hz, 12H), 2.01 – 1.94 (m, 36H), 1.80 – 1.60 (m, 48H), 1.29 – 1.21 (m, 72H). ^{31}P NMR (C_6D_6, 121 MHz) δ 45.5 ppm. UV-vis (C_6H_6) λ_{max}, nm (ε, M^{-1} cm^{-1}): 681 (1090). Anal. Calcd. for $C_{108}H_{184}B_2Fe_2P_6$: C 71.99; H 10.29; N 0. Found: C 71.74; H 10.01; N <0.05.

Synthesis of {[PhBP$^{CH_2Cy}{}_3$]Fe}$_2$(μ-η^5:η^5-1,1'-bicyclohexadienyl), 4.5: A 5 mL benzene solution of {[PhBP$^{CH_2Cy}{}_3$]Fe}$_2$(μ-η^3:η^3-C$_6$H$_6$) (0.050 g, 27.75 μmol) was heated at 60 °C for 20 h. The solution changed from dark green to yellow with precipitation of orange microcrystals. Solids were collected and washed with petroleum ether, benzene,

and THF (0.048 g, 92% yield). Single crystals suitable for X-ray diffraction can be grown from vapor diffusion of petroleum ether into a dichloromethane solution. ^{1}H NMR ($CDCl_3$, 500 MHz) δ 7.33 (m, 4H, H_o of Ph), 7.20 (t, 4H, J = 7.5 Hz, H_m of Ph), 7.02 (t, 2H, J = 7.0 Hz, H_p of Ph), 5.48 (br s, 2H), 4.15 (br s, 4H), 2.12 (br s, 4H), 1.99 (m, 12H), 1.75 – 1.66 (84H), 1.32 – 0.97 (62 H), 0.38 (br s, 12H). ^{31}P NMR (121 MHz, CD_2Cl_2): δ 44.5 (br) ppm. Anal. Calcd. for $C_{114}H_{190}B_2Fe_2P_6$: C 72.84; H 10.19; N 0. Found: C 72.65; H 9.77; N <0.05.

Synthesis of {[PhBP$^{CH_2Cy}_3$]Fe}$_2$(μ-η^5:η^5-azobenzene), 4.6: To a 10 mL THF solution of **4.1** (0.1178 mmol), azobenzene (10.7 mg, 58.72 μmol) was added, and the reaction was stirred for 2 h. The dark-red solution was concentrated under reduced pressure to dryness. The residue was washed with petroleum ether and ether until the washings were nearly colorless. The residue was then extracted with dichloromethane and concentrated under reduced pressure to a red powder (0.075 g, 38% yield). Single crystals suitable for X-ray diffraction can be grown from vapor diffusion of diethyl ether into a dichloromethane solution. ^{1}H NMR (300 MHz, $CDCl_3$): δ 7.31 (d, J = 7.5 Hz, 2H), 7.20 (t, J = 7.5 Hz, 2H), 7.04 (t, J = 7.5 Hz, 1H), 5.07 (m, 2H), 4.91 (m, 1H), 4.45 (m, 1H), 3.81 (m, 1H), 1.97 (m, 6H), 1.73 - 1.67 (m, 42H), 1.26 – 0.99 (m, 30H), 0.44 (br s, 6H). ^{13}C NMR (126 MHz, CD_2Cl_2): δ 166.2 (br), 146.4, 131.8, 127.3, 123.5, 96.0, 95.0, 69.6, 68.1, 62.2, 43.1 (br), 40.9 (br), 37.6, 37.2, 37.1, 36.0, 35.8, 27.4, 27.1, 26.8, 14.3 (br m). ^{31}P NMR (121 MHz, CD_2Cl_2): δ 47.4 ppm. UV-vis (C_6H_6) λ_{max}, nm (ε, M^{-1} cm^{-1}): 465 (19,700), 324 (35,500). Anal. Calcd. for $C_{114}H_{188}B_2Fe_2N_2P_6$: C 71.84; H 9.94; N 1.47. Found: C 72.13; H 9.64; N 1.57.

Synthesis of {[PhBP$^{CH_2Cy}{}_3$]Fe}$_2$(μ-CO)(μ-O), 4.7: A 10 mL THF solution of **4.1** (0.1116 mmol) was transferred to a 50 mL reaction vessel with a Teflon-plug stopcock. The solution was cooled in LN_2 and evacuated under high vacuum. The vessel was then attached to a gas bulb (55.39 cm^3). Gaseous CO_2 (18.5 cm Hg, 0.5578 mmol) was added to the bulb and condensed into the vessel using LN_2. After exposure to the gas, the vessel was sealed, and the reaction was allowed to warm to rt. Immediately, the solution turned to an even darker green color. After 6 h, the solution was evacuated under reduced pressure to dryness. The residue was extracted with benzene. Vapor diffusion of petroleum ether into the benzene solution afforded dark-green crystals (0.0641 g, 65% yield). ^{1}H NMR (500 MHz, C_6D_6): δ 8.07 (d, *J* = 7.0 Hz, 4H), 7.54 (t, *J* = 7.0 Hz, 4H), 7.24 (t, *J* = 7.0 Hz, 2H), 2.31 (m, 12H), 2.05 (m, 24H), 1.95 (m, 24H), 1.71 (m, 24H), 1.56 (d, *J* = 10.5 Hz, 12H), 1.37 – 1.15 (m, 72H). ^{13}C NMR (126 MHz, C_6D_6): δ 164.6 (br), 132.1, 127.9, 124.7, 40.9, 37.8, 37.4, 36.2, 27.4, 27.0, 26.8, 13.8 (br m). ^{31}P NMR (121 MHz, THF): δ 51.9 ppm. IR(THF, KBr): ν(CO) = 1644 cm^{-1}. Anal. Calcd. for $C_{103}H_{178}B_2Fe_2O_2P_6$: C 69.98; H 10.15; N 0. Found: C 69.84; H 9.92; N 0.06.

4.4.6 X-ray Experimental Data

Crystallographic procedures are described in Section 2.4.8. Crystallographic data are summarized in Table 4.1 and Table 4.2.

Table 4.1. Crystallographic data for [PhBP$^{CH_2Cy}{}_3$]Fe(PMe$_3$), **4.2**; [PhBP$^{CH_2Cy}{}_3$]Fe(NAd), **4.3**; and {[PhBP$^{CH_2Cy}{}_3$]Fe}$_2$(μ-η^3:η^3-C$_6$H$_6$), **4.4**.

	4.2	**4.3**	**4.4**·3C$_7$H$_8$
chemical formula	$C_{54}H_{98}BFeP_4$	$C_{61}H_{104}BFeNP_3$	$C_{108}H_{184}B_2FeP_6 \cdot 3C_7H_8$
fw	937.86	1011.02	2078.09
T (K)	100	100	100
λ (Å)	0.71073	0.71073	0.71073
a (Å)	11.2942(6)	11.2710(7)	16.800(2)
b (Å)	14.0920(8)	23.084(2)	19.670(2)
c (Å)	17.6538(9)	22.384(1)	18.232(2)
α (°)	89.927(1)	90	90
β (°)	87.422(1)	91.328(1)	105.532(2)
γ (°)	80.938(1)	90	90
V (Å^3)	2771.8(3)	5822.3(6)	5805(1)
space group	*P-1*	*P2$_1$/c*	*P2$_1$/n*
Z	2	4	2
D_{calc} (g/cm^3)	1.124	1.153	1.189
μ (cm^{-1})	4.20	3.79	3.81
R1, wR2[a] ($I > 2\sigma(I)$)	0.0465, 0.0804	0.1185, 0.1912	0.0774, 0.1410

[a] $R1 = \Sigma||F_o| - |F_c||/\Sigma|F_o|$, $wR2 = \{\Sigma[w(F_o^2 - F_c^2)^2]/\Sigma[w(F_o^2)^2]\}^{1/2}$

Table 4.2. Crystallographic data for {[PhBP$^{CH_2Cy}{}_3$]Fe}$_2$(μ-η^5:η^5-1,1'-bicyclohexadienyl), **4.5**; and {[PhBP$^{CH_2Cy}{}_3$]Fe}$_2$(μ-η^5:η^5-azobenzene), **4.6**.

	4.5·$C_4H_{10}O$	**4.6**·$2C_4H_8O$ ·$2CH_2Cl_2$
chemical formula	$C_{114}H_{190}B_2Fe_2P_6$ ·$C_4H_{10}O$	$C_{114}H_{188}B_2N_2Fe_2P_6$ ·$2C_4H_8O$·$2CH_2Cl_2$
fw	1959.97	2219.86
T (K)	100	100
λ (Å)	0.71073	0.71073
a (Å)	28.3106(8)	22.734(2)
b (Å)	21.7915(7)	15.576(1)
c (Å)	22.8536(7)	17.650(1)
α (°)	90	90
β (°)	126.572(1)	110.288(1)
γ (°)	90	90
V (Å^3)	11323.1(6)	5862.1(7)
space group	*C2/c*	*P2$_1$/c*
Z	4	2
D_{calc} (g/cm^3)	1.150	1.258
μ (cm^{-1})	3.88	4.72
R1, wR2[a] ($I > 2\sigma(I)$)	0.1005, 0.1613	0.1009, 0.1747

[a] $R1 = \Sigma||F_o| - |F_c||/\Sigma|F_o|$, $wR2 = \{\Sigma[w(F_o^2 - F_c^2)^2]/\Sigma[w(F_o^2)^2]\}^{1/2}$

References Cited

1 (a) Nicolet, Y.; Lemon, B. J.; Fontecilla-Camps, J. C.; Peters, J. W. *Trends Biochem. Sci.* **2000**, *25*, 138. (b) Peters, J. W. *Curr. Opin. Struct. Biol.* **1999**, *9*, 670. (c) Peters, J. W.; Lanzilotta, W.N.; Lemon, B. J.; Seefeldt, L. C. *Science* **1998**, *282*, 1853. (d) Nicolet, Y.; Piras, C.; Legrand, P.; Hatchikian, E. C.; Fontecilla-Camps, J. C. *Structure* **1999**, *7*, 13. (e) Que Jr., L.; Watanabe Y. *Science* **2001**, *292*, 651. (f) Burgess, B. K. *Chem. Rev.* **1990**, *90*, 1377.

2 (a) Sellmann, D. *ACS Symposium Series* **1993**, *535*, 332. (b) Chong, D.; Georgakaki, I. P.; Mejia-Rodriguez, R.; Sanabria-Chinchilla, J.; Soriaga, M. P.; Darensbourg, M. Y. *Dalton Trans.* **2003**, 4158. (c) Mejia-Rodriguez, R.; Chong, D.; Reibenspies, J. H.; Soriaga, M. P.; Darensbourg, M. Y. *J. Am. Chem. Soc.* **2004**, *126*, 12004. (d) Razavet, M.; Borg, S. J.; George, S. J.; Best, S. P.; Fairhurst, S. A.; Pickett, C. *J. Chem. Commun.* **2002**, 700. (e) Nicolet, Y.; de Lacey, A. L.; Vernede, X.; Fernandez, V. M.; Hatchikian, E. C.; Fontecilla-Camps, J. C. *J. Am. Chem. Soc.* **2001**, *123*, 1596. (f) De Lacey, A. L.; Stadler, C.; Cavazza, C.; Hatchikian, E. C.; Fernandez, V. M. *J. Am. Chem. Soc.* **2000**, *122*, 11232. (g) Boyke, C. A.; Rauchfuss, T. B.; Wilson, S. R.; Rohmer, M.-M.; Be´nard, M. *J. Am. Chem. Soc.* **2004**, *126*, 15151.

3 (a) Betley, T. A.; Peters, J. C. *J. Am. Chem. Soc.* **2003**, *125*, 10782. (b) Holland, P. L. *Can. J. Chem.* **2005**, *83*, 296. (c) Smith, J. M.; Sadique, A. R.; Cundari, T. R.; Rodgers, K. R.; Lukat-Rodgers, G.; Lachicotte, R. J.; Flaschenriem, C. J.; Vela, J.; Holland, P. L. *J. Am. Chem. Soc.* **2005**, *128*, 756. (d) Smith, J. M.; Lachicotte, R. J.; Pittard, K. A.; Cundari, T. R.; Lukat-Rodgers, G.; Holland, P. L.

J. Am. Chem. Soc. **2001**, *123*, 9222. (e) Vela, J.; Stoian, S.; Flaschenriem, C. J.; Münck, E.; Holland, P. L. *J. Am. Chem. Soc.* **2004**, *126*, 4522.

4 (a) Thomas, C. M.; Mankad, N. P.; Peters, J. C. *J. Am. Chem. Soc.* **2006**, *128*, 4956. (b) Brown, S. D.; Betley, T. A. *J. Am. Chem. Soc.* **2003**, *125*, 322. (c) Daida, E. J.; Peters, J. C. *Inorg. Chem.* **2004**, *43*, 7474. (d) Kisko, J. L.; Hascall, T.; Parkin, G. *J. Am. Chem. Soc.* **1998**, *120*, 10561.

5 Betley, T. A.; Peters, J. C. *Inorg. Chem.* **2003**, *42*, 5074.

6 Nakamoto, K. *Infrared and Raman Spectra of Inorganic and Coordination Compounds*, *Part B*: 5th ed.; Wiley: New York, 1997.

7 (a) Butts, M. D.; Bergman, R. G. *Organometallics* **1994**, *13*, 2668. (b) Nolan, S. P.; Hoff, C. D.; Stoutland, P. O.; Newman, L. J.; Buchanan, J. M.; Bergman, R. G.; Yang, G. K.; Peters, K. G. *J. Am. Chem. Soc.* **1987**, *109*, 3143. (c) Luo, L.; Li, C.; Cucullu, M. E. Nolan, S. P. *Organometallics* **1995**, *14*, 1333.

8 For examples on cobalt, see: a) Shay, D. T.; Yap, G. P. A.; Zakharov, L. N.; Rheingold, A. L.; Theopold, K. H. *Angew. Chem. Int. Ed.* **2005**, *44*, 1508. (b) Dai, X. L.; Kapoor, P.; Warren, T. H. *J. Am. Chem. Soc.* **2004**, *126*, 4798. (c) Jenkins, D. M.; Betley, T. A.; Peters, J. C. *J. Am. Chem. Soc.* **2002**, *124*, 11238. (d) Hu, X.; Meyer, K. *J. Am. Chem. Soc.* **2004**, *126*, 16322.

9 (a) Jonas, K.; Koepe, G.; Schieferstein, L.; Mynott, R.; Krüger, C.; Tsang, Y.-H. *Angew. Chem. Int. Ed. Engl.* **1983**, 22, 620. (b) Konze, W. V.; Scott, B. L.; Kubas, G. J. *J. Am. Chem. Soc.* **2002**, *124*, 12550. (c) Thomas, J. C.; Peters, J. C. *J. Am. Chem. Soc.* **2003**, *125*, 8870.

10 For general references on bridging-arene complexes, see: (a) Wadepohl, H. *Angew. Chem. Int. Ed. Engl.* **1992**, *31*, 247. (b) Budzelaar, P. H. M.; Moonen, N. N. P.; de Gelder, R.; Smits, J. M. M.; Gal, A. W. *Chem. Eur. J.* **2000**, *6*, 2740.

11 (a) Astruc, D. *Chem. Rev.* **1988**, *88*, 1189. (b) Hamon, J.-R.; Astruc, D.; Michaud, P. *J. Am. Chem. Soc.* **1981**, *103*, 758. (c) Nesmayanov, A. N.; Vol'kenau, N. A.; Petrakova, V. A. *Izv. Akad. Nauk SSSR, Ser. Khim.* **1974**, *9*, 2159. (d) Moinet, C.; Román, E.; Astruc, D. *J. Organomet. Chem.* **1977**, *128*, C45. For related couplings in Mn systems, see: (e) Lee, S.; Lovelace, S. R.; Arford, D. J.; Geib, S. J.; Weber, S. G.; Cooper, N. J. *J. Am. Chem. Soc.* **1996**, *118*, 4190. (f) Gaudet, M. V.; Hanson, A. W.; White, P. S.; Zaworotko, M. J. *Organometallics* **1989**, *8*, 269. (g) Shao, L.; Geib, S. J.; Badger, P. D.; Cooper, N. J. *J. Am. Chem. Soc.* **2002**, *124*, 14812.

12 de Lange, J. J.; Robertson, J. M.; Woodward, I. *Proc. R. Soc. London A* **1939**, *171*, 398.

13 Brown, S. D.; Peters, J. C. *J. Am. Chem. Soc.* **2004**, *126*, 4538.

14 Fujita, E. "Carbon dioxide reduction" in AccessScience@McGraw-Hill, http://www.accessscience.com.

15 Evans, D. J. *Coord. Chem. Rev.* **2005**, *249*, 1582.

16 For catalytic reactions, see: (a) Laitar, D. S.; Müller, P.; Sadighi, J. P. *J. Am. Chem. Soc.* **2005**, *127*, 17196. (b) Bogdanovic, B.; Leitner, W.; Six, C.; Wilczok, U.; Wittmann, K. *Angew. Chem., Int. Ed. Engl* **1997**, *36*, 502. (c) Eisenschmid, T. C.; Eisenberg, R. *Organometallics* **1989**, *8*, 1822. For stoichiometric reactions, see: (d) Castro-Rodriguez, I.; Meyer, K. *J. Am. Chem. Soc.* **2005**, *127*, 11242. (e)

Bryan, J. C.; Geib, S. J.; Rheingold, A. L.; Mayer, J. M. *J. Am. Chem. Soc.* **1987**, *109*, 2826. (f) Fachinetti, G.; Floriani, C.; Chiesi-Villa, A.; Guastini, C. *J. Am. Chem. Soc.* **1979**, *101*, 1767. (g) Procopio, L. J.; Carroll, P. J.; Berry, D. H. *Organometallics* **2003**, *12*, 3087. (h) Ziegler, W.; Nicholas, K. M. *J. Organomet. Chem.* **1992**, *423*, C35-37.

17 (a) Evans, W. J.; Seibel, C. A.; Ziller, J. W. *Inorg. Chem.* **1998**, *37*, 770. (b) Fröhlich, H.-O.; Schreer, H. *Z. Chem.* **1983**, *23*, 348. (c) Barret Adams, D. M. Y.; Kahwa, I. A.; Mague, J. T. *New J. Chem.* **1998**, *22*, 919. (d) Farrugia, L. J.; Lopinski, S.; Lovatt, P. A.; Peacock, R. D. *Inorg. Chem.* **2001**, *40*, 558. (e) Stibrany, R. T.; Schugar, H. J.; Potenza, J. A. *Acta. Cryst.* **2005**, *E61*, m1904.

18 Typically, the isolated metal products are either an oxo-bridged dimer (with loss of CO) or a terminal oxo species with a CO ligand.

19 (a) Brown, S. D.; Peters, J. C. *J. Am. Chem. Soc.* **2005**, *127*, 1913. (b) Brown, S. D.; Mehn, M. P.; Peters, J. C. *J. Am. Chem. Soc.* **2005**, *127*, 13146.

20 Raising the temperature greater than 60 °C results in decomposition of **4.7** and the minor species.

21 Lee, C.; Yang, W.; Parr, R. G. *Phys. Rev. B* **1988**, *37*, 785.

Appendix A: Catalytic Copolymerization of CO and Ethylene with a Charge Neutral Palladium(II) Zwitterion

The text in this chapter is reproduced in part with permission from:

Lu, C. C.; Peters, J. C. *J. Am. Chem. Soc.* **2002**, *124,* 5272.

A.1 Introduction

Late transition metal polymerization catalysts currently enjoy widespread scrutiny in academia and industry,[1] partly because their low oxophilicity relative to early metal systems is desirable for polar comonomer incorporation.[2] The cationic polymerization systems are frequently generated by methide or halide abstraction with an activator such as a Lewis acidic borane.[3] We are pursuing an alternate approach whereby charge neutral zwitterions incorporating a borate counteranion might themselves serve as polymerization catalysts.[4,5] Aside from eliminating the need for a cocatalyst, one might anticipate significant differences between zwitterionic and traditionally cationic systems due to (i) differences in their relative electrophilicities, (ii) differences in donor ligand lability, and (iii) reduced or completely eliminated ion-pairing effects in the zwitterionic systems by comparison to their cationic counterparts. To begin to understand the utility of zwitterionic systems in polymerization catalysis, well-defined comparative model studies are required.[6]

In this manuscript, we describe a zwitterionic palladium(II) alkyl complex supported by the anionic ligand $[Ph_2B(CH_2PPh_2)_2]^-$ (abbreviated as $[Ph_2BP_2]$).[7] This system serves as a charge neutral relative to the highly active class of cationic, phosphine-supported palladium CO/ethylene copolymerization catalysts such as $[(dppp)Pd(Me)(solv)]^+$ (dppp = bis-diphenyl(phosphino)propane)).[8,9] We specifically address whether a related zwitterionic palladium system is active for CO and ethylene copolymerization by comparing its reactivity to cationic systems supported by structurally similar bidentate phosphines (Figure A.1). Notably, neutral group 10 systems

supported by anionic LX-type ligands are generally regarded as poor catalysts for CO/ethylene copolymerization.[8b,10]

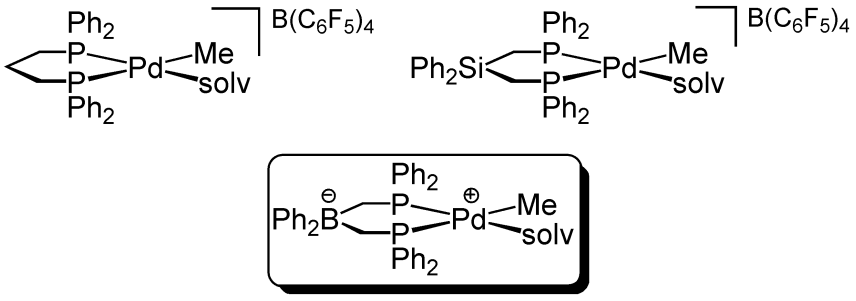

Figure A.1. Comparing a neutral palladium zwitterion with its prototypical cationic relatives.

A.2 Results and Discussion

Preparation of the target palladium alkyl complex proceeds first by reaction of an acetonitrile solution of the bis(phosphino)borate ligand, [ASN][Ph_2BP_2] **(**ASN = 5-azonia-spiro[4.4]nonane), with a benzene solution of (tmeda)$PdMe_2$ (tmeda = N,N,N',N'-tetramethylethylenediamine). The resulting anionic product, [ASN][(Ph_2BP_2)$PdMe_2$] (**A.1**), is then protonated by the ammonium salt [HN^iPr_2Et][BPh_4] to cleanly generate the target zwitterion, [Ph_2BP_2]PdMe(THF) (**A.2**), as a light peach solid (Scheme A.1).

Scheme A.1

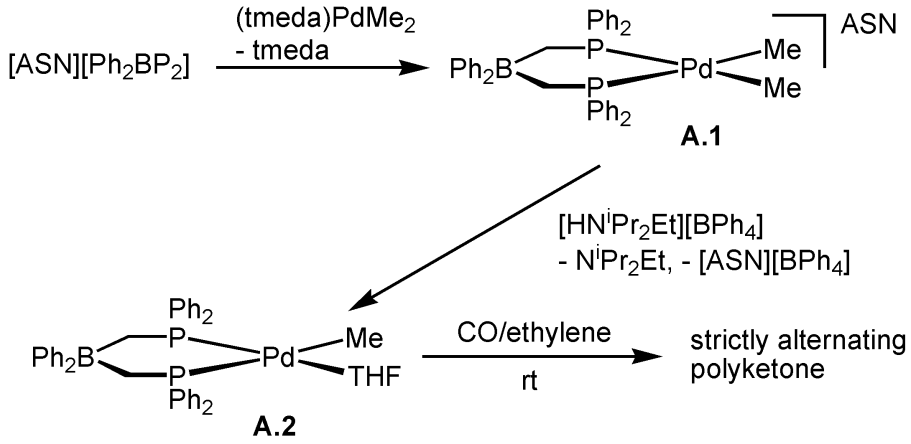

With the solvento adduct **A.2** in hand, we examined the scope of its reactivity under CO and ethylene gas. A light yellow solution results when a dilute THF solution (ca. 10 μM) of **A.2** is exposed to a CO atmosphere. The unstable product, $[Ph_2BP_2]Pd(C(O)Me)(CO)$ (**A.3**), is related to a cationic derivative, $[(dppp)Pd(C(O)Me)(CO)][B(3,5\text{-}(CF_3)_2\text{-}C_6H_3)_4]$, recently reported by Brookhart and coworkers.[11,12] At 30 psi of CO and 30 psi of ethylene, an appreciable quantity of strictly alternating polyketone material rapidly precipitates from the yellow solution (established by ^{13}C NMR and MALDI-TOF). The activity of catalyst **A.2** was examined at higher pressures (200 psi, *vide infra*), and calculated TON values (kg polymer mol^{-1} catalyst h^{-1}) establish that it is a very active catalyst for polyketone production at room temperature (Table A.1).

Table A.1. Copolymerization results for catalysts [Ph_2BP_2]PdMe(THF), **A.2**; [(dppp)Pd(Me)(THF)][$B(C_6F_5)_4$], **A.7**; and [($PhSiP_2$)Pd(Me)(THF)][$B(C_6F_5)_4$], **A.8**.[a]

Catalyst	activity (TON)[b]	yield (g polymer)[c]	M_w (10^3)[d]	M_n (10^3)[d]	M_w/M_n
A.2	39 ± 1	0.36 ± 0.01	138 ± 1	112 ± 3	1.3
A.7	35 ± 2	0.32 ± 0.02	130 ± 1	99 ± 2	1.3
A.8	45 ± 1	0.42 ± 0.01	190 ± 1	130 ± 5	1.5

[a] Conditions: 9.3 x 10^{-6} mol Pd catalyst in 10 mL THF; 100 psi CO; 100 psi ethylene; 23 ºC; 1 h. [b] TON values are expressed as kg polymer per mol catalyst per h. [c] Average mass of polymer obtained from eight independent runs. [d] Determined by GPC using polystyrene standards for calibration (1,3-cresol, 1 mL/min, 120 ºC, duplicate runs).

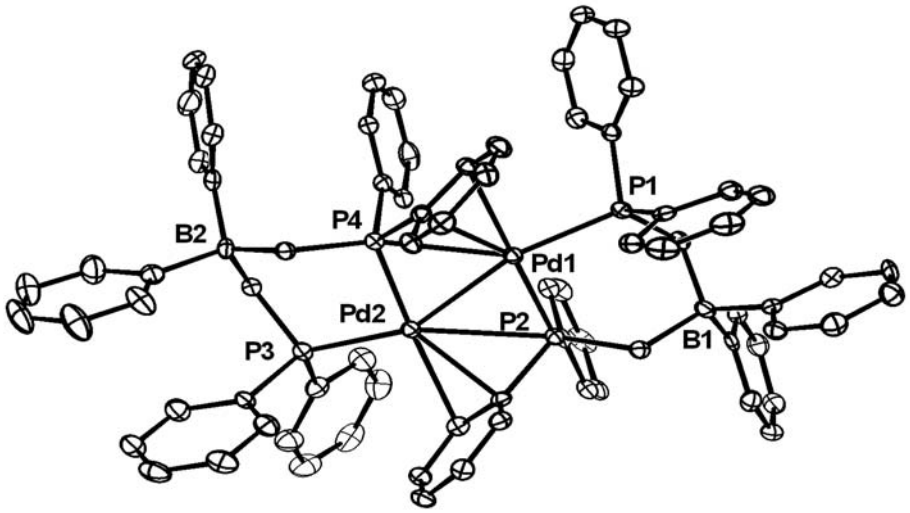

Figure A.2. 50% thermal ellipsoid representation of {[Ph_2BP_2]Pd}$_2$ (**A.4**). Hydrogen atoms and three CH_2Cl_2 molecules have been omitted for clarity. Selected bond distances (Å) and angles (deg) for **A.4**: Pd1–Pd2 2.7281(6), Pd1–P1 2.331(1), Pd1–P2 2.232(1), Pd1–P4 2.695(1), Pd2–P3 2.351(1), Pd2–P4 2.235(1), Pd2–P2 2.781(1), P1–Pd1–P2 92.83(5), P3–Pd2–P4 92.33(5).

Interestingly, the reactivity of catalyst **A.2** with CO gas, in the absence of ethylene, is concentration-dependent. At high concentrations of **A.2** (ca. 0.01M), exposure to an atmosphere of CO produces an orange solution (^{31}P NMR, singlet at 22 ppm),[13] which turns red (two doublets at 11 and 30 ppm) upon replacing the CO atmosphere with dinitrogen. The final red product is accessible by other routes (*vide infra*), and its crystallographic characterization establishes it to be the dimeric palladium(I) complex, $\{[Ph_2BP_2]Pd\}_2$ (**A.4**),[14,15] shown in Figure A.2 and Scheme A.2.

An alternative method for cleanly generating dimeric **A.4** is the exposure of **A.2** to ethylene gas in the absence of CO. In this case, the color change to red is rapid. Monitoring this transformation under ethylene at low temperature (from -78 °C to -10 °C) establishes one observable intermediate, assigned as an insertion product, $[Ph_2BP_2]Pd(C_2H_5)(H_2C{=}CH_2)$ (**A.5**). A related cationic species, $[(dppp)Pd(C_2H_5)(H_2C{=}CH_2)][B(3,5\text{-}(CF_3)_2\text{-}C_6H_3)_4]$, has also been reported by Brookhart and coworkers. Storage of intermediate **A.5** at -10 °C under excess ethylene effects the catalytic production of butenes. On warming, the only new species detectable by ^{31}P NMR is the red dimer **A.4**. The expected product of β-hydride elimination, $[Ph_2BP_2]Pd(H)(L)$ (**6**) (L = THF or ethylene), was not observed. Furthermore, an independent attempt to generate the hydride **A.6** by addition of H_2 to **A.2**, while generating dimeric **A.4** quantitatively, offered no evidence for a detectable hydride intermediate. Considered collectively, the data suggest that the conversion of **A.2** to **A.4** under ethylene may occur as follows (Scheme A.2): initial ethylene insertion and rapid β-hydride elimination, followed by a second ethylene insertion, generates the observable intermediate **A.5**. Intermediate **A.5** can undergo further chemistry with ethylene to

generate butenes. At higher temperatures, a bimolecular path competes in which the unobservable hydride **A.6**, generated by a β-hydride elimination step, reacts with a palladium alkyl, such as **A.5**, to produce alkane and the dimeric palladium(I) species **A.4**. Notably, gas analysis of a reaction mixture from the conversion of **A.2** to **A.4** under ethylene showed no evidence for hydrogen production. Bimolecular loss of H_2 from a hydride intermediate such as **A.6** does not occur.

Scheme A.2

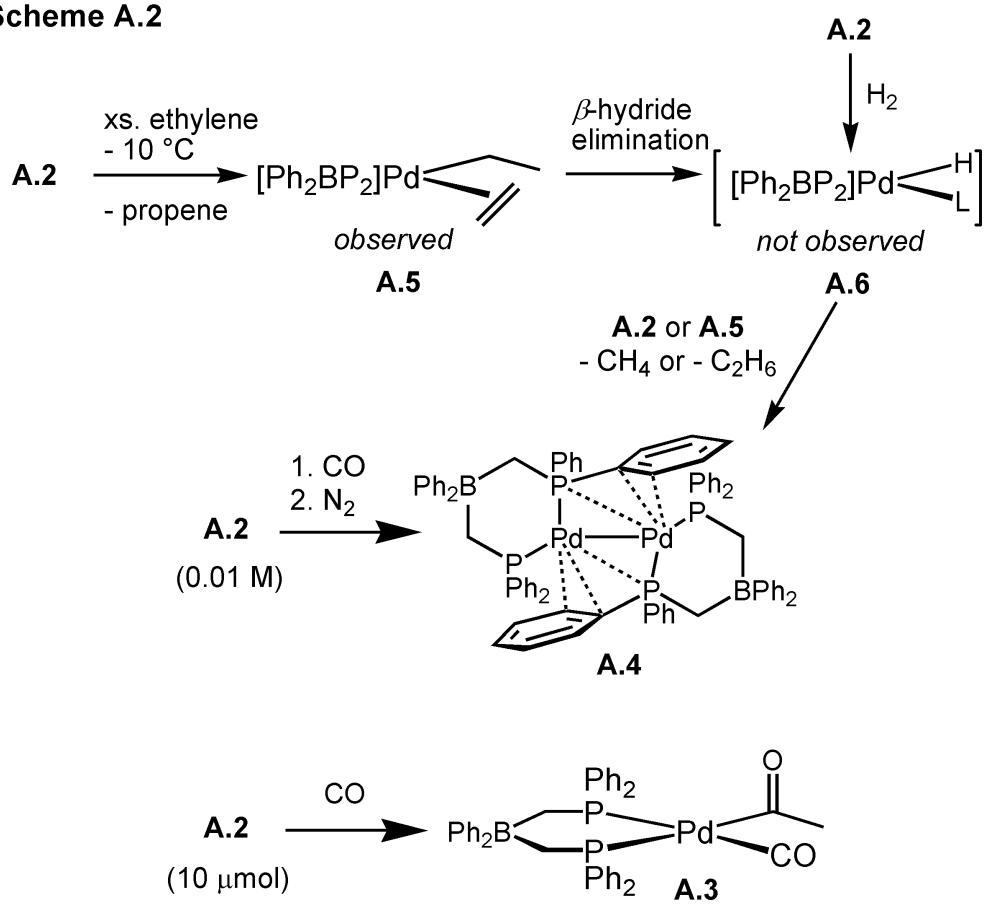

Having established some of the comparative reaction chemistry between charge neutral **A.2** and its cationic dppp counterpart, [(dppp)Pd(Me)(solv)][$B(C_6F_5)_4$], we sought to compare their relative activities with respect to the CO/ethylene copolymerization reaction of interest. The THF adduct complex, [(dppp)Pd(Me)(THF)][$B(C_6F_5)_4$] (**A.7**), was thus prepared, and its copolymerization activity was measured (Table A.1). To our

surprise, under analogous conditions, zwitterionic **A.2** proved to be a slightly better copolymerization catalyst from the perspective of total amount of polyketone produced per unit time (Table A.1). To examine whether the slightly increased activity of the [Ph_2BP_2] system was perhaps due to the difference in relative charge between the palladium centers in **A.2** and **A.7**, we sought a second comparison. A cationic complex more structurally related to neutral **A.2,** [(Ph_2SiP_2)Pd(Me)(THF)][$B(C_6F_5)_4$] (**A.8**), was prepared using the neutral phosphine chelate ($Ph_2Si(CH_2PPh_2)_2$ (abbreviated (Ph_2SiP_2)).[16] Under analogous conditions, cationic **A.8** proved to be a slightly better catalyst than zwitterionic **A.2** (Table A.1), indicating that the phenyl substituents incorporated within the ligand backbones of **A.2** and **A.8** might also contribute to slight differences in reactivity by comparison to the dppp system **A.7**.

Because differences in bulk activity are difficult to interpret, a closer examination of the elementary steps in the polymerization mechanism is desirable. Indeed, Brookhart and coworkers have measured the rates and calculated the activation barriers for migratory insertion reactions in the dppp system, specifically for the complexes: (dppp)PdMe$(CO)^+$, (dppp)PdC(O)Me$(C_2H_4)^+$, and (dppp)PdMe$(C_2H_4)^+$.[12a] The latter represents an olefin misinsertion step during the polymerization. We attempted to study all three migratory insertions for the zwitterionic analogues, but thus far, only the kinetics of [Ph_2BP_2]PdMe(C_2H_4) (**A.9**) have yielded fruitful results. Compound **A.9** is generated *in situ* by the addition of ethylene to **A.2** at low temperatures. The migratory insertion showed no dependence on ethylene concentration. The rate constant at -45.8 ºC, k_{obs} = 1.16 x 10^{-4} s^{-1} (with $\Delta G^{\ddagger}$ = 17.3(1) kcal/mol), is ca. four times slower than that observed for the dppp system (k_{obs} = 4.9 x 10^{-4} s^{-1} and $\Delta G^{\ddagger}$ = 16.6(1) kcal/mol at -45.6 ºC). The

temperature dependence of the reaction rate was also investigated from -58 to -41 ºC. An Eyring plot of this data is shown in Figure A.3, from which the activation parameters, $\Delta H^{\ddagger}$ = 15.4(4) kcal/mol and $\Delta S^{\ddagger}$ = -8.4(1.9) eu, were extracted. Surprisingly, these parameters are identical within error to those reported for the dppp system, $\Delta H^{\ddagger}$ = 15.2(7) kcal/mol and $\Delta S^{\ddagger}$ = -6.2(2.9) eu.

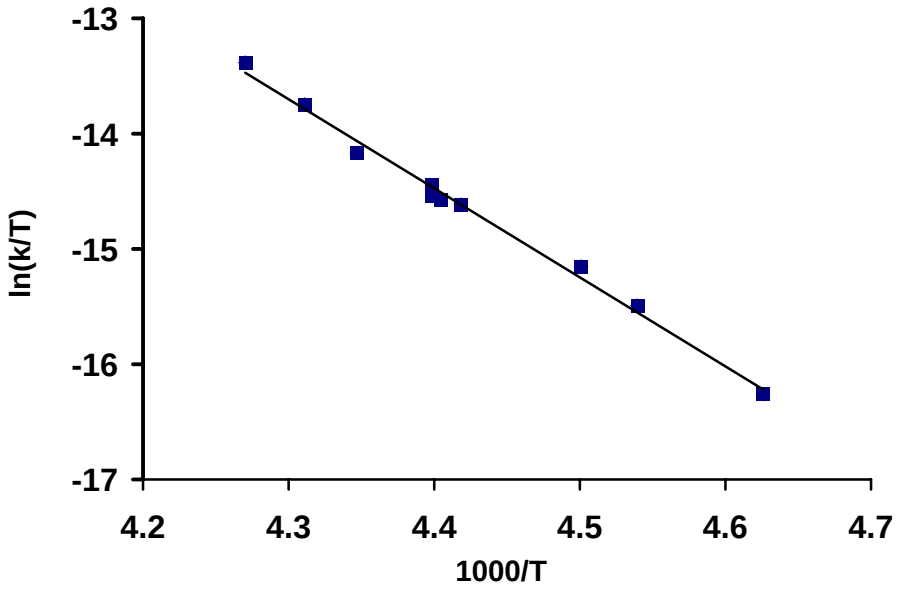

Figure A.3. Eyring plot for the migratory insertion reaction in $[Ph_2BP_2]PdMe(C_2H_4)$ (**A.9**), from -58 to -41 ºC, $\Delta H^{\ddagger}$ = 15.4(4) kcal/mol and $\Delta S^{\ddagger}$ = -8.4(1.9) eu.

A.3 Conclusions

In summary, the zwitterionic palladium(II) complex **A.2** is an active catalyst for the copolymerization of CO and ethylene at ambient temperature. A significant finding is that the charge neutral $[Ph_2BP_2]$ system is essentially as active as more typical dppp and

(Ph_2SiP_2) systems based upon cationic palladium. Complementary infrared studies of CO adducts in analogous platinum systems establish that the palladium center in zwitterionic **A.2** should be appreciably more electron rich than in the cations **A.7** and **A.8**.[17] We therefore suggest that the cationic character of these phosphine-supported copolymerization catalysts might be less relevant to their high activity than has been previously considered. The degree of electrophilicity required for high copolymerization activity is an important factor to consider in the design of future zwitterionic catalysts.

A.4 Experimental Section

A.4.1 General Considerations

All manipulations were carried out using standard Schlenk or glovebox techniques under a dinitrogen atmosphere. Unless otherwise noted, solvents were deoxygenated and dried by thorough sparging with N_2 gas, followed by passage through an activated alumina column. Diethyl ether, tetrahydrofuran, petroleum ether, and benzene were typically tested with a standard purple solution of sodium benzophenone ketyl in tetrahydrofuran in order to confirm effective oxygen and moisture removal. Deuterated acetone and benzene were purchased from Cambridge Isotope Laboratories, Inc. The solvents were dried over activated 3 Å molecular sieves and degassed by repeated freeze-pump-thaw cycles prior to use. Elemental analyses were performed by Desert Analytics, Tucson, AZ. A Varian Mercury-300 NMR spectrometer and a Varian Inova-500 NMR spectrometer were used to record ^1H and ^{13}C NMR spectra unless otherwise stated. ^1H and ^{13}C NMR chemical shifts were referenced to residual solvent. Proton peaks were assigned based on TOCSY-1D and ^{31}P-decoupled ^1H NMR studies.

^{31}P NMR chemical shifts are reported relative to an external standard of 85% H_3PO_4. IR measurements were obtained using a Bio Rad Excalibur FTS 3000 with a KBr solution cell. Polymer analyses were performed by MALDI-TOF MS on an Applied Biosystems Voyager DE-PRO with a matrix of 2-(4-hydroxyphenylazo)-benzoic acid in hexafluoroisopropanol with sodium iodide/ethanol [25 kV, 150 shots, linear, positive ion mode].

A.4.2 Starting Materials and Reagents

The preparations of (tmeda)$PdMe_2$,[18] (dppp)$PdMe_2$,[12] [ASN][$Ph_2B(CH_2PPh_2)_2$],[7] and [$H(Et_2O)_2$][$B(C_6F_5)_4$][19] were carried out following literature procedures. CP grade ethylene and CO were used without further purification for polymerization.

A.4.3 Synthesis of Compounds

Synthesis of [ASN][$Ph_2B(CH_2PPh_2)_2PdMe_2$], A.1: A benzene solution of (tmeda)$PdMe_2$ (0.466 g, 1.85 mmol) was added dropwise to a stirring suspension of [ASN][$Ph_2B(CH_2PPh_2)_2$] (1.273 g, 1.85 mmol) in acetonitrile (20 mL). Within 30 min, the reaction turned from cloudy white to a transparent yellow. The reaction was stirred overnight, and all volatiles were then removed *in vacuo* to give a mixture of off-white and yellow solids. The residue was submerged in Et_2O and stirred vigorously for 30 min to afford a fine powder. The solids were collected on a frit, washed with Et_2O and then with 15 mL Et_2O/CH_3CN (4:1), and dried *in vacuo* to give white **A.1** (1.284 g, 84% yield). ^{1}H NMR (d^6-acetone, 500 MHz) δ 7.35 (m, 8H, H_o of PPh_2), 7.11 (app t, J = 8.0 Hz, 4H, H_p of PPh_2), 7.05 (app t, J = 8.0 Hz, 8H, H_m of PPh_2), 6.95 (br s, 4H, H_o of BPh_2), 6.66 (app t, J = 7.0 Hz, 4H, H_m of BPh_2), 6.60 (tt, J = 1.0 and 7.0 Hz, 2H, H_p of BPh_2), 3.67 (m, 8H, $N(CH_2CH_2)_2$), 2.24 (m, 8H, $N(CH_2CH_2)_2$), 1.79 (br s, 4H, CH_2PPh_2),

-0.18 (d, J = 0.5 Hz, 6H, Pd(CH_3)$_2$). ^{13}C NMR (d^6-acetone, 125 MHz) δ 166.8 (br, C_{ipso} of BPh_2), 141.2 (app t, J = 13.8 Hz, C_{ipso} of PPh_2), 134.4 (t, J = 5.3 Hz, C_o of PPh_2), 133.6 (C_o of BPh_2), 128.1 (C_m of BPh_2), 127.6 (t, J = 4.0 Hz, C_m of PPh_2), 126.3 (C_p of PPh_2), 122.1 (C_p of BPh_2), 63.8 (t, J = 3.1 Hz, N(*C*H_2CH_2)$_2$), 22.8 (N(CH$_2$*C*H$_2$)$_2$), 22.3 (br, *C*H_2PPh_2), 5.61 (br dd, Pd(*C*H_3)$_2$). ^{31}P NMR (d^6-acetone, 121 MHz) δ 22.4. Anal. Calcd. for ($C_{48}H_{56}BNP_2Pd$): C 69.78; H 6.83; N 1.70. Found: C 69.69; H 6.91; N 1.62.

Synthesis of [Ph$_2$B(CH$_2$PPh$_2$)$_2$]PdMe(THF), A.2: A THF solution of [HNEt^{i}Pr$_2$][BPh_4] (43.2 mg, 96.1 μmol) was added to a stirring THF solution of **A.1** (79.4 mg, 96.1 μmol). The reaction solution immediately turned cloudy pink. After stirring for 30 min, the reaction mixture was filtered through a glass wool pipette to remove white solids. A small amount of petroleum ether (5 mL) was added to the light-pink filtrate to further precipitate the white solids. After filtering, the cycle was repeated until all of the [ASN][BPh_4] was removed (^{1}H NMR). Finally, copious petroleum ether (7 mL) was added to precipitate a light-peach solid, which was collected and dried *in vacuo* to give 49.7 mg of product (71% yield). ^{1}H NMR (THF-d$_8$, 300 MHz, -70 °C) δ 7.40 - 7.25 (m, 12H, aryl H's of PPh_2 and P′Ph_2), 7.16 (app t, J = 7.20 Hz, 8H, aryl H's of PPh_2 and P′Ph_2), 6.68 (m, 4H, H_o of BPh_2), 6.59 - 6.57 (m, 6H, H_m and H_p of BPh_2), 3.62 (m, 4H, (CH$_2$C*H*$_2$)$_2$O), 2.01 (dd, J = 4.20 and 16.49 Hz, 2H, C*H*$_2$PPh_2), 1.82 - 1.76 (m, 6H, (C*H*$_2$CH$_2$)$_2$O and C′*H*$_2$PPh_2), -0.12 (d, J = 7.80 Hz, 3H, PdC*H*$_3$). ^{31}P NMR (THF-d$_8$, 121 MHz, -70 °C) δ 47.1 (d, J = 47 Hz, P trans to Me), 19.1 (d, J = 47 Hz, P trans to THF). Anal. Calcd. for ($C_{43}H_{45}BOP_4Pd$): C 68.23; H 5.99; N 0.00. Found: C 68.01; H 5.84; N 0.18.

Synthesis of $[Ph_2B(CH_2PPh_2)_2]Pd(C(O)Me)(CO)$, A.3: Obtaining spectroscopic data for the CO insertion product **A.3** was difficult due to the ease of formation of dimeric **A.4** at concentrations suitable for NMR analysis. However, when THF solvent was first sparged with CO gas, followed by dissolution of pale-peach **A.2** in the CO-containing solvent, a rapid color change to yellow was observed. IR analysis of the solution showed two intense ν(CO) bands at 2108 and 1694 cm^{-1}, indicative of the CO insertion product **A.3**. Compound **A.3** reverts back to starting material **A.2** in the absence of a CO atmosphere. Spectroscopic NMR data was obtained by generating **A.3** *in situ* as described above in CD_2Cl_2. ^1H NMR (CD_2Cl_2, 300 MHz) δ 7.41 - 7.32 (m, 6H, aryl H's), 7.27 – 7.02 (m, 18H, aryl H's), 6.93 – 6.82 (m, 6H, H_m and H_p of BPh_2), 3.68 (m, 4H, free THF), 2.07 (br d, J = 15 Hz, 2H, CH_2PPh$_2$), 1.95 (s, 3H, C(O)*Me*), 1.83 (m, 4H, free THF), 1.72 (br d, 2H, C′H_2P′Ph$_2$). ^{31}P NMR (CD_2Cl_2, 121 MHz) δ 22.3 (d, J = 71.4 Hz), 11.0 (d, J = 71.4 Hz). IR(CH_2Cl_2, KBr): ν(CO) = 2110 cm^{-1}, ν(*C*(*O*)Me) 1686 cm^{-1}.

Synthesis of $[Ph_2B(CH_2PPh_2)_2Pd]_2$, A.4: A THF solution (5 mL) of compound **A.2** (39.8 mg, 52.6 μmol) was sparged with ethylene for 1 h. The dark-red solution was concentrated *in vacuo*, and petroleum ether (5 mL) was added to precipitate red-orange solids (34 mg, 99%). Single crystals suitable for X-ray diffraction studies were grown from vapor diffusion of petroleum ether into a CH_2Cl_2/CH_3CN solution of **A.4** at -30 ºC. ^1H NMR (C_6D_6, 500 MHz) δ 7.46 (br d, J = 7.0 Hz, 4H, H_o of BPh_2), 7.23 (t, J = 7.50 Hz, 4H, H_m of BPh_2), 7.17 (t, J = 7.50 Hz, 2H, H_p of BPh_2), 7.05 (dd, J = 7.50 and 10.50 Hz, 4H, H_o of PPh_2), 6.87 (m, 2H, H_p of P′Ph$_2$), 6.75 (m, 8H, H_m of P′Ph$_2$, H_o of P′Ph$_2$), 6.66 (t, J = 7.00 Hz, 4H, H_m of PPh_2), 6.53 (t, J = 7.50 Hz, 2H, H_p of PPh_2), 2.24 (br d, J = 15.50 Hz, 2H, CH_2PPh$_2$), 1.97 (br d, J = 10.50 Hz, 2H, C′H_2P′Ph$_2$); ^{13}C NMR (C_6D_6, 125

MHz) δ 163.2 (br s, C_{ipso} of BPh_2), 134.9 (t, J = 16.0 Hz, C_{ipso} of PPh_2), 133.4 (m, C_o of BPh_2 , C_o of PPh_2), 131.7 (C_p of P′Ph_2), 130.6 (m, C_m of P′Ph_2), 129.4 (m, C_m of PPh_2), 128.9 (C_p of PPh_2), 127.5 (app t, J = 4.5 Hz, C_o of P′Ph_2), 127.2 (C_m of BPh_2), 123.4 (C_p of BPh_2), 112.4 (app d, J = 49.7 Hz, C_{ipso} of P′Ph_2), 25.3 (br, *C*H_2PPh_2), 21.1 (br, *C*′H_2P′Ph_2); ^{31}P NMR (THF, 121 MHz) δ 29.9 (d, J = 55 Hz), 11.3 (d, J = 55 Hz). Anal. Calcd. for ($C_{76}H_{68}B_2P_4Pd_2$): C 68.13; H 5.11; N 0.00. Found: C 68.68; H 4.75; N 0.21.

Synthesis of ($Ph_2Si(CH_2PPh_2)_2$)$PdMe_2$: The compound (tmeda)$PdMe_2$ (0.190 g, 0.752 mmol) was dissolved in cold benzene (5 mL) and added dropwise to a cold (-30 °C) stirring suspension of $Ph_2Si(CH_2PPh_2)_2$ (0.437 g, 0.752 mmol) in acetonitrile (15 mL). Within ten min, the solution became homogeneous. After stirring overnight, all volatiles were removed *in vacuo* to give an off-white powder. The solids were collected on a frit, washed liberally with petroleum ether, and dried *in vacuo* to give an off-white powder (0.404 g, 75% yield). ^{1}H NMR (C_6D_6, 500 MHz) δ 7.55 (tt, J = 8.50 and 1.50 Hz, 8H, H_o of PPh_2), 7.04 - 6.93 (m, 14H, aryl H's of $SiPh_2$, H_p of PPh_2), 6.88 (br d, J = 4.00 Hz, 8H, H_m of PPh_2), 2.01 (br d, J = 7.50 Hz, 4H, C*H*$_2PPh_2$), 0.925 (d, J = 3.00 Hz, 6H, Pd(C*H*$_3$)$_2$). ^{13}C NMR (C_6D_6, 125 MHz) δ 136.7 (app t, J = 15 Hz, C_{ipso} of PPh_2), 136.4 (m, C_{ipso} of $SiPh_2$), 134.7, 134.1 (t, J = 5.91 Hz), 129.9, 129.6, 128.5 (m), 11.1 (br, *C*H_2PPh_2), 8.36 (dd, J = 14.95 and 95.5 Hz, Pd(*C*H_3)$_2$). ^{13}C NMR (d^6-acetone, 125 MHz) δ 136.9 - 136.6 (m, C_{ipso} of $SiPh_2$, C_{ipso} of PPh_2), 134.8 (C_o of $SiPh_2$), 134.2 (t, J = 6.4 Hz, C_o of PPh_2), 130.3 (C_p of $SiPh_2$), 129.9 (C_p of PPh_2), 128.7 (t, J = 4.3 Hz, C_m of PPh_2), 128.5 (C_m of $SiPh_2$), 10.8 (t, J = 5.0 Hz, *C*H_2PPh_2), 7.16 (dd, J = 97.3 and 15.0 Hz, Pd(*C*H_3)$_2$). ^{31}P NMR (C_6D_6, 121 MHz) δ 11.63. Anal. Calcd. for ($C_{40}H_{40}P_2PdSi$): C 66.99; H 5.62; N 0.00. Found: C 66.70; H 5.75; N 0.13.

Generation of cationic catalysts [(dppp)PdMe(THF)][$B(C_6F_5)_4$], A.7 and [($PhSiP_2$)PdMe(THF)][$B(C_6F_5)_4$], A.8: To a THF solution of the catalyst precursors (dppp)$PdMe_2$ (25.5 mg, 4.65 x10^{-5} mol) or ($PhSiP_2$)$PdMe_2$ (33.3 mg, 4.65 x10^{-5} mol) was added [$H(Et_2O)_2$][$B(C_6F_5)_4$] (38.5 mg, 4.65 x10^{-5} mol). Consumption of the starting neutral precursors was verified by ^{31}P NMR spectroscopy, which also established clean conversion to the cationic catalysts. Compound **A.7**: ^{31}P NMR (THF, 121 MHz) δ 33.1 (d, *J* = 40 Hz), 6.1 (d, *J* = 40 Hz). Compound **A.8**: δ 33.2 (d, *J* = 53 Hz), 0.5 (d, *J* = 53 Hz).

A.4.4 Ethylene and CO Copolymerization Studies

In a typical polymerization experiment, 9.3 x10^{-6} mol of palladium catalyst (**A.2**, **A.7**, or **A.8**) in 10 mL of THF, obtained from stock solutions, were transferred to a small bottleneck glass vessel with a 1 ¼" teflon stir bar. The glass vessels were placed inside a Parr reactor, which was then charged with 100 psi CO and 100 psi ethylene. After vigorously stirring for one h at 23 °C, the reactions were quenched with MeOH. A white precipitate was collected, washed with MeOH, and thoroughly dried *in vacuo*. A total of 8 polymerization experiments were performed for each catalyst system to establish reliable polymer weights for TON value comparisons.

A.4.5 X-ray Experimental Data

X-ray diffraction studies were carried out in the Beckman Institute Crystallographic Facility on a Bruker Smart 1000 CCD diffractometer under a stream of dinitrogen. Data were collected using the Bruker SMART program, collecting ω scans at 5 ϕ settings. Data reduction was performed using Bruker SAINT v6.2. Structure solution and structure refinement were performed using SHELXS-97 (Sheldrick, 1990) and

SHELXL-97 (Sheldrick, 1997). All structural representations were produced using the Diamond software program. Crystallographic data are summarized in Table A.2.

Table A.2. Crystallographic data for $\{[Ph_2BP_2]Pd\}_2$, **A.4**.

	A.4·$3CH_2Cl_2$
chemical formula	$C_{76}H_{68}B_2P_4Pd_2 \cdot 3CH_2Cl_2$
fw	1594.38
T (K)	98
λ (Å)	0.71073
a (Å)	22.389(3)
b (Å)	20.690(2)
c (Å)	16.382(2)
α (°)	90
β (°)	106.779(2)
γ (°)	90
V (Å^3)	2186.0(3)
space group	$P2_1/c$
Z	4
D_{calc} (g/cm^3)	1.458
μ (cm^{-1})	8.48
R1, wR2[a] ($I > 2\sigma(I)$)	0.0606, 0.1173

[a] $R1 = \Sigma||F_o| - |F_c||/\Sigma|F_o|$, $wR2 = \{\Sigma[w(F_o^2 - F_c^2)^2]/\Sigma[w(F_o^2)^2]\}^{1/2}$

References Cited

1 For two recent reviews see: (a) Ittel, S. D.; Johnson, L. K.; Brookhart, M. *Chem Rev*. **2000**, *100*, 1169. (b) Mecking, S. *Coord Chem. Rev*. **2000**, *203*, 325.

2 Younkin, T. R.; Conner, E. F.; Henderson, J. I.; Friedrich, S. K.; Grubbs, R. H.; Bansleben, D. A. *Science* **2000**, *287*, 460.

3 (a) Chen, E. Y.-X.; Marks, T. J. *Chem. Rev*. **2000**, *100*, 1391. (b) Lee, B. Y.; Bazan, G. C.; Vela, J.; Komon, Z. J. A.; Bu, X. H. *J. Am. Chem. Soc.* **2001**, *123*, 5352.

4 For a recent review on zwitterions in organometallic chemistry see: Chauvin, R. *Eur. J. Inorg. Chem*. **2000**, 577.

5 For lead papers dealing with the reactivity of inorganic zwitterions see: (a) Amer, I.; Alper, H. *J. Am. Chem. Soc*. **1990**, *112*, 3674. (b) Westcott, S. A.; Blom, H. P.; Marder, T. B.; Baker, R. T. *J. Am. Chem. Soc*. **1992**, *114*, 8863. (c) Dai, C.; Marder, T. B.; Robins, E. G.; Yufit, D. S.; Howard, J. A. K.; Scott, A. J.; Clegg, W. *Chem. Commun*. **1998**, 1983. (d) Winter, R. F.; Hornung, F. M. *Inorg. Chem*. **1997**, *36*, 6197.

6 (a) Piers, W. E. *Chem. Eur. J*. **1998**, *4*, 13. (b) Bochmann, M. *Topics Catal*. **1999**, *7*, 9. (c) Piers, W. E., Sun, Y., Lee, L. W. M. *Topics Catal*. **1999**, *7*, 133.

7 Thomas, J. C.; Peters, J. C. *J. Am. Chem. Soc.* **2001**, *123*, 5100.

8 (a) Sen, A. *Acc. Chem. Res*. **1993**, *26*, 303. (b) Drent, E.; Budzelaar, P. H. M. *Chem. Rev.* **1996**, *96*, 663.

9 For lead references on this topic see: (a) Mul, W. P.; Drent, E.; Jansens, P. J.; Kramer, A. H.; Sonnemans, M. H. W. *J. Am. Chem. Soc.* **2001**, *123*, 5350. (b)

Shultz, C. S.; DeSimone, J. M.; Brookhart, M. *Organometallics* **2001**, *20*, 16. (c) Murtuza, S.; Harkins, S. B.; Sen, A. *Macromolecules* **1999**, 32, 8697. (d) Margl, P.; Ziegler, T. *J. Am. Chem. Soc*. **1996**, *118*, 7337. (e) Svensson, M.; Matsubara, T.; Morokuma, K. *Organometallics* **1996**, *15*, 5568.

10 Unlike classical LX-type ligands that are regarded as 3-electron donors, the [Ph_2BP_2] ligand is regarded as a 4-electron donor ligand in the zwitterionic depiction.

11 Complex **A.3** shows two very intense bands at 1694 {ν(*C*(*O*)Me} and 2108 {ν(*CO*)} cm^{-1} by infrared spectroscopy.

12 (a) Shultz, C. S.; Ledford, J.; DeSimone, J. M.; Brookhart, M. *J. Am. Chem. Soc.* **2000**, *122*, 6351. (b) Tempel, D. J.; Johnson, L. K.; Huff, L. M.; White, P. S.; Brookhart, M. *J. Am. Chem. Soc.* **2000**, *122*, 6686.

13 We suspect the orange species initially produced to be the dimeric palladium(I) species {[Ph_2BP_2]Pd(μ-CO)}$_2$.

14 X-ray data for (**A.4**·3CH_2Cl_2), MW = 1594.38, red plate, collection temp. = 98K, monoclinic, space group = $P2_1/c$, a = 22.389(3) Å, b = 20.690(2) Å, c = 16.3816(18) Å, β = 104.361(5)º, V = 7265.2(14) $Å^3$, Z = 4, R_1 = 0.0606 [I>2σ(I)], GOF = 2.522.

15 A related, dicationic species, [{(dppp)Pd}$_2$][OTf]$_2$, has been previously obtained by hydrogenation of (dppp)Pd(OTf)$_2$. See Budzelaar, P. H. M.; van Leeuwen, W. N. M; Roobeek, C. F.; Orpen, G. A. *Organometallics* **1992**, *11*, 23.

16 $Ph_2Si(CH_2PPh_2)_2$ is a neutral ligand designed as a close structural model for the anionic borato ligand $[Ph_2BP_2]$ on square planar complexes. See Thomas, J. C.; Peters, J. C. *J. Am. Chem. Soc.* **2003**, *125*, 8870.

17 The CO stretching frequency for the cationic complex $[(Ph_2SiP_2)PtMe(CO)]^+$ is ca. 24 cm^{-1} higher than for neutral $[Ph_2BP_2]PtMe(CO)$. See reference 16.

18 van Asselt, R.; Rihnberg, E.; Elsevier, C. J. *Organometallics* **1994**, *13*, 706.

19 Jutzi, P.; Mueller, C.; Stammler, A.; Stammler, H-G. *Organometallics* **2000**, *19*, 1442.

Appendix B: Synthetic, Structural, and Mechanistic Aspects of an Amine Activation Process Mediated at a Zwitterionic Palladium(II) Center

The text in this chapter is reproduced in part with permission from:

Lu, C. C.; Peters, J. C. *J. Am. Chem. Soc.* **2004,** *126,* 15818.

B.1 Introduction

Exploiting transition metals to functionalize tertiary amines via initial C-H bond activation is a growing area of synthetic interest.[1] For instance, Murai and coworkers have described a catalytic process for the carbonylation of tertiary amines at the position adjacent to the amine N-atom using a rhodium(I) precursor.[2] This system requires amine substrates with pendant directing groups to chelate the metal catalyst. More recently, Murahashi *et al.* have reported a ruthenium catalyst for the cyanation of tertiary amines without the requirement of directing groups.[3] Iminium adducts of ruthenium, while not observed, were proposed as key intermediates in the Murahashi system. Precedent for this type of reactivity had been previously demonstrated at osmium by the Harman group,[4] who provided spectroscopic data to support the generation of an Os(II) η^2-iminium hydride complex via β-hydride elimination upon reduction of an Os(III) amine complex. A final noteworthy example of a catalytic transformation of tertiary amines comes from Goldman's group with the report that iridium(III) dihydride precursors can mediate the dehydrogenation of tertiary amines to produce enamines in the presence of a H_2-acceptor (i.e., NEt_3 + alkene → $Et_2NCH{=}CH_2$ + alkane).[5]

Previous work from our lab has concerned mechanistic aspects of aromatic C-H bond activations mediated by a zwitterionic platinum(II) center.[6] With an interest in extending this effort we turned to developing a related palladium system. In this report a reactive palladium(II) complex is described, $[[Ph_2BP_2]Pd(THF)_2][OTf]$ (**B.1**) where $[Ph_2BP_2]$ represents the bis(phosphino)borate ligand $[Ph_2B(CH_2PPh_2)_2]^-$, that stoichiometrically activates a variety of trialkylamines at a secondary C-H position adjacent to the amine N-atom in a stochiometric manner. Formal proton loss accompanies

the activation process, and structurally unusual iminium adduct complexes of palladium are obtained. The reaction system is particularly well-suited to mechanistic examination, and we have therefore undertaken such a study. We attempt to address the reaction's overall selectivity and suggest a plausible operational mechanism. The amine activation processes may be mechanistically germane to the mode of palladium-catalyzed alcohol oxidations[7] (Figure B.1), and also to the *in situ* reduction of palladium(II) precursors by trialkyamines[8] in palladium(0)-catalyzed reactions, as for example in the Heck reaction.[9] These processes are also of potential relevance to β-hydride elimination processes of palladium amides[10] and to β-hydride eliminations that generate imines from secondary amines.[11]

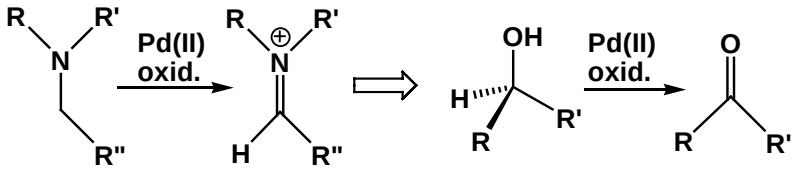

Figure B.1. Relationship between amine-to-iminium ion and alcohol-to-ketone oxidation reactions.

B.2 Results

B.2.1 Synthesis and Structural Characterization of [[Ph_2BP_2]Pd(THF)$_2$][OTf] (B.1) and [Ph_2BP_2]Pd(THF)(OTf) (B.1′)

To activate C-H bonds, a reactive [Ph_2BP_2]Pd(II) system was required. A labile triflate derivative, [Ph_2BP_2]Pd(OTf)(L), was targeted, and the following protocol (Scheme B.1) afforded the species of interest. Mixing [Ph_2BP_2][NBu_4] and $PdCl_2(NCPh)_2$ in THF afforded a mixture of two products, [[Ph_2BP_2]$PdCl_2$][NBu_4] (**B.2**) and

{[Ph_2BP_2]Pd(μ-Cl)}$_2$ (**B.3**). The mixture of **B.2** and **B.3** was converted completely to {[Ph_2BP_2]Pd(μ-Cl)}$_2$ (**B.3**) by the addition of a slight excess of $NaBPh_4$ to the reaction mixture (Scheme B.1). Crystals of **B.3** were grown from THF/CH_2Cl_2 solutions at -30 °C in 73% overall yield (based upon $PdCl_2(NCPh)_2$). Dimeric **B.3** was then converted to the more reactive species, [[Ph_2BP_2]Pd(THF)$_2$][OTf] (**B.1**), by the addition of AgOTf in THF. As indicated by its formula, complex **B.1** exists in THF solution predominantly as a bis(solvento) cation, which is consistent with (a) a single resonance (s, δ = 48.2 ppm) at 23 ºC in the ^{31}P NMR spectrum, (b) integrations consistent with two equivalents of THF in the ^{1}H NMR spectrum, and (c) combustion analysis data. Nonetheless, an X-ray diffraction analysis of a single crystal grown from a purified sample in THF at -30 °C revealed a zwitterionic, mono-THF adduct, [Ph_2BP_2]Pd(THF)(OTf) (**B.1′**) (Figure B.2), and an unbound THF molecule. The THF co-ligands of **B.1** are appreciably labile and in rapid exchange with the competitive triflate ligand. This exchange process, **B.1** ⇌ **B.1′** + THF, was observed by ^{31}P VT NMR spectroscopy in CD_2Cl_2 solution. A broad signal is evident at 47 ppm, indicative of fluxional behavior at ambient temperature. Upon cooling the sample to -85 °C, two signals become fully resolved with a peak separation of 916 Hz. These peaks coalesce at -42.3 °C, and a barrier of 16.2 kcal/mol has been calculated for the THF and triflate exchange at -42.3 °C.[12]

Scheme B.1

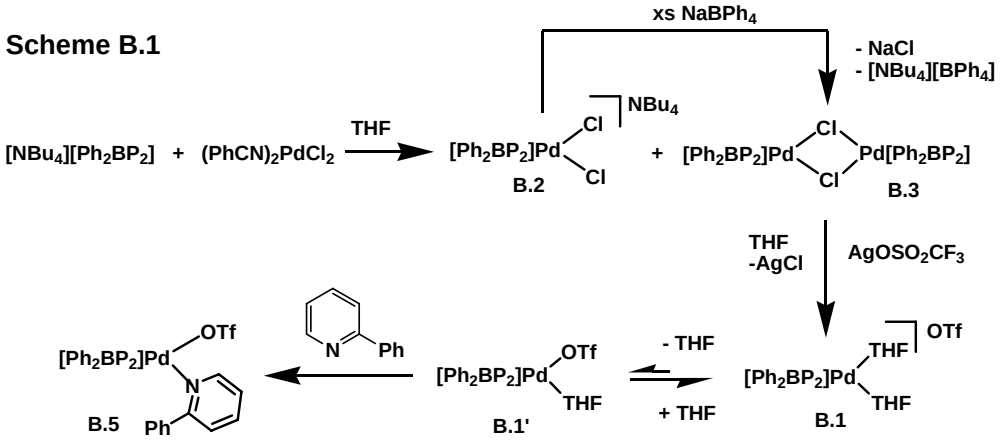

The crystal structure of **B.1′** shows an essentially square planar complex with bond angles that deviate only slightly from their ideal values. The O(1)-Pd-O(2) and O(1)-Pd-P(2) bond angles are 86.52(7) and 92.33(6)º, respectively. The Pd-O bond distances for each of the oxygen donors are identical (2.157(2) and 2.155(2) Å for the THF and triflato donors, respectively). Complex **B.1′** has few structurally authenticated congeners in the palladium literature. The most comparable structures are those of the complexes [(dppp)Pd(H_2O)(X)][X] (where X = OTf and OTs) reported separately by Stang and Toniolo.[13] The Pd-O bond distances in **B.1′**, and also its Pd-P bond distances (2.2378(8) Å and 2.2309(9) Å), compare favorably with these examples.

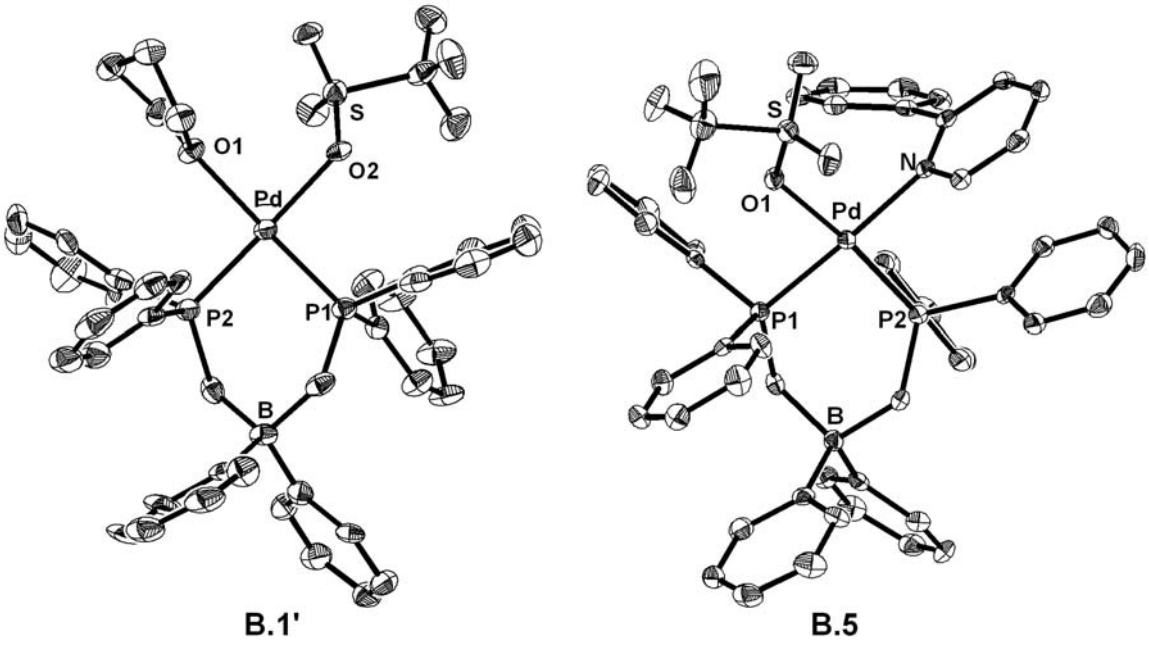

Figure B.2. (A) 50% thermal ellipsoid representation of $[Ph_2BP_2]Pd(THF)(OTf)$ (**B.1′**). Selected bond distances (Å) and angles (deg.): Pd–O1, 2.157(2); Pd–O2, 2.155(2); Pd–P1, 2.2378(8); Pd–P2, 2.2309(9); O1–Pd–O2, 86.52(7); P1–Pd–P2, 89.16(3), O1–Pd–P2, 92.33(6); O2–Pd–P1, 91.90(5). (B) 50% thermal ellipsoid representation of $[Ph_2BP_2]Pd$(*o*-phenylpyridine)(OTf) (**B.5**). Selected bond distances (Å) and angles (deg.): Pd–O1, 2.195(2); Pd–N, 2.139(3); Pd–P1, 2.2718(9); Pd–P2, 2.2503(9); O1–Pd–N, 89.85(9); P1–Pd–P2, 88.43(3), O1–Pd–P1, 88.00(6); N–Pd–P2, 93.87(7). Hydrogen atoms and a THF molecule for **B.5** were omitted for clarity.

B.2.2 Reactivity of B.1 with Arene Substrates

The possibility for complex **B.1** to mediate aryl C-H bond activation was briefly examined by dissolving **B.1** in benzene solution in the presence of the sterically encumbered amine base N^iPr_2Et. Our lab had observed phenyl transfer from benzene to a platinum(II) triflate complex in the presence of N^iPr_2Et, which served as a formal H^+ acceptor to produce $[HN^iPr_2Et][OTf]$.[14] In the present case, adding an excess of N^iPr_2Et to a benzene solution of **B.1** at 25 °C indeed generated a stoichiometric equivalent of $[HN^iPr_2Et][OTf]$. However, the major palladium-containing species generated (> 70% of the mixture by ^{31}P NMR spectroscopy) was the previously reported palladium(I) dimer, $\{[Ph_2BP_2]Pd\}_2$ (**B.4,** Equation B.1).[15] A second diamagnetic species was also evident (^{31}P NMR), but none of the anticipated aryl transfer product, $[Ph_2BP_2]Pd(Ph)(THF)$, was detected.[16] Several observations from the literature suggest that $[Ph_2BP_2]Pd(Ph)(THF)$ may be unstable. For example, it is known that biphenyl and other biaryls can be liberated from palladium(II) aryl species.[17] Biphenyl has also been derived directly from a benzene C-H activation process mediated by palladium(II).[18] Related aryl coupling processes are known for phosphine-supported platinum(II) systems.[19,6b] In the present $[Ph_2BP_2]Pd(II)$ system, however, benzene-derived biphenyl could not be identified (^1H NMR, GC/MS).

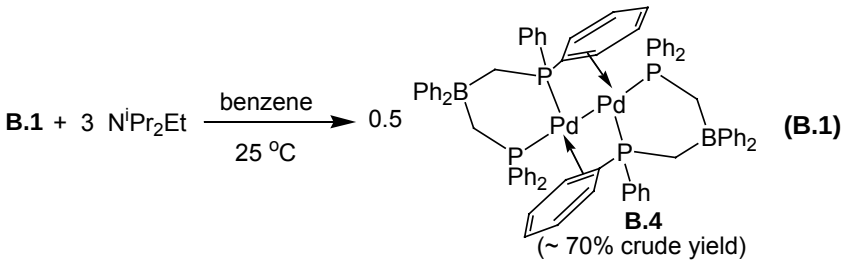

To further explore whether **B.1** might activate aryl C-H bonds, *o*-phenylpyridine was tested as a substrate assuming that a favorable chelate stabilization might encourage metalation of the arene ring. Several platinum(II) and palladium(II) halide and pseudo-halide precursors are known to react with *o*-phenylpyridine in the presence of a sacrificial base to produce cyclometalated products.[20] Exposure of **B.1** to either stoichiometric or excess *o*-phenylpyridine afforded a single product, the adduct complex, $[Ph_2BP_2]$Pd(*o*-phenylpyridine)(OTf) (**B.5**), which was verified by X-ray crystallography. Complex **B.5** is quite hindered, as can be gleaned from its solid-state crystal structure (Figure B.2). At rt in solution, its ^{1}H NMR resonances are broad presumably due to hindered rotation about the Pd-N bond. These peaks sharpen upon cooling to -40 ºC, and the expected four resonances for the ligand methylene protons become well resolved. Relative to **B.1'**, the Pd-OTf interaction of **B.5** is modestly elongated (2.195(2) versus 2.155(2) Å), which is also true of the Pd-P bond distances (2.25 to 2.27 versus 2.23 to 2.34 Å). These relative bond lengths reflect the steric congestion suffered by **B.5**, which nonetheless is unexpectedly robust. For example, no reaction occurred when **B.5** was incubated in THF at 80 ºC in the presence of either excess *o*-phenylpyridine or excess K_2CO_3.

B.2.3 Activation of Trialkylamines by Complex B.1

Treating **B.1** with 20 equivalents of N^iPr_2Et in THF solution at ambient temperature resulted in the gradual consumption of starting material and the rise of a single new palladium product, along with a stoichiometic equivalent of $[HN^iPr_2Et][OTf]$. The new palladium species exhibited resonances in the ^{31}P NMR spectrum that compared well to a minor product that was observed when **B.1** was exposed to N^iPr_2Et in benzene solution (*vide supra*). Single crystals of this species were grown from a THF/petroleum

ether solution, and an X-ray diffraction study revealed it to be the 3-membered palladacycle $[Ph_2BP_2]Pd(N,C:\eta^2\text{-}N^iPr_2CHCH_3)$ (**B.6**, Equation B.2). This formulation was consistent with the complex's spectral data in solution. For example, the $^{13}C\{^1H\}$ NMR spectrum features a signature resonance at 62.6 ppm (dd, $^2J_{C\text{-}Pcis}$ = 13.8 Hz, $^2J_{C\text{-}Ptrans}$ = 56.7 Hz) due to the coupling of an organometallic carbon atom to two nonequivalent phosphorus nuclei.

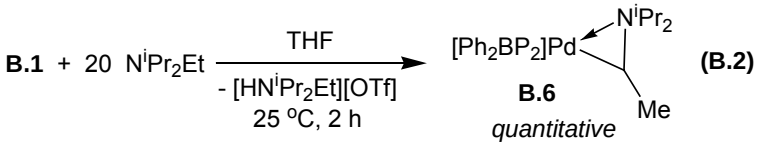

The scope and selectivity of the amine activation process was explored (Scheme B.2). In general, the activation process was found to proceed for trialkylamine substrates that feature secondary C-H bonds adjacent to the N-atom. Palladacycle products that feature 3-membered rings appear to be formed exclusively, with no inclination to form larger metallacycles. To test the reaction's selectivity, the amine NCy_2Et was chosen as a substrate as it contains both tertiary and secondary C-H bonds that can undergo activation. Treatment of **B.1** with excess NCy_2Et in THF resulted in clean conversion to only one palladacycle, $[Ph_2BP_2]Pd(N,C:\eta^2\text{-}NCy_2CHMe)$ (**B.8**), derived from formal cleavage of a secondary C-H bond of the ethyl group. The substrates *N*-methylpyrrolidene and *N*-methylpiperidene were also examined to compare the reactivity of primary versus secondary C-H bonds. Again, activation at the secondary C-H position occurred exclusively, affording the bicyclic palladacycles $[Ph_2BP_2]Pd(N,C:\eta^2\text{-}NMeCH(CH_2)_3)$ (**B.9**) and $[Ph_2BP_2]Pd(N,C:\eta^2\text{-}NMeCH(CH_2)_4)$ (**B.10**), respectively.

To induce reactivity of primary C-H bonds the reactivity of **B.1** with NCy_2Me and N^iPr_2Me was examined. A steric bias might in these cases be expected to direct the

palladium center towards the methyl position. However, the predominant byproduct (70 to 80%) for these substrates was the familiar palladium(I) dimer, $\{[Ph_2BP_2]Pd\}_2$ (**B.4**) (^{31}P NMR).

Scheme B.2

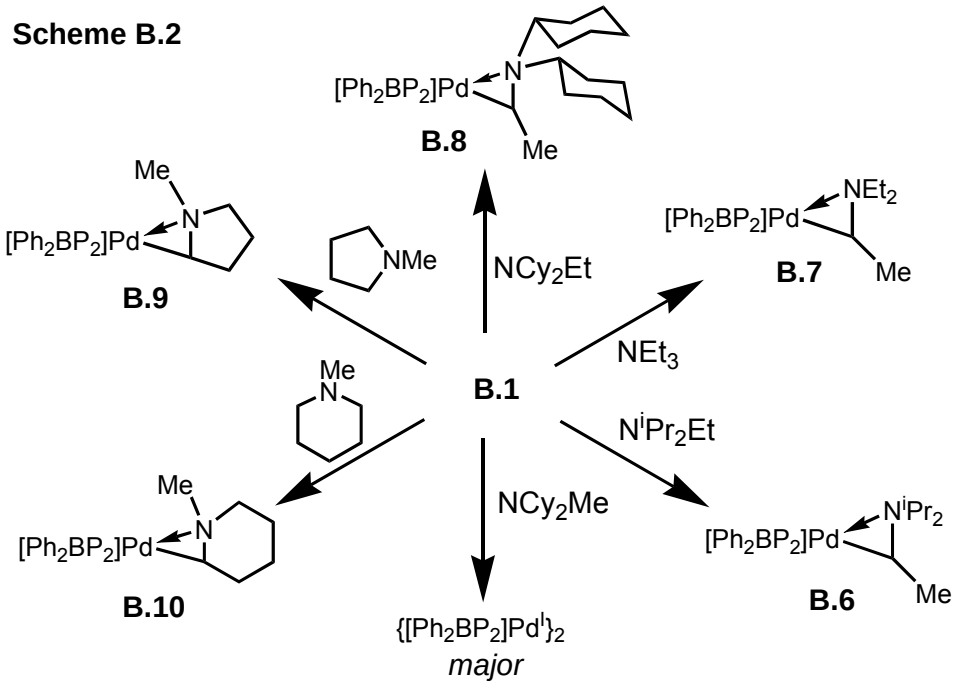

Addition of diisopropyl(2-propenyloxymethyl)amine to **B.1** effected formal C-O rather than C-H bond cleavage to generate $[Ph_2BP_2]Pd(N,C:\eta^2\text{-}N^iPr_2CH_2)$ (**B.11**, Equation B.3) in good yield. Allyl ethers are known to react with Pd(0) sources to generate palladium allyl products via formal C-O cleavage.[21] The high-yield isolation of **B.11** shows quite clearly that $[Ph_2BP_2]Pd(N,C:\eta^2\text{-}NR_2CH_2)$ are viable products of amine activation, and it is therefore puzzling that a similar product is not formed when **B.1** is treated with N^iPr_2Me (*vide infra*).

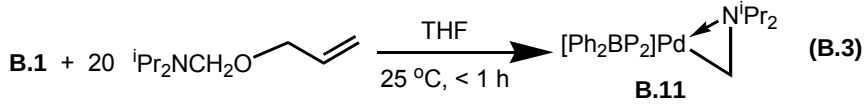

(B.3)

B.2.4 Molecular Structures of the Palladacycles B.8 and B.9

X-ray diffraction studies of the palladacycles were pursued to gain insight into the structural nature of the Pd-N-C core. Crystals of **B.6** and **B.11** suffered from disorder of the iminium group, $R_2C=N^iPr_2$, which sits in two orientations. Derivatives **B.8** and **B.9** provided more reliable structural parameters (Figure B.3, Table B.1). In each structure, the bond angles around palladium are largely distorted from 90º, though all four atoms coordinated to palladium lie in a well-defined plane. Specifically for **B.8** and **B.9**, the N-Pd-C_α angles are acute (39.7(1) and 38.3(2), respectively), and the P(1)-Pd-N angles (122.3 and 120.9º) are significantly larger than the P(2)-Pd-C_α angles (104.0 and 107.6º).

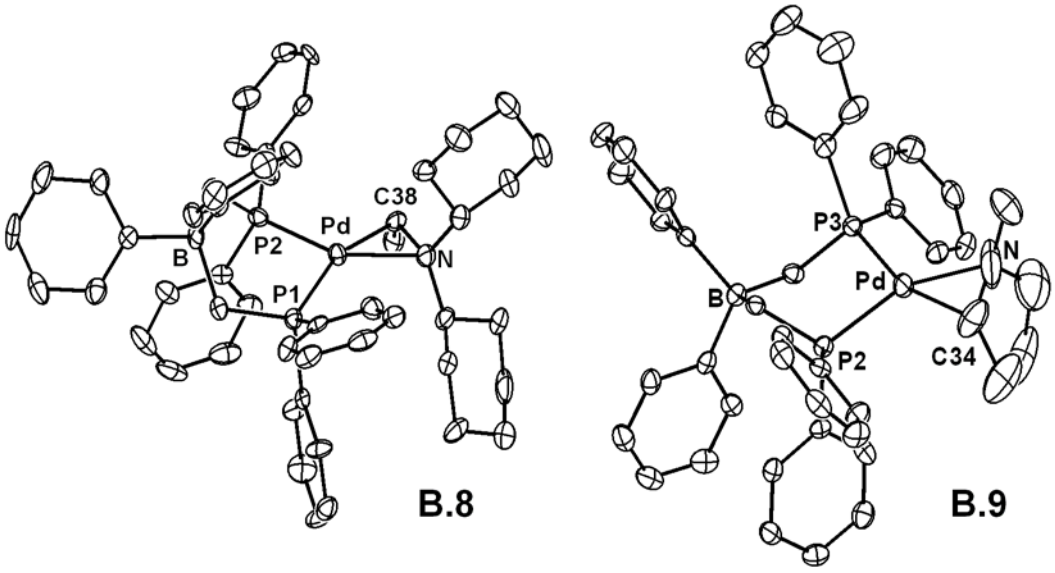

Figure B.3. 50% thermal ellipsoid representations of $[Ph_2BP_2]Pd(N,C:\eta^2\text{-}NCy_2CHMe)$ (**B.8**) and $[Ph_2BP_2]Pd(N,C:\eta^2\text{-}NMeCH(CH_2)_3)$ (**B.9**). Hydrogen atoms have been omitted for clarity.

Table B.1. Selected bond distances (Å) and angles (deg.) for $[Ph_2BP_2]Pd(N,C:\eta^2\text{-}NCy_2CHMe)$ (**B.8**) and $[Ph_2BP_2]Pd(N,C:\eta^2\text{-}NMeCH(CH_2)_3)$ (**B.9**).

Complex **B.8**		Complex **B.9**	
Pd-C(39)	2.037(3)	Pd-C(43)	2.048(4)
Pd-N	2.180(3)	Pd-N	2.104(3)
Pd-P(1)	2.3641(9)	Pd-P(1)	2.3354(8)
Pd-P(2)	2.2549(9)	Pd-P(2)	2.2945(8)
N-C(39)	1.438(4)	N-C(43)	1.361(5)
N-C(41)	1.502(4)	N-C(39)	1.460(5)
N-C(47)	1.484(4)	N-C(40)	1.420(6)
P(1)-Pd-P(2)	93.60(3)	P(1)-Pd-P(2)	93.49(3)
P(1)-Pd-N	122.31(7)	P(1)-Pd-N	120.9(1)
P(2)-Pd-C(39)	104.04(9)	P(2)-Pd-C(43)	107.6(2)
N-Pd-C(39)	39.7(1)	N-Pd-C(43)	38.3(2)
C(39)-N-C(41)	115.8(3)	C(43)-N-C(39)	117.4(4)
C(39)-N-C(47)	117.9(3)	C(43)-N-C(40)	108.0(4)
C(41)-N-C(47)	119.3(2)	C(39)-N-C(40)	117.0(4)

Palladacycles akin to **B.8** and **B.9** have not to our knowledge been described. However, metallaaziridines featuring other transition metals are well established, although they are formed from different methods of preparation.[22] For example, a family of nickel aziridines $(PR_3)(X)Ni(N,C:\eta^2\text{-}CH_2NMe_2)$ that are structurally related to the palladacycles described here were first reported nearly three decades ago.[22d] Two limiting resonance forms are to be considered with respect to the Pd-N-C core (Figure B.4).[22a,d] The first emphasizes a palladium(0) form of the complex with an anionic $\{[Ph_2BP_2]Pd\}^-$ fragment coordinated by an iminium cation ($RHC{=}NR_2^+$). This formulation is analogous to the many olefin complexes of palladium(0) that are known. The other limiting resonance form assigns the alkylamine functionality as a 3-electron LX-type organometallic ligand. In this latter view, a palladium(II) center is formally coordinated to an alkyl ligand with a β-amine donor occupying the fourth site.

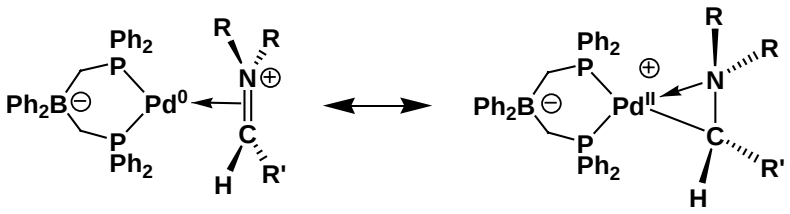

Figure B.4. Limiting resonance forms for the palladacycles.

Close examination of the structural parameters of **B.8** and **B.9** does not unambiguously distinguish between the two resonance forms. The Pd-C_α distances observed for **B.8** and **B.9** are unusually short for *cis*-bis(phosphine)Pd complexes. Their respective distances of 2.037(3) and 2.048(4) Å are just below both the minimum Pd-C(sp^3) and Pd-C(sp^2-alkene) bond distances reported for palladium supported by two phosphines in *cis* relation. The N-C_α bond lengths for complexes **B.8** and **B.9** are between those of free iminium cations (ca. 1.32 Å) and N-C single bonds (ca. 1.50 Å), but are also quite different from one another (1.438(4) Å for **B.8** and 1.361(5) Å for **B.9**). The latter N-C bond distance is the shortest thus far reported for mononuclear metallaaziridines of related structure (range: 1.392 to 1.548 Å, mean of 1.440 Å, SD = 0.03, Cambridge Structural Database[23]). The bond angles around the nitrogen atom are nearly 120º for complex **B.8**,[24] suggesting that the nitrogen atom is perhaps better formulated as sp^2- rather than sp^3-hybridized.

B.2.5 Probing the Reversibility of Palladacycle Formation

To probe whether the formation of the palladacycles [Ph_2BP_2]Pd(N,C:η_2:NR_2CHR') might be reversible we examined whether deuterium would scramble into the palladacycle aliphatic positions upon incubation in the presence of a deuterated ammonium salt. Exposure of **B.1** to $^{i}Pr_2NCH_2CH_2CH_3$ proceeded in

similar fashion to provide the expected palladacycle $[Ph_2BP_2]Pd(N,C:\eta_2{}^iPr_2NCHCH_2CH_3)$ (**B.12**). A homogeneous solution of the complex **B.12** and 15 equivalents of $[DN^iPr_2Et][OTf]$ were stirred at 25 °C for several days. Complex **B.12** was stable under these conditions: no degradation was evident in the ^{31}P NMR spectrum of the reaction solution. Upon examination of the ^2H NMR spectrum, however, it was evident that deuterium had scrambled into the α- and β-carbon positions of the iminium ligand in an approximate ratio of 1:5 respectively (Equation B.4).

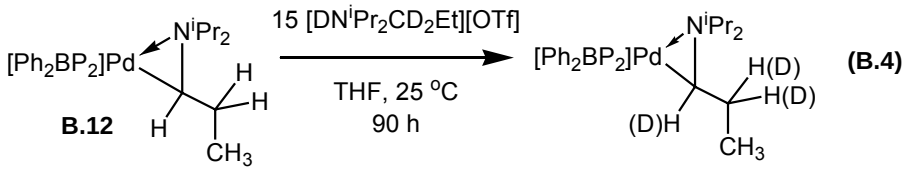

(B.4)

In a related experiment we examined whether iminium ligand substitution would proceed in the presence of an ammonium salt and a trialkylamine. The palladacycle $[Ph_2BP_2]Pd(N,C:\eta_2:N^iPr_2CHCH_3)$ **B.6** was incubated with 15 equivalents of $[HNEt_3][OTf]$ and 15 equivalents of NEt_3 in THF at 80 °C. Under these conditions, none of the palladacycle $[Ph_2BP_2]Pd(N,C:\eta_2:NEt_2CHCH_3)$ **B.7** could be detected after several days (Equation B.5). If **B.6** could undergo protonation to produce $[Ph_2BP_2]Pd(N^iPr_2Et_2)(OTf)$ at some reasonable rate, then we would expect a detectable degree of exchange to occur (i.e., $[Ph_2BP_2]Pd(N^iPr_2Et)(OTf) + NEt_3 \rightarrow [Ph_2BP_2]Pd(NEt_3)(OTf) + N^iPr_2Et$).

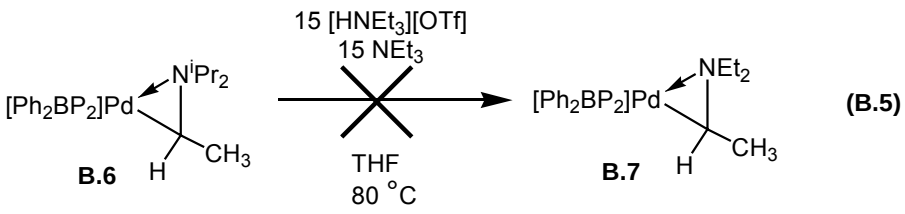

(B.5)

B.2.6 Addition of *tert*-Butyl Isocyanide and Sodium Cyanide to [Ph_2BP_2]Pd(N,C:η^2-NEt_2CHCH_3) (B.7)

The addition of excess *tert*-butyl isocyanide to **B.7** resulted in a single new palladium complex, [Ph_2BP_2]Pd(C(H)=N^{t}Bu)(CN^{t}Bu) (**B.13**), and concomitant expulsion of the enamine $Et_2NC(H)=CH_2$ (Equation B.6). Complex **B.13** is characterized by two intense vibrations in its infrared spectrum (ν(H*C*=*N*^{t}Bu) = 1608 cm^{-1}, ν(*C*≡*N*^{t}Bu) = 2195 cm^{-1}; CH_2Cl_2/KBr) and a signature ^{1}H NMR resonance at 8.75 ppm for the iminoformyl proton Pd(C(*H*)=N^{t}Bu).[25] The release of the enamine $Et_2NC(H)=CH_2$ was confirmed by comparing the crude reaction spectrum with that of an independently prepared sample.

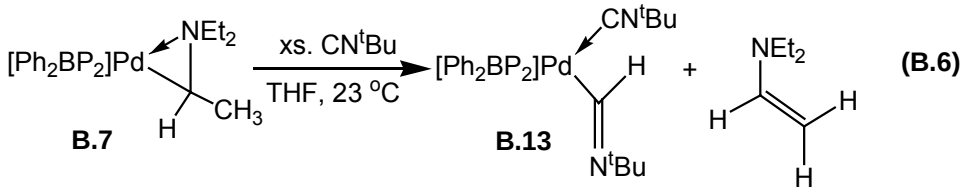

(B.6)

Addition of cyanide anion to **B.7** effected the release of the iminium ligand as a functionalized amine product via generation of a new C-C bond at the α position (Equation B.7). Treatment of **B.7** with 5 equivalents of NaCN in methanol/THF produced $Et_2NCH(CN)CH_3$, confirmed by GC-MS and ^{1}H NMR analysis following work-up. A ^{1}H NMR spectrum of the reaction solution immediately following the addition in CD_3OD/THF-d_8 established that the consumption of **B.7** is very rapid at rt and that the $Et_2NCH(CN)CH_3$ byproduct is released quantitatively. The palladium product(s) of the reaction have not been identified.

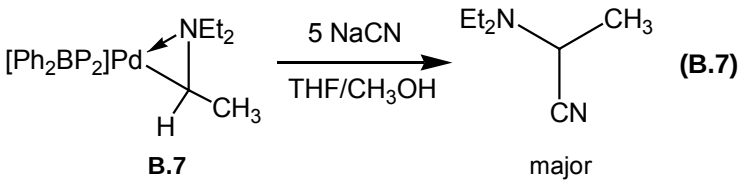

B.2.7 Kinetic Data

The decay of complex **B.1** (0.044 M) in the presence of 20 equivalents of N^iPr_2Et was monitored by ^{31}P NMR spectroscopy and exhibits clean first-order decay in THF at 23 °C. The reaction rate was conveniently determined by integrating the ^{31}P NMR resonance of complex **B.1** versus an internal standard of $Ph_3P{=}O$, sealed as a CH_2Cl_2 solution within a capillary tube. During the reaction course the starting material **B.1** and the product **B.6** were the only two species observed. The rate constant, k_{obs} = 5.6(1) x 10^{-4} s^{-1}, is obtained as the average of three independent runs. Perhaps a more meaningful constant is k′, where $k_{obs} = k'[N^iPr_2Et]/[THF]^2$ (*vide infra*). By assuming constant concentrations of N^iPr_2Et and THF, a value of k′ = 5.6(1) x 10^{-2} s^{-1} is obtained ($[N^iPr_2Et]_i$ = 0.88 M and $[THF]_i$ = 9.33 M). The temperature dependence of the reaction rate was explored between 0 and 35.3 °C. An Eyring plot of this data is provided in Figure B.5 from which the activation parameters $\Delta H^‡$ = 17.9 ± 0.2 kcal/mol and $\Delta S^‡$ = –4 ± 1 eu can be extrapolated. The effect of the amine concentration $[N^iPr_2Et]$ on the reaction rate was also examined by monitoring the rate of decay of **B.1** in the presence of 3 to 30 equivalents of N^iPr_2Et at 23 ºC in THF. The rate data for consumption of **B.1** versus $[N^iPr_2Et]$ are plotted in Figure B.6 and indicate a rate that is first order in $[N^iPr_2Et]$.

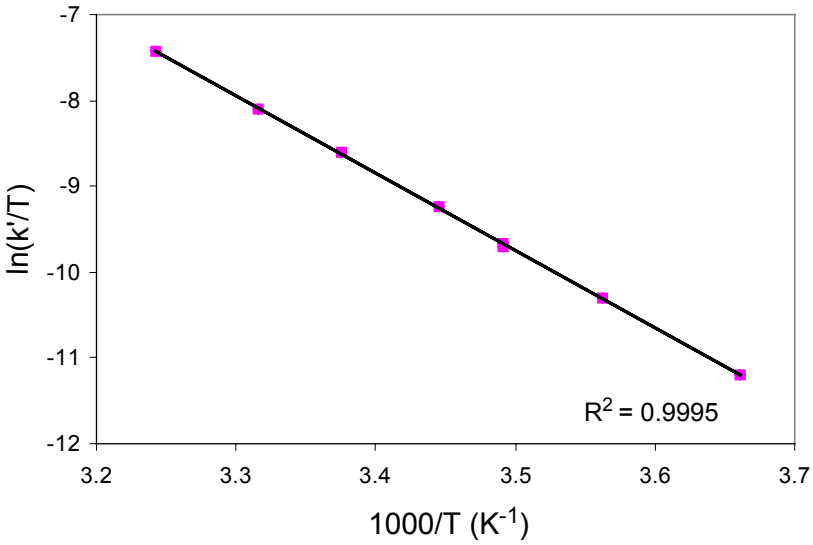

Figure B.5. Eyring plot for the reaction of **B.1** with 20-fold N^iPr_2Et, from 273.2 to 308.5 K, $\Delta H^{\ddagger} = 17.9 \pm 0.2$ kcal/mol, $\Delta S^{\ddagger} = -4 \pm 1$ eu.

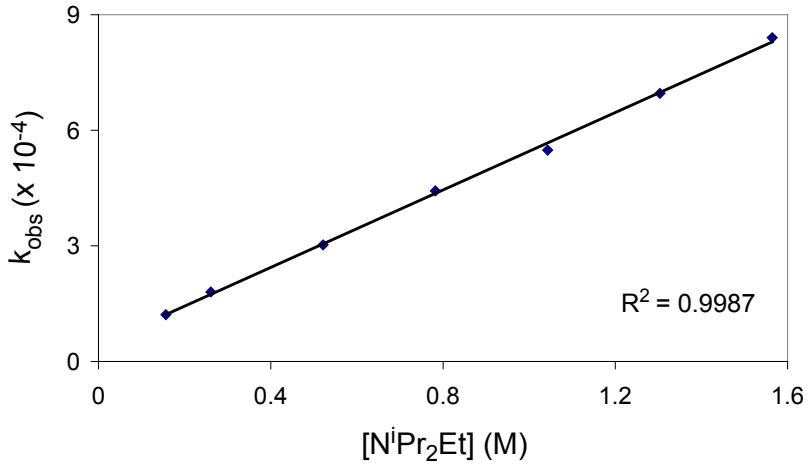

Figure B.6. Rate dependence on $[N^iPr_2Et]$. Reaction conditions: [**B.1**] = 0.052 M; $[N^iPr_2Et]$ is varied between 0.16 M and 1.56 M at 296 K in THF (0.6 mL total solution volume).

The relative rate of the reaction between **B.1** (0.044 M) and the substrates N^iPr_2Et or $N^iPr_2CD_2Me$ (0.88 M) was examined in THF. A dramatic attenuation in rate was observed for the deuterated amine substrate (k_{obs} = 9.9(6) x 10^{-5} s^{-1}), providing a kinetic deuterium isotope effect, $k_{rel}(k_H/k_D)$, of 5.9. For the case of $N^iPr_2CD_2Me$, a small amount of an intermediate species was detected in the ^{31}P NMR spectrum. This species featured a pair of doublets at 28.5 and 39.4 ppm with $^2J_{PP}$ = 62 Hz and can be tentatively assigned as the amine adduct complex, $[Ph_2BP_2]Pd(N^iPr_2CD_2Me)(OTf)$, based upon its similarity in chemical shift to $[Ph_2BP_2]Pd$(*o*-phenylpyridine)(OTf) (**B.5**). We presume that $[Ph_2BP_2]Pd(N^iPr_2CD_2Me)(OTf)$ accumulates due to the attenuated C-D activation rate.

Inspection of the ^1H and ^2H NMR spectra of the reaction between **B.1** and $N^iPr_2CD_2Me$, subsequent to the complete consumption of **B.1,** revealed that the palladacycle product **B.6** contained deuterium at the α- and β-carbon positions in a nearly statistical ratio of 1 : 4 (Equation B.8). The ammonium salt byproducts, $[DN^iPr_2CD_2CH_3]^+$ and $[HN^iPr_2CD_2CH_3]^+$, showed no evidence for deuterium scrambling into the β-carbon position. The extent of deuterium scrambling into the alkyl chain was next investigated using the *N*-propyl amine substrate $^iPr_2NCD_2CH_2CH_3$. In this case deuterium incorporation occurred only at the α- and β-carbon positions and in a statistical ratio of 1:2. No scrambling into the γ-carbon position was detected (Equation B.9).

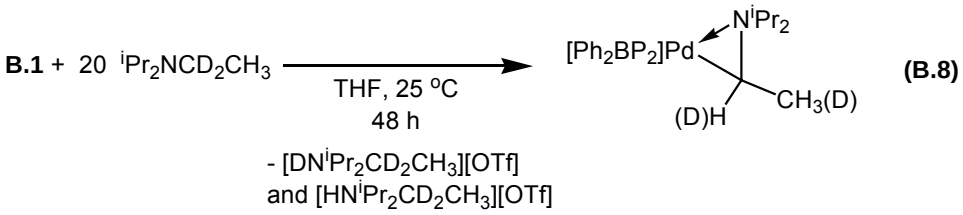

(B.8)

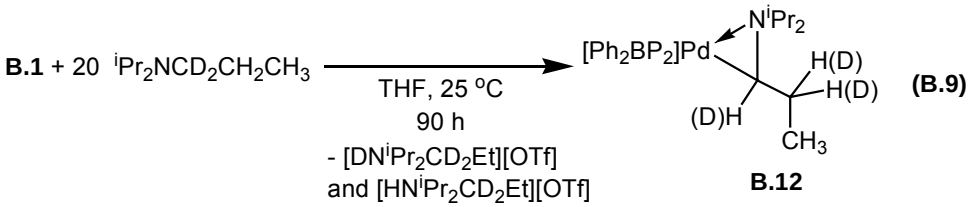

B.2.8 Observation of Intermediates by VT NMR Spectroscopy Using NEt_3 in Toluene

Intermediates during the amine activation reaction were difficult to study because of their low concentrations in THF. Unfortunately, THF is the only solvent that mediates the quantitative conversion of **B.1** and amine to the corresponding palladacycle product. A reasonable compromise was found by studying the activation reaction at low temperature in toluene. Recall that in benzene or toluene, the treatment of **B.1** with N^iPr_2Et (or NEt_3) at rt generates $\{[Ph_2BP_2]Pd\}_2$ (**B.4)** as the major product and only a small amount of the palladacycle **B.6** (or **B.7**). At low temperature (toluene, -35 to 0 ºC), however, the palladacycle products dominate. The case of NEt_3 was examined in detail because of its slightly simplified ^1H NMR spectrum in the aliphatic region. A toluene-d_8 solution of **B.1** in the presence of 50 equivalents of NEt_3 was examined from -50 ºC to 0 ºC by both ^1H and ^{31}P NMR spectroscopy (Figure B.7). In the low temperature regime (-50 ºC), two broad resonances are observed in the ^{31}P NMR spectrum (42.7 ppm, 45.2 ppm) due to slow exchange between **B.1** and **B.1′**. As noted previously, a similar spectrum is observed for **B.1** in CD_2Cl_2 at -50 ºC in the absence of amine. At -35 ºC the two signals have coalesced into a single resonance that is centered at 45 ppm, indicating that **B.1** and **B.1′** are in fast exchange. As the sample is further warmed to -20 ºC, precursor **B.1** decays and four new doublets arise that represent two independent species. The more downfield pair of doublets (45.0 and 29.5 ppm, J_{PP} = 25.9 Hz) is relatively

similar in chemical shift to the resonances observed for the *o*-phenylpyridine adduct complex **B.5** (46.3 and 35.3 ppm). By analogy, this intermediate is proposed to be the amine adduct complex $[Ph_2BP_2]Pd(NEt_3)(OTf)$. An alternative and perhaps equally reasonable formulation for this intermediate would be to suggest that an agostic C-H bond from the amine ligand fills the fourth site and that the triflate anion is outer-sphere. However, examination of the ^1H NMR spectrum between -60 ºC and -20 ºC provided no evidence for an agostic C-H proton.

The other pair of doublets (32.5 and 18.0 ppm, $^2J_{PP}$ = 36.0 Hz), which correspond to another intermediate, are more complex in the proton-coupled ^{31}P NMR spectrum (Figure B.7, inset (a)). The doublet centered at 18 ppm splits into a doublet of doublets with a rather large secondary coupling constant of ~200 Hz. The ^1H NMR spectrum shows a doublet of doublets centered at -8.62 ppm ($^3J_{HP}$ (*cis*) = 30.5 Hz and $^3J_{HP}$ (*trans*) = 200.4 Hz). This resonance simplifies to a singlet when the ^{31}P nuclei are decoupled. These data collectively intimate a square planar "$[Ph_2BP_2]Pd(H)(L)$" hydride intermediate. As discussed below, this intermediate is proposed to be the hydride iminium adduct $[[Ph_2BP_2]Pd(H)(\eta^2\text{-}N(Et_2)=CHCH_3)][OTf]$.

The two detectable intermediates decayed as the concentration of palladacycle **B.7** increased. As the reaction proceeded at -20 ºC, the intermediates maintained a ~ 1:1 ratio until they were practically consumed. Integration of the final ^{31}P NMR spectrum acquired at 0 ºC established that **B.7** had been generated in ~ 80% yield. As shown in Figure B.7, the palladium dimer $\{[Ph_2BP_2]Pd\}_2$ **B.4** was present in only trace quantity (doublets at ~ 10 and 27 ppm). Many of the observed impurities comprise the resonances between 44 and 47 ppm and are unassigned.

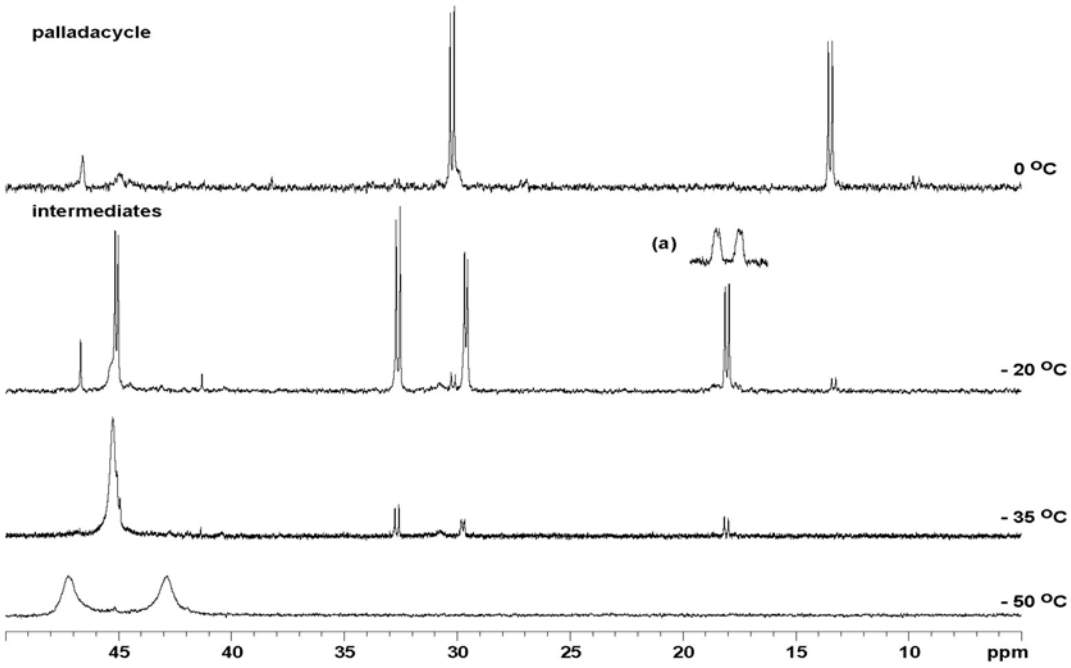

Figure B.7. Reaction profile followed by $^{31}P\{^{1}H\}$ NMR spectroscopy of **B.1** and 50 equivalents NEt_3 in d_8-toluene. The temperature was gradually warmed from -50 to 0 ˚C. (a) Inset shows splitting of peak upon removing proton decoupling. Spectra and inset correspond to the scale shown at the bottom.

B.2.9 Comparison to the System $[(Ph_2SiP_2)Pd(THF)_2][OTf]_2$

The lack of precedent for the palladaziridines described herein was surprising given their thermal stability and the fact that 5- and 6-membered palladacycles are rather common.[26] To inquire as to whether the choice of the anionic $[Ph_2BP_2]$ phosphine ligand was serendipitous, a palladium system supported by the neutral bis(phosphine) ligand $Ph_2Si(CH_2PPh_2)_2$ (abbreviated as Ph_2SiP_2) was studied. The ligand Ph_2SiP_2 is a structurally faithful, neutral analogue of $[Ph_2BP_2]$ that gives rise to reaction profiles very similar to the more familiar bis(diphenylphosphino)propane (dppp) ligand. The desired

precursor complex, $(Ph_2SiP_2)Pd(OTf)_2$ (**B.14**), was conveniently prepared in two steps in 87% overall yield by reaction of Ph_2SiP_2 with $PdCl_2(NCPh)_2$ to generate $(Ph_2SiP_2)PdCl_2$ (**B.15**), followed by treatment with two equivalents of AgOTf to give **B.14**.

Similar to $[[Ph_2BP_2]Pd(THF)_2][OTf]$ (**B.1**), $(Ph_2SiP_2)Pd(OTf)_2$ (**B.14**) coordinated *o*-phenylpyridine in THF but did not effect aryl metalation in the temperature range between 25 °C and 80 °C. Moreover, like **B.1**, complex **B.14** is quite reactive towards trialkylamine substrates. Indeed, complex **B.14** was fully consumed in less than 1 h at rt, releasing a stoichiometric equivalent of $[HN^iPr_2Et][OTf]$ when exposed to just 3 equivalents of N^iPr_2Et in THF. Complete consumption of **B.1** on a similar timescale requires 20 equivalents of N^iPr_2Et. Despite these promising signs, the major palladium-containing product in the case of **B.14** is the dimeric palladium(I) complex $[\{(Ph_2SiP_2)Pd\}_2][OTf]_2$ (**B.16**) (Equation B.10). A second set of NMR signals (^{31}P and ^{13}C NMR) were also present, albeit in much lower concentration relative to **B.16**, that may be attributed to $[(Ph_2SiP_2)Pd(N,C:\eta^2\text{-}N^iPr_2CHCH_3)][OTf]$. The ^{13}C NMR spectrum showed a characteristic resonance at 47 ppm, roughly the chemical shift expected for the Pd-bound carbon atom of the iminium ligand. Other tertiary amines provided similar results, and in no case were the secondary reaction products isolated or more thoroughly characterized due to their low concentrations and the difficulty in separating them from dimeric **B.16**. Gentle warming of a solution that presumably contains $[(Ph_2SiP_2)Pd(N,C:\eta^2\text{-}N^iPr_2CHCH_3)][OTf]$ does not lead to its conversion to **B.16**.

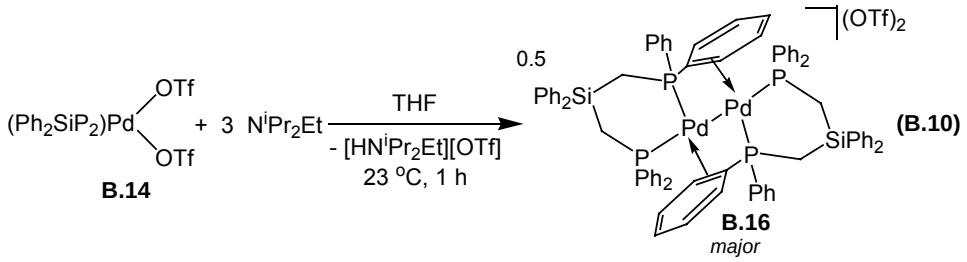

B.3 Discussion

B.3.1 General Summary

Access to the chemistry described herein required a synthetic route to $[Ph_2BP_2]Pd(THF)_2][OTf]$ (**B.1**). Starting with $[Ph_2BP_2]$ and commercially available $(PhCN)_2PdCl_2$, complex **B.1** is readily prepared in three steps and in an overall isolated yield of 67%. The THF and triflate ligands of **B.1** are highly labile. Consequently, complex **B.1** reacts as an unsaturated Pd(II) center with two open *cis* sites. The reactivity of **B.1** with trialkylamines is marked in its rapidity at rt. Moreover, the reaction conditions and work-up are fairly general for the various amine substrates examined. The palladacycles are produced cleanly and isolable in high yields (typically 80%). Extremely bulky amines, however, result in lower isolated yields (e.g., 38% yield for $[Ph_2BP_2]Pd(N,C:\eta^2\text{-}NCy_2CHMe)$ (**B.8**)). The decreased yields are likely the result of the difficultly in separating the palladacycles from the ammonium salt byproduct due to the decreased solubility associated with the increased rigidity of the more encumbered palladacycles.

The amine activation process is selective for secondary C-H bonds. The bias against tertiary C-H bonds is presumably of steric origin, while the bias against primary C-H bonds is consistent with C-H bond dissociation energies (methylene CH_2 < primary

CH_3). While the focus of this paper centers on amine activation exclusively, the transformations described may prove to be more general. One clue that this might be the case comes from the curious reaction that converts **B.1** to **B.11** upon addition of diisopropyl(2-propenyloxymethyl)amine (Equation B.3). A mechanistic sequence that would account for this transformation invokes coordination of an O-atom lone pair to palladium(II) followed by a β-hydride elimination step. The oxonium intermediate formed could then rearrange to **B.11** along with the release of acrolein (Scheme B.3). Comparing C-H bond dissociation energies, the allylic C-H bond is expected to be weaker and thus is preferentially cleaved.

Scheme B.3

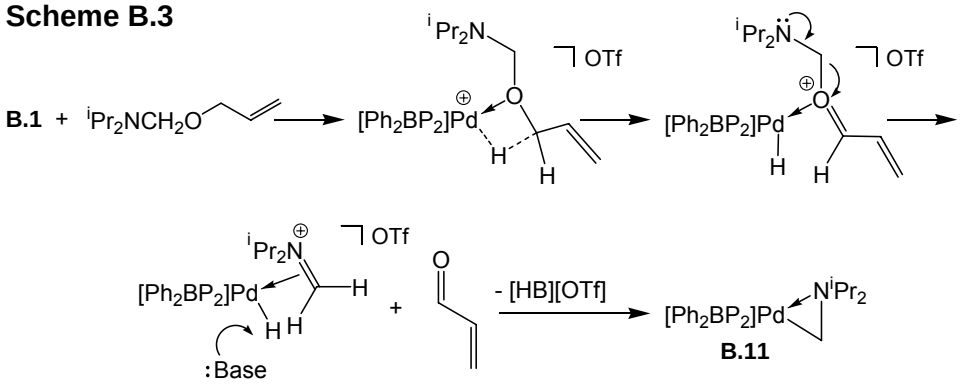

B.3.2 Reactivity of the Palladacycles

The observation that deuterium can scramble from a deuterated ammonium salt into the aliphatic positions of the neutral palladacycles suggests that the palladacycles are not static species (Equation B.4), but rather are capable of dynamic β-hydride elimination/olefin re-insertion processes in accord with cationic palladium alkyls such as Brookhart's (α-diimine)Pd(alkyl)$^+$ systems.[27] Facile chain walking would allow deuterium to wash into the α- and β-carbon positions. Curiously, deuterium does not wash into the γ-carbon position. This discrepancy may arise from differences in the

stability of the palladium hydride intermediates that lie along the path leading to deuterium incorporation (Scheme B.4). Incorporation of deuterium at the α and β positions is expected to proceed via a palladium enamine hydride species, whereas incorporation at the γ position is expected to proceed through a palladium allylamine hydride species. It may be that this latter species is conformationally disfavored and hence deuterium scrambling traverses exclusively along the lower three paths shown in Scheme B.4. It is also plausible to suggest that electronic factors would play a role in destabilizing a Pd allylamine hyride species. In the Pd enamine hydride, the N-atom lone pair should increase the π-basicity of the olefin ligand. This would not be true of an allylamine hydride species.

Although the palladium enamine hydride complexes appear to be intermediates in solution, they have not been directly observed. They can, however, be chemically trapped. For instance, the addition of excess *tert*-butylisocyanide to $[Ph_2BP_2]Pd(N,C:\eta^2\text{-}NEt_2CH_2)$ (**B.7**) liberates enamine and traps the inferred hydride to generate the complex $[Ph_2BP_2]Pd(C(H)=N^tBu)(CN^tBu)$ (**B.13**, Equation B.6).

Scheme B.4

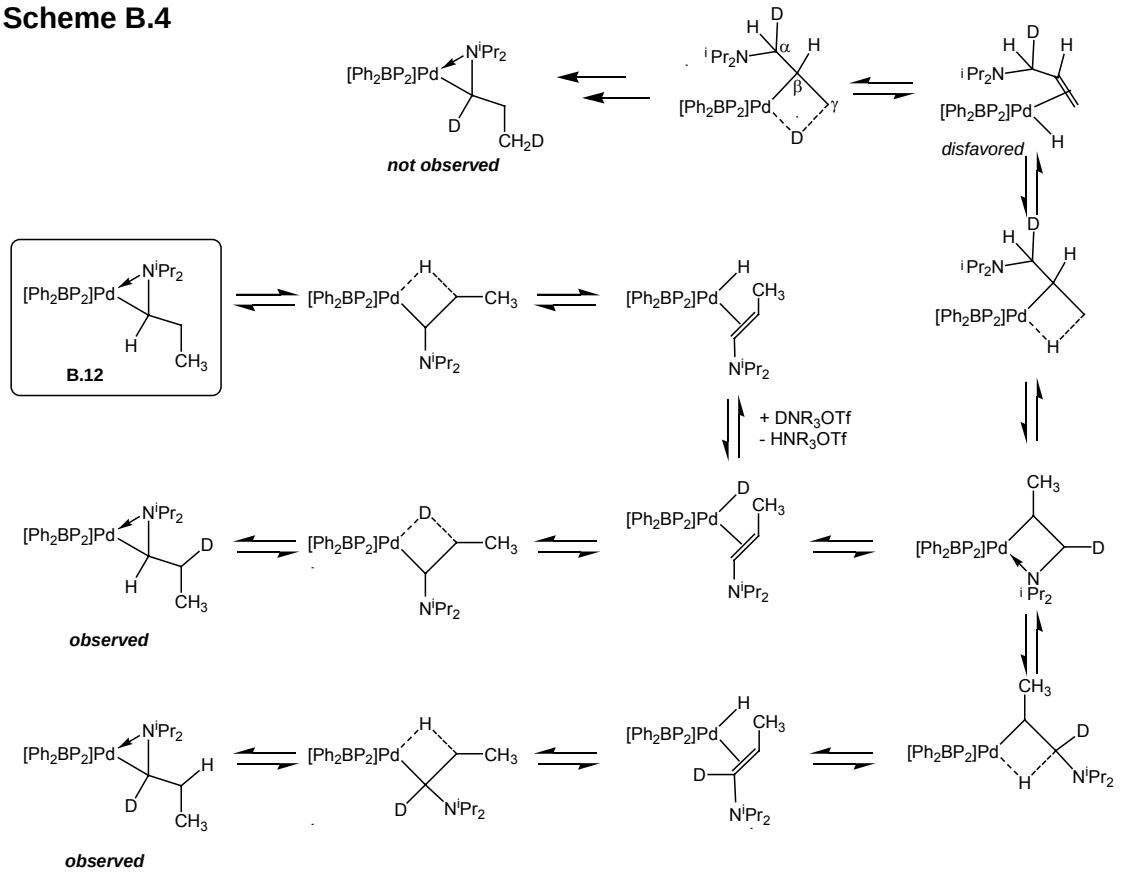

The reactivity of **B.7** with NaCN to generate a new C-C bond is consistent with nucleophilic attack of cyanide at an electrophilic iminium ion bound to Pd(0) (Equation B.7). Though we have not thoroughly explored the reactivity of these palladacycles, it is apparent that the Pd-N-C core shows reactivity consistent with both of its limiting resonance forms: as a Pd(0) iminium adduct (NaCN), and as a Pd(II) alkyl complex with an amine donor (*β*-hydride elimination, deuterium scrambling).

B.3.3 Mechanism

Three limiting mechanisms for the amine C-H activation process are presented in Scheme B.5. Common to each path is an amine adduct of **B.1**. The amine adduct **A** is designated with a triflate ligand coordinated to palladium, although THF and triflate are likely in rapid exchange in THF solvent. Intermediate **A** presumably rearranges to species

B, whereby an intramolecular C_α-H bond replaces the donor ligand (OTf or THF) in the site adjacent to the amine donor. At the formal C-H bond-breaking step, the proposed paths diverge. Path I invokes β-hydride elimination to generate the palladium iminium hydride complex **C**, which is then deprotonated by an exogenous base to give the palladacycle product. Another possibility, path II, suggests that the agostic proton in **B** is directly deprotonated. Alternatively, the agostic C-H bond may undergo oxidative addition to a Pd(IV) alkyl hydride complex **D**, which like **C**, is subsequently deprotonated (path III).

Proposed intermediate **B** is common to each of the three paths. While no direct spectroscopic evidence for **B** has been obtained, its intermediacy to either a β-hydride elimination process (path I) or an oxidative addition step (path III) seems reasonable to infer. Moreover, an agostic C-H proton coordinated to a positively charged palladium center should have markedly increased acidity, which would facilitate its direct deprotonation by a Brönsted base (path II). A wealth of mechanistic information has been collected for cationic $P_2Pd(II)$ alkyl complexes by Brookhart and coworkers. In some favorable cases an agostic C-H proton coordinated to a cationic palladium(II) center can be directly observed (e.g., (dippp)Pd(CH_2CH_2-μ-H)$^+$).[28] The topological analogy between inferred **B** and $P_2Pd(R)^+$ systems is apparent (Figure B.8).

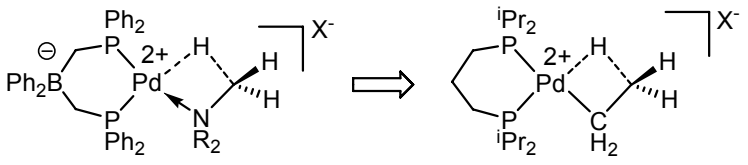

Figure B.8. Comparison of intermediate **B** and (dippp)Pd(CH_2CH_2-μ-H)$^+$.

Scheme B.5

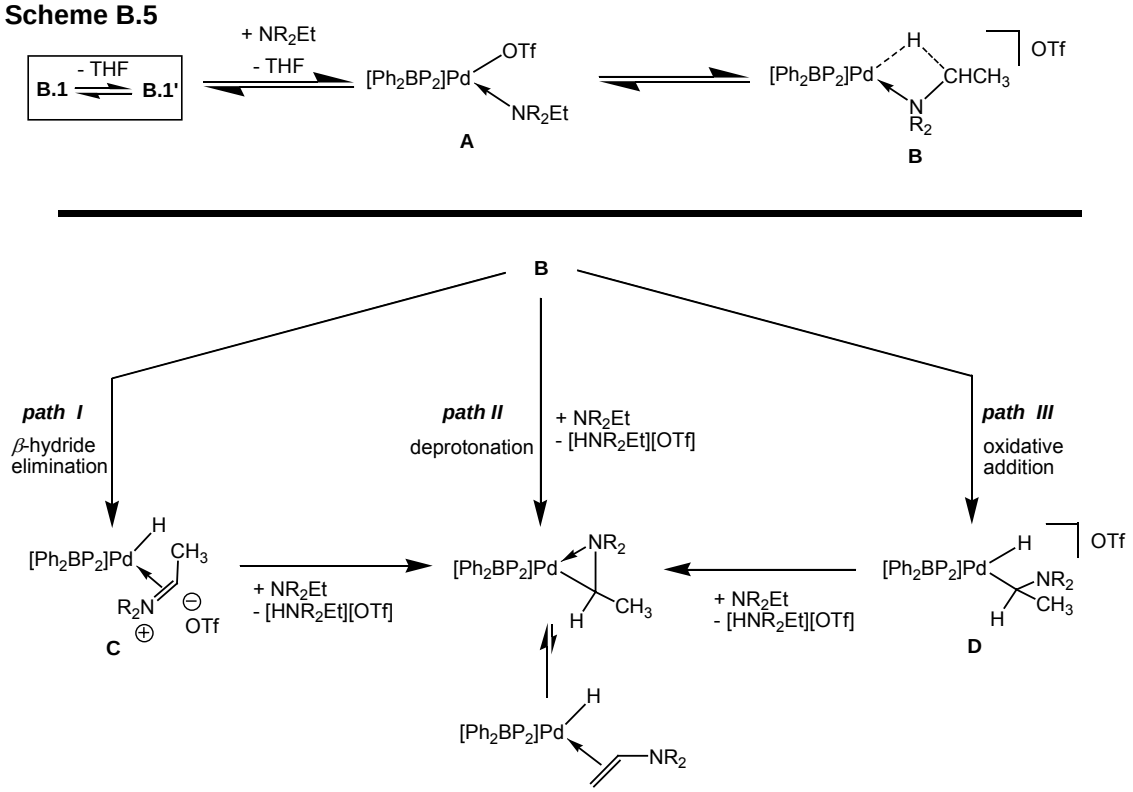

The spectroscopic observation of an intermediate palladium hydride species at low temperature in d_8-toluene solution is the best evidence against path II. A possible counterargument is that this intermediate lies along a non-productive path and is in equilibrium with **B**. If path II is operative, however, then the deprotonation step would have to be rate-determining to give rise to the large KIE observed. The rate law of the reaction would then be expected to show a second-order dependence on amine concentration, assuming exogenous amine to be the base. The observation of a first-order dependence of rate on amine concentration therefore appears to be inconsistent with path II.

Experimentally discriminating between paths I and III is less straightforward. Both paths invoke palladium hydride intermediates, both are expected to exhibit a primary KIE, and both could exhibit a first-order dependence on amine. The prevalence of β-hydride elimination processes in Pd(II) complexes of similar structure to **B** favors

path I. Given the lack of a well-defined Pd(II/IV) redox couple associated with a C-H bond cleavage step, there is no compelling reason to invoke such a scenario here (i.e., path III).[29]

In the context of path I, the work of Murahashi *et al.* is relevant. These authors proposed the intermediacy of an η^2-iminium hydride of Pd(II), $Pd(H)(RHC{=}NR^1R^2)^+$ in their trialkylamine redistribution reactions ($NR^1{}_2R^2 \rightarrow NR^1{}_3 + NR^2{}_3 + NR^1{}_2R^2 + NR^1R^2{}_2$, where $R^1 \neq R^2$) catalyzed by palladium black at 200 ºC.[30] Formal oxidative insertion of Pd(0) into a secondary C-H bond adjacent to an amine N-atom was invoked as the key bond-breaking step. In the present system, we suggest β-hydride elimination from Pd(II) to be the C-H bond-cleaving step. An additional system that appears to be mechanistically related to the present case comes from Harman and coworkers, who have provided spectroscopic data to suggest that one-electron reduction of an Os(III) amine complex induces *β*-hydride elimination to generate an Os(II) η^2-iminium hydride complex.

B.3.4 Rate Law in THF

The mechanism for the amine activation process in THF is represented below as elementary steps (Scheme B.6). All steps are drawn as reversible except for the deprotonation step, which appears to be irreversible based upon the lack of overall iminium exchange in the palladacycles (Equation B.5). Inclusion of intermediate **B** would not alter the rate law and has therefore been excluded.

Scheme B.6

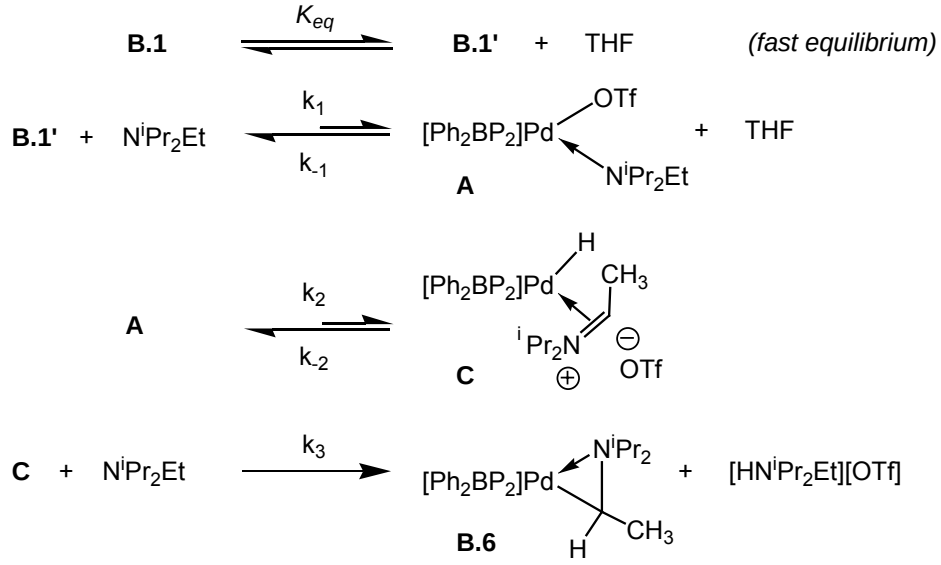

The following rate law is derived by treating **B.1** ⇌ **B.1′** as a fast equilibrium with a constant K_{eq} and applying the steady-state approximation to intermediates **A** and **C**:

$$\text{rate} = \frac{K_{eq}\, k_1\, k_2\, k_3\, [\mathbf{B.1}]\, [N^iPr_2Et]^2}{k_{-1}\, k_3\, [THF]^2[N^iPr_2Et] + k_{-1}\, k_{-2}\, [THF]^2 + k_2\, k_3\, [N^iPr_2Et][THF]} \quad \textbf{(B.11)}$$

In the limit where THF is in vast excess and $k_3\,[N^iPr_2Et] >> k_{-2}$, the rate equation simplifies to:

$$\text{rate} = \frac{K_{eq}\, k_1\, k_2\, [\mathbf{B.1}]\, [N^iPr_2Et]}{k_{-1}\, [THF]^2} \quad \text{and} \quad k_{obs} = \frac{K_{eq}\, k_1\, k_2\, [N^iPr_2Et]}{k_{-1}\, [THF]^2} \quad \textbf{(B.12)}$$

The reduced rate law is in agreement with the experimental data wherein the reaction rate is pseudo first order in both $[N^iPr_2Et]$ and [**B.1**]. Moreover, the rate law can be applied to the kinetic studies performed in THF with 20-fold amine for which k_{obs} was measured. The rate constant k′ (k′ = $K_{eq}k_1k_2/k_{-1}$) comprises two equilibrium constants and the rate of the β-hydride elimination step (k_2). Future studies would be needed to ascertain K_{eq} and k_1/k_{-1} and to obtain a value for k_2. Reports of the isolated

rate constants for β-hydride elimination steps are few in number. The most related case is Harman's osmium system, which is reported to undergo β-hydride elimination at a rate of 6 x 10^{-2} s^{-1} at 25 °C. The rate constant k′ reported here (k′ = 5.6(1) x 10^{-2} s^{-1}) is of similar magnitude.

Table B.2. Summary of observations for various reaction conditions.

	Intermediates		Crude product distribution[a]	
	A	**C**	palladacycle	$\{[PhBP_2]Pd\}_2$ (**B.4**)
THF, 23 °C	–	–	quantitative	–
toluene/benzene, 23 °C	–	–	minor	major
toluene, -20 °C	observed	observed	major	trace

B.3.5 Reaction Profile as a Function of Solvent and Temperature

The reaction profile changes dramatically upon varying the solvent and temperature (Table B.2). The variation in product distribution between low and ambient temperatures in toluene may suggest that $\{[PhBP_2]Pd\}_2$ (**B.4**) is the thermodynamic product and that the palladacycles are the kinetic products. Nonetheless, the palladacycles are thermally quite stable. They show no proclivity to convert to **B.4** at high temperatures upon isolation (up to 90 °C). We presume that complex **B.4**, like the palladacycles, is formed from the Pd iminium hydride intermediate (**C**). Owing to the low polarity of toluene, the transition state for deprotonation of **C** must be sufficiently raised that the competitive loss of iminium triflate dominates the reaction profile. Such a step would generate "$[Ph_2BP_2]PdH$," which in the absence of a strong donor is known to be quite unstable and leads to the generation of $\{[Ph_2BP_2]Pd\}_2$ (**B.4**). For the case of the more polar solvent THF, the barrier to deprotonation is presumably very low relative to the barrier for iminium dissociation. Consequently, complex **B.1** funnels cleanly into the

palladacycle product in THF. In toluene, intermediates **A** and **C** appear to be in equilibrium. In this case, β-hydride elimination *cannot* be rate-limiting.[31] Instead, deprotonation becomes both rate-limiting and product-determining in toluene.

B.3.6 Reaction Profile as a Function of Charge on Palladium

Solvent is not the only factor contributing to the observed product distribution. The electrophilicity of the palladium species also seems to play a role in determining how competitive iminium release from intermediate **C** will be relative to deprotonation. For example, when $(Ph_2SiP_2)Pd(OTf)_2$ **B.14**, the (Ph_2SiP_2)-supported analogue of **B.1**, is exposed to N^iPr_2Et, an analogous Pd iminium hydride intermediate may be invoked, but the iminium ligand is presumably more labile in this case. Thus, a pathway leading to a dimeric Pd(I) product, $[(Ph_2SiP_2)Pd]_2[OTf]_2$ **B.16**, would be favored. Several previous studies have shown that the anionic $[Ph_2BP_2]$ ligand is appreciably more electron-releasing than (Ph_2SiP_2).[6,15] It is therefore reasonable to anticipate that a π-bonded iminium ligand in the adduct complex, $[(Ph_2SiP_2)Pd(H)(R_2N{=}CHCH_3)]^{2+}$, would be more labile than such a ligand in the complex $[[Ph_2BP_2]Pd(H)(R_2N{=}CHCH_3)]^{+}$ (**C**). The anionic charge of the $[Ph_2BP_2]$ chelate thus appears to play an important role with respect to the generation of these unusual palladacycle species.

B.4. Conclusions

In summary, iminium adducts of palladium supported by a bis(phosphino)borate ligand are readily generated from *β*-hydride elimination of amines at a coordinatively unsaturated Pd(II) center. It is rare to isolate or even observe intermediates relevant to the *in situ* reduction of Pd(II) by amines, or the Pd(II)-catalyzed oxidation of alcohols. Thus,

the isolable Pd(0)-iminium adducts, and the mechanistic observations accompanying this study, may provide important mechanistic information regarding the nature of these processes. Moreover, this study also alludes to an attractive opportunity for incorporating Pd(II) species in the presence of an oxidant within the broader synthetic context of new methods for the catalytic functionalization of tertiary amines.

B.5 Experimental Section

B.5.1 General Considerations

All manipulations were carried out using standard Schlenk or glovebox techniques under a dinitrogen atmosphere. Unless otherwise noted, solvents were deoxygenated and dried by thorough sparging with N_2 gas, followed by passage through an activated alumina column. Diethyl ether, tetrahydrofuran, petroleum ether, and benzene were typically tested with a standard purple solution of sodium benzophenone ketyl in tetrahydrofuran in order to confirm effective oxygen and moisture removal. Deuterated solvents were purchased from Cambridge Isotope Laboratories, Inc. The solvents were dried over activated 3 Å molecular sieves and degassed by freeze-pump-thaw cycles prior to use. Elemental analyses were performed by Desert Analytics, Tucson, AZ. A Varian Mercury-300 NMR spectrometer and a Varian Inova-500 NMR spectrometer were used to record ^{1}H, ^{13}C, ^{19}F, and ^{31}P NMR spectra unless otherwise stated. ^{1}H and ^{13}C NMR chemical shifts were referenced to residual solvent. Proton peaks were assigned based on TOCSY-1D and ^{31}P-decoupled ^{1}H NMR studies. ^{31}P NMR chemical shifts are reported relative to an external standard of 85% H_3PO_4. ^{19}F NMR chemical shifts are reported relative to an external standard of hexafluorobenzene. IR

measurements were obtained with a KBr solution cell using a Bio-Rad Excalibur FTS 3000 spectrometer controlled by Bio-Rad Merlin Software (v. 2.97) set at 4 cm^{-1} resolution. X-ray diffraction experiments were performed in the Beckman Institute Crystallographic Facility on a Bruker Smart 1000 CCD diffractometer.

B.5.2 Starting Materials and Reagents

The preparation of $Et_2NC(H)=CH_2$,[32] diisopropyl(2-propenyloxymethyl)amine,[33] $(COD)PdCl_2$,[34] Ph_2SiP_2, and $[NBu_4][Ph_2BP_2]$[35] were carried out following literature procedures. Amines and *o*-phenylpyridine were purchased from Aldrich, dried over CaH_2, distilled or vacuum transferred, and stored over activated 3 Å molecular sieves. The reagents $(PhCN)_2PdCl_2$ and AgOTf were purchased from Strem; the latter was dried under vacuum with heating at 80 °C for 12 h, and the former used without further purification. The reagent NaCN (99%) was dried under vacuum with heating at 80 °C. *Tert*-butyl isocyanide was dried over 3 Å molecular sieves and used without further purification.

B.5.3 Synthesis of Compounds

Synthesis of $[[Ph_2BP_2]Pd(THF)_2][OTf]$, B.1: A THF solution of AgOTf (72.9 mg, 142 μmol) was added to a THF suspension of $\{[Ph_2BP_2]Pd(\mu\text{-}Cl)\}_2$ (0.200 g, 142 μmol). The reaction was stirred for 7 h and filtered through glass wool. The bright yellow filtrate was dried *in vacuo* for 9 h to give a yellow foam-powder (0.252 g, 92% yield). ^1H NMR (C_6D_6, 500 MHz) δ 7.41 (dd, J = 7.0 & 12.0 Hz, 8H, H_o of PPh_2), 7.23 (br d, J = 7.0 Hz, 4H, H_o of BPh_2), 7.09 (t, J = 7.5 Hz, 4H, H_m of BPh_2), 7.04 (tt, J = 1.0 & 7.5 Hz, 2H, H_p of BPh_2), 6.97 (dd, J = 6.5 & 8.0 Hz, H_p of PPh_2), 6.89 (app t, 8H, H_m of PPh_2), 3.44 (m, 8H, $O(CH_2CH_2)_2$), 1.95 (br dd, J = 5.0 & 14.5 Hz, 4H, CH_2PPh_2), 1.26

(m, 8H, $O(CH_2CH_2)_2$). ^{13}C NMR (d_6-benzene, 75 MHz) δ 160.3 (br, C_{ipso} of BPh_2), 133.1 (app t, J = 5.4 Hz, C_o of PPh_2), 132.6 (C_o of BPh_2), 131.9 (C_p of PPh_2), 129.8 (d, J = 55.8 Hz, C_{ipso} of PPh_2), 129.0 (app t, J = 5.4 Hz, C_m of PPh_2), 127.7 (C_m of BPh_2), 124.0 (C_p of BPh_2), 118.7 (d, J = 319 Hz, CF_3), 69.9 ($O(CH_2CH_2)_2$), 25.9 ($O(CH_2CH_2)_2$), 18.6 (br, CH_2PPh_2). ^{31}P NMR (C_6D_6, 121 MHz) δ 48.2; ^{19}F NMR (C_6H_6, 282 MHz) δ −73.5. Anal. Calcd. for ($C_{47}H_{50}BF_3O_5P_2PdS$): C 58.61; H 5.23; N 0. Found: C 58.66; H 5.18; N 0.08.

Synthesis of $[NBu_4][[Ph_2BP_2]PdCl_2]$, B.2: A THF solution (10 mL) of $(COD)PdCl_2$ (0.600 g, 2.10 mmol) was added dropwise to a stirring suspension of $[NBu_4][Ph_2BP_2]$ (1.694 g, 2.10 mmol) in THF (13 mL). The reaction mixture immediately became homogeneous and turned burnt orange. After stirring for 30 min, all volatiles were removed *in vacuo.* The resulting orange oil was taken up in benzene to precipitate the product as a light yellow crystalline solid. The solids were collected on a frit and washed with benzene and petroleum ether to give light yellow **2** (0.410 g, 40% yield). ^1H NMR (d_6-acetone, 500 MHz) δ 7.56 (m, 8H, H_o of PPh_2), 7.24 (app t, J = 7.0 Hz, 4H, H_p of PPh_2), 7.11 (td, J = 1.5 & 7.5 Hz, 8H, H_m of PPh_2), 6.85 (br d, J = 6.5 Hz, 4H, H_o of BPh_2), 6.70 (app t, J = 7.5 Hz, 4H, H_m of BPh_2), 6.65 (tt, J = 1.5 & 7.5 Hz, 2H, H_p of BPh_2), 3.35 (m, 8H, $N(CH_2CH_2CH_2CH_3)_4$), 1.76 (br d, J = 10.5 Hz, 4H, CH_2PPh_2), 1.73 (m, 8H, $N(CH_2CH_2CH_2CH_3)_4$), 1.38 (sextet, J = 7.5 Hz, 8H, $N(CH_2CH_2CH_2CH_3)_4$), 0.95 (t, J = 7.5 Hz, 12H, $N(CH_2CH_2CH_2CH_3)_4$). ^{13}C NMR (d_6-acetone, 125 MHz) δ 163.3 (br, C_{ipso} of BPh_2), 135.5 (dd, J = 4.3 and 55.6 Hz, C_{ipso} of PPh_2), 134.5 (m, C_o of PPh_2), 132.7 (C_o of BPh_2), 129.8 (C_p of PPh_2), 127.7 (m, C_m of PPh_2), 126.7 (C_m of BPh_2), 122.6 (C_p of BPh_2), 59.3 (t, J = 2.4 Hz, $N(CH_2CH_2CH_2CH_3)_4$), 24.4 ($N(CH_2CH_2CH_2CH_3)_4$),

21.6 (br, CH_2PPh_2), 20.3 ($N(CH_2CH_2CH_2CH_3)_4$), 13.9 ($N(CH_2CH_2CH_2CH_3)_4$). ^{31}P NMR (d_6-acetone, 121 MHz) δ 35.46. Anal. Calcd. for ($C_{54}H_{70}BCl_2NP_2Pd$): C, 65.96; H, 7.18; N, 1.42. Found: C 65.83; H 7.60; N 1.63.

Synthesis of {[Ph_2BP_2]Pd(μ-Cl)}$_2$, B.3: A THF solution of $PdCl_2(NCPh)_2$ (1.4856 g, 3.834 mmol) was added rapidly to a stirring THF solution of [NBu_4][Ph_2BP_2] (3.0900 g, 3.834 mmol). The orange-yellow solution was filtered through Celite and dried *in vacuo*. The residue was washed profusely with Et_2O to give pale-yellow solids, which by ^{31}P NMR were a mixture of compounds **B.2** and **B.3**. The solids were dissolved in THF (150 mL) in a 300 mL RB flask with a stir bar, and $NaBPh_4$ (1.3123 g, 3.834 mmol) was added in the dark. After stirring for 8 h in the dark, yellow solids precipitated from the brown solution. The solids were collected and washed sparingly with THF and a 1:1 THF/Et_2O solution. To remove NaCl, the solids were dissolved in CH_2Cl_2 and filtered through Celite. The bright-yellow solution was dried *in vacuo* to give yellow crystalline solids. A second crop of product was collected from the concentrated brown filtrate at -30 ºC. The crops were combined to give 1.911 g of **B.3** (73% yield). ^1H NMR ($CDCl_3$, 300 MHz) δ 7.30-7.18 (m, 12H, H_p and H_o of PPh_2), 7.07 (t, J = 7.8 Hz, 8H, H_m of PPh_2), 6.91-6.82 (m, 10H, aryl H's of BPh_2), 1.79 (br d, J = 10.5 Hz, 4H, CH_2PPh_2). ^{13}C NMR ($CDCl_3$, 125 MHz) δ 161.4 (br, C_{ipso} of BPh_2), 133.3 (m, C_o of PPh_2), 132.1 (C_o of BPh_2), 131.5 (d, J = 56.0 Hz, C_{ipso} of PPh_2), 130.7 (C_p of PPh_2), 128.1 (m, C_m of PPh_2), 126.8 (C_m of BPh_2), 123.0 (C_p of BPh_2), 17.7 (br, CH_2PPh_2). ^{31}P NMR ($CDCl_3$, 121.5 MHz) δ 43.07. Anal. Calcd. for ($C_{76}H_{68}B_2Cl_2P_4Pd$): C 64.71; H 4.86; N 0.00. Found: C 64.80; H 4.83; N <0.05.

Synthesis of [Ph_2BP_2]Pd(*o*-phenylpyridine)OTf, B.5: To a bright-yellow THF solution of **B.1** (75.0 mg, 78.0 μmol) was added *o*-phenylpyridine (11.1 μL, 84.0 μmol). The solution immediately turned off-white and slightly turbid. Petroleum ether (5 mL) was added to precipitate solids. The white solids were collected and washed liberally with Et_2O. The solids were dried *in vacuo* to give 69 mg of a pale-yellow powder (91% yield). Complex **B.5** is rapidly fluxional in solution at rt. ^{1}H NMR ($CDCl_3$, 300 MHz, -40 ˚C) δ 8.35 (d, J = 4.8 Hz, 1H, H_o of pyr), 7.69 – 7.52 (m, 12H, aryl), 7.32 – 7.07 (m, 10H, aryl), 6.84 (t, 2H, J = 6.4 Hz, H_p of BPh_2), 6.72 – 6.67 (m, 12H, aryl), 6.24 (br d, J = 7.5 Hz, 2H, aryl), 2.55 (d, J = 13.5 Hz, 1H, C*H*H′PPh_2), 1.93 (d, J = 14 Hz, 1H, CH*H*′PPh_2), 1.65 (d, J = 14 Hz, 1H, C*H*H′P′Ph_2), 1.53 (d, J = 13.8 Hz, 1H, CH*H*′P′Ph_2). ^{31}P NMR ($CDCl_3$, 121 MHz, -40 ˚C) δ 46.3 (d, J = 20 Hz), 35.3 (d, J = 20 Hz). ^{19}F NMR ($CDCl_3$, 282 MHz, -40 ˚C) δ -81.6. Anal. Calcd. for ($C_{50}H_{43}BF_3NO_3P_2PdS$): C, 61.65; H, 4.45; N, 1.44. Found: C 61.80; H 4.21; N 1.54.

Synthesis of [Ph_2BP_2]Pd(N,C:η^2-N^{i}Pr$_2$CHCH$_3$), B.6: Compound **B.6** was prepared with N^{i}Pr$_2$Et using a procedure identical to that used for compound **B.7** (68.0 mg, 82% yield). ^{1}H NMR (C_6D_6, 300 MHz) δ 7.32 - 7.50 (m, 14H, aryl H), 7.00 - 7.14 (m, 16H, aryl H), 3.38 (app quintet d, J = 1.8 & 6.9 Hz, 1H, PdNC*H*CH_3), 2.95 (septet, J = 6.0 Hz, 1H, N(C*H*Me_2)C′HMe_2), 2.74 (septet, J = 6.0 Hz, 1H, N(CHMe_2)C′*H*Me_2), 2.18 - 2.42 (m, 4H, C$H_2$$PPh_2$ & C′H_2P′Ph_2), 0.88 (d, J = 6.9 Hz, 3H, N(CHMe_2)C′H*Me*$_2$), 0.835 (d, J = 6.3 Hz, 3H, N(CH*Me*$_2$)C′HMe_2), 0.73 (td, J = 9.6 & 15.9 Hz, 3H, PdNCHC*H*$_3$), 0.50 (d, J = 5.4 Hz, 6H, N(CH*Me*$_2$)C′H*Me*$_2$). ^{13}C NMR ($CDCl_3$, 125 MHz) δ 163.8 (br, C_{ipso} and C'_{ipso} of BPh_2), 141.5 (d, J = 24.3 Hz, C_{ipso} of PPh_2), 139.1 (d, J = 35.4 Hz, C'_{ipso} of PPh_2), 137.9 (d, J = 29.3 Hz, C_{ipso} of P′Ph_2), 137.1 (d, J = 40.5 Hz, C'_{ipso}

of P′Ph_2), 133.9 (d, *J* = 31.5 Hz, C_o of PPh_2), 133.3 (d, *J* = 12.7 Hz, C_o′ of PPh_2), 133.0 (C_o of BPh_2), 132.6 (C_o′ of BPh_2), 132.1 (d, *J* = 11.6 Hz, C_o of P′Ph_2), 132.0 (d, *J* = 10.8 Hz, C_o′ of P′Ph_2), 129.0 (d, *J* = 2.0 Hz, C_p of PPh_2), 128.9 (d, *J* = 1.9 Hz, C_p′ of PPh_2), 128.4 (d, *J* = 2.3 Hz, C_p of P′Ph_2), 128.1 (d, *J* = 1.5 Hz, C_p′ of P′Ph_2), 128.0 (d, *J* = 9.2 Hz, C_m of PPh_2), 127.7 – 127.9 (m, C_m′ of PPh_2, C_m and C_m′ of P′Ph_2), 126.2 (C_m of BPh_2), 126.1 (C_m′ of BPh_2), 122.3 (C_p of BPh_2), 122.2 (C_p′ of BPh_2), 62.6 (dd, *J* = 13.8 & 56.7 Hz, PdN(*C*HMe)), 54.6 (N(*C*HMe_2)$_2$), 50.4 (N(*C*′HMe_2)$_2$), 26.1 (N(CH*Me*$_2$)$_2$), 24.8 (N(CH*Me*′$_2$)$_2$), 23.4 (N(C′H*Me*$_2$)$_2$), 21.2 (N(C′H*Me*′$_2$)$_2$), 20.5 - 22 (br m, *C*H_2PPh_2 and *C*′H_2PPh_2), 15.9 (dd, *J* = 2 & 5.3 Hz, PdN(CH*Me*)). ^{31}P NMR ($CDCl_3$, 121 MHz) δ 32.1 (d, *J* = 32.0 Hz), 14.1 (d, *J* = 32.0 Hz). Anal. Calcd. for ($C_{46}H_{52}BNP_2Pd$): C, 69.23; H, 6.57; N, 1.76. Found: C 68.62; H 6.77; N 1.77.

Synthesis of [Ph_2BP_2]Pd(N,C:η^2-NEt_2CHCH_3), B.7: Compound **B.1** (100.0 mg, 103.9 μmol) and NEt_3 (290 μL, 2.081 mmol) were dissolved in THF. The reaction mixture turned from yellow to a burnt orange. After 3 h, all volatiles were removed *in vacuo*, and petroleum ether was added to precipitate salmon powder and to wash away the excess amine. The solids were dissolved in benzene and flashed through a silica plug. The pale-pink filtrate was dried *in vacuo* to give light-pink crystalline solids (78.0 mg, 98% yield). ^{1}H NMR (C_6D_6, 300 MHz) δ 7.62 (br d, *J* = 6.9 Hz, H_o of BPh_2), 7.11 - 7.41 (m, 14H, aryl H), 6.97 – 7.00 (m, 12H, aryl H), 2.97 (app hextet, *J* = 6.0 Hz, 1H, PdNC*H*CH_3), 2.46 (septet d, *J* = 3.6 & 6.9 Hz, 1H, N(C*H*H′Me)Et′, 2.17 – 2.45 (m, 7H, N(CH*H*′Me)C′*HH*′Me, CH_2PPh_2 and C′H_2P′Ph_2), 0.75 (td, *J* = 8.1 & 10.2 Hz, 3H, PdNCHCH_3), 0.47 (m, 6H, N(CH_2Me)C′H_2Me). ^{13}C NMR ($CDCl_3$, 125 MHz) δ 163.4

(br, C_{ipso} and C'_{ipso} of BPh_2), 140.7 (d, J = 26.1 Hz, C_{ipso} of PPh_2), 139.2 (d, J = 34.3 Hz, C'_{ipso} of PPh_2), 139.1 (d, J = 28.0 Hz, C_{ipso} of $P'Ph_2$), 138.3 (d, J = 37.8 Hz, C'_{ipso} of $P'Ph_2$), 133.6 (C_o of BPh_2), 133.2 (d, J = 13.1 Hz, C_o of PPh_2), 133.1 (C_o' of BPh_2), 132.8 (d, J = 12.7 Hz, C_o' of PPh_2), 132.34 (d, J = 13.2 Hz, C_o of $P'Ph_2$), 132.31 (d, J = 11.6 Hz, C_o' of $P'Ph_2$), 128.8 (d, J = 2.3 Hz, C_p of PPh_2), 128.62 (d, J = 1.9 Hz, C_p' of PPh_2), 128.59 (d, J = 1.5 Hz, C_p of $P'Ph_2$), 128.2 (d, J = 2.0 Hz, C_p' of $P'Ph_2$), 127.95 (d, J = 6.2 Hz, C_m of PPh_2), 127.8 – 127.9 (m, C_m' of PPh_2, C_m and C_m' of $P'Ph_2$), 126.4 (C_m of BPh_2), 126.1 (C_m' of BPh_2), 122.73 (C_p of BPh_2), 122.66 (C_p' of BPh_2), 64.3 (dd, J = 13.5 & 57.9 Hz, PdN(*C*HMe)), 52.2 (s, N(*C*H_2Me)), 45.6 (s, N(*C'*H_2Me)), 20.6 (br m, *C*H_2PPh_2 and *C'*H_2PPh_2), 16.1 (app t, J = 3.5 Hz, PdN(CH*Me*)), 13.1 (s, N(CH_2*Me*)), 12.5 (s, N(CH_2*Me'*)). ^{31}P NMR (C_6D_6, 121 MHz) δ 32.2 (d, J = 35.7 Hz), 15.7 (d, J = 35.7 Hz). Anal. Calcd. for ($C_{44}H_{48}BNP_2Pd$): C, 68.63; H, 6.28; N, 1.82. Found: C 68.82; H 5.99; N 1.88.

Synthesis of [Ph_2BP_2]Pd(N,C:η^2-NCy_2CHCH_3), B.8: Compound **B.8** is only sparingly soluble in benzene, so the work-up was slightly modified. Compound **B.1** (200.0 mg, 207.86 μmol) and $NEtCy_2$ (0.96 mL, 4.17 mmol) were dissolved in THF. After stirring for 3 h, the solution was dried *in vacuo*. The residue was washed with petroleum ether, benzene, and acetonitrile. The remaining dull-pink powder was dissolved in CH_2Cl_2 and filtered through Celite (69 mg, 38% yield). Single crystals suitable for X-ray diffraction studies were grown from vapor diffusion of petroleum ether into a CH_2Cl_2 solution of **8** at -30ºC. ^{1}H NMR ($CDCl_3$, 300 MHz) δ 7.11 – 7.36 (m, 24H, aryl H), 6.80 – 6.93 (m, 6H, aryl H), 3.38 (app quintet d, J = 1.1 & 2.9 Hz, 1H, PdNC*H*CH_3), 2.79 (app q, J = 4.9 Hz, 1H, NC*H*$(CH_2)_5$), 1.08 – 2.07 (m, 25H, aliphatic

H's), 0.96 (td, *J* = 5.4 & 9.0 Hz, 3H, PdNCHC*H*$_3$). ^{13}C NMR ($CDCl_3$, 125 MHz) δ 164.2 (br, C_{ipso} and C'_{ipso} of BPh_2), 141.6 (d, *J* = 23.9 Hz, C_{ipso} of PPh_2), 139.6 (d, *J* = 34.6 Hz, C'_{ipso} of PPh_2), 137.7 (d, *J* = 28.8 Hz, C_{ipso} of $P'Ph_2$), 137.2 (d, *J* = 38.2 Hz, C'_{ipso} of $P'Ph_2$), 133.96 (d, *J* = 13.4 Hz, C_o of PPh_2), 133.4 (d, *J* = 13.2 Hz, C_o' of PPh_2), 133.1 (C_o of BPh_2), 132.7 (C_o' of BPh_2), 131.88 (d, *J* = 10.7 Hz, C_o of $P'Ph_2$), 131.85 (d, *J* = 11.2 Hz, C_o' of $P'Ph_2$), 129.0 (d, *J* = 2.0 Hz, C_p of PPh_2), 128.9 (d, *J* = 1.9 Hz, C_p' of PPh_2), 128.4 (d, *J* = 2.4 Hz, C_p of $P'Ph_2$), 128.0 (d, *J* = 9.2 Hz, C_m of PPh_2), 127.9 (d, *J* = 1.5 Hz, C_p' of $P'Ph_2$), 127.72 (d, *J* = 8.8 Hz, C_m' of PPh_2), 127.70 (d, *J* = 10.1 Hz, C_m of $P'Ph_2$), 127.68 (d, *J* = 8.0 Hz, C_m' of $P'Ph_2$), 126.2 (s, C_m of BPh_2), 126.1 (s, C_m' of BPh_2), 122.3 (C_p of BPh_2), 122.2 (C_p' of BPh_2), 64.5 (dd, *J* = 13.4 & 56.7 Hz, PdN(*C*HMe)), 63.8 (N(*C*H$(CH_2)_5$)), 59.9 (d, *J* = 3.1 Hz, N(*C'*H$(C'H_2)_5$)), 36.5 (Cy), 35.4 (Cy), 35.2 (Cy), 32.71 (Cy), 26.7 (Cy), 26.4 (Cy), 26.22 (Cy), 26.18 (Cy), 25.5 (2 overlapping s, Cy), 20.4 – 21.9 (br m, *C*H_2PPh_2 and *C'*H_2PPh_2), 15.7 (d, *J* = 4.3 Hz, PdN(CH*Me*)). ^{31}P NMR ($CDCl_3$, 121 MHz) δ 31.8 (d, *J* = 31.1 Hz), 13.2 (d, *J* = 31.1 Hz). Anal. Calcd. for ($C_{52}H_{60}BNP_2Pd$): C, 71.12; H, 6.89; N, 1.59. Found: C 70.77; H 6.65; N 1.36.

Synthesis of [Ph_2BP_2]Pd(N,C:η^2-$NCH_3CH(CH_2)_3$), B.9: Compound **B.9** was prepared with *N*-methylpyrrolidene using a procedure identical to that used for compound **B.7** (67 mg, 82% yield). Single crystals suitable for X-ray diffraction studies were grown from vapor diffusion of petroleum ether into a THF solution of **B.9** at -30ºC. ^{1}H NMR (C_6D_6, 300 MHz) δ 7.63 (br t, *J* = 6.3 Hz, 4H, aryl H), 7.38 (dd, *J* = 8.7 and 9.6 Hz, 2H, H_o of PPhPh'), 7.11 – 7.30 (m, 12H, aryl H's), 6.96 – 6.99 (m, 12 H, aryl H's), 2.86 (m, 1H, PdN(Me)C*H*$(CH_2)_3$), 2.75 (m, 1H, aliphatic H on pyrrolidene), 2.32 – 2.25 (m, 2H,

C*HH*′PPh_2), 2.14 – 2.10 (m, 2H, C′*HH*′P′Ph_2), 2.07 (d, *J* = 3.3 Hz, 3H, N*Me*), 1.71 – 1.87 (m, 2H, aliphatic H's on pyrrolidene), 1.56 (m, 1H, aliphatic H on pyrrolidene), 1.21 – 1.37 (m, 2H, aliphatic H's on pyrrolidene). ^{13}C NMR ($CDCl_3$, 125 MHz) δ 163.6 (br, C_{ipso} and C'_{ipso} of BPh_2), 140.2 (d, *J* = 26.0 Hz, C_{ipso} of PPh_2), 139.4 – 138.8 (m, C'_{ipso} of PPh_2, C_{ipso} and C'_{ipso} of P′Ph_2), 133.6 (C_o of BPh_2), 133.2 (C_o′ of BPh_2), 133.0 (d, *J* = 13.1 Hz, C_o of PPh_2), 132.8 (d, *J* = 13.7 Hz, C_o′ of PPh_2), 132.2 (d, *J* = 13.1 Hz, C_o of P′Ph_2), 131.9 (d, *J* = 11.4 Hz, C_o′ of P′Ph_2), 128.9 (C_p of PPh_2), 128.6 (C_p′ of PPh_2), 128.5 (C_p of P′Ph_2), 128.3 (C_p′ of P′Ph_2), 128.0 – 127.9 (m, C_m and C_m′ of PPh_2, C_m and C_m′ of P′Ph_2), 126.3 (C_m of BPh_2), 126.2 (C_m′ of BPh_2), 122.8 (C_p and C_p′ of BPh_2), 69.5 (dd, *J* = 14.6 & 61.8 Hz, PdN(Me)*C*H), 60.3 (N(*C*H_2)), 45.5 (d, *J* = 3.8 Hz, N*Me*), 31.6 (*C*H_2 of pyrrolidene), 26.1 (*C*H_2 of pyrrolidene), 20.2 (br m, *C*H_2PPh_2), 17.9 (br m, *C*′H_2PPh_2). ^{31}P NMR (C_6D_6, 121 MHz) δ 32.7 (d, *J* = 39.5 Hz), 16.9 (d, *J* = 39.5 Hz). Anal. Calcd. for ($C_{43}H_{44}BNP_2Pd$): C, 68.50; H, 5.88; N, 1.86. Found: C 68.53; H 5.96; N 2.06.

Synthesis of [Ph_2BP_2]Pd(N,C:η^2-$NCH_3CH(CH_2)_4$), B.10: Compound **B.10** was prepared with *N*-methylpiperidene using a procedure identical to that used for compound **B.7.** Yield 54.1 mg, 69%. ^{1}H NMR (C_6D_6, 300 MHz) δ 7.67 (br d, 2H, *J* = 6.9 Hz, H_o of BPhPh′), 7.61 (br d, 2H, *J* = 6.0 Hz, H_o′ of BPhPh′), 7.31 – 7.39 (m, 8H, H_o and H_o′ of PPhPh′ and P′PhPh′), 7.25 (t, *J* = 6.9 Hz, 2H, H_p and H_p′ of BPhPh′), 7.10 – 7.14 (m, 4H, H_m and H_m′ of BPhPh′), 6.95 – 6.98 (m, 12 H, H_m, H_m′, H_p, and H_p′ of PPhPh′ and P′PhPh′), 2.98 (m, 1H, PdN(Me)C*H*$(CH_2)_4$), 2.29 – 2.42 (m, 3H, C*HH*′PPh_2 and C*H*H′P′Ph_2), 2.11 (br d, *J* = 12.3 Hz, 1H, CH*H*′P′Ph_2), 2.04 (d, *J* = 3.3 Hz, 3H, N*Me*), 1.82 (app q, *J* = 12. 3 Hz, 1H, aliphatic H on piperidene), 1.71 (m, 1H, aliphatic H on

piperidene), 1.07 – 1.15 (m, 4H, aliphatic H's on piperidene), 0.86 – 0.88 (m, 2H, aliphatic H's on piperidene). ^{13}C NMR ($CDCl_3$, 125 MHz) δ 163.4 (br, C_{ipso} and C'_{ipso} of BPh_2), 140.7 (d, J = 25.9 Hz, C_{ipso} of PPh_2), 139.5 (d, J = 28.2 Hz, C'_{ipso} of PPh_2), 139.1 – 139.5 (m, C_{ipso} and C'_{ipso} of $P'Ph_2$), 133.7 (C_o of BPh_2), 133.1 (C_o' of BPh_2), 132.9 (d, J = 13.1 Hz, C_o of PPh_2), 132.2 (m, C_o' of PPh_2, C_o and $C_o'$of $P'Ph_2$), 128.8 (C_p of PPh_2), 128.6 (C_p' of PPh_2), 128.5 (C_p of $P'Ph_2$), 128.3 (C_p' of $P'Ph_2$), 127.9 - 128.0 (br m, C_m and C_m' of PPh_2, C_m and C_m' of $P'Ph_2$), 126.4 (C_m of BPh_2), 126.1 (C_m' of BPh_2), 122.8 (C_p and C_p' of BPh_2), 66.9 (dd, J = 13.8 & 60.4 Hz, PdN(Me)*C*H), 51.4 (N(*C*H_2)), 49.7 (N*Me*), 22.6 (*C*H_2 of piperidene), 22.4 (*C*H_2 of piperidene), 20.7 (br m, *C*H_2PPh_2), 17.8 (br m, *C'*H_2PPh_2), 16.6 (*C*H_2 of piperidene). ^{31}P NMR (C_6D_6, 121 MHz) δ 32.7 (d, J = 39.5 Hz), 16.9 (d, J = 39.5 Hz). Anal. Calcd. for ($C_{44}H_{46}BNP_2Pd$): C, 68.81; H, 6.04; N, 1.82. Found: C 67.93; H 6.39; N 1.41.

Synthesis of [Ph_2BP_2]Pd(N,C:η^2-N^{i}Pr$_2$CH$_2$), B.11: Compound **B.1** (100.4 mg, 104.4 μmol) and diisopropyl(2-propenyloxymethyl)amine (357.4 mg, 2.088 mmol) were dissolved in THF. The reaction mixture turned from yellow to orange-red immediately, but faded to pale yellow after stirring for 5 min. After 1 h, all volatiles were removed in vacuo, and petroleum ether was added to precipitate powder and wash away the excess amine. The solids were dissolved in benzene and flashed through a silica plug. The filtrate is dried *in vacuo* to give pale-yellow solids (63.7 mg, 78% yield). ^{1}H NMR (C_6D_6, 300 MHz) δ 7.55 (br d, J = 6.9 Hz, H_o of BPh_2), 7.32 – 7.44 (m, 8H, aryl H's), 7.08 – 7.18 (m, 6H, aryl H's), 6.98 – 7.02 (m, 12H, aryl H's), 2.61 (m, 2H, N(C*H*$Me_2)_2$), 2.51 (app t, J = 5.1 Hz, 2H, PdNC*H*$_2$), 2.29 (m, 4 H, C*H*$_2PPh_2$), 0.70 (d, J = 6.9 Hz, 6H, N(CH*Me*Me')$_2$), 0.59 (d, J = 6.0 Hz, 6H, N(CHMe*Me'*)$_2$). ^{13}C NMR (C_6D_6, 75 MHz) δ

163.8 (v br, C_{ipso} of BPh_2), 140.6 (d, J = 28.7 Hz, C_{ipso} of PPh_2), 139.8 (d, J = 38.3 Hz, C_{ipso} of $P'Ph_2$), 133.9 (C_o of BPh_2), 133.4 (d, J = 12.6 Hz, C_o of PPh_2), 133.0 (d, J = 12.0 Hz, C_o of $P'Ph_2$), 128.3 – 129.1 (m, C_p and C_m of PPh_2 and $P'Ph_2$), 127.0 (C_m of BPh_2), 123.2 (C_p of BPh_2), 54.5 (d, J = 2.0 Hz, PdN($CHMe_2$)$_2$), 50.1 (dd, J = 56 & 13 Hz, NCH_2), 24.1 (N(CHMeMe′)$_2$), 21.7 (N(CHMeMe′)$_2$), 20.3 (br m, CH_2PPh_2 and $CH_2P'Ph_2$). ^{31}P NMR (C_6D_6, 121 MHz) δ 31.5 (d, J = 39.3 Hz), 16.3 (d, J = 39.3 Hz). Anal. Calcd. for ($C_{45}H_{50}BNP_2Pd$): C, 68.93; H, 6.43; N, 1.79. Found: C 68.66; H 6.73; N 1.64.

Synthesis of [Ph_2BP_2]Pd(N,C:η^2-N^{i}Pr$_2$CHCH$_2$CH$_3$), B.12: Compound **B.12** was prepared with N^{i}Pr$_2$^{n}Pr using a procedure identical to that used for compound **B.7** (78% yield). ^{1}H NMR (C_6D_6, 500 MHz) δ 7.37 - 7.51 (m, 14H, aryl H), 6.96 - 7.19 (m, 16H, aryl H), 3.19 (m, 1H, PdNCHEt), 2.86 (d septet, J = 3.0 & 6.5 Hz, 1H, N(CHMe$_2$)C′HMe$_2$), 2.81 (septet, J = 6.5 Hz, 1H, N(CHMe$_2$)C′HMe$_2$), 2.19 - 2.38 (m, 4H, CH_2PPh$_2$ & C′H_2P′Ph$_2$), 1.28 (m, 2H, PdNCHCH_2Me), 1.00 (d, J = 6.5 Hz, 3H, N(CHMe_2)$_2$), 0.91 (d, J = 6.0 Hz, 3H, N(CHMe_2)$_2$), 0.57 (d, J = 6.5 Hz, 3H, N(CHMe_2)$_2$), 0.53 (d, J = 7.0 Hz, 3H, N(CHMe_2)$_2$), 0.47 (t, J = 7.0 Hz, 3H, PdNCHCH$_2$CH_3). ^{13}C NMR ($CDCl_3$, 125 MHz) δ 164.1 (br, C_{ipso} and C'_{ipso} of BPh_2), 140.7 (d, J = 25.0 Hz, C_{ipso} of PPh_2), 139.1 (d, J = 28.0 Hz, C'_{ipso} of PPh_2), 138.3 (dd, J = 2.0 & 37.0 Hz, C_{ipso} of $P'Ph_2$), 138.1 (d, J = 36.2 Hz, C'_{ipso} of $P'Ph_2$), 133.5 (d, J = 12.8 Hz, C_o of PPh_2), 133.1 (C_o of BPh_2), 132.9 (d, J = 12.3 Hz, C_o' of PPh_2), 132.7 (C_o' of BPh_2), 132.63 (d, J = 11.1 Hz, C_o of $P'Ph_2$), 132.62 (d, J = 11.9 Hz, C_o' of $P'Ph_2$), 128.8 (d, J = 2.3 Hz, C_p of PPh_2), 128.7 (d, J = 1.9 Hz, C_p' of PPh_2), 128.6 (d, J = 1.5 Hz, C_p of $P'Ph_2$), 128.2 (d, J = 1.6 Hz, C_p' of $P'Ph_2$), 128.0 (d, J = 9.3 Hz, C_m of PPh_2), 127.8 – 127.7 (m, C_m' of PPh_2, C_m and

C_{m}' of $P'Ph_2$), 126.2 (C_m of BPh_2), 126.1 (C_{m}' of BPh_2), 122.3 (C_p of BPh_2), 122.2 (C_{p}' of BPh_2), 70.2 (dd, J = 14.1 & 56.5 Hz, PdN(*C*HEt)), 54.1 (N(*C*H$Me_2)_2$), 50.7 (N(*C*′H$Me_2)_2$), 26.1 (N(CH*Me*$_2)_2$), 26.0 (N(CH*Me*′$_2)_2$), 23.4 (N(C′H*Me*$_2)_2$), 23.1 (PdN(CH*C*H_2Me)), 22.0 (br q, *C*H_2PPh_2), 21.5 (N(C′H*Me*′$_2)_2$), 20.3 (br q, *C*′H_2PPh_2), 15.3 (dd, J = 7.8 & 8.5 Hz, PdN(CHCH$_2$*Me*)). ^{31}P NMR (C_6D_6, 121 MHz) δ 32.3 (d, J = 30.2 Hz), 13.7 (d, J = 30.2 Hz). Anal. Calcd. for ($C_{47}H_{54}BNP_2Pd$): C, 69.51; H, 6.70; N, 1.72. Found: C 69.23; H 6.67; N 1.42.

Synthesis of [Ph_2BP_2]Pd(C(N^{t}Bu)H)(CN^{t}Bu), B.13: Compound **B.7** (32.0 mg, 41.6 μmol) and *tert*-butylisocyanide (15 μL, 248.5 μmol) were dissolved in benzene. The reaction mixture turned to a bright yellow. After 1 h, all volatiles were removed *in vacuo*, and the residue was taken up in a benzene/petroleum ether solution. After storing at -30 °C, microcrystalline solids precipitated. The solids were collected and washed with petroleum ether and diethyl ether (27.9 mg, 80% yield). IR(CH_2Cl_2, KBr): ν(H*C*=*N*^{t}Bu) = 1608 cm^{-1}, ν(*C*≡*N*) = 2195 cm^{-1}. ^{1}H NMR (C_6D_6, 300 MHz) δ 8.75 (dd, J = 38.8 & 27.5 Hz, 1H, Pd(CN^{t}Bu)*H*), 7.57 – 7.56 (m, 8H, aryl H's), 7.31 (t, J = 9.0 Hz, 4H, aryl H's), 7.21 – 7.08 (m, 6H, aryl H's), 6.95 – 6.87 (m, 12H, aryl H's), 2.28 (d, J = 14.7 Hz, 2H, C*H*$_2$PPh$_2$), 2.13 (d, J = 13.8 Hz, 2H, C*H*′$_2$PPh$_2$), 0.95 (s, 9H, Pd(CN^t*Bu*)H), 0.58 (s, *9*H, Pd(CN^t*Bu*)). ^{13}C NMR ($CDCl_3$, 125 MHz) δ 179.3 (dd, J = 8.6 & 131 Hz, Pd(*C*N^{t}Bu)H), 163.4 (v br, C_{ipso} of BPh_2), 137.4 (d, J = 35.6 Hz), 133.0 (dd, J = 10 & 25 Hz), 132.8, 132.4, 130.5, 129.0 (dd, J = 2 & 69 Hz), 127.8 (dd, J = 11 & 34 Hz), 126.7, 126.4, 123.0, 122.7, 29.9, 29.2, 19 (br m), 16 (br m). ^{31}P NMR (C_6D_6, 121 MHz) δ 23.6 (d, J = 55.8 Hz), 13.1 (d, J = 55.8 Hz). Anal. Calcd. for ($C_{48}H_{53}BNP_2Pd$): C, 68.87; H, 6.38; N, 3.35. Found: C 69.19; H 6.64; N 3.06.

Synthesis of $(Ph_2SiP_2)Pd(OTf)_2$, 14: A THF solution of AgOTf (455.0 mg, 1.77 mmol) was added dropwise to a THF solution of $Ph_2Si(CH_2PPh_2)_2PdCl_2$ (671.2 mg, 0.886 mmol). The reaction turned bright-yellow and cloudy. The reaction mixture was filtered through Celite, and the filtrate concentrated *in vacuo* to a thick yellow goo. Upon addition of petroleum ether and vigorous stirring, **B.14** was isolated as a yellow powder in 98% yield (854 mg). ^{1}H NMR (d_6-acetone, 300 MHz) δ 7.89 (dd, J = 7.5 & 12.9 Hz, 8H, H_o of PPh_2), 7.67 (br t, J = 7.5 Hz, 4H, H_p of PPh_2), (td, J = 2.1, 7.5 Hz, 8H, H_m of PPh_2), 7.38 – 7.33 (m, 6H, H_o and H_p of $SiPh_2$), 7.20 (t, J = 7.5 Hz, 4H, H_m of $SiPh_2$), 3.01 (dd, J = 6.9 & 17.0 Hz, 4H, CH_2SiPh$_2$). ^{13}C NMR ($CDCl_3$, 125 MHz) δ 135.0 (C_o of $SiPh_2$), 134.5 (m, C_o of PPh_2), 134.3 (C_p of PPh_2), 133.0 (m, C_{ipso} of PPh_2), 131.2 (C_p of $SiPh_2$), 130.4 (m, C_m of PPh_2), 129.0 (C_m of $SiPh_2$), 127.4 (d, J = 59.9 Hz, CF_3), 6.6 (m, CH_2PPh_2) (C_{ipso} of $SiPh_2$ was not clearly visible). ^{31}P NMR (d_6-acetone, 121 MHz) δ 36.4; ^{19}F NMR (d_6-acetone, 282 MHz) δ –74.3. Anal. Calcd. for ($C_{40}H_{34}F_6O_6P_2PdS_2Si$): C 48.76; H 3.48; N 0. Found: C 48.36; H 3.46; N <0.05.

Synthesis of $(Ph_2SiP_2)PdCl_2$, B.15: A THF solution of $PdCl_2(NCPh)_2$ (398.3 mg, 1.038 mmol) was added rapidly to a stirring THF solution of $Ph_2Si(CH_2PPh_2)_2$ (603.0 mg, 1.038 mmol). After stirring for 1 h, the solution was filtered through Celite and dried *in vacuo*. The residue was washed profusely with Et_2O/CH_3CN and Et_2O/THF (> 4:1) and dried under vacuum overnight to give pale-lime-yellow powder (768.3 mg, 89%). ^{1}H NMR ($CDCl_3$, 300 MHz) δ 7.62 (dd, J = 7.5 & 12.3 Hz, 8H, H_o of PPh_2), 7.39 (dd, J = 6.9 & 8.4 Hz, 4H, H_p of PPh_2), 7.34 – 7.25 (m, 10H, H_m of PPh_2 and H_p of $SiPh_2$), 7.12 (t, J = 7.5 Hz, 4H, H_m of $SiPh_2$), 7.20 (d, J = 6.9 Hz, 4H, H_o of $SiPh_2$), 2.11 (dd, J = 5.4 & 15.0 Hz, 4H, CH_2SiPh$_2$). ^{13}C NMR ($CDCl_3$, 75 MHz) δ 133.8 (C_o of $SiPh_2$), 133.7 (app t,

J = 6.0 Hz, C_o of PPh_2), 132.9 (m, C_{ipso} of PPh_2), 131.6 (C_{ipso} of $SiPh_2$), 131.5 (C_p of PPh_2), 130.2 (C_p of $SiPh_2$), 128.4 (app t, *J* = 6.0 Hz, C_m of PPh_2), 128.3 (C_m of $SiPh_2$), 9.4 (dd, *J* = 13.1 & 15.8 Hz, *C*H_2PPh_2). ^{31}P NMR ($CDCl_3$, 121 MHz) δ 22.66. Anal. Calcd. for ($C_{38}H_{34}Cl_2P_2PdSi$): C 60.21; H 4.52; N 0. Found: C 59.34; H 4.52; N <0.05.

Synthesis of [(Ph_2SiP_2)Pd)$_2$][OTf]$_2$, B.16: Diisopropylethylamine (54 μL, 0.310 mmol) was added dropwise to a THF solution (8 mL) of **B.14** (100.5 mg, 0.102 mmol). Within 5 min, the solution turned from yellow to burnt orange. The reaction was monitored by ^{31}P NMR. After 20 h, all volatiles were removed *in vacuo*. After washing with Et_2O, the residue was redissolved in CH_3CN and filtered through Celite. Et_2O was added to the solution to precipitate orange crystalline solids. The solids were collected, washed with Et_2O/CH_3CN (9:1), and dried *in vacuo* to afford 59.3 mg of **B.16** (70% yield). ^{1}H NMR ($CDCl_3$, 300 MHz) δ 7.8 – 7.6 (m, 8H, aryl H's), 7.4 – 7.0 (m, 44H, aryl H's), 6.9 (d, 8H, aryl H's), 2.6 (d, 4H, C*H*$_2$SiPh$_2$), 1.7 (d, 4H, C′*H*$_2$Si′Ph$_2$). ^{13}C NMR ($CDCl_3$, 125 MHz) δ 134.9 (C_p of PPh_2), 134.2 – 134.1 (m, C_o of PPh_2 and C_p of P′Ph$_2$), 133.3 (d, *J* = 11 Hz, C_m of PPh_2), 133.1 (m, C_{ipso} of PPh_2), 131.5 (C_{ipso} of $SiPh_2$), 130.6 (d, *J* = 11 Hz, C_m of P′Ph$_2$), 129.9 (C_p of $SiPh_2$), 129.3 (m, C_{ipso} of P′Ph$_2$), 128.8 (m, C_o of P′Ph$_2$), 128.3 (C_m of $SiPh_2$), 108.0 (br m, CF_3), 13.8 (*C*H_2SiPh$_2$), 12.5 (*C*′H_2SiPh$_2$); ^{19}F NMR ($CDCl_3$, 282 MHz) δ -74.7. ^{31}P NMR ($CDCl_3$, 121 MHz) δ 22.2 (d, *J* = 50 Hz), -0.2 (d, *J* = 50 Hz). Anal. Calcd. for ($C_{78}H_{68}F_6O_6P_4Pd_2S_2Si_2$): C, 56.02; H, 4.10; N, 0. Found: C 55.93; H 3.83; N <0.05.

Synthesis of [(Ph_2SiP_2)Pd(2-phenylpyridine)OTf][OTf] *o*-Phenylpyridine was added dropwise to a THF solution of **B.14**. This compound was generated *in situ* for the specific purpose of this experiment and has not been isolated in crystalline form. ^{31}P

NMR (THF, 121 MHz) δ 37.1 (d, J = 14.5 Hz), 22.8 (d, J = 14.5 Hz); ^{19}F NMR (THF, 282 MHz) δ -75.3, -75.9.

B.5.4 Kinetic Studies

Standard kinetic protocol, measurement of reaction rates: Complex **B.1** (30.0 mg, 31.2 μmol) was dissolved in 0.6 mL THF, transferred to a J-Young NMR tube, and chilled inside a glovebox cold-well below -50 °C. Diisopropylethylamine (109 μL, 626 μmol) was then added to the cold solution. The tube was inserted into an NMR probe at 23 °C, and the temperature was allowed to equilibrate for 10 min. The decay of complex **B.1** was monitored by ^{31}P{^{1}H} NMR spectroscopy against an internal integration standard, which consisted of a sealed capillary tube containing a 1.6 M solution of $Ph_3P{=}O$ in CH_2Cl_2. Spectra were taken at intervals of ca. 3 min for ca. 3.5 half-lives. Besides the integral standard, the only observable peaks arise from **B.1** and the palladacycle **B.6**. The data were satisfactorily fit to an exponential decay, and the first-order rate constant was obtained from the ln(**B.1**) versus time plot. The reaction was carried out in triplicate, giving k_{obs} = 5.63, 5.49, and 5.76 x 10^{-4} s^{-1}. This protocol was also used in determining KIE data, measuring the rate dependence on amine concentration, and generating the Eyring plot.

KIE studies: $N^{i}Pr_2CD_2CH_3$ was prepared by reducing the amide $N^{i}Pr_2C(O)CH_3$ with $LiAlD_4$ under standard conditions.[36] The amine was extracted with petroleum ether and filtered through a silica plug to give spectroscopically pure $N^{i}Pr_2CD_2CH_3$. The reaction was carried out in triplicate, giving k_{obs} = 9.36, 9.65, and 10.57 x 10^{-5} s^{-1}.

Rate dependence on amine concentration: Seven kinetic runs were conducted in which the concentration of $N^{i}Pr_2Et$ was varied from 0.16 to 1.56 M (3 to 30 equivalents

relative to **B.1**). The total volume of the samples was kept constant at 0.6 mL. The following values for k_{obs} (x 10^{-4} s^{-1}) were obtained: 1.21 (3 equivalents of amine), 1.80 (5), 3.03 (10), 4.43 (15), 5.49 (20), 6.96 (25), and 8.41 (30).

Activation parameters ($\Delta H^{\ddagger}$, $\Delta S^{\ddagger}$) for the overall amine activation: A series of reactions were conducted over a 35 °C temperature range (0.0 to 35.3 °C). The NMR probe temperatures were measured using an anhydrous MeOH standard. The following values for k_{obs}*$[THF]_i/[N^iPr_2Et]_i$ (x 10^{-3} s^{-1}) were obtained: 0.40 (0.0 °C), 1.01 (7.5 °C), 1.88 (13.3 °C), 1.95 (13.3 °C), 3.01 (17.1 °C), 5.80 (23.1 °C), 9.81 (28.4 °C), and 19.73 (35.3 °C). The data provided a satisfactory linear fit in the Eyring plot, from which the activation parameters were calculated, $\Delta H^{\ddagger}$ = 17.9 ± 0.2 kcal/mol, $\Delta S^{\ddagger}$ = -4 ± 1 eu. Regression analyses of the data were performed using Microsoft Excel, and the activation parameters are reported with 95% confidence.

VT NMR studies: Complex **B.1** (20.0 mg, 20.8 μmol) was dissolved in 0.6 mL toluene-d_8, transferred to a J-Young NMR tube, and chilled inside a glovebox cold-well. Triethylamine (145 μL, 1.04 mmol) was then added to the cold solution. The tube was inserted into an NMR probe at -50 °C. As the temperature was slowly raised up to 0 °C, the reaction was monitored by ^1H and ^{31}P NMR spectroscopy. Conversion to the palladacycle **B.7** was relatively clean (~ 80% crude yield by ^{31}P NMR spectroscopy).

B.5.5 X-ray Experimental Data

X-ray diffraction studies were carried out in the Beckman Institute Crystallographic Facility on a Bruker Smart 1000 CCD diffractometer under a stream of dinitrogen. Data were collected using the Bruker SMART program, collecting ω scans at 5 ϕ settings. Data reduction was performed using Bruker SAINT v6.2. Structure solution

and structure refinement were performed using SHELXS-97 (Sheldrick, 1990) and SHELXL-97 (Sheldrick, 1997). All structural representations were produced using the Diamond software program. Crystallographic data are summarized in Table B.3 and Table B.4.

Table B.3. Crystallographic data for $[Ph_2BP_2]Pd(THF)(OTf)$, **B.1′**; $[Ph_2BP_2]Pd$(*o*-phenylpyridine)(OTf), **B.5**.

	B.1′·C_4H_8O	**B.5**·$2CH_2Cl_2$
chemical formula	$C_{43}H_{42}BF_3O_4P_2PdS\cdot C_4H_8O$	$C_{50}H_{43}BF_3NO_3P_2PdS\cdot 2(CH_2Cl_2)$
fw	963.08	1143.92
T (K)	98	98
λ (Å)	0.71073	0.71073
a (Å)	13.2666(7)	16.358(1)
b (Å)	17.483(1)	17.415(1)
c (Å)	19.212(1)	19.542(1)
α (°)	90	90
β (°)	95.855(1)	112.188(1)
γ (°)	90	90
V (Å^3)	4432.7(4)	5154.9(6)
space group	$P2_1/n$ (# 14)	$P2_1/n$ (# 14)
Z	4	4
D_{calc} (g/cm^3)	1.443	1.474
μ (cm^{-1})	5.96	7.24
R1, wR2[a] ($I>2\sigma(I)$)	0.0478, 0.0701	0.0489, 0.0802

[a] $R1 = \Sigma||F_o| - |F_c||/\Sigma|F_o|$, $wR2 = \{\Sigma[w(F_o^2 - F_c^2)^2]/\Sigma[w(F_o^2)^2]\}^{1/2}$

Table B.4. Crystallographic data for $[Ph_2BP_2]Pd(N,C:\eta^2\text{-}NCy_2CHMe)$, **B.8**; and $[Ph_2BP_2]Pd(N,C:\eta^2\text{-}NMeCH(CH_2)_3)$, **B.9**.

	B.8	**B.9**
chemical formula	$C_{52}H_{60}BNP_2Pd$	$C_{43}H_{44}BNP_2Pd$
fw	876.16	753.94
T (K)	98	98
λ (Å)	0.71073	0.71073
a (Å)	12.978(1)	11.616(1)
b (Å)	19.442(2)	29.268(2)
c (Å)	18.121(2)	11.5305(9)
α (°)	90	90
β (°)	107.570(1)	113.573(1)
γ (°)	90	90
V (Å^3)	4358.7(6)	3593.1(5)
space group	$P2_1/c$ (# 14)	$P2_1/c$ (# 14)
Z	4	4
D_{calc} (g/cm^3)	1.338	1.394
μ (cm^{-1})	5.4	6.4
R1, wR2[a] ($I>2\sigma(I)$)	0.0497, 0.0953	0.0485, 0.0870

[a] $R1 = \Sigma||F_o| - |F_c||/\Sigma|F_o|$, $wR2 = \{\Sigma[w(F_o^2 - F_c^2)^2]/\Sigma[w(F_o^2)^2]\}^{1/2}$

References Cited

1. Doye, S. *Angew. Chem. Int. Ed.* **2001**, *40*, 3351.

2. (a) Chatani, N.; Asaumi, T.; Ikeda, T.; Yorimitsu, S.; Ishii, Y.; Kakiuchi, F.; Murai, S. *J. Am. Chem. Soc*. **2000**, *122*, 12882. For Rh-catalyzed carbenoid insertions into C-H bonds α to N, see: (b) Davies, H. M. L.; Hansen, T.; Hopper, D. W.; Panaro, S. A. *J. Am. Chem. Soc.* **1999**, *121*, 6509. (c) Davies, H. M. L.; Venkataramani, C.; Hansen, T.; Hopper, D. W. *J. Am. Chem. Soc.* **2003**, *125*, 6462. (d) Davies, H. M. L.; Venkataramani, C. *Angew. Chem. Int. Ed.* **2002**, *41*, 2197. For a related example of imine activation, see: (e) Sakaguchi, S.; Kubo, T.; Ishii, Y. *Angew. Chem. Int. Ed.* **2001**, *40*, 2534.

3. Murahashi, S.-I.; Komiya, N.; Terai, H.; Nakae, T. *J. Am. Chem. Soc*. **2003**, *125*, 15312. For other Ru examples: (b) Chatani, N.; Asaumi, T.; Yorimitsu, S.; Ikeda, T.; Kakiuchi, F.; Murai, S. *J. Am. Chem. Soc*. **2001**, *123*, 10935. (c) Chatani, N.; Fukuyama, T.; Tatamidani, H.; Kakiuchi, F.; Murai, S. *J. Org. Chem.* **2000**, *65*, 4039.

4. (a) Barrera, J.; Orth, S. D.; Harman, W. D. *J. Am. Chem. Soc.* **1992**, *114*, 7316. (b) Orth, S. D.; Barrera, J.; Rowe, S. M.; Helberg, L. E.; Harman, W. D. *Inorg. Chim. Acta* **1998**, *270*, 337.

5. Zhang, X.; Fried, A.; Knapp, S.; Goldman, A. S. *Chem. Commun*. **2003**, 2060.

6. (a) Thomas, J. C.; Peters, J. C. *J. Am. Chem. Soc*. **2001**, *123*, 5100. (b) Thomas, J. C.; Peters, J. C. *J. Am. Chem. Soc.* **2003**, *125*, 8870.

7. For mechanistic considerations pertaining to these types of reactions see: (a) Nishimura, T.; Onoue, T.; Ohe, K.; Uemura, S. *J. Org. Chem.* **1999**, *64*, 6750. (b)

Mueller, J. A.; Sigman, M. S. *J. Am. Chem. Soc.* **2003**, *125*, 7005. (c) Jensen, D. R.; Schultz, M. J.; Mueller, J. A.; Sigman, M. S. *Angew. Chem. Int. Ed.* **2003**, *42*, 3810. (d) Steinhoff, B. A.; Stahl, S. S. *Org. Lett.* **2002**, *23*, 4179. (e) Steinhoff, B. A.; Fix, S. R.; Stahl, S. S. *J. Am. Chem. Soc.* **2002**, *124*, 766. (f) Mueller, J. A.; Jensen, D. R.; Sigman, M. S. *J. Am. Chem. Soc.* **2002**, *124*, 8202. (g) ten Brink, G.-J.; Arends, I. W. C. E.; Sheldon, R. A. *Adv. Synth. Catal.* **2002**, *344*, 355. (h) Trend, R. M.; Stoltz, B. M. *J. Am. Chem. Soc.* **2004**, *126*, 4482. (i) For a review on this topic see: Muzart, J. *Tetrahedron* **2003**, *59*, 5789.

8. See Trzeciak, A. M.; Ciunik, Z.; Ziółkowski, J. J. *Organometallics* **2002**, *21*, 132 and references therein.

9. (a) Tsuji, J. *Palladium Reagents and Catalysts– Innovations in Organic Synthesis*; John Wiley & Sons: New York, 1995; 125. (b) Beletskaya, I. P.; Cheprakov, A. V. *Chem. Rev.* **2000**, *100*, 3009 and references therein.

10. (a) Hartwig, J. F. *Angew. Chem. Int. Ed.* **1998**, *37*, 2046. (b) Hartwig, J. F.; Richards, S.; Barañano, D.; Paul, F. *J. Am. Chem. Soc.* **1996**, *118*, 3626.

11. (a) Strieter, E. R.; Blackmond, D. G.; Buchwald, S. L. *J. Am. Chem. Soc.* **2003**, *125*, 13978. (b) Guram, A. S.; Rennels, R. A.; Buchwald, S. L. *Angew. Chem., Int. Ed. Engl.* **1995**, *34*, 1348.

12. Gasparro, F. P.; Kolodny, N. H. *J. Chem. Educ.* **1977**, *54*, 258.

13. (a) Stang, P. J.; Cao, D. H.; Poulter, G. T.; Arif, A. M. *Organometallics* **1995**, *14*, 1110. (b) Benetollo, F.; Bertani, R.; Bombieri, G.; Toniolo, L. *Inorg. Chim. Acta* **1995**, *233*, 5.

14. Harkins, S. B.; Peters, J. C. *Organometallics* **2002**, *21*, 1753.

15. Lu, C. C.; Peters, J. C. *J. Am. Chem. Soc*. **2002**, *124*, 5272.

16. We note that $[Ph_2BP_2]Pd(Ph)(CH_3CN)$ can be generated in solution and spectroscopically identified by reaction of $\{[Ph_2BP_2]Pd(\mu\text{-}Cl)\}_2$ with PhMgBr in the presence of acetonitrile.

17. Yagyu, T.; Hamada, M.; Osakada, K.; Yamamoto, T. *Organometallics* **2001**, *20*, 1087.

18. Ackerman, L. J.; Sadighi, J. P.; Kurtz, D. M.; Labinger, J. A.; Bercaw, J. E. *Organometallics* **2003**, *22*, 3884.

19. Konze, W. V.; Scott, B. L.; Kubas, G. J. *J. Am. Chem. Soc.* **2002**, *124*, 12550.

20. (a) Constable, E. C.; Thompson, A. M. W. C.; Leese, T. A.; Reese, D. G. F.; Tocher, D. A. *Inorg. Chim. Acta* **1991**, *182*, 93. (b) Wong-Foy, A. G.; Henling, L. M.; Day, M.; Labinger, J. A.; Bercaw, J. E. *J. Mol. Catal. A: Chem.* **2002**, *189*, 3.

21. See Yamamoto, T.; Akimoto, M.; Saito, O.; Yamamoto, A. *Organometallics* **1986**, *5*, 1559 and references therein.

22. For pertinent examples, see: (a) Crawford, S. S.; Knobler, C. B.; Kaesz, H. D. *Inorg. Chem.* **1977**, *16*, 3201. (b) Matsumoto, M.; Nakatsu, K.; Tani, K.; Nakamura, A.; Otsuka, S. *J. Am. Chem. Soc*. **1974**, *96*, 6777. (c) Abel, E. W.; Rowley, R. J.; Mason, R.; Thomas, K. M. *J. Chem. Soc., Chem. Commun.* **1974**, 72. (d) Sepelak, D. J.; Pierpont, C. G.; Barefield, E. K.; Budz, J. T.; Poffenberger, C. A. *J. Am. Chem. Soc*. **1976**, *98*, 6178.

23. Allen, F. H. *Acta Cryst.* **2002**, *B58*, 380.

24. For complex **B.9**, the bond angles around nitrogen are also near 120° with the exception of the pyrrolidene ring angle, which is restrained by the ring.

25. (a) Ciriano, M.; Green, M.; Gregson, D.; Howard, J. A. K.; Spencer, J. L.; Stone, F. G. A.; Woodward, P. *J. Chem. Soc., Dalton Trans.* **1979**, *8*, 1294. (b) Kayaki, Y.; Shimizu, I.; Yamamoto, A. *Bull. Chem. Soc. Jpn.* **1997**, *70*, 917. (c) Veya, P.; Floriani, C.; Chiesi-Villa, A.; Rizzoli, C. *Organometallics* **1994**, *13*, 441.

26. (a) Canty, A. J.; Patel, J.; Skelton, B. W.; White, A. H. *J. Organomet. Chem.* **2000**, *607*, 194. (b) Dunina, V. V.; Gorunova, O. N.; Averina, E. B.; Grishin, Y. K.; Kuz'mina, L. G.; Howard, J. A. K. *J. Organomet. Chem.* **2000**, *603*, 138. (c) Ryabov, A. D. *Chem. Rev.* **1990**, *90*, 403.

27. (a) Tempel, D. J.; Johnson, L. K.; Huff, R. L.; White, P. S.; Brookhart, M. *J. Am. Chem. Soc.* **2000**, *122*, 6686. (b) Shultz, L. H.; Tempel, D. J.; Brookhart, M. *J. Am. Chem. Soc.* **2001**, *123*, 11539.

28. (a) Ledford, J.; Schultz, C. S.; Gates, D. P.; White, P. S.; DeSimone, J. M.; Brookhart, M. *Organometallics* **2001**, *20*, 5266. (b) Shultz, L. H.; Brookhart, M. *Organometallics* **2001**, *20*, 3975.

29. For examples of Pt(II/IV) redox couples associated with C-H bond cleavage see: (a) Wick, D. D.; Goldberg, K. I. *J. Am. Chem. Soc.* **1997**, *119*, 10235. (b) Jensen, M. P.; Wick, D. D.; Reinartz, S.; White, P. S.; Templeton, J. L.; Goldberg, K. I. *J. Am. Chem. Soc.* **2003**, *125*, 8614. (c) Stahl, S. S.; Labinger, J. A.; Bercaw, J. E. *Angew. Chem., Int. Ed.* **1998**, *37*, 2180. (d) Labinger, J. A.; Bercaw, J. E. *Nature* **2002**, *417*, 507.

30. Murahashi, S.-I.; Hirano, T.; Yano, T. *J. Am. Chem. Soc.* **1978**, *100*, 348.

31. We studied the product distribution for the reaction of **B.1** and $Et_2NCD_2CD_3$ in toluene to obtain a KIE of 2.0. This primary KIE does not help to establish whether or not β-hydride elimination is rate-determining in toluene. For instance, a primary KIE would also be consistent with deprotonation of the Pd-H as the rate-limiting step.

32. Laban, G.; Mayer, R. *Z. Chem.* **1967**, *7*, 12.

33. Arenz, T.; Frauenrath, H.; Raabe, G.; Zorn, M. *Liebigs Ann. Chem.* **1994**, 931.

34. Drew, D.; Doyle, J. R. *Inorg. Synth.* **1990**, *28*, 346.

35. Peters, J. C.; Thomas, J. C. *Inorg. Synth.* **2004**, *34*, 8.

36. March, J. *Advanced Organic Chemistry– Reactions, Mechanisms, and Structure*; John Wiley & Sons: New York, 1992; 448.